

Visual-auditory visualisation of dynamic multi-scale heterogeneous objects



Evgeniya Malikova

Faculty of Media and Communication
Bournemouth University

This dissertation is submitted for the degree of
Doctor of Philosophy

Abstract

The multi-scale phenomena analysis is an area of active research that is connecting simulations with experiments to get a correct insight into the compound dynamic structure. Visualisation is a challenging task due to a large amount of data and a wide range of complex data representations. The analysis of dynamic multi-scale phenomena requires a combination of geometric modelling and rendering techniques for the analysis of the changes in the internal structure in the case of data coming from different sources of various nature. Moreover, the area often addresses the limitations of solely visual data representation and considers the introduction of other sensory stimuli as a well-known tool to enhance visual analysis. However, there is a lack of software tools allowing perform an advanced real-time analysis of heterogeneous phenomena properties. The hardware-accelerated volume rendering allows getting insight into the internal structure of complex multi-scale phenomena. The technique is convenient for detailed visual analysis and highlights the features of interest in complex structures and is an area of active research. However, the conventional volume visualisation is limited to the use of transfer functions that operate on homogeneous material and, as a result, does not provide flexibility in geometry and material distribution modelling that is crucial for the analysis of heterogeneous objects. Moreover, the extension to visual-auditory analysis emphasises the necessity to review the entire conventional volume visualisation pipeline. The multi-sensory feedback highly depends on the use of modern hardware and software advances for real-time modelling and evaluation.

In this work, we explore the aspects of the design of visual-auditory pipelines for the analysis of dynamic multi-scale properties of heterogeneous objects that can allow overcoming well-known problems of complex representations solely visual analysis. We consider the similarities between light and sound propagation as a solution to the problem. The approach benefits from a combination of GPU accelerated ray-casting, geometry, optical and auditory properties modelling. We discuss how the modern GPU techniques application in those areas allows introducing a unified approach to the visual-auditory analysis of dynamic multi-scale heterogeneous objects. Similarly to the conventional volume rendering technique based on light propagation, we model auditory feedback as a result of initial impulse propagation through 3D space and its digital representation as a sampled sound wave obtained with the

ray-casting procedure. The auditory stimuli can complement visual ones in the analysis of the dynamic multi-scale heterogeneous object.

We propose a framework that facilitates the design of dynamic multi-scale heterogeneous objects visual-auditory pipeline and discuss the framework application for two case studies. The first is a molecular phenomena study that is a result of molecular dynamics simulation and quantum simulation. The second explores microstructures in digital fabrication with an arbitrary irregular lattice structure. For considered case studies, the visual-auditory techniques facilitate the interactive analysis of both spatial structure and internal multi-scale properties of volume nature in complex heterogeneous objects.

A GPU-accelerated framework for visual-auditory analysis of heterogeneous objects can be applied and extend beyond this research. Thus, to specify the main direction of such extension from the point of view of the potential users, strengthen the value of this research as well as to evaluate the vision of the application of the techniques described above, we carry out a preliminary evaluation. The user study aims to compare our expectations on the visual-auditory approach with the views of the potential users of this system if it is implemented as a software product. A preliminary evaluation study was carried out with limitations imposed by 2020/2021 restrictions. However, it confirms that the main direction for the visual-auditory analysis of heterogeneous objects has been identified correctly and visual and auditory stimuli can complement each other in the analysis of both volume and spatial distribution properties of heterogeneous phenomena. The user reviews also highlight the necessary enhancements that should be introduced to the approach in terms of the design of more complex user interfaces and consideration of additional application cases. To provide a more detailed picture on evaluation results and recommendations introduced, we also identify the key factors that define the user vision of the approach further enhancement and its possible application areas, such as users experience in the area of complex physical phenomena analysis or multi-sensory area.

The discussed in this work aspects of heterogeneous objects analysis task, theoretical and practical solutions allow considering the application, further development and enhancement of the results in multidisciplinary areas of GPU accelerated High-performance visualisation pipelines design and multi-sensory analysis.

Acknowledgements

First of all, I would like to express my gratitude to my amazing supervisory team, Dr Oleg Fryazinov, Prof. Alexander Pasko, Dr Valery Adzhiev for their continued support and advice.

I also wish to express my sincere gratitude to Dr Panos Amelidis and Dr Elena Kartasheva their insightful comments, suggestions and discussion of crucial aspects of this research.

I would also like to thank the researchers and my colleagues that took part in the evaluation study and provided very useful comments on this work.

Declaration

This thesis has been created by myself and has not been submitted in any previous application for any degree. The work in this thesis has been undertaken by myself except where otherwise stated. The list of related to this research publication is shown in appendix B

Contents

Acknowledgements	v
Declaration	vii
List of Figures	xv
List of acronyms	xxiii
1 Introduction	1
1.1 Problem statement	2
1.2 Research questions, aims and objectives	3
1.3 Contributions	4
1.4 Applications	6
1.5 Structure	6
2 Related Works	9
2.1 Challenges and requirements of visual analysis of heterogeneous multi-scale phenomena	10
2.1.1 Visual pipeline optimisation and execution	10
2.1.2 Dynamic and multi-scale geometry representation	11
2.1.3 Complexity and quality in visual analysis of volume objects	15
2.1.4 Interactive exploration of scientific data	16
2.2 Challenges of auditory analysis of heterogeneous phenomena	18
2.2.1 Exploration of physical properties of spatial structures	19
2.2.2 Auditory mappings for volume structures	20
2.2.3 Spatial orientation and navigation	21
2.3 Summary	22

3	Background	23
3.1	Overview	23
3.2	Heterogeneous objects representations	25
3.2.1	Cellular representation	26
3.2.2	Voxel representation	28
3.2.3	Point clouds and particle-based data	29
3.3	Material and geometry modelling	30
3.3.1	HyperVolume model	31
3.3.2	Implicit complexes framework for heterogeneous objects	35
3.3.3	Constructive hybrid modelling within IC	37
3.4	Direct Volume ray-casting	37
3.4.1	Computer graphic rendering pipeline	37
3.4.1.1	Rasterisation basics	38
3.4.1.2	Ray-tracing basics	39
3.4.2	Volume Rendering framework	42
3.4.3	Volume ray-casting on unstructured grids	43
3.4.4	Optical model	45
3.4.4.1	Absorption	45
3.4.4.2	Emission	46
3.4.4.3	Emission and absorption	46
3.4.4.4	Emission, absorption, single scattering	47
3.5	Auditory feedback and sound propagation	47
3.5.1	Core principles of sound modelling and analysis	48
3.5.2	Physically based sound synthesis	51
3.5.3	3D spatial sound computation	56
3.5.3.1	Modelling 3D sound propagation through environment	57
3.5.3.2	Sound-listener interaction	60
3.5.4	Auditory analysis of generated sound wave	62
3.6	Interactive exploration and multimodal feedback	65
3.6.1	Overview	65
3.6.2	Widgets and avatars	66
3.6.3	Continuous multi-dimensional modelling and sampling issues in real-time user interaction	68
4	Theoretical framework	71
4.1	Overview	71
4.2	An approach to visual-auditory analysis	72

4.2.1	General scheme	72
4.2.2	Initial data pre-possessing and representation	75
4.2.2.1	Preprocessing	76
4.2.3	Visual-auditory scene representation and mapping	79
4.2.4	Analysis of visual-auditory stimuli and rendering	81
4.2.4.1	Colour and music scale	81
4.2.4.2	Optical and auditory models	83
4.2.4.3	Getting an insight into the internal volume structure	84
4.2.5	User interaction for visual-auditory scene exploration	85
4.2.5.1	Avatar based interaction	87
4.2.5.2	GUI extension	88
4.3	Constructive geometry modelling	88
4.3.1	From explicit to implicit cell	90
4.3.2	Geometry, topology and shape dynamic changes	92
4.3.3	Modelling of multi-scale features with composite cells	94
4.3.4	Lattices and irregular structure modelling on the sets of cells	97
4.4	Visual-auditory materials modelling	101
4.4.1	Constructive material modelling	101
4.4.2	Multi-dimensional TF	105
4.5	Visual-auditory rendering	106
4.5.1	Overview	106
4.5.2	Intersection with multi-dimensional geometry	107
4.5.3	Visual-auditory properties accumulation	109
4.5.3.1	General concepts	109
4.5.3.2	Optical properties accumulation	110
4.5.3.3	Auditory properties accumulation	111
4.6	Interactive visual-auditory exploration	115
4.6.1	Constructive modelling with interaction avatar	115
4.6.2	Measurement with auditory feedback	117
4.6.2.1	Auditory feedback generation as a part of ray-casting	117
4.6.2.2	Numerical measurements with ray-casting	119
4.6.3	Modelling the region of two heterogeneous structures overlap	120
4.6.4	User Interface for manipulating visual-auditory scene	121
4.7	Summary	124

5	Algorithms and implementation	125
5.1	Overview	125
5.2	Ray-casting inspired visual-auditory pipeline for dynamic heterogeneous objects	127
5.2.1	Overview	127
5.2.2	General principles	127
5.2.3	Bounding volume hierarchy	129
5.2.4	Sphere-tracing	130
5.2.4.1	Ray-geometry intersection	130
5.2.4.2	Local optical and auditory model integration	131
5.2.5	Visual-auditory pipeline optimisation and efficiency	131
5.3	Ray-tracing API for IC hybrid structure rendering	132
5.3.1	Acceleration structures in visual-auditory pipeline	133
5.3.2	Data storage and intra-shader communication for various volume ray-casting strategies	140
5.3.3	Types of ray-tracing pipelines for heterogeneous objects	145
5.3.4	GPU modelling and storage of hybrid constructive geometry	147
5.3.5	Visual and auditory rendering passes	150
5.4	Visual-auditory API	151
5.4.1	Overview	151
5.4.1.1	Naming structure	152
5.4.1.2	Prerequisites	152
5.4.2	Data-flow in GPU-accelerated visual-auditory analysis	152
5.4.3	Handling GPU programs	156
5.4.4	Data readers and SDF geometry mapping	157
5.4.5	Setting up Mapper and Actor for visual-auditory Rendering	159
5.4.6	Window, GUI and Interactor	160
5.4.7	Constructive modelling	161
5.4.8	Rendering	164
5.4.9	Interactive widgets	167
5.4.10	Timings	170
6	Case studies	175
6.1	Molecular simulation case study	175
6.1.1	Molecular phenomena representation and visual analysis	176
6.1.2	An overview of multi-modal visualisation of molecular data	178
6.1.2.1	Constructive modelling of visual-auditory molecular scene	179

6.1.2.2	Visual-auditory analysis of molecular structures	180
6.1.3	Case studies	181
6.1.3.1	CPK and Ball-and-Stick representations for molecular dynamics results visual-auditory study	181
6.1.3.2	Visualisation of dynamic multi-scale molecular structures example	184
6.1.3.3	Quantum chemistry example	187
6.2	Microstructures in digital fabrication	190
6.2.1	Problem overview	191
6.2.1.1	Modelling of multimaterial microstructures	191
6.2.1.2	Rendering multimaterial volume objects	192
6.2.2	Case study overview	193
6.2.2.1	GPU modelling geometry and material	193
6.2.2.2	Accelerated volume ray-casting of semitransparent multi- material microstructures	194
6.2.3	Examples	195
6.2.3.1	Multimaterial lattice-type microstructures	195
6.2.3.2	Modelling on the sets of cells within lattice microstructures	199
6.2.3.3	Composite material modelling on microstructures	199
7	Preliminary evaluation	205
7.1	Design	206
7.1.1	Introduction	206
7.1.2	Sample population description	207
7.1.3	Independent and dependent variables	207
7.1.4	Data analysis structure	208
7.1.5	Questionnaire structure and limitations of the procedure	209
7.2	Analysis of the results	210
7.2.1	2D scanning for volume rendering to highlight visual perception issues in superconductor field	210
7.2.1.1	Comparison of two different visual-auditory techniques	214
7.2.1.2	Impression on visual-auditory volume rendering across population	217
7.2.2	3D sound	220
7.2.2.1	Visual-auditory exploration of molecular structures	220
7.2.2.2	Overall vision of extension of visual-auditory volume ren- dering	224

7.2.3	Auditory perception based user interaction	225
7.3	Summary	229
8	Conclusions and discussion	231
8.1	Overall conclusions	231
8.2	Future research	233
8.2.1	HPC and complex GPU tasks within visualisation pipeline	234
8.2.2	User interaction with multisensory feedback	234
Appendix A	Additional materials	237
Appendix B	List of Publications	239
Bibliography		241

List of Figures

3.1	(a) General representation of visualisation pipeline. Initially introduced in (Haber & McNabb 1990) (b) View on structure of volume visualisation in (Chaudhary et al. 2019) that relies on regular structured grids (Kaufman & Mueller 2005)	24
3.2	Schematic representation of basic FEM simulation pipeline and visualisation of the results. The visualisation example from (<i>GLVis gallery</i> 2018): the case of High-order Lagrangian hydrodynamics. Grey blocks represent procedures and black input/output data structures. 1)Input BRep representation that is a result of CAD parametric modelling 2) 3D meshing of BRep into tetrahedral volume 3) FEM-based simulation 4) The result of simulation: 3D mesh with distribution of attributes within cellular subdivision 5) Visualisation of the results of simulation.	27
3.3	Schematic representation of basic medical imaging pre-processing and visual analysis. The visualisation example from (<i>MITK Release notes 2016</i> 2016): the segmented tissues on CT scan. Grey blocks represent procedures and black input/output data structures. 1) Input image data that is obtained experimentally with scanning devices 2) Registration and segmentation procedures that combine various image data and extract tissues for analysis 3) The result of image processing that is the labelled volumes that represent substructures of interest (tissues) 4) Visualisation of labelled volume data	29
3.4	Examples of modelling and visualisation of heterogeneous objects. a) Volume rendering of dynamical process of molecular structure geometry optimisation; b) Modelling and visualisation of porous structure; c) Volume geological structure with layers of different materials, cavities and a drilled well. d) Brain labelled data volume rendering by standard VTK means (data from <i>Volume Rendering with Python and VTK</i> (n.d.)	34
3.5	Rasterization pipeline. Image from (Deng et al. 2017)	38

3.6	Dataflow in rasterization pipeline. Image from (Subtil 2018)	39
3.7	Ray-tracing scheme	40
3.8	Dataflow in ray-tracing pipeline. Image from (Subtil 2018)	41
3.9	Volume ray-casting of most common heterogeneous objects representations: point-based data and tetrahedral meshes . The integration of optical properties is evaluated only on ray-segment of length $ x_1 - x_0 $ computed as a result of ray intersection with bounding box	44
3.10	Scheme of input convolution with LTI impulse response. Image from Cook (2002)	50
3.11	Mass/spring system. Image from Cook (2002)	52
3.12	Modal resonant filter based synthesis, schematic representation from Cook (2002)	54
3.13	Simulation of ideal string a) Basic idea of describing string through trav- elling wave components $y(x, t) = y_r(x - ct) + y_l(x + ct)$. b) A schematic representation of travelling wave components as string is picked through time c) Waveguide string model with loss	55
3.14	Impulse response for ear modelled as a result of propagation(a) and entire scheme for HRIR ray-tracing (b). Images from (Röber et al. 2006)	60
3.15	HRTF scheme	61
3.16	Reverberation paths. Image from Funkhouser et al. (1998)	62
4.1	Visual auditory analysis process unified by concepts of light and sound propagation (input as $g(t), l(t), c(t)$, data - heterogeneous object initial data representation, remove HV	73
4.2	Initial data representation	76
4.3	Bounding volume construction for a basic case of multi-scale geometry with dynamic features (a) A bounding volume for the dynamic geometry (b) A bounding volume for the static multi-scale geometry (one frame is considered)	77
4.4	Modelling of visual-auditory scene	79
4.5	Basic colour scale and introduced "music scale" in volume rendering frame- work for analysis of scalar field simultaneously via optical and auditory properties	81
4.6	Light transport in the conventional volume rendering for analysis of the internal structure of the scalar field	82
4.7	Sound propagation in the proposed approach for auditory volume rendering	84

4.8	Interactive exploration of heterogeneous objects with spatially distributed properties	86
4.9	Examples of constructive trees for molecular point-based data and FEM tetrahedral meshes a) 1D case of molecular data b) 3D case of tetrahedral meshes as mapping of explicit cells data is performed	91
4.10	Dynamic changes in shape for 0D data.	92
4.11	Various dynamic changes in shape and topology from 0D to 1D variations. (a) Microstructure type geometry G_1 mapping $M_{i1} : C_1 \rightarrow I_1$ (b,c) balls and sticks type geometries G_2, G_3 mappings M_{i2}, M_{i3} of 1D explicit cells with different topological structure. A transition between output implicit cells I_{i1}, I_{i2}, I_{i3} is modelled with geometry interpolation M_g and dynamic morphing of shapes M_s	93
4.12	Macro and micro scale features for dynamic water cluster	95
4.13	Visualisation of multi-dimensional geometry by a combination of interactive LOD and dynamic rendering techniques	95
4.14	An example of constructive modelling of dynamic geometry on "macro" (cluster fluctuations) and "micro" (individual molecule vibrations) scales controlled with parameters t_1, t_2 for water cluster.	96
4.15	Using tetrahedral mesh subdivision as a basis for modelling of arbitrary geometry on set of cells	98
4.16	Ice crystal lattice-based microstructure a) Lattice b) Unit cell	99
4.17	Modelling within the selection of unit cells. The lattice structure or "blobby" structure within each regions is highlighted with different colour (green, pink, violet, yellow)	100
4.18	Material modelling and application scheme. a) G_1, G_2, G_3, G_4, G_5 are geometry regions of semitransparent homogeneous material. G_6 is computed as subtraction from cube of G_1, G_2, G_3, G_4, G_5 represents a region of homogeneous materials blending $f(x) = RBGW$ and blended material as blending function over two constant $f(X) = Blend(f_1(x), f_2(x))$ where f_1 and f_2 are functions returning material distribution within the bounding volume. b) Geometry c) Result of material application rendered with proposed sphere-traced sampling d) Comparison to regular volume sampling	101
4.19	Geometry and material modelling within one cell with Si-O basic individual element. A1 and A2 are regions of homogeneous materials on geometries G_1, G_2 and A3 is defined as blending of A1, A2. Additional bounding subvolumes (yellow spheres) include blending of bond with one of its atoms	102

4.20	Examples of material blending modelling within various structures	104
4.21	Constructive modelling of geometry and optical properties for dynamic HCN molecule	106
4.22	Intersection with multidimensional geometry for further optical and auditory properties integration.	108
4.23	Auditory scene volume ray-casting for molecular structure where each region of constant acoustic material is defined on "atom" geometry.	112
4.24	Constructive modelling of hand based of hand interaction with object that was considered in Fig. 4.21	116
4.25	Frames of example of constructive modelling on base of hand interaction	116
4.26	The scheme of auditory feedback generation with digital waveguide model of plucked string.	118
4.27	Examples of evaluation of distance properties on between cells and additionally modelled representations (SDF blobby structure) within proposed geometry model. d1 - euclidean distance between points that are centres of cells, d2 - distance from cell centre x_1 to surface SDF, d3 - distance from cell centre to surface SDF along the ray computed with sphere tracing (general algorithm is discussed in section 5.2.4)	119
4.28	Example of volumes overlapping evaluation and complex modelling. Region of overlapping is modelled as "composite material injection" volumes	121
4.29	Isosurface extraction for tetrahedral mesh volume rendering	122
4.30	Interaction via Midi keyboard a) Music pattern definition with Midi Keyboard b) Highlighting of scalar field areas, corresponding to defined pitch pattern	123
5.1	An approach to volume ray-casting of heterogeneous objects. Step1. intersection with bounding volume $BV_i^{l_2}$ - BVH acceleration. Step2. Intersection with "lower level" bounding volumes and decomposition of constructive tree. Sphere-tracing (Hahn et al. 1998) of SDF subtree for exact intersection with geometry domain G_i . Step3. Local volume integration of Ao_i and As_i with the ray-segment parameters for integration of constant and "blended" materials computed with sphere-tracing	128
5.2	Examples of TLAS and BLAS for scene with different types of objects: polygonal plane composed of 2 triangles (BLAS), SDF primitives without BLAS acceleration and molecular structures those atoms are accelerated with BLAS	134
5.3	Bounding volumes deployment for basic dynamic geometry	134
5.4	Monte-carlo ray-tracing of CPK molecular structure (surface)	135

5.5	General scheme for testing and evaluation of intersection with i_{th} cell. . . .	137
5.6	Splitting of constructive tree for composite cell with bounding volumes $BV_{ij}^{l_0}$ of dynamic and multi-scale nature. The technique suggests rendering of overlapping geometries.	138
5.7	Decomposition of ray-cell intersection for constructively modelled heterogeneous structure.	139
5.8	Example of complex BLAS accelerated intersection case. We do not know if intersection point computed with BLAS is the closest one for geometry G_1	140
5.9	Ray-tracing APIs shaders and the execution logic (image from (Usher 2020)). During traversal, rays are tested against primitives in the leaf nodes (IC cells in our case) of the acceleration structure. (c) If an intersection is found the Any Hit Shader is called. After the traversal is complete (d) if defined the Closest Hit Shader of the hit geometry is called if a hit was found, otherwise (e) the Miss Shader is called. These shaders then return control to the caller of TraceRay, or can make recursive trace call.	141
5.10	Iterative accumulation of optical and auditory properties for basic type of volume ray-casting pipeline	142
5.11	General optical and auditory volume ray-casting algorithm. Ray-tracing API shader domains and their augmentation with callable shaders accessed directly or from Per ray data array	144
5.12	Heterogeneous objects architecture to define the logic of volume ray-casting	146
5.13	Types of volume ray-casting architectures	148
5.14	Hybrid constructive tree implemented as a set of Optix Buffers with explicit cell representation and Callable programs ids.	149
5.15	Interaction	149
5.16	The structure of communication between classes and shaders management	153
5.17	A structure of proposed framework for volume rendering of heterogeneous objects. Visual-auditory pipeline is constructed according to data-flow concept with two main procedures to be user defined: mapping geometry primitive (SDF) and TF	154
5.18	An example of calling GPU accelerated API from Python	155
5.19	Execution in Python based scientific environment for conventional visualisation APIs (1) and the proposed API (2) that minimises CPU-GPU data exchange	156
5.20	Core classes	157
5.21	Reading classes	157

5.22	Constructive geometry modelling classes, including heterogeneous objects modelling framework	162
5.23	A example of constructively modelled geometry	164
5.24	Optical and auditory models	167
5.25	Widgets	168
5.26	Registration of widget geometry (sphere) and molecular surface object. (a) The ray-casting based scanning of local surface patch for assumed local registration area. For this the user interactively moves widget in specified direction (b) Result of least-squares registration of two defined point sets.	169
5.27	Examples of input data with dynamic microstructure shape modelled within defined heterogeneous subdivision a) Heat equation mesh; b) Diffuse membrane (molecular data) d) Slice of diffuse membrane	172
5.28	Pipeline evaluation time depending on number of cells for models 1,2,3	173
5.29	Averaged FPS depending on number of cells for models 1,2,3	173
6.1	Volume ray-casting of various representations of molecular phenomena that is a result of molecular dynamics simulation	180
6.2	Dynamic frames of rendering of molecular dynamic representations for CPK and Ball-and-Stick like blending(surface ray-casting)	182
6.3	Volume ray-casting of various molecular structures	183
6.4	Visual-auditory volume ray-casting of various molecular structures	185
6.5	Visualisation of molecular structure with dynamic features om both macro and micro scale	186
6.6	Selected frames of dynamic Volume Rendering of the chemical transformation from HCN to the HNC isomer. Ball-and-Stick model (a) and quantum chemistry model (b)	187
6.7	Volume Rendering of the HCN molecule. Rendering with introduced TF and the following optical models: a) without scattering; b) with basic single scattering.	189
6.8	Sphere-tracing of cell with sparse geometry within lattice microstructure. The shape is a part of representation of dynamic cell within microstructure presented in Fig. 6.11	194
6.9	Comparison of regular volume sampling and ray-segment integration (Max & Chen 2010) where ray-segments are computed with sphere-tracing for constant and blended material regions	196
6.10	The frames from the animation that demonstrates the dynamic changes of shape and topology within subdivision defined by tetrahedral mesh	197

6.11	The frames from the animation that demonstrates the dynamic changes of shape and topology within subdivision defined by crystal lattice	198
6.12	(a) irregular lattice structure modelling scheme (b)initial ice cell (c) The scheme of "meta" regions modelling on crystal lattices from paper (Pham et al. 2019)	200
6.13	Frames of dynamic modelling within the selection of unit cells. The lattice structure within each regions is highlighted with different colour (green, pink, violet, yellow)	201
6.14	Various cases of cells ray-casting	202
6.15	The frames of volume rendering of the multimaterial microstructure	203
7.1	The screenshots of the results obtained with implemented visual-auditory techniques used for the analysis of superconductor field symmetry features	211
7.2	Visual detection of small geometric features (changes in symmetry and distortion) in a scalar field. (a) Simultaneous scan the field areas that are supposed to be equal due to symmetrical field properties, for example, lines $\langle 0, 8 \rangle, \langle 1, 7 \rangle \dots \langle 3, 5 \rangle$, in Fig. 7.1 a) (b)Tracking the possible vortex distortion due to external influence applied to a field that changes its symmetrical properties and shapes of vortexes. The scanning vortexes 1,2,3,4 and) is a centre of symmetry in Fig. 7.1 b).	213
7.3	Overall experience on two considered visual-auditory techniques that were applied to superconductor fields analysis problem	215
7.4	Screenshot of Analysis ToolPack linear regression results for the analysis of user preference of the visual-auditory techniques that minimise either memory or time issues	216
7.5	T-test on sample for preference of the visual-auditory analysis technique	216
7.6	Power analysis. Estimation of sample size for defined II-type error with effects size of 0.78.	217
7.7	Summary on preference to enhanced volume rendering technique . The screenshot of the linear regression results from the Analysis Toolpack(a) The regression with all independent variables (significant variables marked with yellow) (b) Regression for significant variables only	218
7.8	Approximated line plots for significant variables for enhanced volume rendering technique	219
7.9	T-test results on population sample	219
7.10	Power analysis. Estimation of sample size for defined II-type error with effects size of 0.71.	220

7.11	Visual-auditory volume ray-casting of the complex spatial object (molecule). Highlighting of "activated" with auditory impulse atoms	221
7.12	Auditory scanning of different layers of membrane molecular structure . . .	221
7.13	3D sound for navigation and exploration. (a) Deployment of substructures localisation tasks in visual-auditory scene (atoms in molecular structure) (b) Deployment of solely auditory stimuli as source of additional information on substructure. The auditory feedback is based on 2 molecular membrane layers	223
7.14	Screenshot of Analysis ToolPack linear regression results for the analysis of user vision of auditory analysis tools within volume rendering framework, in particular vision of using auditory analysis only as additional tool to visual analysis. The significant variables are marked with yellow.	224
7.15	T-test results on population sample	225
7.16	Power analysis. Estimation of sample size for defined II-type error with effects size of 0.49	225
7.17	Interaction with volume data on base of obtained auditory image of the phenomena.	226
7.18	Summary on preference to enhanced volume rendering technique . The screenshot of the linear regression results from the Analysis Toolpack(a) The regression with all independent variables (significant variables marked with yellow) (b) Regression for significant variables only	227
7.19	Approximated line plots for significant variables for vision of user interaction with visual-auditory image of the phenomena	228
7.20	T test results for user visual-auditory interaction vision within used popula- tion sample	228

List of acronyms

FREP	Function Representation
HV	HyperVolume
SDF	Signed Distance field
TF	Transfer function
VRep	Voxel representation
SVO	Sparse Voxel Octree
IC	Implicit complex
FEM	Finite element method
GPGPU	General-purpose computing on graphics processing units
HCI	Human–computer interaction
HPC	High Performance Computing
HPG	High Performance Graphics
ML	Machine learning
CAD	Computer-aided design
CAE	Computer-aided engineering
BREP	Boundary representation
HV	Hyper Volume
BRDF	Bidirectional reflectance distribution function
HRTF	Head-related transfer function
AR	Augmented reality
VR	Virtual reality
XR	Mixed reality or cross-reality environment

BLAS	Bottom level acceleration structure
TLAS	Top level acceleration structure
ROI	Region of interest
SSBO	Shader storage Buffer Object
GUI	Graphic user interface
UI	User interface
LOD	Level-of-detail
SBT	Shader binding table
PSO	Pipeline state object
BVH	Bounding volume hierarchy
MIDI	Musical Instrument Digital Interface

Chapter 1

Introduction

The complexity of modern scientific and engineering workflows along with the rapid progress in the area of digital fabrication boost the need in methods and tools that can simultaneously operate, store and visualise several representations of volume objects that come from various sources. The results of such complex scientific and engineering workflows are often referred to as heterogeneous objects. A heterogeneous object is a general term for representations of the volume objects that use different representations of multi-scale and dynamic features that are modelled on the spatial subdivision. Such subdivision can be introduced as a result of parallel CPU/GPU accelerated simulation and preprocessing tasks that are an essential part of scientific and engineering workflows. The most common examples of such heterogeneous objects are molecular structures, the results of Finite Element Methods and microstructures in digital fabrication.

The analysis of such objects is not straightforward. A combination of the results of experiments and computer simulations with several representations leads to the necessity of heterogeneous multi-scale objects modelling and rendering within the visualisation pipeline. However, conventional visualisation solutions can not address challenges imposed by heterogeneous objects since they deal primarily with the homogeneous material distribution. Moreover, the complexity of such objects raises the issues of analysis quality and visual stimuli overload.

The recent advances in graphics hardware allow addressing the problems with interactive exploration and multimodal techniques. The multisensory perception allows extending the analysis of such complex structures as heterogeneous objects. Different sensory stimuli are well known to efficiently complement each other in the analysis process via real-time user interaction with multisensory feedback. Introduction of multisensory features in the scientific visualisation is often considered in a context of virtual reality (VR) or augmented reality (AR) application that emphasises real-time decision making and interactive exploration. The

design tasks demand real-time computationally expensive geometric modelling in the context of user interaction and high update rate rendering requirements.

In this work, we are dealing with visual-auditory rendering and analysis of the heterogeneous objects. We focus on the principles that push forward the modern volume rendering and sound modelling solutions those are based on the latest GPU hardware features. We take advantage of commonalities in light and sound propagation to introduce a unified approach. We construct a visual-auditory pipeline as a result of continuous optical and auditory properties modelling and consider a visual-auditory image rendering and analysis unified by concepts of light/sound propagation. We demonstrate those principles application by designing a framework for fast prototyping of volume visualisation solutions for heterogeneous objects study. We provide examples of the application of the framework for visual-auditory case studies of molecular structures and microstructures in digital fabrication.

1.1 Problem statement

The analysis of dynamic heterogeneous objects is an area of active research that is connecting simulations with experiments to get a correct insight into the compound dynamic structure. The problem of dynamic multi-scale phenomena analysis arises in many research areas, such as computational chemistry, medical data analysis, physical phenomena studies or engineering and digital fabrication workflows. The visual analysis of such multi-scale phenomena is a challenging task due to a large amount of data and a wide range of complex data representations. The task may demand simultaneous analysis of various dynamic representations that include discrete or continuous scalar fields, particle-based data and polygonal meshes. The data describes different features and underlying processes that characterise the studied phenomena. The modelling of dynamic multi-scale geometry and optical properties distribution within a heterogeneous structure takes place in the multidimensional space. Such representation requires a large number of 3D objects and should allow real-time or interactive exploration of the multi-scale properties of the phenomena (Kouřil et al. 2019).

The complexity and the multi-scale nature of heterogeneous objects require a combination of geometric modelling and rendering techniques and often takes place in the context of GPU-accelerated methods. Due to the nature of the problem, heterogeneous representation uses a wide range of geometry models within a spatial subdivision. The conventional mesh-based geometric models are not convenient for the multi-scale dynamic phenomena (Wang et al. 2011) and unsuitable for many scenarios. For example a large dynamic data that is a result of computer simulation, cannot be visualised conveniently by using traditional mesh-based methods (Muzic et al. 2015)(Miao, Klein, Kouřil, Mindek, Schatz, Gröller,

Kozlíková, Isenberg & Viola 2019). Moreover, the complexity of heterogeneous objects raises the issues of analysis quality and facilitation in terms of human-computer interactions and multisensory data exploration (Kozlikova et al. 2017). The wrong insight on complex data can fail the entire analysis process (Keim et al. 2008). The sensory stimuli are well known to operate differently and successfully complement each other.

The volume rendering framework establishes high-quality requirements for the visual analysis of phenomena. The technique core is a physical concept of light propagation through volume object and evaluation of optical model by iterative computation of interaction with each subvolume element. The approach provides flexibility in visual analysis improvement (Kniss et al. 2002, Johnson 2004). By enhancement of optical model, the technique allows addressing such issues as highlighting features of interest in complex phenomena (Jung et al. 2018) , image quality and human perception limitation (Djurcilov et al. 2001). However, the conventional volume visualisation framework is not suitable for heterogeneous objects analysis. Also, the computationally expensive multisensory user interaction with such structures impose additional efficiency requirements.

1.2 Research questions, aims and objectives

This research tackles the three main questions:

1. How optical and auditory properties can be modelled within heterogeneous structure independently from the restrictions imposed by geometry, and how these properties can be efficiently rendered to visual-auditory stimuli?
2. How the visual-auditory pipelines can be constructed from basic blocks in a unified way for complex virtual scenes, thus allowing users creating flexible solutions for visual-auditory analysis of the dynamic multi-scale heterogeneous objects?
3. How visual-auditory pipeline implementation can benefit from the modern GPU hardware?

The main aim of this research is to provide a unified framework for the visual-auditory analysis of dynamic multi-scale heterogeneous objects with the distribution of heterogeneous properties in volumes. Moreover, the solution should naively support the design of pipelines oriented on real-time visual-auditory exploration and user interaction.

In this work, we consider extending the volume ray-casting technique with auditory stimuli. Therefore, it can be interpreted that we move from a conventional graphical representation of the multi-scale phenomena to a multisensory scene. The research explores an

object with heterogeneous representation with optical and auditory properties that is obtained as a result of hybrid modelling. To introduce a visual-auditory scene rendering based on the ray-casting the work takes advantage of similarities between light and sound propagation. The auditory stimuli are employed to enhance the analysis of dynamic multi-scale molecular phenomena and complement visual stimuli in the conventional volume rendering technique.

The main objectives of this research are:

1. To explore the problem areas that discuss the analysis of the heterogeneous objects, such as FEM, molecular simulation, medical imaging and digital fabrication and specify the input data structures in those research areas that the designed solution can contribute to.
2. To reconsider the visualisation pipeline in terms of use of modern GPU hardware and algorithms for efficient analysis of dynamic multi-scale heterogeneous objects.
3. To propose a general framework for visual-auditory analysis of heterogeneous objects with a unified structure that takes advantage of the concepts of light and sound propagation.
4. To specify a mathematical framework for continuous modelling of dynamic and multi-scale geometry with a distribution of optical and auditory properties in heterogeneous objects.
5. To implement and evaluate an original prototype software that allows GPU data flow for visual-auditory analysis and demonstrating practical applications

1.3 Contributions

In this work, we propose a complex visual-auditory solution to problems arising in the area of heterogeneous objects analysis. The main contributions of the research are:

1. The analysis of heterogeneous objects impose challenges that conventional volume visualisation frameworks are not designed to address, in particular multi-dimensional continuous modelling of dynamic and multi-scale properties on various types of a cellular subdivision. We provide a unified multi-dimensional continuous representation of dynamic multi-scale properties. We pay particular attention to the control of shape and topology in the geometry representation as we visualise the dynamic and multi-scale features changes. In our research, we consider a blend of ray-casting and geometry and volume material modelling to address complex and computationally

- expensive tasks such as accelerated rendering multi-dimensional properties, continuous geometry modelling and real-time user interaction procedures.
2. We propose a universal approach to the visual-auditory analysis of such complex objects that takes advantage of similarities in light and sound propagation to obtain a visual-auditory image of heterogeneous phenomena. We discuss the visual-auditory rendering as a procedure that can be computed with ray-casting that evaluates the light and sound interaction for optical and auditory properties that are modelled within a heterogeneous structure. Thus, we introduce the unified design of a visual-auditory pipeline and simultaneous visual-auditory analysis based on the analysis of the distribution of optical and auditory properties. The approach deals with the following visualisation blocks:
 - (a) A mapping procedure for modelling of distribution of volume optical and auditory properties;
 - (b) The rendering of the visual-auditory scene as evaluation of light and sound propagation through the heterogeneous volume computed with the ray-casting procedure;
 - (c) Analysis of data that represents the initial heterogeneous object as analysis of visual and auditory stimuli produced by individual components of heterogeneous objects with optical and auditory properties of the entire object;
 3. We provide the examples and discuss how various initial data representations influence the design of GPU accelerated visual-auditory pipeline for analysis of such objects. We consider such representations of heterogeneous objects as point-based and voxel data for molecular structures that are the result of molecular dynamics or quantum simulation, tetrahedral meshes that are the result of FEM, procedural modelling of lattice-based microstructures on a base of crystal data. We demonstrate such various representations of heterogeneous objects can be conveniently handled by the introduced concept of a ray-casting inspired visual-auditory pipeline that operates a hybrid multi-dimensional structure.
 4. We test the examples on a selected set of potential users of this approach to assess the applicability of the method.

1.4 Applications

We see the main application area of the designed tools as facilitation of the design of the high-quality heterogeneous objects visualisation solution for scientific analysis or educational purposes.

There is a lack of general visualisation solutions that simultaneously address such aspects of heterogeneous objects nature as volume nature of internal properties and spatial subdivision (unstructured data) to describe those internal properties of distribution. Moreover, the real-time introduction of additional sensory stimuli into such pipelines is not a straightforward task. In this research, we have demonstrated the benefits of the design of the GPU-accelerated visualisation pipeline on the base of ray-tracing technique principles. We design an API on a top of the ray-tracing APIs and benefits of GPU data flow, object-oriented architecture and Python bindings for the design of real-time interactive solutions in integration into scientific workflows. Moreover, we extend the proposed solution to the case of visual-auditory analysis and consider the principles of multimodal feedback that is becoming an essential part of VR/AR experience.

We provide the practical examples implemented with the designed API that address the problem of heterogeneous objects analysis in various areas including molecular data analysis, analysis of FEM results and microstructures analysis in digital fabrication. The implemented API is an open-source project that implements the proposed concepts for multimodal exploration of heterogeneous objects and combines continuous multi-dimensional geometry, modelling of optical and auditory properties and volume ray-casting techniques.

Due to data-flow principles and object-oriented architecture, it is easy to further extend the functionality of API, for example, introduce various types of heterogeneous objects. The main geometric representation in this work is Signed Distance Fields (SDF), but the concept assumes a potential for a combination of different geometry modelling techniques (hybrid modelling).

All this makes allows using the output of this research work for the design of high-quality visualisations for scientific analysis or educational purposes.

1.5 Structure

Chapter 2 gives an overview of the heterogeneous object analysis problem and aspects of volume rendering technique application. We discuss the cases of heterogeneous objects auditory analysis, such as sonification of molecular structures. The sonification techniques

are considered in the context of a potential extension of conventional volume rendering or interactive exploration of heterogeneous structure.

Chapter 3 presents the necessary background for the problem of heterogeneous objects analysis area, including volume rendering, geometry and materials modelling on spatial subdivision, physically-based sound synthesis and multi-modal interactive exploration.

Chapter 4 introduces a general theoretical approach to the visual-auditory analysis of heterogeneous objects and specifies the details of the visual-auditory pipeline. Multidimensional modelling of a dynamic multi-scale heterogeneous object with optical and auditory material properties and rendering to visual and auditory stimuli is described.

Chapter 5 provides the details of how the visual-auditory analysis pipeline can be implemented on the modern GPU hardware and outlines the details of the API used for developing the examples and applications.

Some case studies of visual-auditory analysis of molecular structures and microstructures are presented in Chapter 6. This section details the examples which are used to show the applicability of the proposed visual-auditory pipeline.

In Chapter 7 we provide the results of preliminary evaluation by the potential users of visual-auditory pipelines. We discuss the vision of the proposed visual-auditory approach application from its potential users' point of view and identify key factors that define such vision. The section overviews the users' recommendations on the proposed visual-auditory techniques further extension and application outside this research.

Finally, in the section 8 we conclude the work and present the future research directions.

Chapter 2

Related Works

The McCormick (1988) defines visualisation as the process of transforming data into a visual form for data analysis. The reasoning on the visual representation of data involves the hypothesis formulation a set of suppositions about the properties of data (Keim et al. 2008). The introduced hypothesis is confirmed or rejected as the analytical reasoning facilitated by visual representations is applied. The process leads to a better understanding of a phenomenon that data represents. An introduction of a new hypothesis is assumed to be a result of real-time rendering and interactive exploration.

The visual analysis of dynamic multi-scale phenomena is challenging due to a large amount of data and a wide range of representations introduced and analysed simultaneously (Kozlikova et al. 2017). Moreover, the study of heterogeneous objects brings together the necessity of simultaneous analysis of both experimental and numerical simulation data (Luck 1991), (Wang et al. 2016), (Hines et al. 2009). Conveying information about the properties of such large-scale dynamic structures is not straightforward, as it demands interactive exploration and simultaneous analysis of various phenomena representations of multi-scale nature (Wahle & Wriggers 2015),(Wang et al. 2011) or obtained as a result of complex engineering workflows (Hines et al. 2009). Users are not always able to make meaningful conclusions due to object complexity, information miss and visual perception errors. The issues can lead to the wrong hypothesis and understanding of data. The problem is an area of constant research in scientific visualisation (Johnson 2004). The research in area uses various approaches to address the problem (Etiene et al. 2015).

A general definition of visualisation introduced in Foley & Ribarsky (1994) as "a binding (or mapping) of data to a representation that can be perceived" has given the ground to the expansion of visual analysis to become the multisensory analysis (Grinstein & Smith 1990, Gaither et al. 2004). The combination of several sensory stimuli for data representation defines the perceptualisation (Grinstein & Smith 1990, Gaither et al. 2004). The main goal

of the technique is making abstraction perceivable. Extending visual stimuli with auditory (Grinstein & Smith 1990) or visual and tactile/haptic stimuli (Maciejewski et al. 2005) are typical approaches for scientific phenomena analysis. The sophisticated cases consider the simultaneous application of the above all sensory stimuli (Ogi & Hirose 1996). The auditory stimuli have been widely investigated since early 80-s (Yeung 1980, Bly 1982). Sonification is an area of active research (Kaper et al. 1999, Hermann et al. 2011) that uses various sound characteristics to represent and analyse the input data.

The paper concentrates on aspects of visual-auditory analysis of heterogeneous objects, including basic multisensory interactive exploration techniques that are also relevant for the case of auditory interfaces design. We believe that the introduction of auditory stimuli can be particularly beneficial in case of heterogeneous objects analysis. Auditory stimuli can address both issues of handling the visual perception, as well as the complexity of multi-scale and dynamic feature and facilitate navigation and exploration of spatial properties distribution. The work discusses the challenges that the analysis of the heterogeneous object imposes to conventional visualisation frameworks, the algorithms and main research trends in the area.

The potential benefits of auditory interfaces design for complex heterogeneous structures are the focus of this work. The auditory interfaces that are most relevant to the problems of heterogeneous objects analysis are those that deal with objects dynamic nature, the spatial distribution of multi-scale representation. This includes such areas as interactive exploration, spatial navigation, limitation of visual perception, dynamic nature of spatial distributions in data structures.

2.1 Challenges and requirements of visual analysis of heterogeneous multi-scale phenomena

2.1.1 Visual pipeline optimisation and execution

The modern visualisation frameworks allow designing a pipeline from the input data to the rendered image, as a set of modules of specified functional groups that deal with data filtering, mapping, rendering (Moreland 2013). Often those blocks are implemented with the data flow principles (Dyer 1990) and are flexible tools for the design of custom visualisation solutions (Ayachit 2015), (Kikinis et al. 2014).

However, the modern research that deals with large-scale scientific data sets additional requirements to procedural blocks and the entire visualisation pipeline (Weiler et al. 2003). Additional requirements are also imposed by scientific visualisation in the context of VR (Wald et al. 2006) or interactive exploration that involves intensive geometry modelling

2.1 Challenges and requirements of visual analysis of heterogeneous multi-scale phenomena

(Maloca et al. 2018). The new frameworks (Meredith et al. 2012),(Moreland et al. 2011) were designed to reflect new programming models and algorithmic approaches that are suitable for more up to date architectures and can provide flexible support for both CPU and GPU parallelism (Moreland et al. 2016).

Similarly to other research-intensive areas such as high-performance computing (HPC), machine learning and big data exploration, the area of modern visualisation employs CPU (Wald et al. 2017) and GPU distributed systems (Dykes et al. 2016), for visual discoveries in large-scale data. The design of research workflow assumes high flexibility in scaling for diverse architectures, heterogeneous support for both CPU and GPU, possible application within web environments (Franke & Haehn 2020), (Usher & Pascucci 2020).

GPU hardware and algorithms have changed significantly since most of the conventional frameworks have been designed (Schroeder et al. 2006). General solutions in area concentrate not only on the scalability of the process but pay attention to the optimisation of complex scientific workflows as well (Team 2018a). The latter is of particular importance for real-time interactive visualisation.

The real-time exploration of large scale heterogeneous object with different representations of dynamic and multi-scale nature sets additional challenges and requirements that are generally related to geometry modelling. The multi-scale properties of heterogeneous objects demand additional requirements for the efficiency as the pipeline evaluation time grows with the number of basic procedures (Moreland 2013).

The analysis of multi-scale heterogeneous phenomena considers such areas as results of FEM simulations, molecular structures that are results of molecular dynamics simulation. The Grottel et al. (2015) exploit the representation of molecular structures to improve rendering performance (Muzic et al. 2015) and discusses optimisation issues of conventional visualisation pipelines. Chavent et al. (2011) introduces quadric surfaces for real-time modelling and rendering of the dynamic molecular structures on GPU. Similarly, Parulek & Viola (2012) constructs exact solvent-accessible surfaces on GPU combining geometric modelling and ray-casting. The efficiency of considered solutions is obtained as a result of optimisation of GPU-CPU data exchange for large scale data and combination of geometry modelling with rendering techniques. We will discuss the importance of the latter in the next section.

2.1.2 Dynamic and multi-scale geometry representation

GPU hardware and algorithms have changed significantly since most of the conventional frameworks have been designed (Schroeder et al. 2006). Despite considering certain algorithmic advances, the new HPC tools still often rely on mesh-based geometry models and

rasterisation rendering technique that has certain limitations. The limitations of conventional mesh-based modelling tools are obvious when dynamic changes or precision support for objects with non-trivial geometry is required (Crassin et al. 2011) that is a crucial feature of multi-scale heterogeneous objects. In geometry modelling area the subdivision schemes have been developed for polygonal surface to generate convolution surfaces at different LOD (Sherstyuk 1999). The works (Cani & Hornus 2001),(Angelidis & Cani 2002) propose a LOD paradigm for implicit fields using subdivision curve primitives in combination with convolution surfaces with local LOD modelling parameters defined by both implicit field and on surface sampling. The various sampling techniques are conventional tool to address problems of discrete representations (Sik & Krivanek 2013) as they allow for quality control quality on rendering stage or as a part of geometry processing techniques(Sik & Krivanek 2013),(Corsini et al. 2012). The area is a subject to constant research with most advanced algorithms are enhancement of pure Monte-Carlo technique and classified as importance sampling (Ostromoukhov et al. 2004) and adaptive sampling techniques such as Vegas (Lepage 1980) and Miser (Schürer 2004). The main concern of sampling in rendering is quality on numerical approximation of integration of problem of light transport (Kulla & Fajardo 2012),(Raab et al. 2008) that is done as part of ray-tracing of volume ray-casting for numerical solving.

Compared to rendering area where related to geometry sampling problems arise and usually addressed on rendering stage (Morrical et al. 2019), the visualisation often has to deal with very complex geometry mappings that can be directly ray-traced without intermediate representations (Müller et al. 2003),(Tejima et al. 2015). In this context, the main challenge in the analysis of heterogeneous objects, such as molecular structures or medical data, is the simultaneous use of several geometric representations, that can describe both experimental and computer simulation results (Grottel et al. 2015),(Weiler et al. 2003) or procedural modelling techniques (Kurzeja & Rossignac 2019).

The choice of specific geometric representation in conventional rendering pipeline is defined by the availability of rendering algorithms to handle it efficiently. As a result, discrete representations such as polygonal meshes and voxels are considered as convenient for the modern rendering pipeline. For geometry representation of multi-scale and heterogeneous phenomena it is not enough to find ray/geometry intersection for efficient rendering (Silva et al. 2005), (Museth 2013). The additional key requirement is resolution-independency with unlimited complexity and ability to handle various dynamic geometry changes (Crassin 2011), (Museth 2013), (Grottel et al. 2015), (Muzic et al. 2015). As a dynamic nature of multi-scale phenomena is considered, both macro and micro-level dynamic changes should be displayed simultaneously on-demand Ojha et al. (2018). Also, control over dynamic changes

2.1 Challenges and requirements of visual analysis of heterogeneous multi-scale phenomena 13

of both geometry shape and topology is assumed (Museth 2013). Moreover, the essential interactive exploration procedures, the need to operate Level-of-detail (LOD) techniques (Callahan et al. 2006), (Usher et al. 2017) and multi-scale nature of the phenomena benefits from combination of rendering and geometry modelling procedures (Museth 2013), (Grottel et al. 2015).

The modern flexible rendering technique based on the ray-casting simplifies the conventional geometric problems in visual pipeline design (Knoll et al. 2014), (Parulek & Viola 2012), takes advantage of GPU programming (Chaudhary et al. 2018), acceleration structures (Beyer et al. 2015) and on-demand loading of various data representations (Ruijters & Vilanova 2006), (Beyer et al. 2015). The approach allows introducing more flexible compared to polygonal meshes geometry modelling techniques directly on GPU.

For complex tasks, the ray-tracing is used in combination with the implicit/voxel-based geometry models and hierarchical structures that allow efficient storage and manipulation in GPU memory. As alternative to meshes, the implicit (Knoll 2009), (Parulek & Viola 2012) or voxel-based solutions (Putanowicz 2015), (Museth 2013) are often suggested. Both representations are very convenient for geometric modelling with constructive techniques (Chen & Tucker 2000), (Pasko et al. 2011a) and provide high support of quality control in terms of sampling issues (Crassin 2011).

A particular type of implicit representation, the signed distance field (SDF) is used very often due to the availability of efficient ray-casting algorithm (Hart 1996). Conversion of the mesh-based representation to the voxels or SDF is a well-studied and solved problem (Crassin 2011), (Sanchez et al. 2012). The most well known are the adaptive distance field technique (ADF) (Bastos & Celes 2008, Frisken et al. 2000a). The properties of SDF make it very convenient for GPU geometric modelling (Reiner et al. 2011) that often facilitates GPU accelerated image and point clouds processing tasks in the context of real-time rendering (Jones et al. 2006).

The use of hierarchical structures over space partitioning is a further step that is often related to another strategy to optimise the rendering procedure for volume objects - the detection and skipping of empty spaces in heterogeneous structure (Yagel & Shi 1993, Jones et al. 2006). In modern research the use of voxel and implicit representations is related to use of GPU acceleration structures (Parulek & Viola 2012), (Crassin & Green 2012) and hierarchical representations of volume structures Sparse Volume Octree (SVO) (Museth 2013), (Hoetzlein 2016) and "compression" techniques (Villanueva et al. 2017), often in context of ray-tracing technique (Hoetzlein 2016), (Parulek & Viola 2012). An additional requirement for heterogeneous objects is GPU support for dynamic (Museth 2013) and multi-scale features. For the latter, the implicit representation for geometry modelling as

a part of mapping seems to be more flexible for visualisation tasks (Chavent et al. 2011), (Grottel et al. 2015).

We summarise the advantages and limitations of the GPU geometry representations discussed above with respect to the requirements for GPU-based rendering of multi-scale heterogeneous objects:

Geometry representation	Dynamic and multi-scale modelling	Resolution limitations and LOD	Compactness	Fast ray-tracing algorithm
Voxel data (SVO)	Dynamic volumes are supported. However, it lacks of flexibility of procedural approaches and multi-scale modelling is problematic.	Was introduced as mesh alternative to support LOD features	Very compact	Fast for ray-casting
SDF	Highly flexible	Allow fully procedural, precise modelling	Similarly to parametric models can grows very fast as models with lots of details demanding a lot of functional superpositions are considered	Sphere tracing algorithm
Mesh	Very problematic. In dynamics conventionally were used when control over topology is required (FEM)	Well known and most often addressed with conversion to SVO alternatives	Compact	Convenient algorithms that consider rasterisation and accelerated with BVH ray-casting techniques

2.1.3 Complexity and quality in visual analysis of volume objects

The conventional task of scientific visualisation is to get insight into phenomena through its graphical representation. As sole visual stimuli are considered, the increased complexity of the multi-scale phenomena and data scale are addressed with complex queries to extract only the necessary region of interest (ROI) for further analysis (Vitello et al. 2018) and mapping procedures (Miao, Klein, Kouřil, Mindek, Schatz, Gröller, Kozlíková, Isenberg & Viola 2019). We discuss the user interaction for ROI extraction in volume data in next section. The mapping part in volume rendering technique is controlled with transfer functions (TF) (Kniss et al. 2002), (Chaudhary et al. 2018). Compared to frameworks for surface visualisation (Grottel et al. 2015), (Muzic et al. 2015), there is a lack of functional features and research (Knoll et al. 2014), (Weiler et al. 2003) in heterogeneous objects visualisation that is mainly a volume visualisation that highlight internal structure within spatial heterogeneous subdivision (unstructured volume data).

The conventional volume visualisation is limited to the rendering of structured textures in GPU memory Chaudhary et al. (2018). However, the lack of consideration of spatial subdivision modelling nature in such objects leads to quality issues (Silva et al. 2005), (Weiler et al. 2003). Similarly to high-quality rendering of discrete geometry representation, the problem is much related to sampling issues in volume integral evaluation as heterogeneous structures (Morricall et al. 2019), (Kulla & Fajardo 2012). As the requirements for quality are high the integration includes evaluation of two nested integrals that both highly depend on sampling strategy (Kulla & Fajardo 2012), (Raab et al. 2008): transmittance and incoming light (see brief details on volume integral in section 3.4.4). Thus not only consideration of subdivision used for volume heterogeneous structures modelling is of great importance (Morricall et al. 2019), but an aspects of such subdivision modelling are worth considering as complex geometry is modelled within subdivision (Tejima et al. 2015). The modern ray-tracing APIs per-ray memory structures have a potential to control sampling issues and reduce complexity by decoupling various sampling techniques within lighting procedures (Kulla & Fajardo 2012). Similarly, in this work we also discuss the geometry and material modelling within visualisation pipeline that is accessed as part of per-ray data structures evaluated during ray-tracing of heterogeneous structure to provide a visualisation quality control.

As the conventional volume visualisation is considered, the mapping quality aspects controlled with transfer function (TF). The research uses various types of Multidimensional Transfer Functions (compared to conventional 1D TF) to interactively highlight the features of interest in volumes (Kniss et al. 2002). Multidimensional transfer functions that are used to address issues both issues of several scalar fields (Haidacher et al. 2008) simultaneous

analysis and visual analysis quality enhancement in general (Falk et al. 2017, Kniss et al. 2002), (Park & Bajaj 2004, Fang et al. 1998). The multidimensional transfer functions design targets the automatic requested features detection and extraction and hide unnecessary details as acknowledged in Kniss et al. (2002), Ament (2014), Ljung (2006). The technique also targets leveraging the conventional problems of experimentally obtained volume data analysis. The simultaneous analysis of several scan images that contrast features of interest (Martí-Bonmati et al. 2010), (Cebulla et al. 2014). Also, TFs are used in combination with image processing techniques (Park & Bajaj 2004, Fang et al. 1998, Ljung 2006). As it was remarked in Ljung (2006), there is no clear distinction between classification, segmentation (Vasuki et al. 2017) and Multidimensional Transfer Function mapping procedures. Segmentation procedures, in general, can be quite a time consuming and complex, while transfer functions operate data ranges in real-time. However, transfer functions are believed to be less efficient to identify the relevant ROI (Ljung et al. 2016). Moreover, the modern graphics hardware and programming techniques make such combinations very convenient (Allusse et al. 2008).

The more complex optical model consideration is the other approach to address volume rendering quality issue (Ament 2014) that is, however, balanced by computational expensiveness (Jönsson et al. n.d.). The shading and depth perception can provide an addition to 3D shape cues and thus enhance visual analysis and highlight the features of interest Kniss et al. (2003). The Blinn-Phong model Levoy (1988) was an initial enhancement of the classical emission-absorption model (Max & Chen 2010) to highlight features of interest such as edges Jönsson et al. (n.d.). The approach based on a straightforward adaptation of "surface shading" technique had limitations and demanded adjustments Kniss et al. (2003). An optical model with single scattering (Jönsson et al. n.d.) or ambient occlusion (AO) allows to significantly enhance visual analysis quality Wahle & Wriggers (2015). Ambient occlusion is combined with diffuse and specular properties of Blinn-Phong model Schlegel et al. (2011) to highlight the thin, tube-like structures and cavity areas on the surfaces of volumes (Ament 2014) and thus can significantly enhance molecular fields analysis (Wahle & Wriggers 2015). Computation of complex optical models for interactive Volume Rendering takes advantage of modern graphics hardware (Schlegel et al. 2011). The modern algorithms often employ the idea of splitting the optical model computation into separate parts, mainly concerned with the lighting conditions that can be precomputed into textures independently and updated on-demand (Kniss et al. 2003), (Schlegel et al. 2011).

2.1.4 Interactive exploration of scientific data

In modern research, the interactive exploration of scientific data is considered in the context of the introduction of the new modalities (Turk 2014). This includes the introduction of

2.1 Challenges and requirements of visual analysis of heterogeneous multi-scale phenomena 17

additional interactive devices (Silva et al. 2019) or sensory outputs (Tak & Toet 2013). The process targets the facilitation of cognitive load and makes interaction more efficient and intuitive (Lee et al. 2018). The process often uses complex procedures (Turk 2014), such as computer vision-based pre-processing of input devices (Silva et al. 2004), ML assistance and pre-processing (Chen et al. 2020), gesture recognition (Hoell et al. 2018). The techniques not only facilitate the interactive manipulation with complex data (Cassat et al. 2018), but expand conventional graphic user interface procedures (Turk 2014) with new concepts (Yan et al. 2004), (Keefe & Isenberg 2013) such as AR/XR interface paradigms that combines perception of physical and virtual space (Kalkofen et al. 2011), (Silva et al. 2004)

As the new sensory stimuli are introduced into analysis pipeline, a new UI should provide tools for interpretation and manipulation all layers of perception and support unimodal and multimodal interaction techniques (Lee et al. 2018). Moreover, the users have to consider the aspects of integration of such interaction into conventional visualisation pipeline procedures (filtering, mapping, rendering) (Kalkofen et al. 2011), (Sua et al. 2015), (Roberts et al. 2014).

We can roughly distinguish the interactive procedures for heterogeneous objects into two groups. Due to the nature of heterogeneous phenomena, the user tools should allow manipulating both volume properties and access spatial subdivision properties. The latter may involve various procedures, including tracking of dynamic features of multi-scale representations (Arbon et al. 2018), interactive measurements over spatially distributed components (Bagaturyants et al. 2010) or self-positioning tasks (Donalek et al. 2014), (Goddard et al. 2018). In many cases, the interaction with such spatial distributions of heterogeneous data involves computationally expensive computations to generate multi-sensory feedback. The problem is addressed with GPU-accelerated ray-object intersection evaluation (Xu & Barbic 2017) and benefits of acceleration structures and geometry representations conventional for large-scale data ray-tracing (Xu & Barbič 2014, Van & Bergen 2004).

The conventional interactive user interface design for volume data exploration deals with region of interest selection (ROI) or adjustment of the discussed in previous section TF via editors and widgets (Zhou et al. 2012), (Kniss et al. 2002), (Computing & SCI) to control visual mapping. For latest the techniques often uses histograms based preprocessing (Lundström et al. 2006) and clustering (Patric et al. 2016) that can be a part of stroke based/volume painting techniques (Ropinski et al. 2008), ROI selection (Luo & Dingliana 2017), parallel coordinates to access TF ranges for multivariate volumes (Zhao & Kaufman 2010), (Hege et al. 2009). The painting techniques can be performed on 2D slices of volume with further application of image processing or ml techniques (Soundararajan & Schultz 2015) that makes interfaces much similar to conventional medical image semiautomatic segmentation interfaces (*MITK Release notes 2016* 2016). Also, similar to medical image

processing, 3D brushing techniques are used for further conventional region growing (Zhou & Hansen 2013). The other approach is an application of conventional 3D widgets that operate volume data in 3D space (Kniss et al. 2002).

2.2 Challenges of auditory analysis of heterogeneous phenomena

The multisensory technique efficiency is based on the well-known fact that several sensory stimuli operate differently and thus can complement each other (Hermann et al. 2011), (El Saddik et al. 2011). Compared to single sensory stimuli based analysis, this allows straightforward detection of "perception errors" and offers an opportunity for several stimuli cross-evaluation to obtain a correct image of the phenomena as a result of perceptualization (Hermann et al. 2011).

The sonification is defined as "the transformation of data relations into perceived relationships in acoustic signal for purposes of facilitating communication or interpretation" (Kramer 1994). The technique can facilitate the analysis of heterogeneous objects that imposes a challenge of consideration of both spatial distribution (Grottel et al. 2015) and volume nature (Knoll et al. 2014). Among heterogeneous objects, auditory techniques are most often applied for various aspects of molecular phenomena exploration, such as simultaneous analysis of several representations Grond et al. (2010), (Ballweg et al. 2016) or additional properties (Arbon et al. 2018), tracking dynamic features (Florian Grond & Dall'Antonia 2008) or VR/AR application of auditory and haptic/tactile stimuli (Miao, Klein, Kouřil, Mindek, Schatz, Gröller, Kozlíková, Isenberg & Viola 2019) and facilitation of navigation and interaction (Kozlíková et al. 2017). In the area of volume rendering the auditory stimuli are mostly applied for fixing a visual perception issues (Gionfrida et al. 2016). To facilitate the interaction with complex 3D structures many research works take advantage of both auditory and tactile stimuli. (Roodaki et al. 2017) fixes haptic perception issues with auditory analysis. At the same time, in some works use of haptics is closely related to audio data analysis, when audio or music data maps to sound and haptics (Giordano 2016) on the shared wave representation basis.

Sonification research provides a wide variety of auditory mappings (Hermann et al. 2011). There is no hardware limitations that are so common for haptics (May et al. 2019). However, the interpretation of sound wave properties along with the control of the obtained as a result of such mappings auditory representation can be not straightforward (Hermann 2018). Thus, compared to conventional visualisation, the auditory "knowledge discovery" can be trickier

(Hermann et al. 2011). The sonification research still lacks the structure (*Sonification Report: Status of the Field and Research Agenda* 2010). The convenient sonification techniques are an area of constant research (Hermann 2018). Below we consider the auditory interface design areas that are related to various aspects of heterogeneous objects interactive exploratory study.

2.2.1 Exploration of physical properties of spatial structures

The vision perception temporal and spatial resolution limitations (El Saddik et al. 2011) is one of the main motivations of auditory techniques application in the visual analysis of spatial structures (Hermann et al. 2011). The research in auditory analysis often deals with tracking or detection of small changes in data, an area where visual stimuli often demonstrate a resolution limitation. Auditory stimuli effectively complement visual in classification (Bly 1982) detection (Merimaa 2006) or tracking dynamic features (Florian Grond & Dall'Antonia 2008), (Arbon et al. 2018) in spatial structures. Also, the research explores other difficult for solely visual perception cases where auditory stimuli complement or degrade visual performance (Malpica et al. 2020), (Hidaka & Ide 2015), (Lewis et al. 2000) In task of spatial localisation the visual and auditory stimuli are well known to highly influence each other (Boyce et al. 2020), however the "perceptually efficient" visual-auditory integration that is a one that can automatically highlight the features of interest with auditory stimuli, is a complex, not fully understood task where visual limitation often shape the entire procedure (Pérez-Bellido et al. 2015).

The auditory stimuli can address the complexity of multi-scale features that use several representations. The Grond et al. (2010) study multi-scale properties with auditory stimuli for the heterogeneous phenomena that is a molecular structure. The auditory interfaces are widely used to facilitate comprehension of complex molecular relationships Liu & van der Heide (2019) and complement visual analysis (*An overview of auditory display to assist comprehension of molecular information* 2006).

Auditory data exploration is one of the most promising auditory interface design areas. The mapping to sound strategy conventionally considers the several dimensions of sound perception. Among them are the properties that enable categorical perception of sound (e.g. timbre property) or perceived along a "perceptual continuum" (frequency, intensity) (Hermann et al. 2011). The research in area concentrates on an effective combination of those to highlight dynamic features (Arbon et al. 2018) or perform conventional classification (Bly 1982) tasks and considers auditory models that facilitate auditory space of interpretations (Hermann 2018). As well, to simplify the process for the user the auditory interface design concentrates on facilitating data manipulation providing various interaction modes (Ballweg

et al. 2016). The design of the interactive interfaces with auditory feedback is employed to address such problems as protein docking (Férey et al. 2009), auditory perception of the nearby internal structure (Ballweg et al. 2016), highlighting multi-scale molecular features like RNA sequences (Grond et al. 2010).

Compared to more general multi-modal interaction research and haptic research in particular, sonification often concentrates on auditory mappings aspects and does not pay much attention to potential computational inefficiency issues and quality loss as a result of complex user interaction (Xu & Barbic 2017). Moreover, the aspects of universal integration of auditory feedback into the general multi-modal framework is an open research area (Florian Grond & Dall'Antonia 2008), Férey et al. (2009). An exception is the area of analysis of physical properties of dynamic phenomena directly via sound that such phenomena generates (Dobashi et al. 2003). Such areas often address 3D sound generation as a rendering problem (Shi et al. 1993), (Dobashi et al. 2003) that can be addressed with computer graphics techniques. The modern solutions in area of virtual reality often provide a unified approach to visual-auditory stimuli generation, by taking advantages of similarities in light and sound propagation, that form 3D sound properties similarly to visual representation and allows to benefit of GPU acceleration (*VRWorks - Audio* 2018). Also, researchers in area often considers modern GPU ray-tracing APIs, such as OptiX, DirectX Ray-tracing (DXR) and Vulkan as a base to design custom sound rendering solutions (Ulmstedt & Stålberg 2019).

2.2.2 Auditory mappings for volume structures

The additional sensory stimuli are used to control the analysis quality by comparison of phenomena images obtained with different sensory stimuli (Hermann et al. 2011). A relatively new application area for auditory stimuli is enhancement of the visual analysis of volume objects. (Minghim & Forrest 1995) discusses some general auditory application directions. Auditory analysis of continuous scalar fields uses the well-studied advantages of auditory perception, that we have mentioned above, such as effective tracking of small changes, alarming and classification tasks. The techniques assume the analysis of spatial features extracted from the scalar field (Lodha et al. 1997) or compare volumes with auditory stimuli (Gionfrida & Roginska 2017). The sonification of 3D volume data is complex in terms of auditory perception and interpretation. Often the 2D crosssections of volumes are considered as a basis for visual-auditory analysis Gionfrida & Roginska (2017).

The auditory interface very often designed for a typical type of problem and data (Gionfrida & Roginska 2017). So far there was no direct attempt to use auditory analysis for general volume data analysis case, in the context of conventional volume rendering framework (Kniss et al. 2002). Moreover, such a view on the problem demands consideration of aspects of

cross stimuli interpretation. The aspects of simultaneous visual-auditory analysis (Abboud et al. 2014), (MacDonald & Stockman 2014), (Brown et al. 2011) that is often performed in context of user interaction (Frauenberger & Stockman 2009) or stress aspects of music theory and composition for such interfaces design (MacDonald & Stockman 2014),(Abboud et al. 2014). The research in area stresses that sonification principles often use natural cross-modal correspondence for coding visual cues into auditory ones (Spence 2011), (Lepore et al. 2011). The research in area stresses that such conversions can be natural (Evans & Treisman 2010) and particularly welcome when use of visual sensory inputs are problematic (Ward & Meijer 2010). Among others, colour and pitch visual-auditory mappings complement each other or replace.

Musical approaches also have been successfully applied to assist user interaction (Yang et al. 2019). Compared to "strokes and brushing" that are conventional volume interactive techniques, the auditory analysis uses the parameter mapping "Sonic Brushing"(Hunt & Hermann 2011). The approach assumes the selections in a single visual display cause selected data to be presented in real-time by sonification based on musical mappings (Ó Maidín & Fernström 2001).

2.2.3 Spatial orientation and navigation

Auditory feedback often assists the navigation and spatial orientation (Ziemer & Schultheis 2019) that includes various tasks such as a raw estimation of position and orientation based on HRTF (Urbanietz et al. 2019) or precise navigation for object localisation (May et al. 2019).

The auditory stimuli often prove to be more flexible, than visual ones in tasks of object detection and localisation (Auvray et al. 2007) and navigation tasks (Maidenbaum et al. 2013). Similarly to haptic/tactile stimuli (j. van Erp & Self 2008), the sonification often addresses the problems of spatial disorientation. As well, there is an increase of interest to objects sonification and continuous data in particular in augmented reality (Ribeiro et al. 2012) and virtual reality (Begault 1994) that demand consideration of immersive aspects of 3D sound propagation perception and lack of spatial orientation. The sound propagation and the human perception of this process are considered in the modelling of auditory feedback (McArthur et al. 2017). Moreover, ray-tracing of auditory stimuli is an area of active research that takes advantage of the computer graphics approaches and techniques (Schissler & Manocha 2011). Similarities between light and sound propagation (Max & Chen 2010),(Siltanen et al. 2007) have formed the basis for further studies based on visual-auditory approaches.

2.3 Summary

The multi-sensory visualisation requires the simultaneous rendering of several sensory stimuli. The process can impose computational efficiency requirements, especially if problem is considered in context of the real-time user interaction. The introduction of additional sensory stimuli for analysis can also be challenging in terms of a design of a unified framework that will establish the automatic perception and interpretations principles for considered mapping techniques. This work discusses the visual-auditory analysis of multi-scale objects that include interactive exploration with auditory feedback. The similarities in modelling of visual and auditory stimuli allow assuming a unified approach to analysis for complex heterogeneous structures. Such approach to problem provides an advantage of exploiting the modern GPU computational possibilities and architectures for non-trivial tasks that arise in a process of heterogeneous objects analysis, such as GPU volume modelling on complex geometry domain and visual-auditory rendering.

Chapter 3

Background

3.1 Overview

The visualisation frameworks allow designing a visualisation algorithm as a set of customised procedural blocks that often depend on a type and structure of input data. The visualisation frameworks specify several input data representations, such as structured and unstructured data, that are processed differently (Kam et al. 2015). A sequence of procedures of such functional groups as Filtering, Mapping, Rendering, outline a graph-like structure that is referred as visualisation pipeline (Moreland 2013) (see Fig. 3.1(b)).

The user constructs a pipeline from initial data to the rendered image from available functional modules according to specified input data representation and analysis problem. In this work, we emphasise the role of the Mapping group that assume a wide range of geometry and material modelling to be provided by visualisation framework. However, conventionally the visualisation solutions provide such procedures only for surface objects. Volume visualisation inherits its structure from rendering procedure that historically operates only with structural input data stored as 3D texture in GPU memory (Kaufman & Mueller 2005). The technique assumes that only a transfer function is used for mapping structured data to optical properties such as colour and opacity.

However, in many cases, the heterogeneous objects are represented with unstructured data with internal properties modelled within a spatial subdivision. The visual analysis of a geometry representing phenomena boundary and the internal structure changes is required to get an insight into dynamic multi-scale heterogeneous phenomena. A general class of heterogeneous objects impose challenges that can not be addressed with conventional volume rendering framework that compared to the general representation of pipeline (see Fig. 3.1(b)) is highly inflexible. The adaptation of such objects for conventional pipeline by re-sampling

to regular grids inevitably raises further quality issues due to discrete nature of the sampling procedure (Silva et al. 2005).

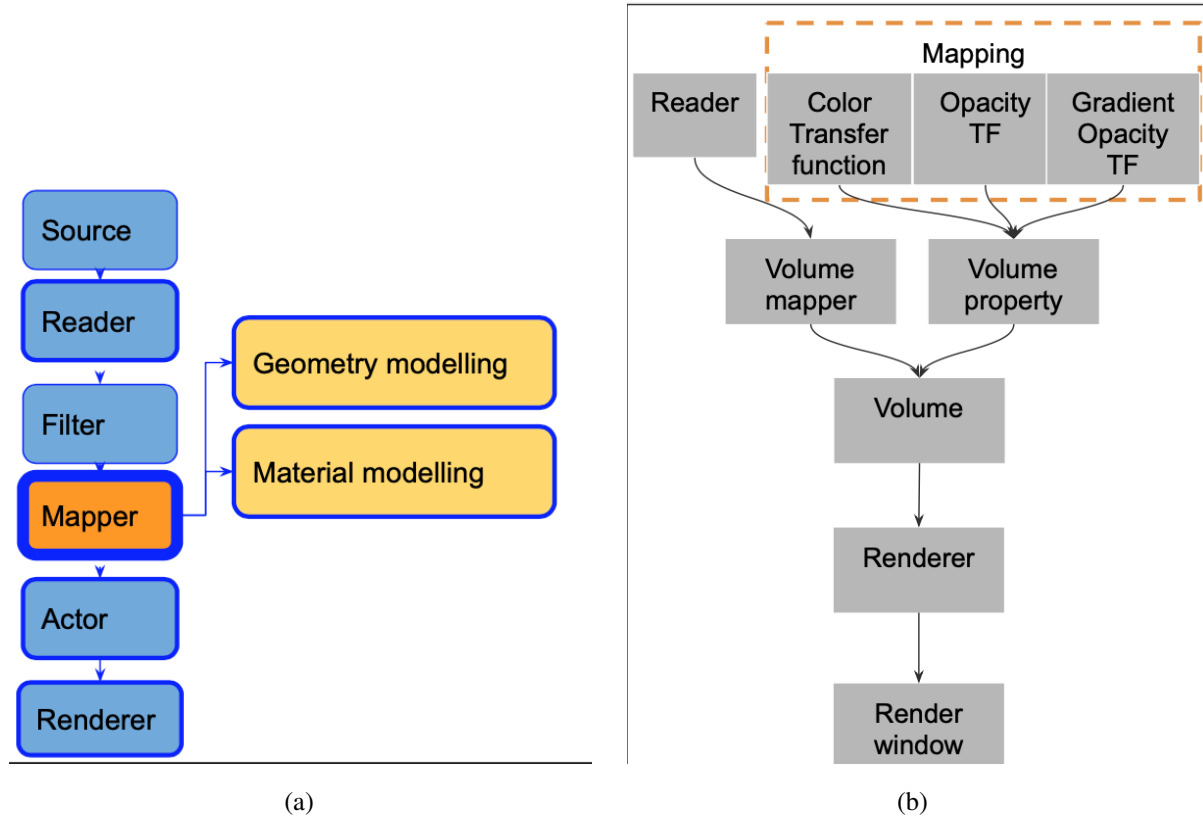


Figure 3.1: (a) General representation of visualisation pipeline. Initially introduced in (Haber & McNabb 1990) (b) View on structure of volume visualisation in (Chaudhary et al. 2019) that relies on regular structured grids (Kaufman & Mueller 2005)

Moreover, the visualisation of dynamic and multi-scale features of such objects uses geometry and material modelling within a spatial subdivision. The research in the area of representation of the volume objects with their internal spatial variations of single or multiple materials explores the methods that provide the efficiency with increased complexity and precision. Wide range of geometric representations can be used for multi-scale phenomena representation as defined by the nature of the problem and scale of the input data. Moreover, as various issues may arise not only on Mapping but on Rendering and Analysis stages as well due to specific requirements to volume rendering of such objects (Rathke et al. 2015, Adamson & Alexa 2006).

Thus, the analysis of the heterogeneous object is a challenging task in terms of quality and efficiency. In this research, we review and refine the conventional approach before extending it to the visual-auditory analysis case. We believe the modern graphics hardware

allows introducing an arbitrary geometry and material mappings to volume visualisation framework (see Fig. 3.1(b)) similarly to the flexibility that visualisation of surface objects provides. The modern multisensory rendering also often takes advantage of conventional computer graphics techniques. Thus, there are similarities in modelling and rendering to visual/auditory/tactile stimuli and as a result, a correlation in the origins of quality and efficiency issues in conventional and multisensory rendering areas.

Below we discuss the main features of the design of visualisation pipeline for analysis of heterogeneous objects. In particular:

1. We overview the representations of the heterogeneous objects in various research areas. We discuss the visual analysis and issues that arise due to initial data representations.
2. We overview the modelling of heterogeneous volume objects. We concentrate on resolution-independent, continuous modelling of geometry and material and discuss user-friendly constructive approaches.
3. We discuss the approaches to hardware-accelerated volume rendering. We overview the two main rendering techniques those are rasterisation and ray-tracing. We discuss the volume ray-casting framework that is defined by approximation of the natural process of light propagation through volume.
4. We explore the similarities in modelling and rendering of visual and auditory stimuli. We discuss how areas of sound synthesis and acoustic rendering take advantage of conventional computer graphics rendering techniques and employ graphics hardware. We discuss the aspects of the auditory analysis of complex sound representations generated as a result of such techniques.
5. We outline the core features of visual-auditory interactive exploration of heterogeneous objects. We discuss the main aspects of multimodal interaction within the visualisation pipeline. We explore how modern computer graphics techniques can be used to facilitate and accelerate user interaction with multisensory feedback.

3.2 Heterogeneous objects representations

Let us consider the examples of volume heterogeneous objects in various research areas and discuss the advantages and limitations of used geometry representations for modelling dynamic and multi-scale features. Below we discuss such examples of heterogeneous structures as molecular structures, tetrahedral meshes obtained by Finite Element Methods (FEM), microstructures in digital fabrication and medical image data.

3.2.1 Cellular representation

Boundary representation (BRep), and various cellular structures such as 3D computational grids and more cellular structures (Hatcher 2000) are widely used in CAD and numerical simulations. One of the examples of how polygonal meshes are used for heterogeneous modelling and visual analysis is a pipeline for finite element modelling (FEM) presented in Fig. 3.2.

The main advantage of BRep (see step 1 in Fig.3.2) is an exact object boundary definition, that is crucial for certain tasks. However, the common problem is that to get final simulation the user has to deal with 3D meshes (see step 2 in Fig.3.2). The process of mesh generation is defined as a subdivision of a continuous geometric space into a topologically valid collection of discrete geometric cells. The process assumes obtaining cells of convex shape, commonly the tetrahedral ones. The cells partitioning is performed on the geometric input domain usually defined with BRep. The core advantage of cellular models is topological control and validation of the entire structure that is crucial for the usage of data structures in Finite element analysis (FEA).

Results of numerical simulations (step 3 of Fig.3.2) is also represented by cell complexes or 3D meshes (including dynamically deforming in time) with computed properties and require further visual analysis (step 5 of Fig.3.2).

The mesh representation, obtained on step 2 of Fig. 3.2 should satisfy certain criteria, otherwise, it will be a potential source of issues, arising on step 3 (Bathe & Zhang 2017). Thus, usually, the pre-processing stage (meshing stage 2 in Fig. 3.2) also includes the visual analysis of the quality and consistency of the obtained mesh (Liu 2013, Kounghelis & Augarde 2008).

In the general case, the cellular structures are composed of elements connected to each other under some rules. Mathematically such structures are described by topological complexes. Various types of complexes differ in allowed elements shapes and restrictions on their connections Hatcher (2000). With material distribution modelled within each cell the entire structure that represents a multi-material heterogeneous object. A cellular complex is constructed iteratively by attaching cells. Cellular complexes are widely used for tasks, that demand additional control over topology as the entire structure uses predefined connectivity information between individual components. The structure allows to efficiently handle various problems where control over topology is required.

Usually, cellular complexes imply conventional explicit representation of cells. The limited precision of explicit geometry description leads to lack of control over quality and dynamic changes of shape of cell. In section 3.3.2 we discuss a more general model that extends the concept by consideration of both explicit and implicit representations inside

cellular structure (Kartasheva et al. 2008) . This model based on notion of an Implicit Complex (IC)(Kartasheva et al. 2005) which combines the advantages of topological and constructive representations with using the feature-based methodology. It provides a valid topological description of heterogeneous objects and allows for the flexible combination of cellular and functional representations of both the geometry of objects and their attributes.

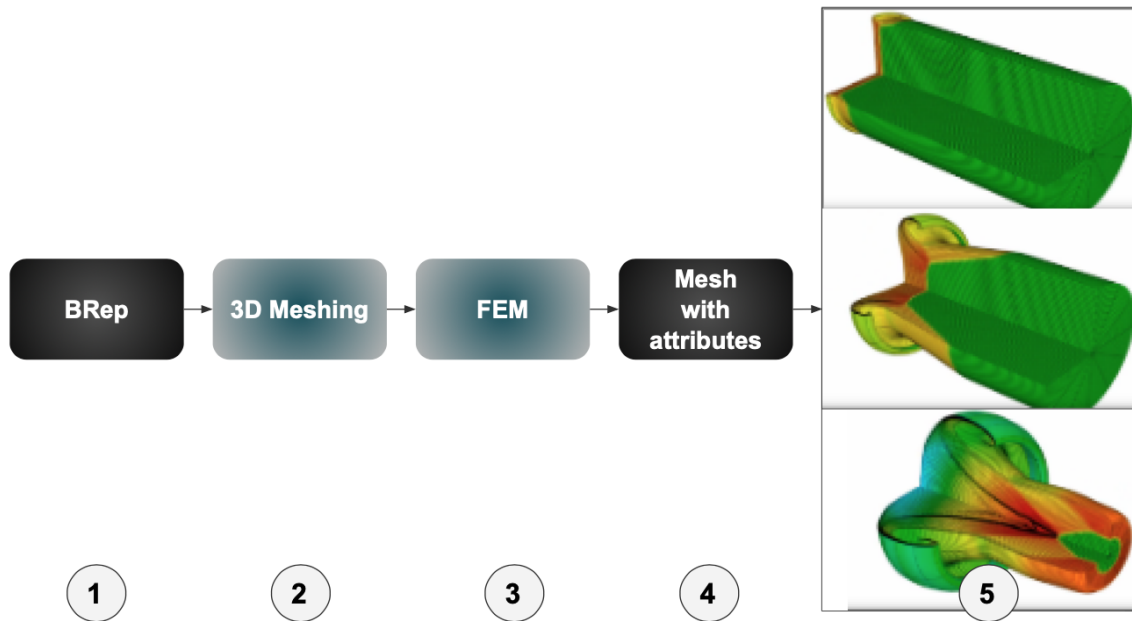


Figure 3.2: Schematic representation of basic FEM simulation pipeline and visualisation of the results. The visualisation example from (*GLVis gallery* 2018): the case of High-order Lagrangian hydrodynamics. Grey blocks represent procedures and black input/output data structures. 1) Input BRep representation that is a result of CAD parametric modelling 2) 3D meshing of BRep into tetrahedral volume 3) FEM-based simulation 4) The result of simulation: 3D mesh with distribution of attributes within cellular subdivision 5) Visualisation of the results of simulation.

Conventional explicit cellular complexes is used in combination with implicit representations in many areas. Application areas include surface reconstruction (Adamson & Alexa 2006) and topological analysis of implicit surfaces. A piecewise smooth surface, represented with point samples can as well be modelled as cell complex with elements of different dimension glued on base of connectivity information (point-sampled cell complex) (Adamson & Alexa 2006). More examples can be found in the review (Kartasheva et al. 2008).

The advantage of the IC based model is that it provides a systematic and topologically valid description of heterogeneous objects as a union of high-level components defined by various models (explicit and implicit, cellular, functional or constructive). Special constraints

on the description of the components and on the mutual dispositions of the components provide a distinctive structure which allows for encapsulation of various numerical calculations inside individual cell representations and getting a result of an operation over a whole IC complex as a combination of results received for separate cells. Detailed descriptions of main operations over ICs, including set-theoretic operations, gridding, ray-intersection, point membership evaluation, implemented in the mentioned above manner can be found in (Kartasheva et al. 2008)

3.2.2 Voxel representation

The voxel-based or Image-based representation is common data representation in the medical imaging area. The initial data is a result of MRI and CT scanning devices that is a discrete scalar field defined on a structured grid (see step 1 of Fig. 3.3). Conventionally the analysis of such volume data requires the internal structures of interest (veins, human organs) to be defined with segmentation procedures (see step 2 of Fig. 3.3). The boundaries can be defined as binary image masks, approximated as polygonal surfaces or by signed distance fields. The visualisation of such structures is often referred to as "labelled volumes" (see step 3 of Fig. 3.3). The data represents the segmented label-field, where each labelled volume represents some internal organ (see step 4 in Fig. 3.3).

In medical image analysis, the main challenge is the simultaneous analysis of several scans obtained by various techniques, also referred as multimodal visualisation (Lawonn et al. 2018). In the general case, the analysis of such structures demands the application of pre-processing procedures such as:

1. Denoising and specific data cleaning techniques. Those techniques aim to remove various types of imperfections and signal corruptions in scanned images brought by scanning technique or used device limitations. A problem is most crucial in MRI scanning and most well-known types are noise (Mohan et al. 2014) and MRI bias correction (Juntu et al. 2005). A survey of a problem and methods of solving those issues is presented in Mohan et al. (2014).
2. Registration of scans obtained in different modalities or with different scanning techniques (rigid and non-rigid). Dynamically obtained scans (time sequences) can also demand the application of this step before being analysed. An example can be a motion correction for the fMRI problem presented in *Basics of fMRI Analysis: Preprocessing, First Level Analysis, and Group Analysis* (2018).

3. Normalisation. The procedure means normalisation of images intensities. As an example, intensity ranges for the same organ can significantly vary for images obtained in different modes or with different scanning devices. The procedure changes image intensity to be consistent between the images, so they can be analysed simultaneously or preprocessed.
4. Segmentation. At this stage, we receive a definition of organ shape that is usually a binary mask, or an approximate polygonal surface defining organ boundary. The techniques can be classified as automatic, which are based mainly on image processing and machine learning procedures, and interactive ones that are based on geometric modelling procedures (Maleike et al. 2009).

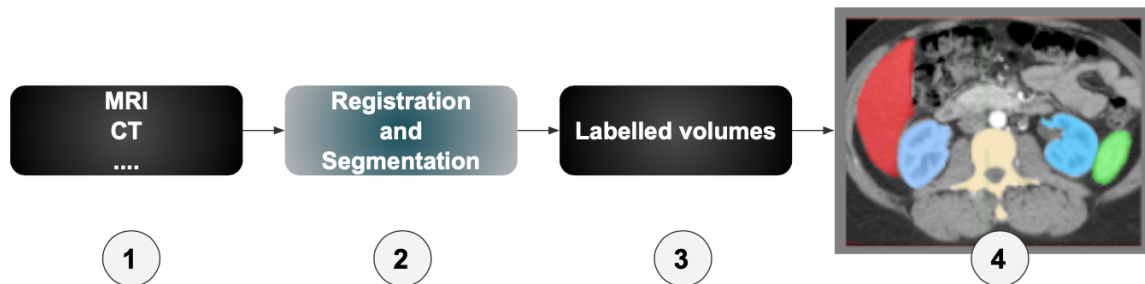


Figure 3.3: Schematic representation of basic medical imaging pre-processing and visual analysis. The visualisation example from (*MITK Release notes 2016* 2016): the segmented tissues on CT scan. Grey blocks represent procedures and black input/output data structures. 1) Input image data that is obtained experimentally with scanning devices 2) Registration and segmentation procedures that combine various image data and extract tissues for analysis 3) The result of image processing that is the labelled volumes that represent substructures of interest (tissues) 4) Visualisation of labelled volume data

Voxel representation is one of the most convenient for further geometry manipulations and highly flexible for sampling quality control issues (Crassin 2011). Geometric modelling on a base of voxels is a well-studied area that makes the most of user-friendly constructive modelling techniques such as Constructive Volume Geometry (CVG) (Chen & Tucker 2000).

3.2.3 Point clouds and particle-based data

The unstructured point clouds are often obtained with depth scanning devices (Berger et al. 2017). Conventionally point clouds represent the surfaces of the objects. The visualisation of such representation demands the application joined surface reconstruction (Carr et al.

2001), (Kazhdan & Hoppe 2013) and registration procedures (Izadi et al. 2011) that return an implicit or voxel representation for further visualisation. Recently the visualisation processes are actively accelerated with subdivision of original scan data into multiple blocks, where for each block the reconstruction or modelling technique is applied with conventional rendering acceleration structures (Liu et al. 2012),(Zhao et al. 2001), (Zhou, Hou, Wang & Guo 2008) in a context of ray-tracing technique application.

The similar structures can be obtained as a result of the molecular or astrophysical simulation (Becciani et al. 2010, Dykes et al. 2018). The structures represent a distribution of particles in a volume that often referred to as particle-based data. The visualisation of such structures with particle splatting is one of the most well-studied areas (Knoll et al. 2019). However, the visualisation of such structures becomes more complicated as it has to deal with the image processing and geometric modelling on a base of unstructured particle data. For example, the common graphical representation of molecular structures is a space-filling model (Berg et al. 2002), where atoms are represented by spheres whose radii are proportional to atomic radii. With GPU-accelerated implicit modelling, the representation is used for the rendering of large scale molecular structures obtained from molecular dynamics (Muzic et al. 2015)(Grottel et al. 2015)

Moreover, as physical processes of interaction between molecular structures are considered, the modelling of "interaction" molecular surfaces based on the point-based data is required (Parulek & Viola 2012). In this context, the arising problems of modelling, acceleration techniques and geometry share a lot in common with the visualisation of large scale point clouds that we have discussed above (Zhou, Gong, Huang & Guo 2008).

The recent techniques in this area can be summarised as follows:

1. Implicit representation and voxel are better suited especially if surface should be reconstructed/ modelled on large scale data (NVIDIA 2018),(Muzic et al. 2015).
2. Spatial partitioning and hierarchical structures are used to facilitate modelling/reconstruction (Parulek & Viola 2012),(Zhou, Gong, Huang & Guo 2008)
3. The acceleration and optimisation of the visualisation is obtained with the modern graphics hardware (Grottel et al. 2015). Moreover, in many cases, the combine GPU-based geometric modelling and ray-tracing based rendering (Grottel et al. 2015).

3.3 Material and geometry modelling

The design of the visualisation pipeline for the analysis of heterogeneous objects obtained as a result of molecular simulation, microstructures modelling or engineering workflows is chal-

lenging. There is a demand for simultaneous control over different geometry representations that appears on various stages of simulation workflow (Hines et al. 2009). The dynamic and multi-scale features impose similar challenges as require the simultaneous storage of several geometrical representations and render them on-demand with Level-of-detail (LOD) visualisation techniques (Zhou 2014),(Fyta 2016). The hybrid models address those challenges by simultaneous storage of both discrete or parametric/continuous representations (Hines et al. 2009) and provide geometric kernels to operate them both. Such hybrid models allow combining advantages of several representations. The core procedures are the evaluation of relationships between models and the ability to perform the conversion from one representation to the other (Hegemann et al. 2013), (Kartasheva et al. 2008). The constructive approach facilitates the modelling of the entire hybrid structure by establishing relationships between various representations that are stored and operated simultaneously. Let us discuss the core advantages of hybrid constructive models application for modelling heterogeneous objects, such as:

1. A model that allows representation of an arbitrary amount of heterogeneous object geometry and material properties and evaluation of defined relationships, which pays particular attention to continuous multi-dimensional modelling (see section 3.3.1)
2. A model that is convenient for modelling the dynamic and multi-scale distribution of arbitrary properties with control over topology and shape (see section 3.3.2)
3. The aspects of constructive hybrid modelling that allow combining various representations (see section 3.3.3)

3.3.1 HyperVolume model

A HyperVolume (HV) (Pasko et al. 2001, Vilbrandt et al. 2009) is a general model that allows combining several independent material representations that may have different description, but are stored and operated within one structure. Initially the approach considered a unified geometry and several materials representation with real-valued functions and considered constructive modelling (Pasko et al. 1995).

The geometry and materials descriptions are exact, compact and easy to interpret. Due to absence of dimension restrictions, the approach is convenient for continuous modelling of dynamic and multi-scale properties. The core feature of the approach is implicit modelling principle applied in context of constructive modelling of geometry and materials. An implicit modelling framework provides a wide set of operations to address issues of continuous multi-dimensional modelling such as blending space time interpolation and morphing operations to

efficiently handle the dynamic transitions in shape. Likewise, it provides a set of operations to handle multidimensional representations and perform transitions from one space to another, such as projection, sweeping, space-time blending, mincowsky sum (Sourin & Pasko 1995), (Pasko & Savchenko 1997), (Pasko et al. 2004a), (Pasko et al. 2003). Moreover, the modern research in area has demonstrated that implicit models are highly convenient in context of modern computer graphics hardware development as model allows direct GPU implementation and close integration with ray-tracing based rendering. Those advantages lead to significant reduce CPU-GPU exchange bandwidth as geometry and material modelling is considered as a part of user interaction or modelling is evaluated as a part of real-time visualisation.

A general HyperVolume model can be expressed as triple (O, Φ, W) , where O is a set of HyperVolume objects, Φ is a set of HyperVolume operations and W is a set of relations for a set of objects.

The HyperVolume object is defined as:

$$O = (G, A_c, A_1, \dots, A_n(t)) : \quad (3.1)$$

$$(F'(X), S'_c(X), S'_1(X), \dots, S'_n(X))$$

Here one component is responsible for the object geometry G and other components serve as the point attribute functions representing object properties of different nature A_k .

$X = (x_1, \dots, x_n)$ is a point in n-dimensional Euclidean space.

The set of operations $\Phi = \{\Phi_m\}, m = 1, \dots, M$ includes types: $\Phi_m : O^m$

where m is a number of operands of an operation; Φ_m is a set of operations of the same type m . The result of an operation it also a HyperVolume object.

For example, given the unary operation Φ_1 , applied to HyperVolume object $O_1 = (G_1, A_{11}, \dots, A_{1m})$, the resulting HyperVolume object O_2 is defined as:

$$O_2 = (G_2, A_{21}, \dots, A_{2k}) = \Phi_1(O_1) = \Phi_1(G_1, A_{11}, \dots, A_{1m}) \quad (3.2)$$

The definition 3.2 corresponds to the composition of the functions on scalar fields:

$$\begin{aligned}
(F_2, S_{21}, \dots, S_{2k}) &= (\Theta(X, F_1, S_{11}, \dots, S_{1m}), \\
&\Omega_1(X, F_1, S_{11}, \dots, S_{1m}), \\
&\dots \Omega_k(X, F_1, S_{11}, \dots, S_{1m}))
\end{aligned} \tag{3.3}$$

, where Θ is a function describing a new geometric point set; Ω_i is a function describing a new attribute.

Relations are defined over HyperVolume objects O_j and, possibly, some objects of another nature Q_k . They are represented in the form of n-valued predicates over functions. The set of relations W includes such relations as

$$\begin{aligned}
w_i(O_1, \dots, O_m, Q_1, \dots, Q_k) &: \Gamma(F_1, S_{11}, \dots, S_{1m}, \dots, F_k, S_{k1}, \dots, S_{km}, Q_1, \dots, Q_k) \\
&, \text{ where } \Gamma \text{ is a predicate.}
\end{aligned}$$

For example, binary relations over point set G can be defined with point and attributes $P_a = (X, a_1, \dots, a_k)$ and HyperVolume object $O = (F, S_1, \dots, S_k)$ as:

$$\Gamma_2(P_a, O) = \begin{cases} 0, F(X) < 0 \\ 1, F(X) \geq 0 \end{cases} \tag{3.4}$$

This means that point belongs to object if it is internal or boundary, without any attributes values check.

The described above rules allow to operate geometry and attributes of objects representing initial data and to define various relations on a unified basis. The underlying process leads to the construction of the tree structure for geometry and attributes. The functions F, S_1, \dots, S_j are evaluated at the given point by a tree traversing procedure.

Flexibility in the modelling of the object with properties of arbitrary nature and its user-friendly nature make the HyperVolume framework a convenient tool for visualisation of a wide range of initial data representations. Fig. 3.4 shows some visualisation examples, where the HV representation is used. In particular, it shows the visualisation of the results of the physical simulation and analysis of molecular fields (Fig. 3.4 (a)), and the modelling of the geological and biological structures (Fig. 3.4(b,c)). The hybrid HyperVolume model has the potential for quite broad application areas that impose restrictions on nature and features of geometry and materials. Conventionally, the HV was applied for modelling with voxel and implicit representations. Those representations are convenient for modelling dynamic changes in shape, however, does provide control over topology.

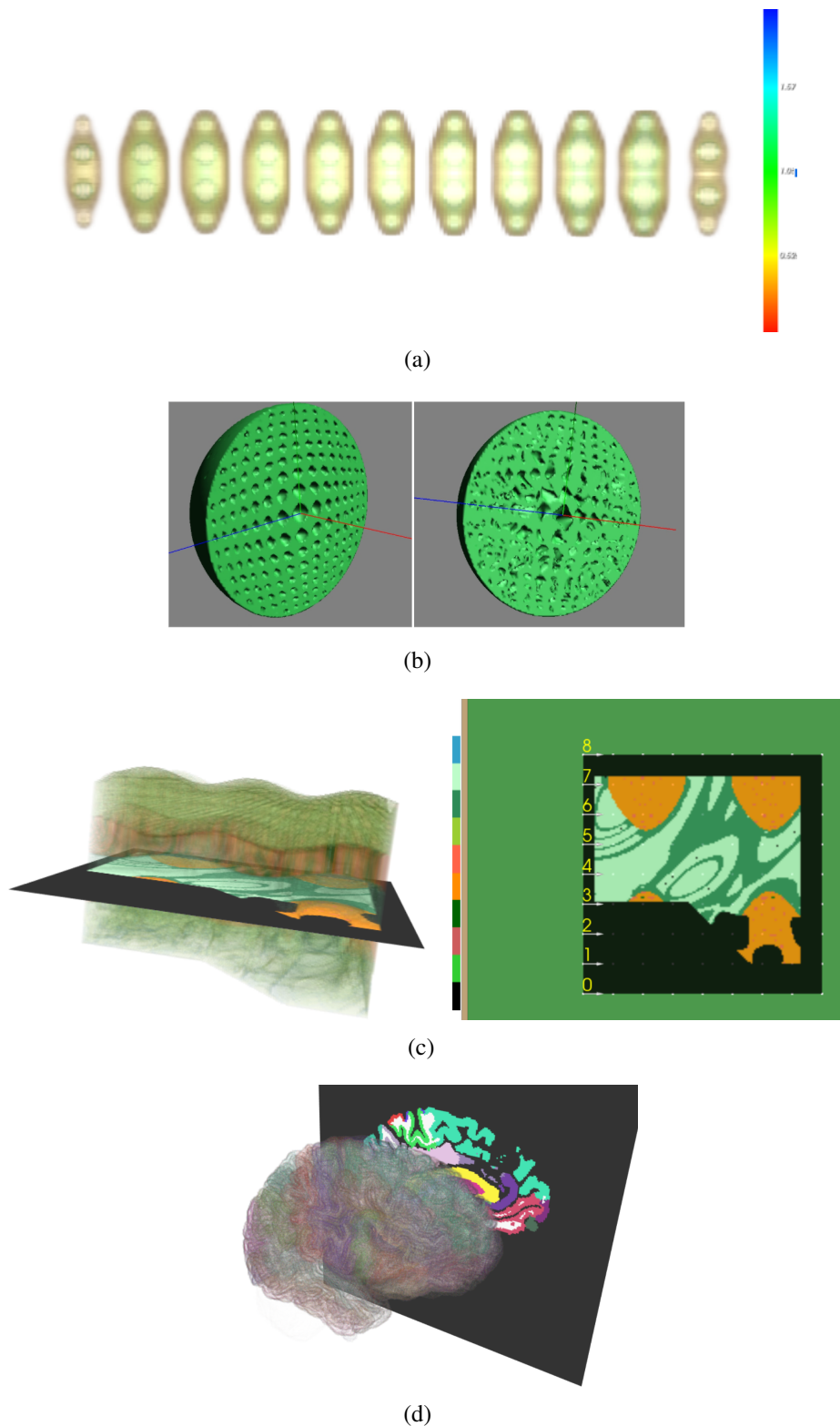


Figure 3.4: Examples of modelling and visualisation of heterogeneous objects. a) Volume rendering of dynamical process of molecular structure geometry optimisation; b) Modelling and visualisation of porous structure; c) Volume geological structure with layers of different materials, cavities and a drilled well. d) Brain labelled data volume rendering by standard VTK means (data from *Volume Rendering with Python and VTK* (n.d.))

3.3.2 Implicit complexes framework for heterogeneous objects

Let us outline the main features of the IC-based framework (Kartasheva et al. 2008). It allows for representing a heterogeneous object by a union of high-level components that are significant for a given application. The components can overlap each other under the special restrictions on their mutual dispositions. Thus IC provides the representation with a distinctive structure that can easily be reduced to the cellular topological subdivision. The intersections of the components are described by the constructive methods which preserve the precision of the representation.

In the IC based framework a hybrid model (Kartasheva et al. 2008) is defined in the Euclidian modelling space as follows. Let $g_i^{q_i} \subset E^3$ be a closed point set called a cell, where i is its index number and q_i is its dimension. Then, a geometric object D is defined as the union of cells $g_i^{q_i}$ under the following conditions:

1. The boundary of each cell $g_i^{q_i}$ is the union of a finite number of cells of lower dimensions;
2. Cells can overlap each other but the intersection of any two cells is either the union of a finite number of cells or is empty. (Note that we call the cells satisfying 1 and 2 conditions as properly joined cells.)
3. Each $g_i^{q_i}$ is unambiguously described by some known geometric representation which provides a set of tools for geometrically and topologically correct discretization of the cell. So, a variety of representations can be used for the description of the cell shapes. However, all of these representations should guarantee a conversion into a mesh described by a polyhedral complex.

A collection K of cells satisfying the above conditions is called an implicit complex (IC), i.e.: $K = \{g_i^{q_i}\}_{i=1}^N$. The dimension of the IC is the maximal dimension of its cells. In accordance with the IC definition, polyhedral, cellular, and CW complexes are also represented in the IC framework.

The above conditions ensure the ability to convert an arbitrary IC K into a polyhedral complex, which approximates, geometrically and topologically, the object D . In fact, the reducibility of each of the used representations to a polyhedral one guarantees a correct execution of any operation on objects described by various representations. However, the IC-based approach allows exploiting advantages of different types of representations, keeping the initial representations for components of the model and using meshes only for the implementation of various numerical procedures applied in topology analysis, computational geometry, and finite element analysis.

An implicit complex provides a consistent description of both the geometry and the topology of a modelling object. The geometry is represented by shapes of the individual cells and the topology is described using the relations between cells. The main relations defining the topology of an IC are the boundary relation and the relation “to contain”. According to the first two conditions of the IC definition, the mutual disposition of any of the IC cells can be evaluated through queries to the main relations.

The attribute values are assigned to points of a heterogeneous object described by the IC using a collection of attribute functions $\{A_i\}$, where each function maps the modelling space into the corresponding attribute value set. Attribute functions can be analytic, piecewise analytic or be defined by interpolation methods. The dimension of an attribute value set and an interpretation of attribute values depends on its nature and specifics. Thus a heterogeneous object D is described by a hybrid model H based on IC complex $K = \{g_i^{q_i}\}_{i=1}^N$ by tuple $H = \langle G, R, A \rangle$, where

1. G is a collection of cells' shapes : $G = \{g_i\}$,
2. R is a collection of boundary B and “to contain” relations C between cells $R = \{B_{ij}, C_{ij}\}$
3. A is a collection of attributes defined at points of D , $A = \{A_k\}$

IC framework was proven to flexibly operate both explicit and implicit representation and perform a conversion between representations (Kartasheva et al. 2005).

The next research (Kartasheva et al. 2008) is focused on the algorithms for the set-theoretic operations on heterogeneous objects represented by implicit complexes and describes a step-by-step procedure for the construction of a hybrid model using these operations. The paper also presents a case-study showing integration of both boundary and function representations, illustrates modelling with attributes and dynamic modelling on the base of the IC. Practical usage of IC-based framework for unified handle implicit, explicit geometry and internal properties in structural modelling and grid generation for reservoir simulation is described in Branets et al. (2015).

The key characteristic of the IC structure for this research is that it allows operating and evaluate relationships for both implicit and explicit cells. The mathematical framework has two advantages. Firstly, it is convenient for the representation of various heterogeneous objects and allows modelling subdomains both explicitly and implicitly. Secondly, the constructive modelling of a hybrid structure allows continuous modelling of dynamic changes with flexible control over topology and shape.

Let us discuss more in details the aspects of hybrid constructive modelling of geometry and material.

3.3.3 Constructive hybrid modelling within IC

The support for constructive hybrid modelling in IC framework is provided via various cell types (Kartasheva et al. 2008). Among those, in context of this research we are interested in the following types:

1. The P-cell is an explicit cell representing a simple polyhedron.
2. The F-cell is an implicit cell described by FRep that is a constructive representation by real-valued functions. In our case F-cells are suitable for involving HyperVolume models into a hybrid representations.
3. The C-cell is a composite cell aggregating cells of various types. Each C-cell is defined as a carrier of a local implicit complex L differing from the complex K containing this C-cell. The complex L can consist of the cells of any types supported within IC framework. In particular cases complex L can be represented by simplicial or a polyhedral complexes. C-cells allow us to specify multi-scale representation.
4. The T-cell is described with a constructive tree. Its leaves represent objects described by cells of all other types. The tree nodes represent operations, in particular, some bijective geometric transformations, non-regularized set-theoretic operations and trimming by 3D manifolds. The T-cells allow for the description of the result of applying set-theoretic operations to cells of different types without the need for converting between representations.

Note that IC-based framework provide flexible unified support for unstructured representations, including the cellular (FEM) and dynamic point-based representations (molecular structures). The flexibility in terms of geometry modelling also provide a base for multi-scale features modelling on spatial subdivision.

3.4 Direct Volume ray-casting

3.4.1 Computer graphic rendering pipeline

The work (Pharr & Humphreys 2004) defines rendering as a process of producing a 2D image from a description of a 3D scene. In terms of scientific visualisation, the obtained 2D image is a graphical representation of the initial data, that users employ to get insight into phenomena this data represents (Haber & McNabb 1990).

The rendering process considers the rasterisation or ray-tracing algorithms (Akenine-Moller et al. 2008). Also, the modern graphics hardware allows introducing a combination of two techniques and introduces hybrid rendering (*Imagination announces PowerVR wizard GPU family: Rogue learns ray tracing* retrieved 2019). The ray-tracing became popular quite recently due to its flexibility and intensive research in the area of hardware support. Recently the graphics hardware is used for computational purposes such as computer simulation, machine learning and geometry modelling tasks. Often those task demand real-time rendering of intermediate or final results of complex modelling or simulation or high-quality rendering. Such tasks make graphics pipeline programming not straightforward. In the context of implementation on modern graphics hardware, the ray-tracing technique becomes more suitable for such problems.

3.4.1.1 Rasterisation basics

The rasterisation is a conventional rendering technique for real-time computer graphics. The core of graphic pipeline is rendering of objects that are created as a 3D meshes, composed of triangles (see Fig. 3.5 for a basic scheme).

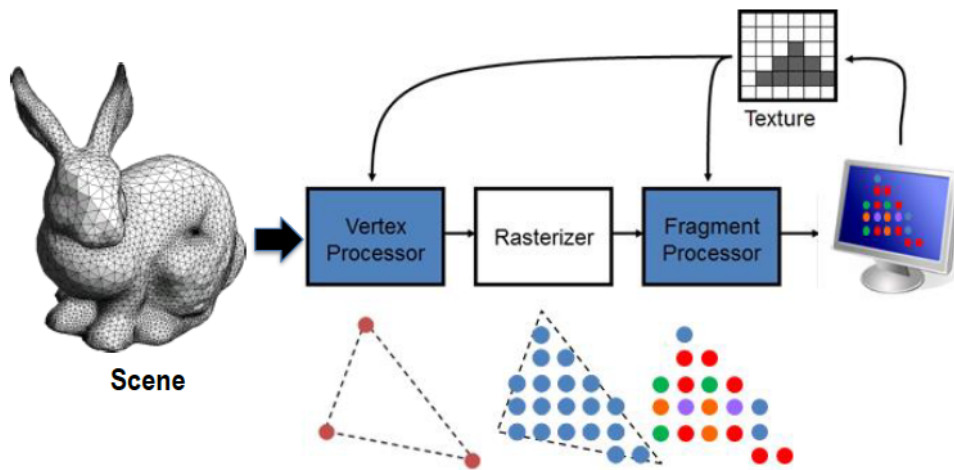


Figure 3.5: Rasterization pipeline. Image from (Deng et al. 2017)

The two basic types of GPU programs for the pipeline are vertex and fragment shaders. The rasterisation is a spatial sampling operation that converts triangles into pixels on a 2D screen to obtain an image that the viewer sees. The pipeline is described with several steps (see Fig. 3.5). First, the mesh as a set of triangles is loaded to the graphic pipeline. The second stage is vertex processing that is followed by triangles spatial sampling. The fragment

processing and other processes like depth or z-buffer follow and the resulting colour of each pixel is sent to frame buffer for rendering.

The rasterisation process is highly optimised for GPU rendering Deng et al. (2017). However, treating each triangle primitive separately limits the flexibility for complex shading calculations that consider multiple primitives simultaneously (Pharr et al. 2016) such as indirect illumination and other complex techniques. Moreover, a lot of aspects of the rendering process that have to be taken into account if the complex light transport model is considered. The modern visualisation imposes the quality requirements, such as support of transparent overlapping geometries, depth and shapes enhanced perception that is only possible due to ambient occlusion and global illumination. However, those techniques are difficult for implementation in a rasterizer (Han et al. 2019). Initially designed as highly optimised for graphics hardware, the rasterisation technique is not flexible for complex procedures as it is highly restrictive in terms of data flow that is a one-way procedure executed by each operation unit (see Fig.3.6).



Figure 3.6: Dataflow in rasterization pipeline. Image from (Subtil 2018)

For comparison, in the ray-tracing pipeline that we consider in Fig. 3.8 the number of working units, those are rays depends on the outcome of previous work units and the entire computational process can be restarted again in the pipeline with programmable stages.

Moreover, as continuous geometry modelling and rendering is required or LOD techniques are assumed the sampling issues of mesh-based rendering becomes crucial (Crassin 2011). The research in area stresses that mesh representations are not suitable for both modelling (Pasko et al. 1999), (Blinn 1982), (*Projection operation for multidimensional geometric modeling with real functions* 1996), (Adzhiev et al. 1999)) and rendering (Crassin 2011). One of the particular features of the ray-tracing technique is its ability to adapt to input geometry via customising ray-primitive intersection procedures.

3.4.1.2 Ray-tracing basics

The ray-tracing was introduced more than 50 years ago (Appel 1968). The approach was inspired by real-world processes of how we see the objects. As the light from source illuminates the object, the photons (particles) bounce from one object to another till it reaches the viewer's eyes. The ray-tracing reverses the process of tracking photons by shooting rays

from camera or viewer position. Each pixel of the rendered image is obtained as the path of light is traced backwards (see Fig. 3.7).

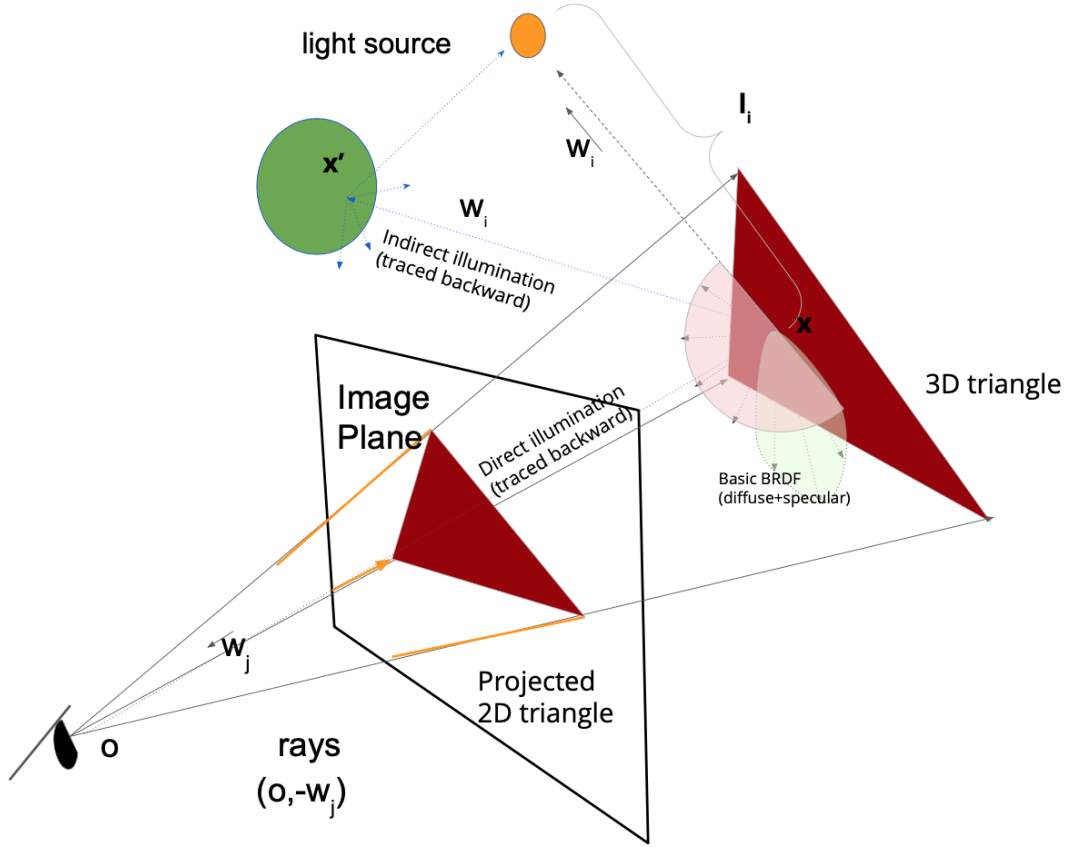


Figure 3.7: Ray-tracing scheme

The Fig. 3.7 demonstrates that the realistic approximation assumes the iterative process of ray shooting to compute indirect light coming that "bounces" from another object on the scene. Global illumination technique conventionally uses random, semi-sphere sampled rays shooting and is referred to as path tracing (Deng et al. 2017). The modern graphics hardware allows real-time iterative tracing of ray in a backward direction from the viewer for realistic rendering advanced shading effects, such as reflection, shadows (Whitted 1980).

The ray-tracing is a direct method to solve a rendering problem that is generally formulated by Kajiya's rendering equation for illumination model and is stated as:

$$L(x, \omega_j) = L_e(x, \omega_j) + \int_S f_r(x, \omega_i \rightarrow \omega_j) L(x', \omega_i) G(x, x') V(x, x') d\omega_i \quad (3.5)$$

where (see Fig.3.7: ω_j - generic direction along j -th ray ω_i - secondary directions, including light direction and indirect illumination L_l - point light source intensity l_i - ray

length from light source or secondary object to intersection with object surface o - ray origin x - point location along ray (intersection with surface) $L(x, \omega_j)$ - intensity reflected from position x in ray direction ω_j $L_e(x, \omega_j)$ - light emitted from x by object itself or background contribution $f_r(x, \omega_i \rightarrow \omega_j)$ is a Bidirectional reflectance distribution function (BRDF) of surface at point x , transforming incoming light w_i to reflected w_j

$L(x', \omega_i)$ light from x' on another object arriving along ω_i

$G(x, x')$ - geometric relationship between x and x'

$V(x, x')$ - visibility test that returns 1 if x can "see" x' and 0 otherwise

In section 3.5.3.1 we will compare main terms of this equation to acoustic rendering equation 3.26 that is derived as a time-dependent version that models acoustic radiation transfer.

The direct propagation of light through volume transparent objects demands more complex computations and light path sampling. The problem is conventionally addressed within volume rendering technique that we will discuss in details in sections 3.1, 3.4.4.

The ray-tracing brings a lot of simplifications to design of complex rendering pipelines and the entire technique is highly flexible as much more programming flexibility is provided per each operation unit/ray (see Fig. 3.8).

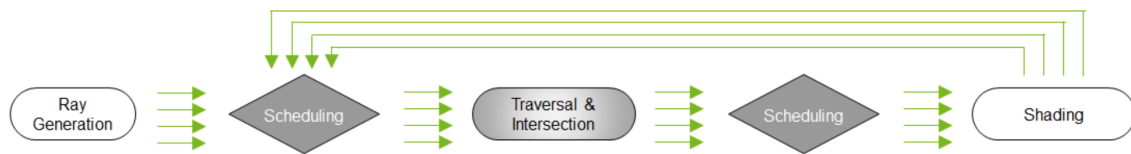


Figure 3.8: Dataflow in ray-tracing pipeline. Image from (Subtil 2018)

Moreover, it benefits from GPU programmable features and considers loading complex data on demand (ray-driven, ray-based rendering). The core of procedure flexibility is an assumption that generally any geometry primitive is directly ray-traced by solving its custom ray-primitive intersection procedure without additional conversion to triangle primitives. Users can employ direct rendering without conversion to triangles of such geometry representations as voxel sparse structures (Crassin 2011) or implicit geometry Grottel et al. (2015). The technique is accelerated with hierarchical structures build on top of the spatial subdivision. This allows accelerating a preliminary intersection, with exact ray-object intersection is programmed for custom geometry primitive (Rincon-Nigro et al. 2014). The well-known applications of ray-tracing/ray-casting concepts are Monte Carlo ray-tracing, voxel cone tracing, sphere-tracing of signed distance fields. The recent research actively uses acceleration structures for space skipping and ray-primitive intersection acceleration in the rendering of heterogeneous volume data distribution, that is a particular area of interest

for this research. The research explores the volume ray-casting of basic static concave shapes that compose a FEM result that is unstructured grid such as tetrahedral meshes (Silva et al. 2005) and molecular point-based data (Knoll et al. 2009). We discuss the aspects of accelerated volume rendering technique in section 3.4.2. In this research, we concentrate on the advantages of direct integration of general-purpose GPU programming (GPGPU) for visualisation tasks.

With the graphics hardware, the graphics pipeline is evolving into a generally programmable stream processor (Purcell et al. 2002), (Chadzynski 2018). Moreover, the research is an area of constant improvement in terms of adapting the working specifics of modern graphics hardware for further ray-tracing procedure optimisation (Wald & Parker 2019), (*Ray Tracing In Vulkan* 2018). Modern ray-tracing solutions address optimise a lot of highly low-level issues and reduce the average cost of ray-object intersection computation allowing the researchers to concentrate on solution design aspects (Parker et al. 2010).

3.4.2 Volume Rendering framework

The principles of volume rendering have straightforward interpretation in the context of ray-tracing as a simulation of the process of light propagation through volume object. In the rendering of surface objects, a user is interested in the reflective properties that are essential for shape highlighting. The analysis of volume objects, however, mostly concentrates on highlighting of internal structure that is perceived due to emission, absorption, scattering properties of individual volume elements (voxels) or ray-segment (Max & Chen 2010).

The conventional and most simple model of light interaction with a volume object considers only emission and absorption (Jönsson et al. n.d.). The model is convenient for real-time interactive rendering of large-scale structures.

The rendering equation that takes into account a single light scattering makes it suitable for real-time rendering (Jönsson et al. n.d.). The optical model allows enhancing quality of visual analysis (Wahle & Wriggers 2015), however, can be still computationally expensive (Jönsson et al. n.d.) for the interactive and dynamic rendering of large structures. Often, the modern interactive Volume Rendering takes advantage of modern graphics hardware (Schlegel et al. 2011) and is limited to single-scattering. The modern algorithms often employ the idea of splitting the optical model computation into separate parts, mainly concerned with the lighting conditions that can be independently precomputed into textures and updated on-demand (Kniss et al. 2003), (Schlegel et al. 2011).

In section 3.4.4 we discuss the optical models in volume ray-casting that describe in general how light interacts and mathematical formulation of the process as a volume rendering integral whose evaluation is approximated with Riemann sum.

The other important component of volume rendering framework is a Transfer Function(TF). We can perceive and interpret the volume structure by operating only two optical attributes: colour and opacity. TF maps the representation of internal volume structure to optical attributes. A basic 1D TF operates the 3D texture scalar value and maps it to colour and opacity to perform a visual classification of heterogeneous data when there is no information on its heterogeneous nature. The fetching operation from 3D textures with trilinear/cubic interpolation of the scalar field is performed on GPU.

A more advanced Multidimensional Transfer Function (TF) assume operation by several scalar values to perform this task. A tool allows visual analysis of more complex objects represented with two and more scalar fields describing various object properties. In this research, we consider a distance-based TF in Volume Rendering that highlights features of interest mostly determined by the distance to reference structures Tappenbeck et al. (2006). The more complex mapping facilitates the visual-classification task Kniss et al. (2003). The use of shading and depth perception that can provide an addition to 3D shape cues and thus enhance visual analysis and highlight the features of interest Kniss et al. (2003). For this, the conventional for surface rendering Blinn-Phong model (Levoy 1988) was considered as an initial enhancement of the classical emission-absorption model that we discuss in section 3.4.4. Designed for surface objects, the direct application of this technique for volumes leads to quality issues Kniss et al. (2003). Still, a model is widely used in Volume Rendering to highlight features of interest such as edges (Jönsson et al. n.d.)

The conventional volume rendering has limited application for the rendering of complex heterogeneous data because it deals only with structured volumes in GPU memory that are stored as 3D textures. A more advanced view on volume rendering of heterogeneous objects allows to review the technique and optimise its efficiency.

3.4.3 Volume ray-casting on unstructured grids

As discussed in section 3.1, the heterogeneous objects are often described within an unstructured spatial subdivision. The problem of such data volume rendering is referred to as the task of unstructured grids volume ray-casting (Weiler et al. 2003),(Silva et al. 2005),(Callahan et al. 2006).

To describe a problem of light transfer problem solving for semitransparent volume object that is approximated with light interaction evaluation at several subvolumes, a ray is parametrised in terms of a distance from the background point x_1 in direction w_j , where each point at distance s is $x(s) = x_1 + w_j s$ (see Fig. 3.9). The volume rendering integral depends on integrating over distance through volume the ray passes and values of fetched 3D

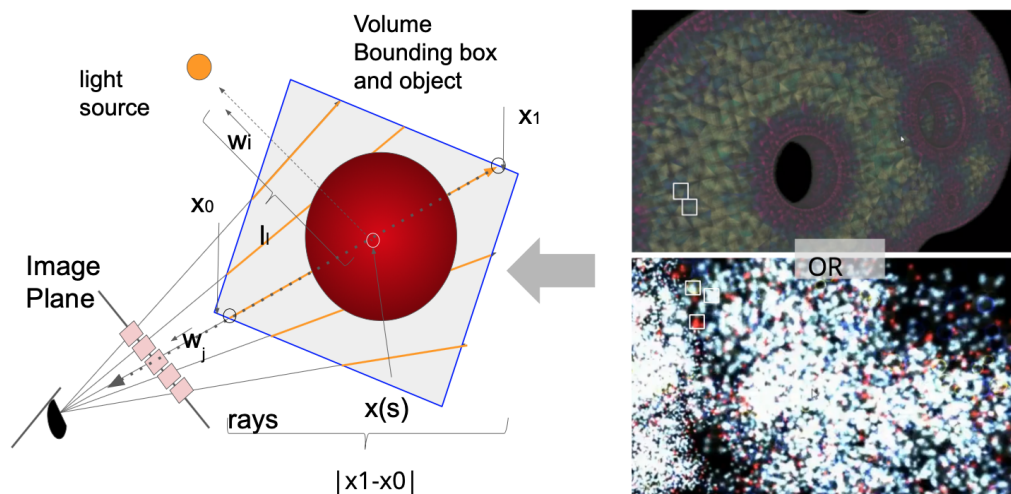


Figure 3.9: Volume ray-casting of most common heterogeneous objects representations: point-based data and tetrahedral meshes . The integration of optical properties is evaluated only on ray-segment of length $|x_1 - x_0|$ computed as a result of ray intersection with bounding box

textures that are mapped to optical properties with TF (see section 3.4.4 for details on optical models used in volume rendering).

For heterogeneous objects, however, usually instead of direct fetching structured 3D textures in GPU memory, the ray-casting procedure firstly operates a GPU-stored hierarchical structures that are used for accelerated access to a part of the heterogeneous volume. As a result, the techniques allow operating both structured and unstructured data (Knoll et al. 2009),(Max et al. 1990) and accelerate the volume rendering by skipping space in the heterogeneous volume as volume integration occurs only on selected region (see Fig. 3.9)

Moreover, storing additional dependencies between subvolumes within a subdivision (i.e. neighbouring cells) on GPU allows extend the technique to cases of reconstruction and modelling of the surfaces of volumetric structures (Zhou, Gong, Huang & Guo 2008), (Parulek & Viola 2012). Moreover, space partitioning over the data can be introduced artificially to provide more intensive control over a topology defined on initial data (Adamson & Alexa 2006).

The technique was mainly considered for volume ray-casting of unstructured volume data those cells were concave shapes, such as tetrahedral meshes (Max et al. 1990) or molecular data (Knoll et al. 2009). The research in area stresses the technical advantages to simplify the preliminary data resampling into the structural grid so that the conventional 3D texture fetching can be applied. Still, the conventional technique can lead to inaccuracies in visual representation and information loss Rathke et al. (2015). In other words the problem should

be addressed as more generic computation of the light propagation through a heterogeneous object with the complex heterogeneous material distribution. In some cases, highlighting of a surface shape properties Parulek & Viola (2012) of individual geometric volumes is required.

A technique introduces a notion of individual subvolume interaction with light within a heterogeneous subdivision, which we revisit later in section 4. In particular, we discuss how the concept allows judging on properties of complex heterogeneous phenomena via optical properties distributed on a complex domain and extend it the more general visual-auditory rendering case.

3.4.4 Optical model

The optical model defines light propagation through a volume object in terms of the geometric optics effects. The optical properties affect the light propagation as three types of light-particle interactions are considered that are absorption, emission or scattering that we will discuss below.

3.4.4.1 Absorption

The light intensity $I(s)$ that passes the distance s in voxels through participating media that is composed of particles that only absorb the light as it was derived at Max & Chen (2010):

$$I(s) = I_0 * T(s) \quad (3.6)$$

where I_0 is initial light intensity as ray enters the volume. The transparency of medium that reaches s is formulated as follows

$$T(s) = \exp\left(-\int_0^s \tau(t) dt\right) \quad (3.7)$$

In this case, τ is defined only by absorption properties. However in a general case $T(s)$ is referred to as an extinction function defined with Beer-Lambert law and τ is an extinction coefficient as discussed below. For this case, it defines the transparency of each element, voxel and is constant within it. The opacity for voxel reached l is defined as $\alpha = 1 - T(l)$ for this case and τ is defined by TF. The Gaussian form of $T(s)$ has a relation to probability modelling and can be interpreted as the probability to traverse the volume along the ray with length $d = s * dt$ without hitting the particle. In (Max & Chen 2010) was demonstrated that if we can divide the entire ray segment Δs into subsegments with $s_i = i\Delta s$ with constant $\tau(t)$ value (the segments are not required to be of the same length Δs) the following approximation

can be introduced for transparency that reaches s_i :

$$T(s_i) = \exp\left(-\int_0^{s_i} \tau(t)dt\right) \approx \prod_{j=1}^i \exp(\tau(s_j)\Delta s) \quad (3.8)$$

3.4.4.2 Emission

The light intensity $I(s)$ is described as :

$$I(s) = I_0 + \int_0^s g(t)dt \quad (3.9)$$

where g is a source term that for this model includes emission only: $g(s) = c(s)\tau(s)$. Like τ , c is one of the values defined by TF. Conventionally those values are defined on a per-voxel base as TF.

3.4.4.3 Emission and absorption

A more general emission-absorption model is formulated through two terms:

1. The light coming from the background I_0 multiplied by participating media total transparency $T(D)$
2. The contribution of the source term $g(s)$ integrated over each element multiplied by the transparency that has reached s -th element.

In terms of probability, the expected colour I for a ray is obtained by averaging colour returned by hitting background that is weighted with event probability and colour of going through transparent volume weighted by the probability of this event. The total equation with an emission-absorption source term $g(s)$ is:

$$I(D) = I_0T(D) + \int_0^D c(s)\tau(s)T(s)ds \quad (3.10)$$

The integral in equation 3.10 is conventionally approximated with Reimann sum for evaluation. The regular small step discrete sampling that suggests accumulation of optical properties on the per-voxel basis is considered. The physical interpretation of those values, in this case, is the light interaction with each voxel element. However, if we have a segment s_i, s_{i+1} with constant $c(s_i)$ and τs_i values we can compute the contribution of i -th as (Max & Chen 2010):

$$I_i = \int_{s_{ci}}^{s_{ci+1}} \tau_i c_i T(s) ds = T(s_{ci}) c_i (1 - \exp(-\tau_i \Delta s_{ci})) \quad (3.11)$$

3.4.4.4 Emission, absorption, single scattering

In the complexity of the optical model in volume, rendering is balanced by its computational expensiveness. In this work, we consider only the in-scattering process within the volume as it allows significantly to enhance volume rendering quality and still can be computed efficiently. In general the source term includes both emission and reflection of external illumination that is indirect light that comes from other part of the medium (scattering) with consideration of absorption through the medium or light blocking (shadows). The source term is formulated as $g(x, \omega) = E(x) + S(x, \omega)$ where $E(x)$ - emissive term (self-glow) and $S(x, \omega)$ -scattering at x with direction ω .

The total global illumination is most often is approximated with local illumination in computationally expensive volume rendering, that is:

$$I(D) = I_0T(D) + \int_0^D (c_g(s) + \sum_{i=1}^k c_r(s, L_i)\tau(s)T(s)ds \quad (3.12)$$

here $c_g(s)$ defined intensity of self-glowing and $c_r(s, L_i)$ the light reflected due to light source L_i .

The model is two-pass (Kajiya & von Herzen 1984). On the first step, we compute the illumination that reaches some point s (second term), the propagation of flux from the light source through the volume to the point (ray-shooting from the light source) that contributes to the brightness of s as described by the first component of equation 3.10. On the next step, this illumination is scattered (reflected) from the viewpoint (conventional rays shooting from a camera) and intensity is gathered along with viewing rays with equation 3.12. Conventionally the first pass is stored and sampled as a 3D texture in GPU memory (Jönsson et al. n.d.).

3.5 Auditory feedback and sound propagation

The sound modelling and preprocessing for further analysis uses various techniques and physical models. Those models are defined in the context of how human auditory system perceives and extract meaningful cues from complex sound wave produced by a set of the vibrating objects with different locations in acoustic environment vibrations. The area explores the relations between such approaches as modelling with a second law of Newton (Leonard & Villeneuve 2019), digital signal processing (Smith 1997), (Anwar & Sung 2009) and sound propagation (Smith 1992), (Murphy et al. 2007), (Elorza 2006).

The digital signal processing establishes the core principles of the linear system and convolution for sound modelling. The technique is a conventional tool for sound wave

decomposition and analysis as well as a synthesis of new sounds. Research in area emphasises the technique related to physical processes of sound propagation. The problem area often adapts computer graphics techniques with consideration of differences in light and sound transport. Also, sound modelling uses the second law of Newton to synthesise a sound as a result of forces generated during user interaction and compute parameters of a linear system. The area of computational auditory scene analysis explores how user auditory system performs automatic decomposition of a complex sound wave performing the inverse procedure that via based on the above principles. The sonification area uses the human ability to perceive, extract a wide range of auditory features and associate them with properties of objects under study and design the techniques according to the established principles of auditory scene analysis.

In this section, we concentrate on the principles of complex sound wave decomposition in the frequency domain and spatial properties interpretation. We discuss how those properties are formed by the physical process of propagation within geometry and further "decoded" by a human auditory system that "reverses" the process.

Below we consider:

1. Mathematical foundation of processing sounds with a complex frequency domain and spatial properties based on the digital signals representation
2. Physically-based sound synthesis and the role of sound propagation in various models. We discuss the basics of formation of sound wave frequency domain characteristics.
3. Basic principles of spatial sound modelling as a result of propagation and interaction with various geometry, including both acoustic environment and listener. We discuss computer ray-tracing technique application aspects in modelling the above interaction
4. The analysis of sound waves in an area of auditory scene analysis and how the design of sonification techniques takes advantage of the area.

3.5.1 Core principles of sound modelling and analysis

How we perceive and "identify" auditory objects is an area of constant research (Hermann et al. 2011). In everyday life, by listening to the music we group auditory objects by timbre and pitch sound characteristics and distinguish the separate music instrument. We can tune our focus to individual sound of just one auditory object and track it (Hermann et al. 2011). We also perceive the complex sound produced by many auditory objects (music instruments) as a whole and understand the entire picture that can be a musical composition. Thus we can analyse both "big picture" represented with several auditory objects and concentrate

on detailed analysis of particular features. Moreover, we can extract the spatial positions of auditory objects from the sound. The principles of processing of the input signals and extracting information by human auditory system processing are related to digital sound processing techniques, such as Fast Fourier Transform(FFT) and convolution. Also, the sound synthesis uses those techniques in combination with the laws of physics to generate the most realistic, accurate and rich sound waves. Let us discuss the basic principles of digital sound processing.

Conventionally digital audio signals have discrete representation that can be formed by sampling continuous signals with regular intervals of time (Cook 2002). The preprocessing and modelling of audio feedback directly operates sampled waves and takes into account their discrete nature, especially on stages of re-sampling and interpolation. Similarly to other discrete representations, the quality and antialiasing issues of auditory stimuli generation are defined by Nyquist theorem and directly related to a range of frequencies auditory system can perceive. For this and several other reasons discussed later, the complex sound waves are often decomposed into separate bandwidths (frequency ranges)(Cook 2002, Essl et al. 2004) that are processed differently. The digital signal processing technique that operates the sampled representations is based on principles of linearity of these discrete systems that establish the principles of homogeneity and superposition and the entire system does not change its behaviour with time (Cook 2002). Linear Time-Invariant Systems (LTI) is a core of auditory perception, analysis and sound modelling principles. Those principles also define sonification area by proving the efficiency of sonification techniques.

The interaction of the input signal with a linear time-invariant system can be described as a decomposition of separate impulse responses: the convolution of input with an impulse response of LTI. The input sequence $x(n)$ is decomposed into time-ordered set of weighted impulses $\delta(n)$ (type of basic sequence) and output sequence $y(n)$ is presented with weighted impulse responses $h(n)$:

$$x(n) = x_0\delta(n-1) + x_1\delta(n-2) + \dots + x_m\delta(n-M) \quad (3.13)$$

where

$$\delta(n) = \begin{cases} 1, n = 0 \\ 0, n \neq 0 \end{cases} \quad (3.14)$$

$$y(n) = x_0h(n-1) + x_1h(n-2) + \dots + x_mh(n-M) \quad (3.15)$$

Convolution allows decomposing signal for analysis or modelling of new sound waves with predefined properties. The technique allows performing such operations as cancelling or

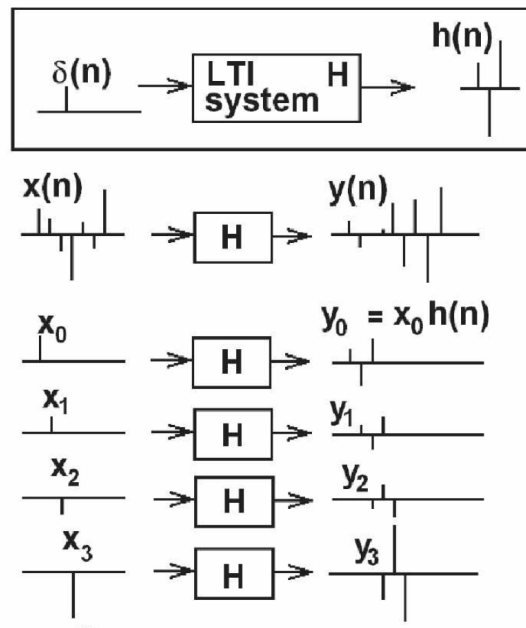


Figure 3.10: Scheme of input convolution with LTI impulse response. Image from Cook (2002)

adding new sounds or correcting the quality of old recordings (*Signal Processing Essentials* 2005). Convolution parameters (acoustic impulse response) can be recorded or computed as a result of the physical process of propagation/interaction of sound in the geometry of acoustic environment (room, concert hall, etc.) (Elorza 2006) or human auditory systems (Röber et al. 2006). Sound spatial properties are formed as a result of propagation and allow localisation of several auditory objects in space.

The other technique for sound analysis and modelling relates to the perception of a periodical component of complex sound waves. We can further decompose and analyse the complex sounds produced by vibrating objects in frequency domain (Cook 2002). The frequency spectrum (harmonic diagram) can be extracted from the recorded sound produced by a real object with Fast Fourier Transform (FFT). The spectrum provides the information to synthesise similar sounds quite accurately with the use of noise, oscillators, envelopes and filters (Bonneel et al. 2008). This model of generated by vibrating sound wave reflects auditory perception aspects, as a human auditory system in the analysis of complex sounds performs a complex signal processing (Pressnitzer & Gnansia 2005) and acts like FFT (Moore 2012).

Precise modelling of sound wave requires consideration of all propagation paths and the human auditory system can process and compare such auditory rays for analysis (see section 3.5.4). Sound modelling for interactive environments can include such procedures

to describe how sound is formed by a vibrating object with sound synthesis (Cook 2002); how it propagates through the geometry of acoustic environment, i.e. acoustics modelling; how the sound wave that reaches the listener interacts with his auditory system so the user perceives spatial properties of sound and locates the auditory source (Takala & Hahn 1992). For these areas the sound propagation plays a crucial role.

3.5.2 Physically based sound synthesis

Sound synthesis often relies on physics principles. The waveguide approach binds the aspects of conventional digital filters applied to the physical process of separate waves propagation (Smith 1997), (Smith 1992), (Murphy et al. 2007), (Duyne & Smith 1993). A general algorithm for synthesizing sound, the modal resonant filters decompose complex sound generation into a linear system those coefficients and parameters are computed as a result generated by interaction forces (O'Brien et al. 2002), (Bonneel et al. 2008), (van den Doel & K. Pai 2003). Research in this area (Essl 2002) demonstrates the relation between such decomposition and propagation in vibrating objects geometry. Let us discuss some aspects of those techniques and how a frequency domain of complex sound wave is formed on the base of those principles.

Mass spring system for deformations modelling Let us consider the model of the vibrating object with deformations occurring as a result of to applied forces. From human perception's point of view, there are visual deformations, for example, soft body deformations, and deformations that can not be seen, but we hear them, such as rigid body deformations. The mass-spring model is often used to model both the deformations in computer graphics and oscillating systems in sound synthesis and haptic rendering (Payandeh & Azouz 2001). Below, we use the mass-spring model as a reference to outline the features of the deformations modelling, physical-based sound synthesis and haptic feedback modelling have in common.

A simple mechanical system is presented in Fig. 3.11

Due to Newton's second law, the equation, describing such a system is:

$$-k \cdot d - m \cdot g - c \cdot \frac{dx}{dt} = m \cdot \frac{d^2x}{dt^2} \quad (3.16)$$

Where

$$F_s = k \cdot x \quad (3.17)$$

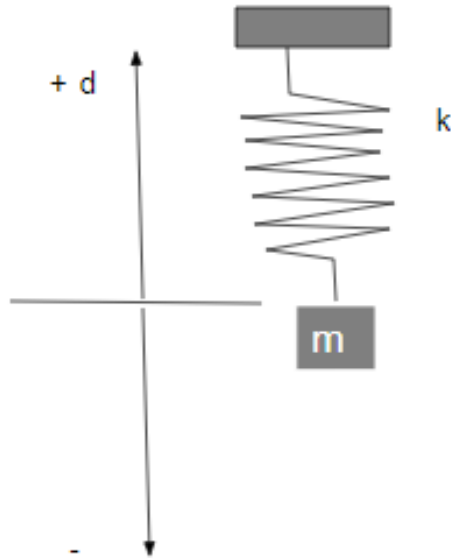


Figure 3.11: Mass/spring system. Image from Cook (2002)

F_s represents spring force and k is spring constant

$$F_d = -c \cdot \frac{dx}{dt} \quad (3.18)$$

F_d damping force, that reflects the loss against motion and c damping coefficient

$$F_g = -g \cdot m \quad (3.19)$$

F_g is a gravity force. It is neglected sometimes.

The main advantage of the model is that it allows describing displacement dependence on applied external force.

The time-dependent solution to the presented simple system is:

$$d(t) = d_0 \cdot \exp\left(\frac{-c \cdot t}{2m}\right) \cdot \cos\left(t \cdot \sqrt{\frac{k}{m} - \frac{c^2}{4m^2}}\right) \quad (3.20)$$

As a result of applied external force (displacement d_0), the system returns to equilibrium without oscillating or oscillates with amplitude gradually decreasing to zero or with a natural frequency.

There is a relation between conventional digital sound processing techniques and general numerical approaches to model complex vibrating/deforming systems via mass/spring systems. As described in Cook (2002), the solution for a basic model can be approximated

with digital filters. In introduced above mechanical mass/spring system, the oscillations are approximated with standard infinite response filter (IIR) filter, those parameters depend on mass, stiffness and damping coefficients, and the use of initial impulse as input. The sound produced by 2D and 3D vibrating systems those deformations are represented with mechanical mass/spring system can also be modelled with similar 2D and 3D digital waveguide systems (Duyne & Smith 1993), (of York n.d.), (Hacihabiboglu et al. 2008).

Modal synthesis The conventional technique to approximate a real-life sound is based on (Fast Fourier Transform) FFT analysis. In basic case the sound is approximated as a sum of partials, modal modes N' , that can be extracted with audio signal processing techniques like Fourier Transform (see Bonneel et al. (2008)):

$$s(t) = \sum_k^{N'} a_k \cdot e^{-\alpha_k \cdot t} \cdot \sin(w_k * t) \quad (3.21)$$

where $\sin(w_k * t)$ are oscillations of modes with frequencies w_k , $e^{-\alpha_k * t}$ - oscillations attenuation in time.

In terms of sound produced by an auditory object (that can be a music instrument), its vibrations are a sum of "modes" characterising object's geometry and internal properties through the sound. The modal synthesis approach takes advantage of this idea and states that the frequencies of the modes do not change for an object (van den Doel & K. Pai 2003). Only the coefficients are weighted as a result of the place of interaction and applied force. Such modes are obtained experimentally by the processing of the recorded sounds (Ren et al. 2013) or analytically via consideration of the relation between a set of modes and sound propagation paths in geometry (Essl 2002). Let us consider the details.

We can approximate the physical object geometry and internal structure with one of the methods of discretization (finite element, finite differences) and model the displacement of each node to compute sound produced by the vibrating object. In O'Brien et al. (2002) demonstrates that as displacements for sound are small the following equation, representing displacements dependence on the force, will describe the system:

$$K \cdot d + C \cdot \dot{d} + M \cdot \ddot{d} = f \quad (3.22)$$

where K, C, M are stiffness, damping and mass matrix and d is displacement vector. Linear algebra matrix transformations allow obtaining the equation that directly states that forces depend on a set of oscillators, those parameters are defined with a diagonal matrix of eigenvalues. The equation states that those oscillators, conventionally modelled with

mass-spring-damper system, do not interact with each other O'Brien et al. (2002) . The system can be decomposed into modes of certain frequencies and only initial amplitude and attenuation parameters are changing. This property is often referred to as "modal shapes". The eigenvalues for modes depend on stiffness and mass for each mode.

The conventional rigid-body simulation can be deployed to compute objects deformation modes or finite element methods to explicitly model the response of an object to external forces and generate audio as a result of computed surface behaviour O'Brien et al. (2002). The additional post-processing with filters extracts the range of produced frequencies within the human-perceived range.

The modal synthesis idea also is extended with the concept of modal resonant filters (Cook 2002), that can be used as an alternative to complex mass/spring systems (see paragraph 3.5.2 below). The general decomposition scheme is presented in Fig. 3.12.

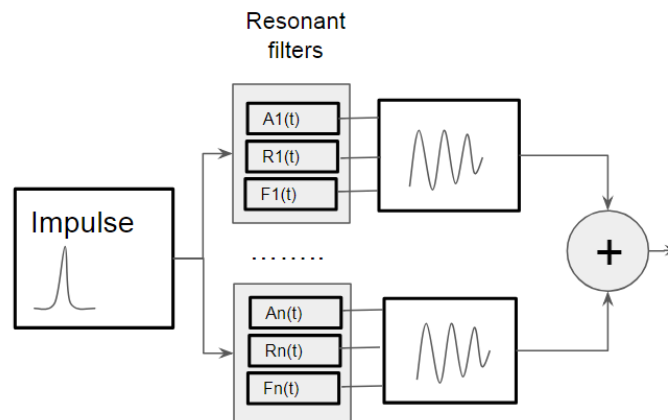


Figure 3.12: Modal resonant filter based synthesis, schematic representation from Cook (2002)

Digital waveguide synthesis One of the aspects of physically-based modelling is a consideration of how sound propagates through space. This propagation may consider sound acoustics area (considered in next section), modelling how sound travels through space to calculate impulse response, or sound synthesis area, where the waveguide approach used to model sounds being produced by objects (Cook 2002).

The start point for digital waveguide synthesis is a travelling wave solution for plucked string. The general solution described in Smith (1992) for sampled plucked string travelling wave $y(x, t)$ can be represented as a sum of rightgoing $y_r(x - ct)$ and leftgoing $y_l(x + ct)$ waves in Fig. 3.13 (a).

In the digital domain, that operates "sampled waves" the solution of the travelling wave can be formulated through spatial samples or digital delay lines. For the variables x, t

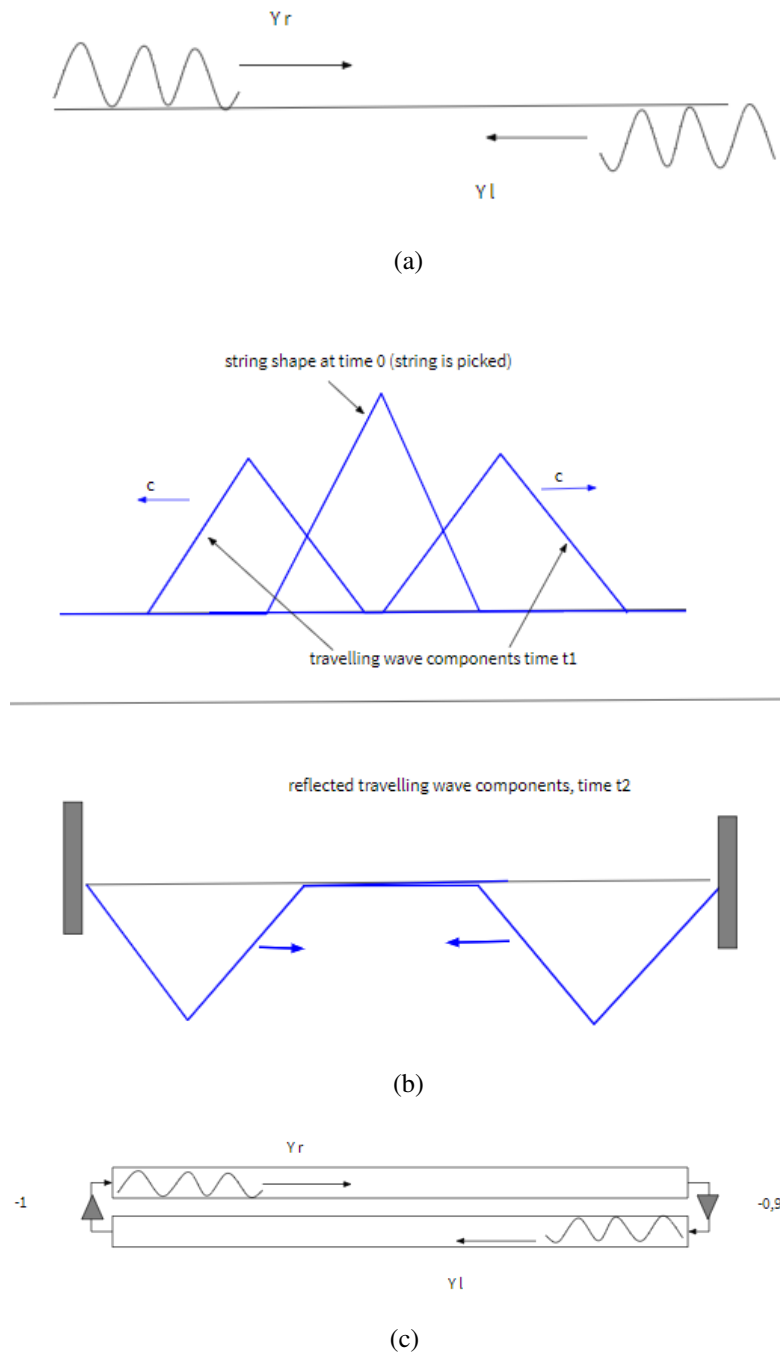


Figure 3.13: Simulation of ideal string a) Basic idea of describing string through travelling wave components $y(x, t) = y_r(x - ct) + y_l(x + ct)$. b) A schematic representation of travelling wave components as string is picked through time c) Waveguide string model with loss

changing $x \rightarrow x_m = mX$, $t \rightarrow tn = nT$, where $X = cT$. y^+ rightgoing component and y^- is leftgoing component, the physical output is:

$$y(t_n, x_m) = y^+(n - m) + y^-(n + m).$$

In other words, a string displacement at sampling point x_m is equal to upper and lower rails at position m along with delay-line pair (Smith 1992).

Those right and left waves are a source of the initial impulse. Considering the boundary and initial conditions, such as a pick position, fixed edges, etc., we get the description of those travelling waves in time (see Fig. 3.13 (b)). In lossless case, a travelling wave between two points in the medium can be simulated using a digital delay line as the initial conditions are injected through input $x(n)$. In a general case, the losses and dispersion are lumped at discrete points (Smith 1992),(Cook 2002).

The Fig. 3.13 (c) summarise the idea of waveguide technique of modelling vibrating string, that is described in Cook (2002). The -1 at left models the wave reflection with the inversion of the wave displacement (fixed string edges, like a guitar string). The -.99 on right models an amount of loss that happens due to internal damping, viscous losses, etc.

The basic idea of the 1D digital waveguide described above was extended for cases of sound propagation in 2D Meshes (Duyne & Smith 1993),(Murphy et al. 2007), that is the case of modelling sound propagation in plates and membranes and has a potential for 3D modelling (Savioja & Välimäki 2002, of York n.d., Hacıhabiboglu et al. 2008).

The Essl (2002) extends the idea to the banded digital waveguide, that states that each mode is activated by travelling ray and final obtained sound depend on the ray path. The final signal is a contribution of all modes. The approach in Cook (2002) unites the ideas introduced in modal and waveguide synthesis. Banded waveguides use sampling in time, space and frequency, as each mode is modelled with a bandpass filter and a delay line. The main advantage of digital waveguide approach as its computation is quite efficient in terms of time and it allows obtaining quite good results (Kapur et al. 2015),(Cook 2002).

The methods used in the digital waveguide and modal synthesis may seem quite similar. However, as summarised in Essl (2002), modal synthesis is based on filters and use of delay lines and bidirectional delay lines, combined with filters use is the main characteristic of Waveguide synthesis.

3.5.3 3D spatial sound computation

Basic techniques of computation of sound that is produced by a vibrating object (can be a musical instrument) are zero-dimensional as they take into account only frequency component and ignore spatial component(Cook 2002). However, the spatial component is crucial for such

areas as computation of sound in acoustic environments (Murphy et al. 2007) or computation of binaural sound.

Depending on problem and level of realism the research used either the 3D structured waveguide meshes or more simple concept of 3D ray propagation paths (Cook 2002). The latter approach uses the propagation similar to computer graphics ray-tracing and mixes it with conventional digital sound processing techniques to address the problem-specific features: individual ray paths are modelled as delay lines, attenuation spreads linearly with distance, etc.

3.5.3.1 Modelling 3D sound propagation through environment

The similarities between sound propagation and visual stimuli rendering are of particular interest in this research. As stated in Takala & Hahn (1992), the principles of light and sound propagation are very similar. They share the wave nature. A wave equation is a general equation that describes a wave propagation through time and wave pressure:

$$c^2 \nabla^2 p = \frac{\partial^2 p}{\partial t^2} \quad (3.23)$$

The propagation of sound and light follows the Huygens principle, that states that every point on a wavefront acts as a spherical wave source. The intensity I at distance r as function of sound source strength P (Elorza 2006):

$$I = \frac{P}{4 * \pi r^2} \quad (3.24)$$

Absorption happens during propagation in air and is described with distance-dependent amplitude exponential attenuation or attenuation as a result of contact with objects. In Elorza (2006) it is described with the equation, similar to those that can model light absorption mechanisms that it passes through semitransparent objects:

$$A(d) = A_{ini} \exp^{-\alpha d} \quad (3.25)$$

,where absorption coefficient α depends on angle of incidence $A = A_{ini}(1 - \alpha)$.

The modelling of realistic sound with sound wave propagation is computationally expensive because it considers all complex interaction with various objects (Röber et al. 2007). A simplification can be made that neglects the wave nature of sound and makes the process very similar to optical properties modelling and rendering in computer graphics. The approach allows real-time spatial sound modelling in interactive environments (*VRWorks - Audio* 2018). Let us discuss the foundation of such techniques.

Sound propagation through the environment can be conveniently modelled in terms of transmitted energy and similarly to optical properties modelling. Following the similarities in light and sound propagation, an acoustic rendering equation was proposed as a time-dependent extension of Kajiya's rendering equation (Siltanen et al. 2007). The outgoing time-dependent acoustic radiance from point x in direction w_j is calculated as:

$$l(x, \omega_j) = l_0(x, \omega_j) + \int_S R(x', x, \omega_j) l(x', \frac{x' - x}{|x' - x|}) dx', \quad (3.26)$$

See Fig.3.7 for similar optic terms in Kajiya's rendering equation 3.5 in section 3.4.1.2 and basic notation used. Here:

$l(x, \omega_j)$ - ongoing acoustic radiance from x' in direction of ω_j

$l_0(x, \omega_j)$ - initial emitted acoustic radiance from x in direction of ω_j that in case of area sound source represent the radiance emitted by the surface (can be compared to optical term $L_e(x, \omega_j)$). For details on calculation for area, point and omnidirectina point sound sources see (Siltanen et al. 2007)

$R(x, x', \omega_j) = v(x, x') * \rho(\frac{x - x'}{|x' - x|}, \omega_j; x') * g(x, x')$ is a reflection kernel in acoustic equation. As the reflection occurs from point x via point x' into direction w_j , a reluctance function includes a visibility and geometry term:

$v(x, x')$ a visibility term (similar to optical term)

$g(x, x')$ acoustic geometry term (similar to optical term), but contains an acoustic propagation operator: $S|x' - x|$. The operator takes into account speed of sound c and distance between points x' and x and as demonstrated in (Siltanen et al. 2007) can be applied to impulse $\delta(t)$ to compute the response of impulse energy in reflections with absorption and as a result used for computation of propagation effects for any initial sound with delays based on reflection paths lengths(see discussion on linear system properties in section 3.5.1).

$\rho(\Omega_i, \Omega_o; x)$ - an acoustic Bidirectional reflectance distribution function (BRDF) at point x for incident angle Ω_i of $-w_i$ direction between normal on object surface at x , and outgoing angle Ω_o between $-w_i$ and normal on object surface at x' .

S is a set of all surface points in the enclosure.

Thus terms in equation 3.26 above are distance-dependent, as they are expressed via neighbour points x and x' as wave travels and sound speed dependent due to propagation operator S .

At any point, the receiver detects a sum of direct and reflected sound energy that has reached him by a particular time t . The model in equation 3.26 is a justification of geometric acoustic modelling methods, like image source methods and ray-tracing. The model allows a sound material interpretation of how an object interacts with a sound wave or acoustic conditions of surface(Savioja & Svensson 2015) and allows the computation of time-dependence

of the impulse response (acoustic) of the acoustic environment depending on the position of source/sources and receiver or listener.

Like the light, modelling sound propagation with ray-based methods can consider only primary (direct illumination) or primary with secondary rays (global illumination) (Röber et al. 2007) (see Fig. 3.16). To calculate the secondary sound waves, the algorithms of Monte-Carlo path tracing and beam tracing are used for better sound rendering (Funkhouser et al. 1998). Depending on the considered problem, the complexity of ray-tracing is reduced and in some cases, the secondary rays can be removed for simplicity whilst still allowing to synthesize the good physically-based sound (O'Brien et al. 2001). Computation of properties of acoustic environments (concert halls, etc.) conventionally split the process into three steps (Gardner et al. 2000): a direct sound that is similar to the computation of objects "visibility" in conventional visual ray-tracing; early reflections that can be compared to ambient occlusion (AO) approximations of illumination from nearby surfaces and late reverberations (fully global illumination). For the case of acoustic rendering such division also is important not only for simplification introduced to remove part procedures that describe high computational expensiveness bring a little increase in quality but the fact that those free types of reflections demand consideration of different processes that should be addressed for sparse and dense sound reflections produced on second and third stage accordingly (Chen et al. 2007).

Thus, similarly to geometric optics that neglects the fitness of the wavelength (Ament 2014), the geometric acoustic methods apply the same idea. However, despite similarities with light, the research considers several assumptions for sound propagation that is different nevertheless, such as:

1. Sound travels slower than light and we can perceive its time dependence as it interacts with objects. The sound propagation time dependence is the main feature that should be taken into account as one model sound propagation through the environment, or how the final signal is formed from initial impulse in a vibrating object.
2. Unlike light propagation modelling, sound modelling is considered a large area of time-dependent frequency bands (Röber et al. 2007). This difference in the light and sound perception results in two ways of modelling the sound. Model sound propagation for lower frequency waves is modelled as a wave, while middle and higher frequencies ranges are modelled with geometry techniques with the sound is treated as a ray or directed line segment. Geometric approach results in the suggestion that sound waves are much smaller than the obstacles in the scene unless the obstacles are too small and can be ignored (Funkhouser et al. 1998).

3. Most materials have specular properties for sound waves, so unlike for light interaction, specular reflections dominate diffuse ones (Funkhouser et al. 1998).

3.5.3.2 Sound-listener interaction

Headphone based sound specialization systems for exploration of sounds in space is one of the most often used as it does not demand expensive hardware. The system takes advantage of the Head Related Transfer Function(HRTF).

Human are able to localise objects in 3D space due to sound wave interaction with human ear (see Fig.3.14 (a)), head and torso (see Fig.3.14 (b)). The main perceptual cues for 3D localisation are interaural differences in time and level, spectral, distance and dynamic cues evaluated as a result of propagation to left and right ear (Huang & Benesty 2004) (see Fig. 3.14(a) and Fig. 3.15). Ideally HRTF is computed for user (Gardner 1994), (Röber et al. 2006) function of direction, distance and frequency that is defined as Fourier Transform of head-related impulse response (HRIR) (frequency domain view).

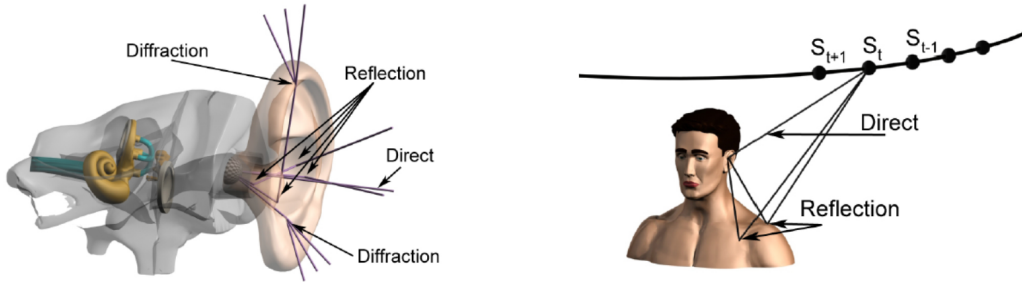


Figure 3.14: Impulse response for ear modelled as a result of propagation(a) and entire scheme for HRIR ray-tracing (b). Images from (Röber et al. 2006)

Application of HRTF suggests extraction of HRIR coefficients and delays and sound convolution. A sound source coordinates are matched with HRTF coordinates and HRIR coefficients and delays are interpolated via bilinear interpolation as the measurements are discrete (Wu & Yu 2016). The sound pressure for left and right ears H_L and H_R (see Fig. 3.15).

$$H_L = \frac{P_L(r, \theta, \phi, f)}{P_0(r, f)}, H_R = \frac{P_R(r, \theta, \phi, f)}{P_0(r, f)} \quad (3.27)$$

where sound source is defined with spherical coordinates (r, θ, ϕ) , P_L and P_R complex sound pressure at the entrance of left and right ear and P_0 is complex sound pressure at centre of listeners head.

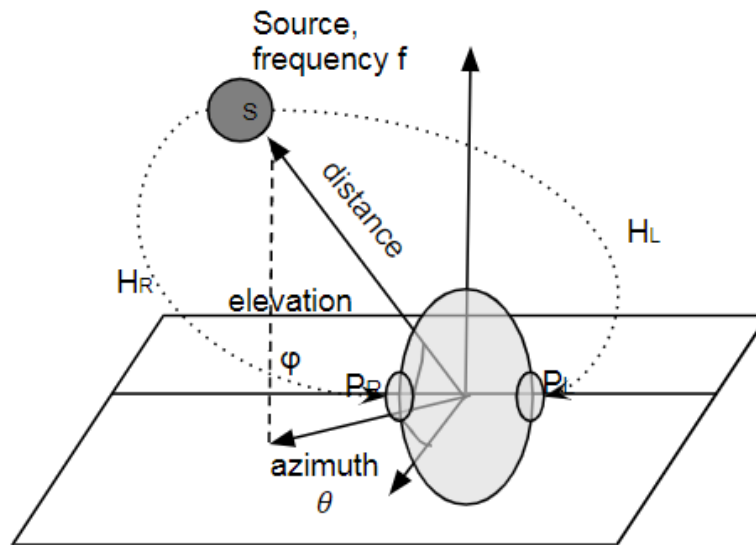


Figure 3.15: HRTF scheme

For simplicity, the virtual environments use a general, not individually computed HRTF (Wenzel et al. 1993, Wu & Yu 2016). Moreover, research introduces additional simplifications. The main problem of precise modelling of total 3D spatial sound is its computational expensiveness. The model considers interactions that occur in the spatial environment and interaction with user (Röber et al. 2006) and precise model considers all interactions (apply convolutions) that form the 3d output. The direct HRTF application of such a binaural display yields a computational cost that scales linearly with several sound sources (Adams & Wakefield 2005). Similarly to light sources, the realistic simulations require consideration of the shape and orientation of sound source (Elorza 2006) that may lead to additional challenges. For the problem of visual stimuli rendering, this is beyond interactive techniques and is an area of constant recent research (Moreau & Clarberg 2019),(Wyman 2020). For sound, the problem imposes an additional challenge on the stage of consideration sound/listener interaction for several auditory objects that can move in space (Adams & Wakefield 2005). Computation of sound spatial properties for big amount of auditory objects localised in different areas of acoustic environment is not straightforward as in addition to ray-tracing impose HTRF application challenges (Adams & Wakefield 2005, Chanda et al. 2006).

Conventionally, the interactive environments introduce simplifications to address the problem. The propagation of sound in the environment or "room effect" was included as a part of HRTF, although the technique assumes HRTF adjustment for dynamic environments

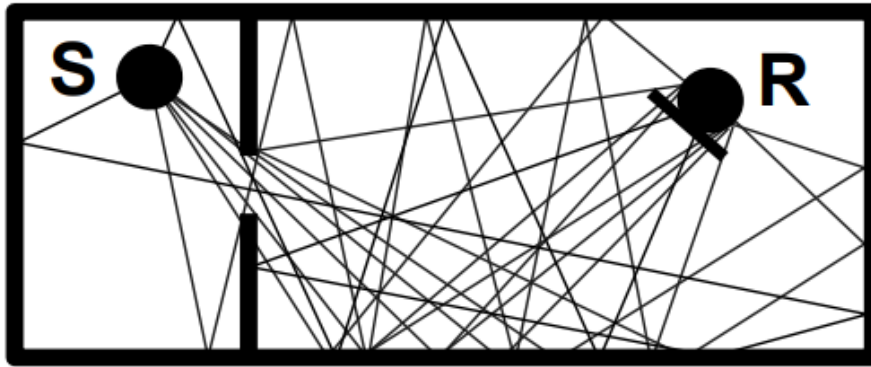


Figure 3.16: Reverberation paths. Image from Funkhouser et al. (1998)

(Barrass & Vickers 2011). Multiple sound sources grouping/clustering approaches were considered in (Chanda et al. 2006), (Adams & Wakefield 2005).

3.5.4 Auditory analysis of generated sound wave

The main requirement to traditional Volume Rendering transfer function (Kniss et al. 2002) is to highlight features of interest via optical attributes, which normally are colour and opacity. Similarly, the auditory model considers the mappings that allow the user to perform analysis with perceived sound wave properties. Depending on the type of auditory mappings, the mixture of sounds reaches the user's ears. The human auditory system processes sound mixture for further interpretation and analysis.

An area of Auditory Scene Analysis (ASA) forms a general background for analysis with auditory stimuli. The area considers how the user perceives the sound, automatically performs such procedures as segregation, integration, considers memory issues in performing those procedures and final interpretation of auditory stimuli (A.S. Bregman 1990),(Sussman 2017),(Sussman 2005). Such areas as hearing aids design, sonification (McGookin & Brewster 2004), music processing (Brown & Cooke 1994) take advantage of those concepts to improve and justify their techniques. As stated in (A.S. Bregman 1990) the user applies ASA principles in two steps:

1. Acoustic signal is decomposed into 'sensory components', that are likely to have been produced by the same event with one or several activated simultaneously sound sources.
2. The user automatically groups obtained sensory component into structures that are processed and interpreted conventionally on a higher level. For grouping, an associative

knowledge of familiar patterns or directly acoustic data is used ("schema driven" and "primitive") (A.S. Bregman 1990).

The principles of ASA play an essential role in the design of auditory tools and are a justification of the principles of sonification techniques (McGookin & Brewster 2004). Let us consider a particular class of approaches to auditory mappings, that take advantage of music theory (Trainor 2015a) and commonly referenced as musical systems (Neuhoff 2011). Musical systems are one of the most well studied by ASA approaches (Trainor 2015b) and is the most structured auditory cognitive representations (Neuhoff 2011).

The approach is extremely flexible in terms of establishing relationships between the auditory mapping and their further perception/interpretation aspects for the users with different level of musical training, starting with no musical experience at all. Such approaches take advantage of the musical experience or a more common user experience of orchestra sound (A.S. Bregman 1990). For orchestra sound, the user automatically separates into several streams related to musical instruments, may neglect the background noise. An average user ear performs basic segregation in everyday life. Moreover, users with music training can "extract" the sound patterns and interpret them as music scores. The area of functional ear training establishes the rules to teach musicians to perform such lower-level analysis of music and recognise and extract from sound such music concepts as "chord sequences"(Trainor 2015a).

If an auditory analysis is considered for an untrained user, the basic auditory dimensions are pitch, loudness and timbre (Neuhoff 2011). The auditory parameters are defined by physical characteristics of a sound wave such as fundamental frequency, amplitude or physical intensity and contribution of a sum of partials into a sound wave. As we have considered in section 3.5.2 are shaped via modal and/or digital waveguide techniques.

The complex sound wave that reaches our ears as a result of vibrations of several objects, where the vibration of each object consist of several sub-waves of partials. Our auditory system (Cook 1999) extracts fundamental frequency that is perceived as pitch or tone and contribution of a sum of partials that form sound quality or timbre characteristic. The last can be described as a sound characterising a particular music instrument that it is producing.

We can rewrite equation 3.21 for the vibration produced single auditory object in the following form for all its modal oscillations:

$$M_i(t) = a_i \cdot e^{-\alpha_i t} \cdot \sin(w_i * t) + \sum_j^N a_j \cdot e^{-\alpha_j t} \cdot \sin(w_{ij} t) \quad (3.28)$$

Here, the sound wave fundamental frequency w_i is directly perceived as pitch and another sum of partials that form timbre characteristic that distinguishes the music instrument.

Among them there are "harmonics", the frequencies related to fundamental as $w_j = jw_i$, where $j = 1, 2, \dots, N$. The harmonics support the pitch perception (Trainor 2015b).

A basilar membrane in human ear automatically performs a sort of Fourier analysis, decomposing a complex sound into frequency components such as in equation 3.21 and maintain them separate channels and further reintegrate them once again in cortex to associate with a sound produced by a particular auditory object with pitch and timbre (Zatorre 1988, Trainor 2015b).

On a basic level, the music systems organise the musical pitch into tonal structures, where the listeners operate and analyse the intervals between two or more pitches of sound waves. Such organisations are studied in music theory as tones within musical scales (Lerdahl 1988). The scale establishes the rules of how each note of the scale is related to the others in terms of pitch relations (Balzano & Clynes 1982). Similarly, the music training techniques often take advantage of the human ability to remember the entire pattern a distinguish the unique interval relationships between each note in the scale and the central one - the tonic (Benbassat n.d., Balzano & Clynes 1982).

The rules of combinations of such tone sequences are an essential part of composition and improvisation. For music systems, assuring that generation of sequences of sound ques is happening according to music scales establishes the formal structure for effective auditory interface building and further analysis and interpretation of auditory stimuli (Vickers & Alty 2002), (Jordan & Shepard 1987).

Moreover, the established rules of perception of intervals between pitches are a basis for technique further extension with much more complex mappings to complex sounds produced by several vibration objects at the same time. The human auditory system is capable of extracting pitches associated with fundamental frequencies w_i and grouping them into musical entities defined within music theory, such as intervals, chords:

$$M(t) = \sum_j^N M_i(t) \quad (3.29)$$

Such mappings provide an additional auditory dimension for perception and analysis, although the complexity is limited by user musical training and experience (Neuhoff et al. 2002). Most cases are limited to extraction up to 3 fundamental frequencies w'_i, w''_i, w'''_i .

In total the human ability to operate and analyse familiar auditory patterns (Winkler et al. 2009), including tonal ones (Watson et al. 1975) much depends on memory issues (Bianco et al. 2020).

The musical systems also have proved to be highly flexible for cross stimuli visual-auditory interpretations and analysis (Brown et al. 2015). For analysis, a set of feature-based

sensory representations should provide insight into object properties. Often visual and auditory sensory stimuli processing is compared together via Gestalt rules that allow grouping low-level features into visual (Ben-Av et al. 1992) and auditory (A.S. Bregman 1990) objects. The later is referenced as ASA and grouping principles are based on similarities on the temporal or melodic level, coherent changes in loudness, frequency and harmony.

The approach can be further augmented with consideration of several auditory objects, in general case dynamic. We recognise and distinguishes several simultaneously vibrating auditory objects not only due to decomposition to harmonics (Trainor 2015*b*) that we have discussed above, but as well operate spatial sound properties that are formed as a result of propagation in an acoustic environment. The wave that is generated as a result of several sound sources the user can localise those objects spatial positions, track them in space, etc. Light and sound in the environment can be automatically transformed into a set of cues, associated with spatial substructures of complex objects such as heterogeneous structure. Those properties can be further interpreted according to user subjective real-world visual and auditory experience.

3.6 Interactive exploration and multimodal feedback

3.6.1 Overview

Multi-sensory interactive exploration is conventionally used to overcome the limitations of conventional visual analysis (Moloney et al. 2018). For complex phenomena analysis, the introduction of multisensory stimuli can enhance the conventional user interactive exploration of complex phenomena, such as facilitation of the analysis process via a selection of a region of interest (ROI). The procedure is a conventional tool for getting insight into complex phenomena (Lee et al. 2018) or handling initial complexity and replacement or refinement of computationally expensive segmentation procedures (Laha & Bowman 2013).

The user interaction in the analysis of scientific heterogeneous objects can involve a wide range of geometric interpretations, especially if the interaction with multi-dimensional volume data is considered (Ward & Yang 2004),(Manssour et al. 2001). Also, the analysis of scientific phenomena may involve the interactive measurements performed over the spatial distribution of heterogeneous components or facilitation of collaboration and self-positioning tasks (Donalek et al. 2014), (Goddard et al. 2018).

The conventional and multimodal user interaction in the context of visual analysis operates one or several of the procedural blocks of the visualisation pipeline (Filtering, Mapping, etc.) (Kalkofen et al. 2011), (Sua et al. 2015), (Roberts et al. 2014). In the general

case, the process involves the interactive changes of visual properties (optical model) and geometry in the virtual scene as a result of selection and manipulation tasks.

In this research, we consider the user exploration task in the context of conventional techniques for interactive manipulation or measurements for heterogeneous phenomena:

1. Through a user interface (UI), by operating a numerical values/ranges of available data attributes, virtual scene optical properties, etc. We are particularly interested in the case of changing optical properties of visual-auditory scene (Zhou et al. 2012),(Kniss et al. 2002).
2. Through introducing an interaction widget (Dai et al. 2013, Hanwell et al. 2015) or avatar (Schwind et al. 2018, Hartling et al. 2004) that that in general case can be arbitrary volume object. The last ones are used in modern research to provide a complex spatial input that is not easily replicated (Hartling et al. 2004) or should reflect specific features of interaction devices (Ostaduy & Lin 2005).

The user interaction with volume objects within virtual reality environments is more challenging compared to surface objects (Kalarat & Koomhin 2019) as it is more computationally demanding (Hänel et al. 2014),(Scholl et al. 2018).

Below we discuss the introduction of avatars and widgets that is a part of complex user interaction, including hand-based interaction (Phillips et al. 2010) (Hoell et al. 2018) that in modern research context involves gesture control devices such as Leap Motion (Laha & Bowman 2014). The ray-casting is highlighted as a core of user interaction for exploration of virtual objects, selection and manipulation tasks. Moreover, the interaction with heterogeneous objects imposes a challenge of exploration of both volume and spatial subdivision properties. The example of the second type of interaction uses ray-casting for real-time measurements (Phillips et al. 2010) that can be a core of evaluation of specific physical properties that are considered in phenomena simulation (Bryer et al. 2019).

We also explore the role of continuous multi-dimensional modelling with GPU acceleration to address the high update rate and sampling issues in modelling and rendering of several sensory stimuli feedback. We discuss the general similarities that rendering to several sensory stimuli shares as well as bottlenecks reflected in various multi-sensory research areas that can be crucial as simultaneous rendering to several sensory stimuli is considered.

3.6.2 Widgets and avatars

In virtual, augmented and mixed environments the multi-sensory feedback often accompanies basic user interactions just as a simple notification. The users have difficulties in

understanding how interaction occurs only due to visual information as multi-sensory cues that are present in the real environment are not integrated into virtual. The understanding and perception of interaction process highly depends on a conventional for scientific visualisation concept of widget (Kniss et al. 2001) or more extended concept of avatar (Schwind et al. 2018),(Hartling et al. 2004) , that represents a virtual copy of the interacting object in physical space, such as interacting haptic device (Otaduy & Lin 2005), hand (Cakmak et al. 2020) or a real person (Leyrer et al. 2011)

The user interaction starts from the identifying of virtual space and a physical environment relationship and where user interaction takes place and positioning of 3D objects such as interaction cursor or avatar. Within the considered virtual scene perception paradigm (Backhaus et al. 2019),(Silva et al. 2019) and the demanded precision of multisensory interaction, there also can be tracking of one or several additional devices. The devices provide information necessary for rendering into sensory stimuli, such as the viewing direction for visual stimuli or listener's head position for auditory stimuli (Berger et al. 2018),(Hurter et al. 2018). In general, the tracking procedure depends on the calibration of external device (Nie et al. 2019, Sarkka et al. 2017) for estimation of parameters of an error model for positioning in the current situation and for the current user. In consumer devices such as eye-gaze (Silva et al. 2019) or gesture control devices (Cakmak et al. 2020) the procedure is usually simplified. This allows the input devices to perform related measurements or track interaction features in a real environment, such as position, orientation or more complex point cloud data that describes an interacting volume to be reconstructed (Izadi et al. 2011) that most often is human hand (Cakmak et al. 2020).

The user interaction is based on the combination of ray-casting and geometric modelling. The process may involve such procedures as collision detection, geometry free form deformations (Seyb et al. 2019a) and pointing operations. The ray-casting is the most common technique for pointing and manipulation (Baloup et al. 2019, Nukarinen et al. 2018). The viewer position in 3D space that is modelled with a virtual camera positioning. In a basic case we obtain the 3D position of the cursor by transforming its 2D coordinates in the camera image plane. Pointing eye-rooted techniques (Argelaguet et al. 2008) also compute the ray-casting direction depending on eye viewing direction, in other words, the virtual camera orientation. This parameter can be obtained with head-tracking, eye-tracking devices or conventionally is defined by mouse input(Saket & Endert 2018). The gestures highly depend on the ability of a self-location to coordinate head, arm, fingers. Current gesture control and VR systems actively use ray casting methods based on different parts of the body, most often head and hand tracing (Argelaguet et al. 2008). A mid-air pointing direction that is one of the main gestures and virtual object selection and derived by ray-casting and further error

compensation models improve this direction (Schwind et al. 2018). Also, machine learning techniques (Fiebrink & Cook 2010) are used for improving the stability of the system.

After the positioning parameters are identified, the selection and manipulation with an object and multisensory rendering are executed. A sense of presence and engagement with the immersive virtual world is possible only due to high quality real-time multi-sensory feedback computation. The procedure often involves computationally expensive geometric modelling. The multisensory rendering for user interaction considers the shape of cursor/avatar (Otaduy & Lin 2005). The realistic sound and haptic feedback computations take advantage of the second Newton law or Hooks law for simulating the real-life user exploration process. Collision detection and computation of the parameters of "assumed penetration" (Zilles & Salisbury 1995) , (Ruspini et al. 1997) (see Fig. ??) into object is used to compute distance/displacement parameters that are directly used within force-dependent haptic/ auditory rendering model. As a result of collision detection, a force is computed for each contact point and feedback is described by the amount of penetration and object behaviour (non-rigid, rigid). The simple model considers avatar as point object for a Hooks law based interaction model (Otaduy & Lin 2005) (see Fig. ??). More realistic models take advantage of mass-spring-damper (McNeely et al. 1999) and depend on the geometry and properties of the interaction avatar as the collision parameters computed for several contact points (6DOF rendering).

As we discuss later, the time-dependent nature of user interaction has to be taken into account and continuous modelling should be performed to address the quality issues of multi-sensory rendering. Below we discuss the aspects of multi-dimensional geometric modelling in user interaction procedures (Xu & Barbic 2017).

3.6.3 Continuous multi-dimensional modelling and sampling issues in real-time user interaction

Similarly to conventional visual stimuli rendering, the quality issues of multisensory feedback are related to sampling issues that are stressed on geometry modelling and rendering stages. The real-time multi-sensory rendering is often challenging due to the need of the high update rate in the context of computationally expensive procedures execution and as a bidirectional task (Rubin 2016).

The haptic and auditory stimuli are more demanding than visual one. Compared to visual rendering 30Hz update rate, the good quality feedback in haptic rendering demands 1000Hz and auditory 44,100 Hz. Sound and tactile feedback are both perceived in time and as a result of pressure or displacement and share a lot in common in terms of representation and

rendering (Rubin 2016), (Strohmeier & Hornbæk 2017). The output representations for visual/auditory and tactile stimuli are discrete and often use the digital sampled sound wave representation (Freeman et al. 2017) or deploy the principles of acoustic radiation force that is a core of ultrasound haptic devices and tactile model it renders (Long et al. 2014).

In the context of bidirectional tasks and cross-modal rendering, when quality depends on algorithms efficiency, the efficiency of rendering to several sensory stimuli and features and limitations of output devices, the high update rate related issues are not easy to control. The problem is addressed with the active combination of the GPU acceleration structures (Salisbury et al. 2004) and GPU geometric modelling (Xu & Barbič 2014, Van & Bergen 2004). With simultaneous rendering to several sensory stimuli, one can observe accumulation of the sampling-related issues that appear on various stages of analysis pipeline. User interaction involves real-time geometry modelling and stresses limitations of resolution-dependent or sampled representations Fuhrmann & Sobottka (2003) arise. Moreover, the problem demands consideration of the time-dependent nature of user interaction that involves a multi-dimensional continuous representations (Xu & Barbič 2014). For high-quality tracking of avatar/virtual scene interaction event, a sweeping of avatar surface trajectory is computed to avoid "slipping" into small gaps or the "tunnelling" effect (Xu & Barbic 2017). The model uses multidimensional modelling and projection into 3D space to detect the exact time of contact within a specified time interval.

As discussed above, the implicit, SDF and voxel representations are very convenient for geometry modelling tasks with high-resolution requirements (Crassin 2011). Within the context of high requirements of multi-sensory rendering and multi-dimensional geometry modelling (Pasko et al. 2001) these two are most often used representations. The SDF representation is a convenient tool to address continuous collision detection in haptic rendering (Xu & Barbic 2017) and is well known for its flexibility in terms of interactive geometric modelling. The crucial advantage of SDF representation is its conventional reliance on the GPU implementation (Schmidt 2020),(Jiang et al. 2019) that allows efficient support for wide range of computationally expensive operations. Similarly to more general implicit representations, SDF can be defined procedurally (Schmidt 2020), as an interpolation of discrete field (He et al. 2020),(Friskens et al. 2000b), skeleton defined (Koschier et al. 2016) or used to reconstruct the initial skeleton (Van Uiter & Bitter 2007),(Tang et al. 2020). The latter category is also the most promising in terms of advantages of hybrid modelling. Conventional implicit modelling with LOD is done on a base of subdivision-curves that are used as a skeleton and allow for flexible control of local changes in blending and deformation (Angelidis & Cani 2002). Such hybrid modelling allows for control of topology of the shape and provide high flexibility for interactive modelling (Cani & Hornus 2001). The SDF

modelling moreover can combine those advantages with specialised ray-tracing techniques to design highly flexible and predictable deformation procedures as a result of user interaction (Seyb et al. 2019b).

Many complex procedures involved in user interaction, such as collision detection, can be treated as a ray-tracing problem combined with GPU geometric modelling accelerated with conventional ray-tracing acceleration structures (Xu & Barbič 2014, Van & Bergen 2004). Construction of BVH over geometry structure for effective collision detection is conventional strategy (Wang et al. 2018), which might be not straightforward for dynamic geometry modelled within spatial subdivision (Garanzha 2008, Pantaleoni & Luebke 2010). As it was demonstrated in (Han et al. 2019), specifying a class of input geometries is a key to finding the most optimal bounding volume structure for the procedure efficiency. To handle more general cases of interaction and dynamic deformations (Tsai 2017), the implicit bounding volumes were considered in (Nguyen 2006). The other approaches take advantage of several layers of bounding volumes within acceleration structure (Han et al. 2019) to facilitate intersection with complex geometry and combine the technique with geometric modelling (Gourmel et al. 2010a). Initially applied for continuous surface reconstruction or modelling tasks the techniques demonstrate acceleration ability not only in terms of optimal bounding volumes construction but a reduction of the evaluation of complex geometry (Parulek & Viola 2012, Gourmel et al. 2010a) that is constructed on top of several elements. The potential speed up mostly depends on the amount of reduced evaluation complexity (Gourmel et al. 2010a).

Thus the continuous, GPU accelerated multidimensional modelling is very convenient real-time multi-sensory user interaction as it provides continuous functions for convenient sampling to multi-sensory output only on rendering stage (Xu & Barbic 2017). In this terms, the SDF representation is very convenient as it combines geometry modelling with the GPU hierarchical structures acceleration (Lehericcy et al. 2015) for more efficient evaluation of ray-casting based time-dependent intersection (Van & Bergen 2004).

Chapter 4

Theoretical framework

4.1 Overview

The visualisation of multi-scale heterogeneous objects is challenging as it simultaneously operates spatial subdivision and volume nature of multi-scale properties that are represented differently. The heterogeneous object's representation is computed as a result of an experimental study, computer simulation or can be modelled procedurally in such areas as digital fabrication or additive manufacturing. Due to the multi-scale nature, geometry subdivision with arbitrary dynamic changes, the support of increased complexity and precision of the volume models is an essential requirement. In this work, we address the analysis complexity with an introduction of auditory stimuli and consider a unified approach to the visual-auditory analysis of heterogeneous objects.

As we have discussed in section 3.6 the introduction of additional sensory stimuli emphasises the efficiency and quality issues that arise during conventional visualisation of heterogeneous objects. The multisensory rendering in many aspects takes advantage of computer graphics techniques and uses GPU acceleration structures from computer graphics rendering pipeline with ray-tracing as well as ray-casting technique itself. The conventional approaches employ structural 3D textures and rasterisation techniques and are not applicable for heterogeneous objects as does not consider their heterogeneous nature. The quality issues inevitably arise with an approximation of heterogeneous materials distribution as structured data. The problem becomes more apparent for multi-scale heterogeneous objects that multi-dimensional nature requires a combination of geometry modelling and rendering techniques. The complex cases of real-time multimodal user interaction for heterogeneous structures are also based on a GPU accelerated continuous multidimensional geometric modelling and imposes high-efficiency requirements.

Thus, compared to the conventional visual pipeline, the multisensory pipeline largely depends on real-time interactive geometry and material modelling that is often implemented in the context of the ray-tracing procedure (see section 3.6.3). For multi-scale heterogeneous objects, the pipeline evaluation time grows with the introduction of dynamic features of various scale. The multi-threading and deployment of distributed systems is a conventional technique of high-performance visualisation to overcome many of the issues. However, the introduction of the real-time multisensory feedback and volume visualisation of heterogeneous phenomena require the GPU-specific implementation of visual and auditory pipelines to address the bottlenecks of the interactive visualisation.

In this chapter, we describe a unified theoretical approach to the interactive visual-auditory analysis of a wide range of dynamic multi-scale heterogeneous structures that address those challenges. In section 3.4.3 we have discussed how the modern ray-tracing based computer graphics pipeline uses the concept of light propagation to provide the flexible GPU solutions to address challenges in the rendering of heterogeneous volume objects. Inspired by approaches and techniques that modern GPU hardware allows to deploy, we introduce a unified approach to visual-auditory pipeline design, by taking advantage of similarities in light and sound propagation and continuous multi-dimensional visual-auditory scene modelling and rendering. We discuss the basic aspects of GPU-accelerated user interaction with heterogeneous objects with the introduced framework as a tool to support and facilitate the visual-auditory analysis via manipulation of both visual and auditory information in the multi-sensory scene.

4.2 An approach to visual-auditory analysis

4.2.1 General scheme

The conventional goal of visualisation is getting an insight into phenomena the data represents (Keim et al. 2008) by using visual stimuli. The design of visual pipeline design is a process that establishes a sequence of mapping from numerical data input to a rendered image. In this work, we consider the concept of light propagation as a core procedure in the design of a visual analysis of the heterogeneous object. Moreover, we take advantage of similarities in light and sound propagation to propose a unified approach to visual-auditory analysis.

As we have discussed in section 3.1 the visualisation pipeline structure is conventionally represented with such blocks as "Data reading", "Mapping", "Rendering" and user analysis of the visual stimuli. Let us consider those procedures and their input/output representation

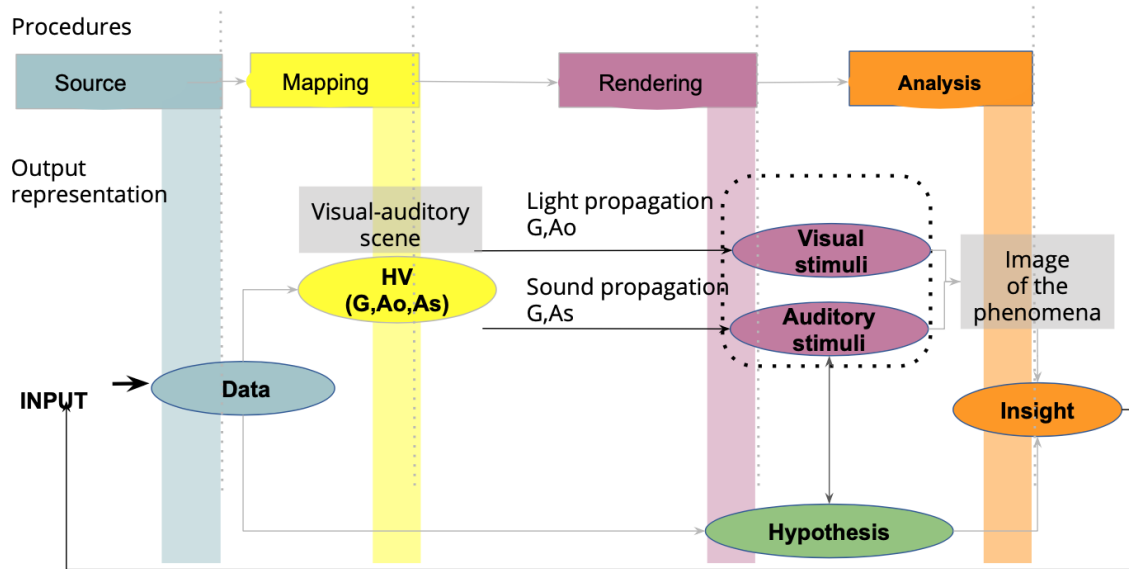


Figure 4.1: Visual auditory analysis process unified by concepts of light and sound propagation (input as $g(t), l(t), c(t)$, data - heterogeneous object initial data representation, remove HV

on each stage of visual-auditory pipeline for a special case of heterogeneous objects (see Fig. 4.1).

By treating visual-auditory analysis as an extension of visual analysis we consider that the user operates the obtained visual-auditory image to get insight into phenomena the object represents (see Fig. 4.1, the procedure "Analysis"). The visual-auditory image is obtained as a result of the rendering of 3D scene representation (see Fig. 4.1, the procedure "Rendering"). The 3D scene representation on other hand is obtained as a result of the mapping of initial data (see Fig. 4.1, the procedure "Mapping").

We propose the following concepts to unify the entire approach and individual procedural blocks.

Firstly, as we have discussed in sections 3.3, 3.6.3, the core pipeline requirement is continuous modelling in multi-dimensional space. This includes both multi-scale and dynamic features of heterogeneous objects and the user interaction with complex data. We consider a general case of visual-auditory scene modelling as the multidimensional object in E^{3+n} dynamic and multi-scale features space with further projection to E^3 space and visual-auditory rendering. Moreover, we treat visual-auditory scene itself as a heterogeneous object with geometry G , optical A_o and auditory properties A_s modelled in multi-dimensional space (see Fig. 4.1, the output representation "Visual-auditory scene"). For this, we use

the HV model discussed in section 3.3.1 and the IC representation of spatial distribution of materials in volumes discussed in section 3.3.2.

Secondly, the rendering to visual and auditory stimuli uses the concept of light and sound propagation through a heterogeneous object that represents this scene. (see Fig. 4.1, the procedure "Rendering"). The multi-dimensional representations are projected to 3D space as a part of the ray-casting procedure. The visualisation of heterogeneous objects implies that the user analyses their properties via optical material distribution that is defined by subdivision introduced by input data structure (see overview in section 3.4.3). Moreover, quality of analysis highly depends on a rendering procedure that uses this subdivision and accumulates optical property at each region (see section 3.4.4). Thus, the analysis of the visual-auditory image (see Fig. 4.1, block "Analysis") can be decomposed into an analysis of optical and auditory properties on individual subvolumes that are used to judge about properties of the heterogeneous object in total. A rendering (see Fig. 4.1, block "Rendering") step evaluates the process of the propagation of light or initial sound impulse through a heterogeneous object. The procedure can be also decomposed into interaction with each individual volume element within the heterogeneous subdivision and evaluation of light/subvolume or sound impulse/subvolume interaction on optical or auditory materials distributions that is followed by accumulation of the above interactions on entire propagation path. Thus, interpretation and rendering concepts that are well established in volume rendering of heterogeneous objects can be further extended to case of visual-auditory framework.

Moreover, we can review the design of visual-auditory pipeline as process driven entirely by concepts of light and sound propagation. We consider subdivision defined by initial data as a key for modelling of optical A_o and auditory A_s materials distributions that are important for a mapping from initial data to visual-auditory scene (see Fig. 4.1, the block "Mapping"). Thus, the geometry, optical and auditory properties modelling procedures are closely related to light and propagation through heterogeneous volume as key concepts of optical and auditory properties modelling and rendering. Moreover, in our work the geometry and materials modelling are combined with ray-casting procedure that imitates light or sound impulse propagation processes along the ray. This allows to facilitate visual-auditory rendering, user interaction modelling, multi-scale properties rendering.

Below we discuss how the proposed framework can address the challenges that impose the problem of visual-auditory analysis of dynamic multi-scale heterogeneous objects. For this we discuss the output representations that are results of visual-auditory pipeline procedural blocks: Data reading that we combine with demanded preprocessing/filtering functionality (see section 4.2.2) Mapping (see section 4.2.3), Visual-auditory rendering (see section 4.2.4), introduction of used interaction into visual-auditory pipeline (see section 4.2.5).

Also, we describe in details the main features of deployed procedural blocks and demonstrate their application for various heterogeneous objects. We discuss such aspects as :

1. Geometry constructive modelling of hybrid structure in section 4.3 (a part of Mapping)
2. Visual-auditory materials modelling in section 4.4 (a part of Mapping)
3. Visual-auditory rendering of hybrid multi-dimensional structure in section 4.5
4. Some aspects of designing interactive interfaces that use hybrid structure to perform visual-auditory feedback as a result of user exploration of heterogeneous structure in section 4.6

4.2.2 Initial data pre-processing and representation

Spatial subdivision is natural for types of data that represent heterogeneous objects. That is the case of 3D meshes, molecular point-based data, the data that represents lattice-based microstructures. (see sections 3.2.1, 3.2.3, 3.2.2). The geometry that defines the material distribution regions and material itself may vary in time and scale. Thus, a typical approach for describing heterogeneous objects is to represent them with a set of disjoint components, each containing homogeneous material distribution, also known as unstructured data. The description of those components includes geometry, material distribution and description of topological dependencies. The last one requires introduction of spatial subdivisions.

We assume that the initial dynamic data are represented within unstructured polyhedral grids where points are specified by its coordinates and cells of higher dimensions are defined topologically by their boundary connections.

The initial dynamic data representation can be described as a tuple $g(t), l(t), a_1(t), \dots, a_m(t)$, that describes a dynamic cellular structure $C = \bigcup_{i=1}^N C_i$, where

$g_i(t)$ - input data on cell geometry representation at the time t ;

$l_i(t)$ - input data on i - th cell topology representation (boundary connections) that changes at the time t ;

$a_1(t), \dots, a_m(t)$ - input data on additional computed properties, a set of attributes that can be scalar values, vectors, tensors and etc. that represent non-geometric properties or pan-geometric properties such as multi-scale representations that depend on the resolution.

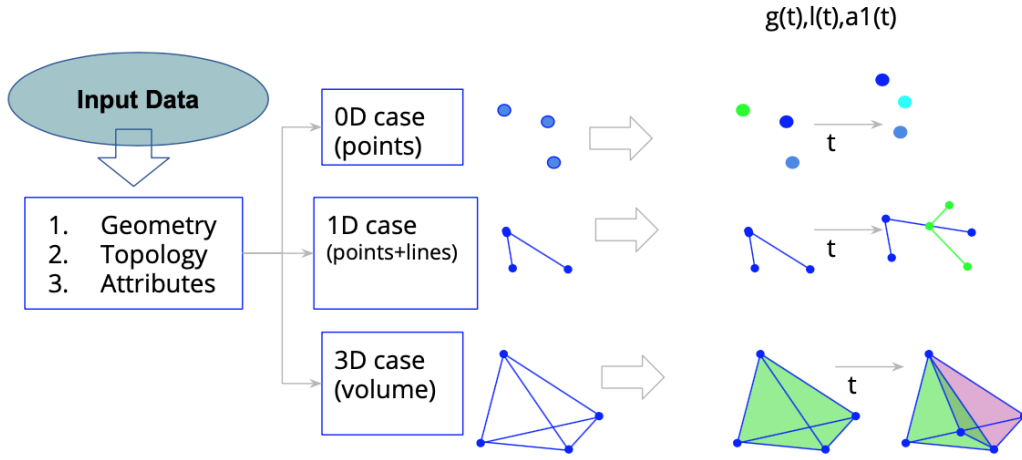


Figure 4.2: Initial data representation

The time should be represented through time span (t_{min}, t_{max}) where input data is defined at each key frame t_j : $g(t_j), l(t_j), a_1(t_j), \dots, a_m(t_j)$. So for each t_j the $C_i(t_j)$ is a polyhedron cell that we have considered as a part of CW cellular complex representation in section 3.2.1. The $C_i(t)$ represents a dynamic cell in E^4 .

In this research we use the input data represented by the cellular complexes C of the following dimensions: 0D (points), 1D (points and lines) and 3D (conventional 3D volume meshes). The cells have corresponding attribute data $a_1(t), \dots, a_m(t)$, i.e. 0D point data, 1D line data and 3D volume data. The examples of data are molecular CPK representation (0D), molecular data balls and sticks representation (1D) and tetrahedral meshes (3D). For details see case studies in sections 6.1, 6.2.

We map the initial cellular structure C to a heterogeneous object $o(t)$ defined by IC complex. Each polyhedral cell $C_i(t)$ is mapped into explicit P-cell geometry G in E^{4+l} in multi-dimensional space that reflect the time and multi-scale features modelling dimension. The l depends on nature of attributes and size of attributes tuple, or whether the attributes will be mapped to geometry or optical and auditory properties.

Moreover, for correct description of multi-scale properties we may need to consider a complex subdivision inside some cells $C_i(t_j)$. Such cells we represented by composite C-cells in the IC structure of object $o(t)$ (see sections 4.3.3 and 4.3.4). The level of complexity depends on the input data and whether we use dynamic changes in shape and topology.

4.2.2.1 Preprocessing

For efficient implementation of mapping and rendering procedures we introduce hierarchical subdivision in E^{4+l} with geometry G in E^{4+l} space that includes multi-scale and dynamic

representations. This is an additional bounding volume structure that simplifies the evaluation of relationships between multi-dimensional cells, their projection into 3D space and further geometric modelling performed on those cells (for example, see the details in section 4.2.4).

Within the subdivision the data is mapped to multi-dimensional geometry as: $G(t) = \bigcup_{i=1}^N G_i(t)$, where $t = (t_0, t_1)$, t_0 is a time parameter, t_1 is a parameter that controls transition between multi-scale representations. In a case of 3D geometry, the modelling space here becomes E^5 .

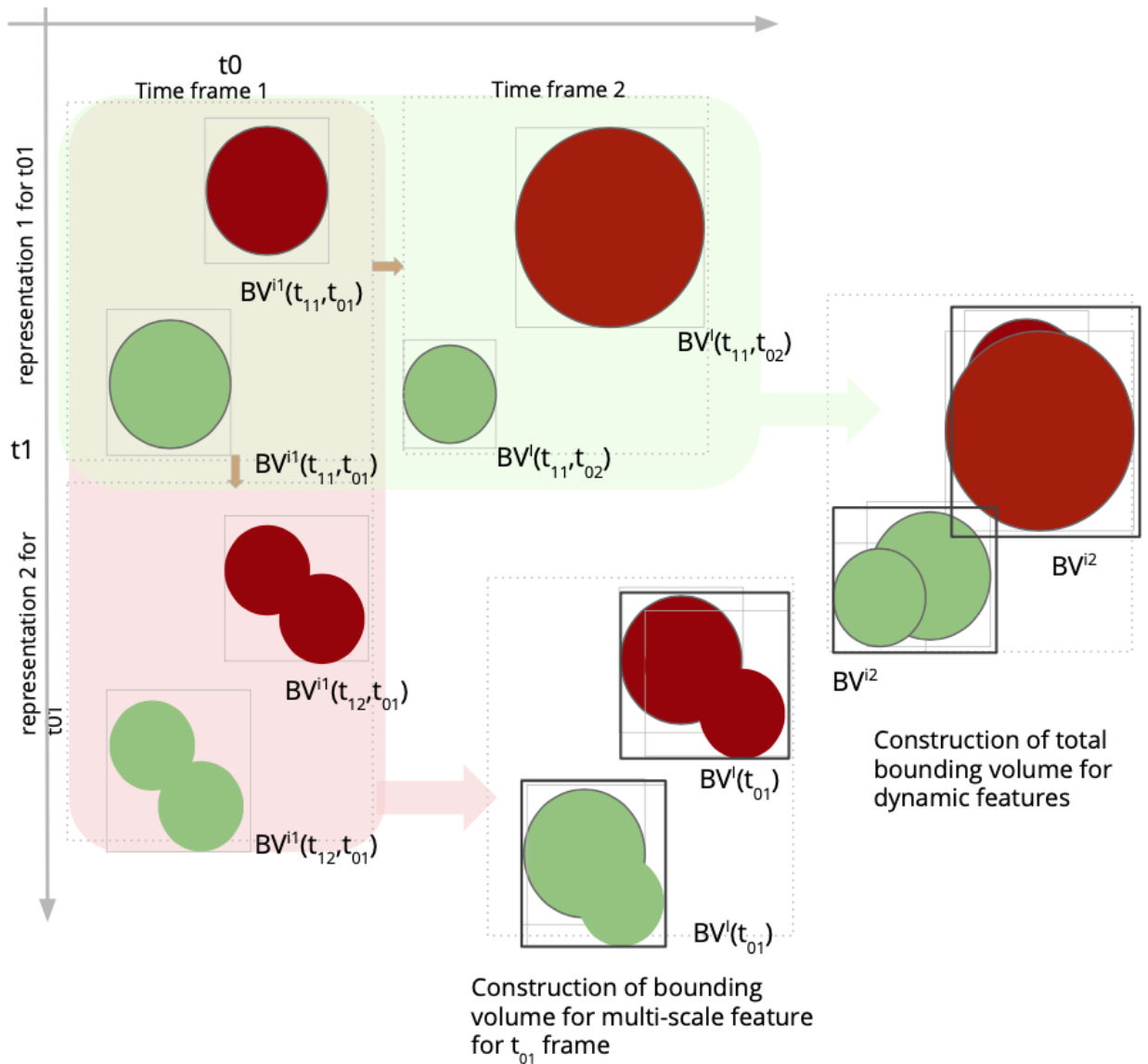


Figure 4.3: Bounding volume construction for a basic case of multi-scale geometry with dynamic features (a) A bounding volume for the dynamic geometry (b) A bounding volume for the static multi-scale geometry (one frame is considered)

The bounding volume structure includes all possible projections of geometry from 5D into 3D space and is the tightest bounding volume for the geometry. We propose to build a bounding volume structure from bottom l_1 to top l_3 level as:

$$BV^{l_1}(t_0, t_1) \subset BV^{l_2}(t_0) \subset BV^{l_3} \quad (4.1)$$

In equation 4.1 $BV^{l_2}(t_0)$ is a set of dynamic bounding volumes in E^4 modelled on subdivision:

$$BV^{l_2}(t_0) = \bigcup_{i=1}^N BV_i^{l_2}(t_0) \quad (4.2)$$

For each cell, the bounding volume $BV_j^{l_2}(t)$ can have explicit or implicit representation and they can overlap. We construct the projection of $BV_j^{l_2}(t)$ into E^3 space as the "swept" bounding volume subdivision BV^{l_3} (see Fig. 4.3 for explanation):

$$BV^{l_3} = \bigcup_{i=1}^N BV_i^{l_3}, \text{ where } BV_i^{l_3} = \bigcup_{t_0=t_{min}}^{t_{max}} BV_i^{l_2}(t_0) \quad (4.3)$$

Due to conventional representation of multi-scale features, the dynamic bounding volume for each cell $BV_i^{l_2}(t_0)$ that includes all its multi-scale representations can be modelled with following simplification. We consider that in t_{1min} and t_{1max} we have a main scale of representation with additional scale, with all being enclosed by a bounding volume. $BV_j^{l_1}(t_0, t_{1min})$ and $BV_j^{l_1}(t_0, t_{1max})$. We can model the bounding volume $BV_j^{l_2}(t_0) = BV_j^{l_1}(t_0, t_{1min}) \cup BV_j^{l_1}(t_0, t_{1max})$ so that any intermediate dynamic multi-scale representation $G_j(t_0, t_{1m}) \subset BV^{l_2}(t_0)$.

Thus, for any time value t_{0n} the i -th cell geometry $G_i(t_{0n}, t_{1m}) \subset BV_i^{l_2}(t_{0n}) \subset BV_i^{l_3}$, where $G_i(t_{0n}, t_{1m})$ is a projection of dynamic cell $G_i(t_{0n}, t_{1m})$ to E^3 space. Note that G_i itself is a composite one represented as a union of other cells of the same or lower dimension, then each of its internal cell should satisfy the above conditions. In some cases the $BV_i^{l_1}(t_0, t_1)$ can be subdivided into $BV_i^{l_1}(t_0, t_1) = \bigcup_{j=0}^N BV_{ij}^{l_0}(t_0, t_1)$, where N is number of subcells in composite cell. We will discuss such cases in sections 4.3.3 and 4.3.4. In other cases, we can benefit from a representation of $BV_i^{l_1}(t_0, t_1)$ in an implicit form, such that it can bound the geometry of the cell tighter.

Thus, we specify the following basic structure $o(t)$, that represents a heterogeneous objects with dynamic and multi-scale properties modelled within with explicit cellular subdivision:

$$o(t) = G'(t), A'_1(t), \dots, A'_m(t) : \langle C(t), BV^{l_2}(t_0) \rangle = \bigcup_{i=1}^N \langle C_i(t), BV_i^{l_2}(t_0) \rangle \quad (4.4)$$

where $A'_1(t), \dots, A'_m(t)$ describe various properties distributed on geometry $G'(t)$ that map to visual-auditory stimuli.

Let us discuss the details of how we obtain a visual-auditory scene $h(t)$ from $o(t)$ in a form of an implicit complex.

4.2.3 Visual-auditory scene representation and mapping

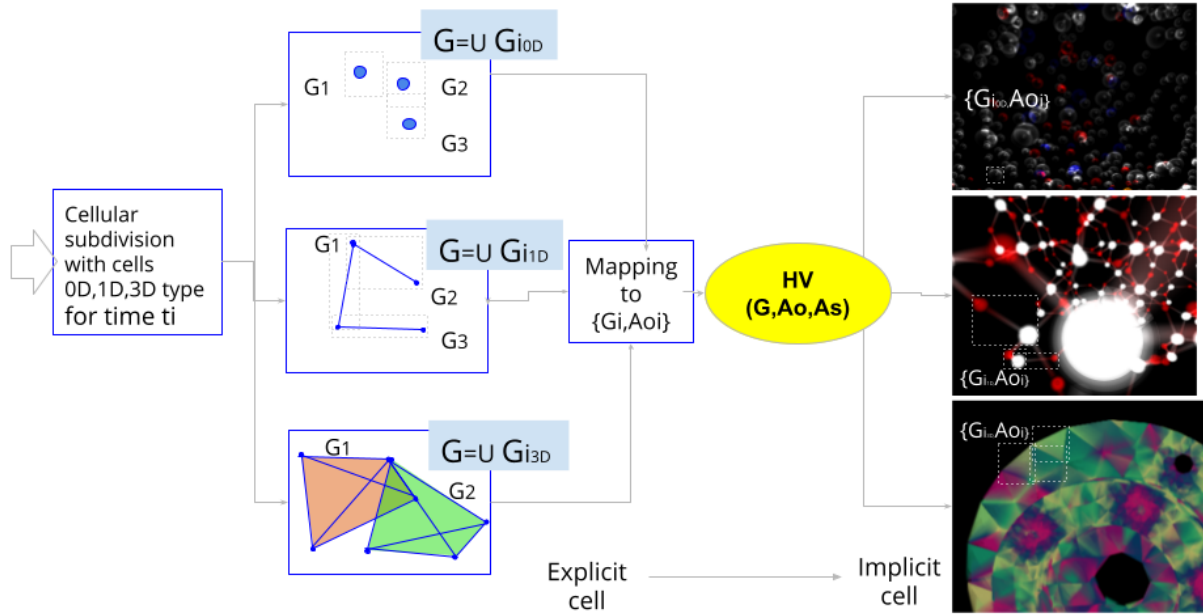


Figure 4.4: Modelling of visual-auditory scene

The visual-auditory scene is described through spatial subdivision $(G, Ao, As) = \bigcup_{i=1}^N G_i, Ao_i, As_i$, where each cell of the cellular complex is represented by a HyperVolume model $HV_i : G_i, Ao_i, As_i$ with

G_i - dynamic multi-scale geometry in E^5 , that is the IC cell of F-type described with a signed distance function $I_i(X|t)$ (SDF implicit cell representation).

Ao_i, As_i - dynamic multi-scale optical and auditory properties on implicit cell geometry G_i that are defined as continuous function representations of attributes $So_i(X|t), Ss_i(X|t)$.

Following the discussion above, we can define the following requirements for the subvolumes (G_i, A_{o_i}, A_{s_i}) :

1. The i -th cell $G_i^5 \subset E^5$ is a closed point set that represents a volume object.
2. $G_i'(t_0) \subset G_i(t_0) \subset BV_i^I$.
3. Each tuple $(G_i', A_{i1}', \dots, A_{im}')$ is modelled over explicit cell C_i with attributes, and each tuple (G_i, A_{o_i}, A_{s_i}) is modelled over the implicit cell $I_i = I(C_i)$ with materials. Each constructive tree for cell geometry G_i returns the signed distance value. The optical and auditory properties A_{o_i}, A_{s_i} have implicit or voxel representation that are used by visual-auditory rendering procedure.
4. The cells G_i^5 can overlap. The intersection of any two cells is empty point set or a closed bounded point set .
5. Within each cell G_i the optical and auditory A_{o_i}, A_{s_i} properties are defined only by geometry and attributes of the explicit cell C_i .
6. An implicit cell I_i is obtained as a result of hybrid constructive modelling of explicit cell C_i and only this cell. The cell C_i can also be a composite cell.
7. The materials A_{o_i}, A_{s_i} are defined per implicit cell I , but may not depend on a constructive tree that models G_i .

With continuous representation of geometry G_i , optical A_{o_i} and auditory A_{s_i} properties, the geometry model of visual-auditory scene is represented as

$$\langle I, BV^{l_2} \rangle = \bigcup_{i=1}^N \langle I_i, BV_i^{l_2} \rangle \quad (4.5)$$

where $I = \bigcup_{i=1}^N I_i$ is a union of dynamic SDF cells that is modelled within subdivision of bounding volumes $BV^{l_2}(t_0) = \bigcup_{i=1}^N BV_i^{l_2}(t_0)$. Each implicit cell I_i description represents a geometry G_i and the optical and auditory properties A_{o_i}, A_{s_i} are defined within i -th subvolume G_i .

The visual-auditory scene $h(t)$ is obtained as a set of mappings from $o(t)$:

$M : (G', A_1, \dots, A_m) \Rightarrow (G, A_o, A_s)$ that can be decomposed into a set of mappings

$M_i : \langle G_i(t), A_{i1}(t), \dots, A_{il}(t) \rangle \Rightarrow \langle G_i(t), A_{io}(t), A_{is}(t) \rangle$

performed on properties of heterogeneous object $o(t)$ to map them to regions of heterogeneous optical and auditory properties of $h(t)$.

The geometry G , optical Ao and auditory As materials are modelled within spatial subdivision based on the explicit geometry $C_k : M_k : \langle C_k, BV^{l_2} \rangle \Rightarrow \langle I_k, BV^{l_2} \rangle$.

The modelling process can be schematically represented with a graph, that is a hybrid constructive modelling of geometry, optical and auditory material distribution (see section 3.3.3 for details on structure). Thus, the hybrid constructive tree structure reflects the mapping logic of visual-auditory pipeline (the block "Mapping" in Fig. 4.1) .

For modelling of optical and auditory materials we use the conventional volume rendering TF (see for details see the section 3.4.2) in more general context of optical and auditory properties constructive modelling. The optical and auditory TFs are treated as nodes in constructive trees. The TFs allow the analysis of internal volume properties through optical and auditory properties, such as colour and pitch. Below we discuss the details of analysis of visual and auditory stimuli.

4.2.4 Analysis of visual-auditory stimuli and rendering

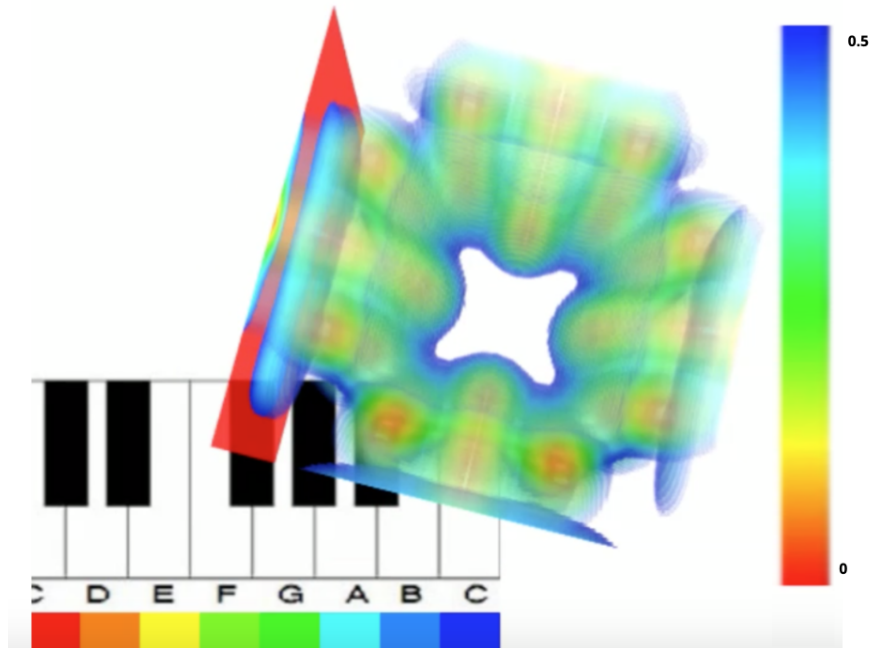


Figure 4.5: Basic colour scale and introduced "music scale" in volume rendering framework for analysis of scalar field simultaneously via optical and auditory properties

4.2.4.1 Colour and music scale

The main goal of the analysis is to get an insight into the initial representation of the heterogeneous object $o(t)$ via analysis of visual-auditory scene $h(t)$. We discussed the

formulation of the conventional visual analysis in the section 3.1. In case of visual-auditory analysis the judgements are made based on a distribution of the optical A_o and auditory A_s properties on the geometry domain G that allows the user to get an insight into phenomena properties A_1, \dots, A_m . As we have discussed in section 3.4.2, optical TF that maps numerical values of to optical properties is a conventional tool to control the quality of the visual analysis and perform backward interpretation of the mapping to visual auditory-scene $(A_o, A_s) \rightarrow (A_1, \dots, A_m)$ in volume rendering.

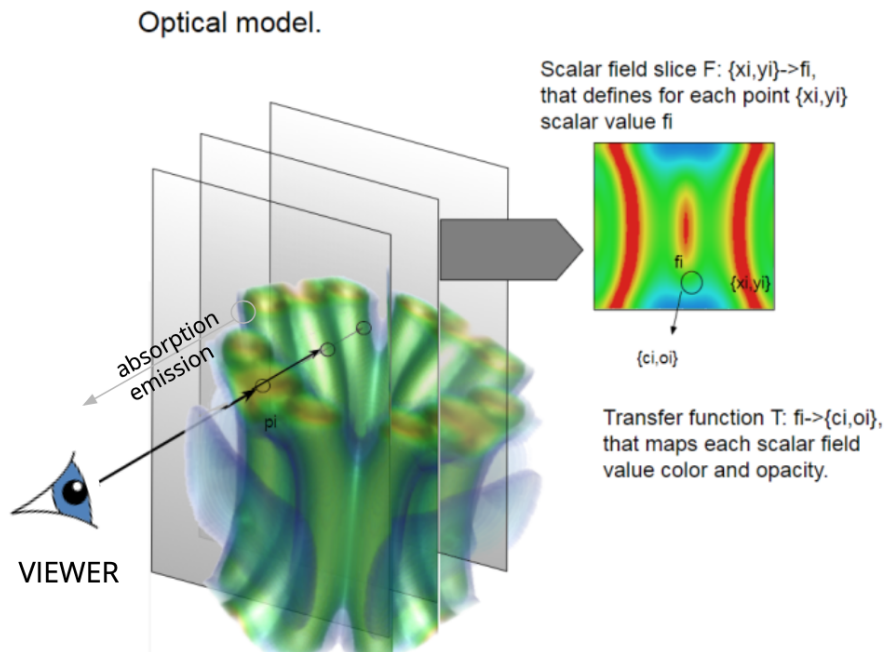


Figure 4.6: Light transport in the conventional volume rendering for analysis of the internal structure of the scalar field

The conventional volume analysis assumes that the user gets the insight into the internal structure described with a scalar field through a perception of colour changes within a defined colour scale. As we have discussed in the section 3.5.4, mapping to auditory properties or sound wave allows for more flexibility. In this work we consider a type of auditory mapping based on the musical systems, as we mentioned in the section 3.5.4. The scalar field is mapped to pitches of a certain range within a space of 1 and 2 octaves with specified division and operates the conventional notion of "music scale". The example of colour scale and similar Cmaj music scale is presented in Fig. 4.5. Thus, if we consider the extension of conventional volume rendering, the mapping of scalar field to both colour and sound are used for simultaneous analysis on scalar value distribution through simultaneous change of a colour and a pitch. The work (Malikova et al. 2019) discusses some aspects of how

conventional visual analysis of scalar fields and optical TF can be evaluated with auditory stimuli and similar auditory TF in terms of perception quality control via id detail analysis of 2D slices of scalar field.

In conventional analysis of 3D volume data the optical properties obtained with TFs are accumulated along the ray as a result of ray-casting or 2D slice blending as a part of rasterisation. Thus, the analysis of volume data is performed by using the concept of light interaction with volume and the accumulation of optical properties.

4.2.4.2 Optical and auditory models

The concept of sound propagation and similarities in modelling of visual and auditory stimuli through light and auditory impulse interaction leads to visual-auditory analysis. We mainly consider emission and absorption interactions for light and auditory impulse as they propagate through heterogeneous structure of the volume as discussed previously in 3.4.4 and provide the results of single scattering for small structure where the auditory feedback is used as a part of user interaction that results in measurement of distance between avatar position and heterogeneous structure (Malikova et al. 2020)).

As discussed previously, the technique is widely used in the spatial sound modelling that applies ray-tracing methods from computer graphics for its sound generation. However, there is a significant difference in concept with geometric acoustic methods. The ray-tracing acoustic methods concentrate on rendering of surface objects where the reflective properties are essential for shape analysis. This research deals with volumes, that are conventionally processed differently as most attention is paid to the emission-absorption interaction that is used to get an insight and to highlight the internal structure within the volume.

As the auditory model ignores reflections, we can introduce further simplifications that allow computing of the spatial sound's properties. In auditory case we consider a heterogeneous object with acoustic properties. The output of interaction is the wave S_j represented with sound impulse propagation along j -th ray through the heterogeneous object and interacting with each geometry region G_i of auditory material definition As_i . An HRTF convolution applied to output of j -th ray approximates interaction with the listener and enables spatial perception of time dependent propagation process, as discussed in the section 3.5.4.

On this stage for auditory stimuli we have to take into account the interaction of result auditory feedback with listener, in other words enable binaural perception of the auditory propagation along j -th ray (see section 3.5.4 for general principles of rendering to auditory stimuli). Such interaction is defined by assumed listener head position and orientation (see Fig. 4.7). We consider the positions of the listener and of the viewer to be the same. To

achieve that, we use the same camera position to imitate the light propagation path from a light source to human eye and the sound propagation from the auditory source to the human ear or back (see Figures 4.6 and 4.7).

As it is discussed in section 3.6.2, the virtual scene perception paradigm may vary depending on the precision of interaction and input devices used such as head-tracking and eye-tracking. The design may assume the viewing direction that is the input parameter for visual stimuli generation to be different from head orientation, one of the main input parameters in the binaural rendering. In this work we consider a basic case, that viewing direction is defined only by head orientation (no eye-tracking). Thus the input parameters for the virtual camera and listener model are similar and can be defined by either head-tracking devices or by conventional mouse input.

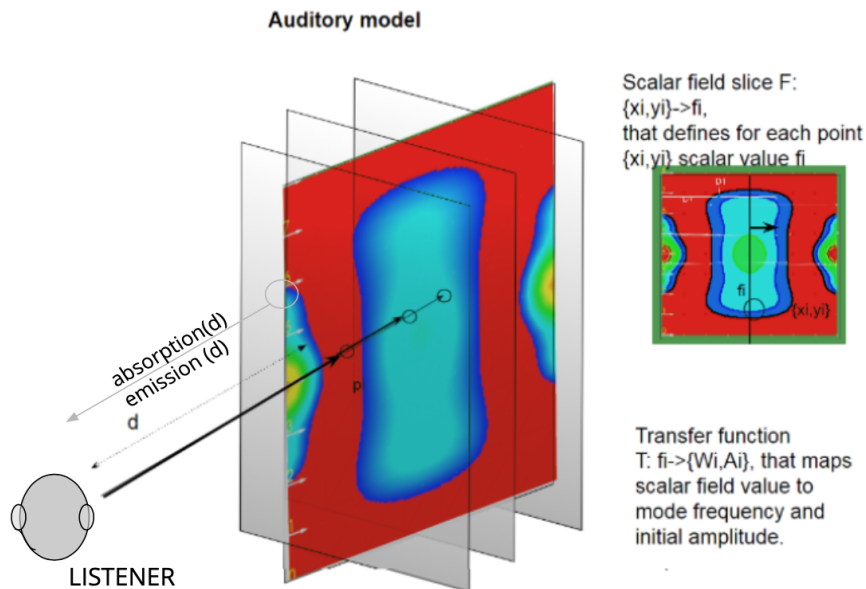


Figure 4.7: Sound propagation in the proposed approach for auditory volume rendering

4.2.4.3 Getting an insight into the internal volume structure

The insight into the volume structure is done with an analysis of the distribution of the optical properties, such as the colour and the opacity defined by optical TF. Similarly, the evaluation of the auditory material properties that highlight substructures in volume, can be done with analysis of distribution of auditory properties defined by auditory TF that can be approximately located in space by using the spatial properties of output sound. With the concept of auditory ray propagation through volume structure in specified direction, the combination of spatial sound and auditory TF highlights the properties and relative positions

of substructures via perception of delays in times of "activation" and pitch. This allows the user to "look inside" the complex volume structure.

As we have discussed above, due to necessity to consider the material distribution on subdivision, the analysis of all the properties of the heterogeneous object with the geometry G_i is separated into analysis of the optical properties Ao_i and auditory properties As_i of its individual components. The visual-auditory rendering procedure follows this process. The rendering is performed as a result of interactions with the geometry of the scene, where the optical and auditory material properties of the HV model $o(t)$ are considered given the time value t_{0j} and current level of the representation t_{1k} . Unlike the conventional volume sampling, the ray-casting procedure evaluates total optical and auditory impact via intersection with geometry G_i within subdivision to result in its optical and auditory Ao_i, As_i material properties.

4.2.5 User interaction for visual-auditory scene exploration

In conventional visual analysis interpretation the user interaction accesses and adjusts the one or several of the procedural blocks of visual pipeline (filtering, mapping and etc.) (Kalkofen et al. 2011), (Sua et al. 2015), (Roberts et al. 2014). Thus establishing the principles of integration of various interaction procedures into conventional volume visualisation pipeline for heterogeneous objects analysis can be not straightforward due to lack of consideration of spatial distribution of properties that is often used by measurement procedures. Our approach combines the constructive geometric modelling with volume ray-casting. This allows facilitating many aspects of visual-auditory pipeline design, including the integration of interactive feedback that operates both volume and spatial subdivision properties.

The interaction procedures change the representation of geometry G_{sc} , optical Ao_{sc} or auditory As_{sc} properties of object h_{sc} the user interacts with, that we previously referred as visual-auditory scene representation (see Fig. 4.8).

We are modelling the geometry G_{sc} as a union of dynamic implicit cells $I = \bigcup_{i=1}^N I_i$ within subdivision of bounding volumes $BV^{l_2}(t_0) = \bigcup_{i=1}^N BV_i^{l_2}(t_0)$, that is:

$$G_{sc} = \langle I^{sc}, BV^{sc l_2} \rangle = \bigcup_{i=1}^N \langle I_i, BV_i^{sc l_2} \rangle \quad (4.6)$$

In this work we assume that the interactive exploration of the heterogeneous object h_{sc} targets highlightment and analysis of a certain region of interest (ROI). This can be done by selecting a geometry domain $Go_2 \subset G_{sc}$, that is a ROI geometry domain or the user can directly manipulate the Ao_{sc} or As_{sc} to adjust visual/ auditory image.

In the first case, the user is interested in detailed exploration of the properties distributed within $Go2$. This can be done by further highlighting /changing the optical $Aoo2$ and/or the auditory $Aso2$ properties distributed on $Gos \subset G_{sc}$ or by performing a certain measurements on Gos as a result of user interaction and mapping those results to auditory feedback.

Consider the visual-auditory feedback as a result of two different groups of interaction techniques: via interaction widget or avatar and via user graphic interface (GUI). In this work we assume the first type of interaction uses the "selection" of ROI geometry domain and second type of interaction adjust the $Aosc$ or $Assc$ representations.

The generic scheme of the exploration and how it can be integrated into visual-auditory pipeline is shown in Fig. 4.8.

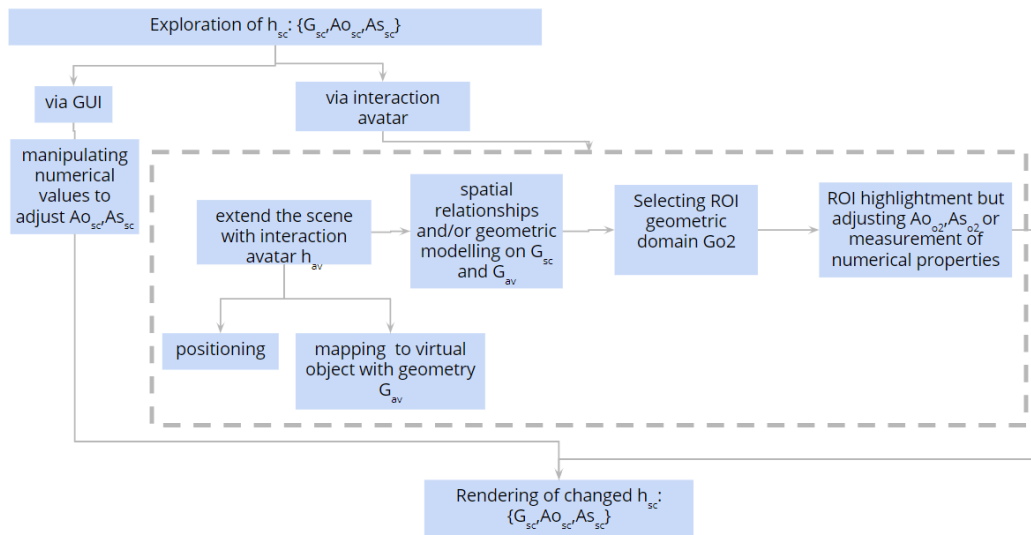


Figure 4.8: Interactive exploration of heterogeneous objects with spatially distributed properties

The user interaction performed with interactive widget or with GUI that targets a real-time adjustment of visual, optical or geometry model of visual-auditory scene. As a result, the general way to model and represent the result of interaction is through constructive approach as additional integration into pipeline. This interaction can be performed via interactive widgets or UI extension that takes advantage of new concepts and devices to manipulate additional layer of auditory information.

In this work we consider the examples of basic procedures that highlight different aspects of user interaction design within visual-auditory pipeline. Those procedures use both visual and auditory feedback as part of user interaction:

1. Performing the distance measurements

2. The visual notification of the overlapped region as a result of interaction/overlap between two complex structures
3. The ROI selection as a result of auditory layer direct manipulation with specialised device, such as the MIDI keyboard

We discuss these procedures in more details below in the section 4.6.

4.2.5.1 Avatar based interaction

As discussed previously in sections 3.6.1, 3.6.2 the volume object that is used for interaction by using widgets or avatars, in general case can be represented as a compound object and thus should be treated as a heterogeneous object. Thus, for user interaction in addition to visual-auditory scene representation h_{sc} we use the h_{av} that is a representation of interaction avatar/widget.

The geometry G_{av} of h_{av} has a structure similar to G_{sc} and is modelled with similar concepts:

$$G_{av} = \langle I^{av}, BV^{avl2} \rangle = \bigcup_{i=1}^N \langle I_i, BV_i^{avl2} \rangle \quad (4.7)$$

The set of possible procedures that operate G_{av} and G_{sc} to obtain a ROI G_{o2} is described within a triple (O, Φ, W) , where O is a set of initial objects represented with G_{sc} and G_{av} ; Φ a set of constructive modelling operations performed on G_{sc} and G_{av} ; W a set of relations used on G_{sc} and G_{av} (see section 3.3.1)

A new geometry domain G_{o2} can be obtained as a result of:

1. A set of constructive modelling operations $\Phi_m, m = 1, \dots, N$ applied on top of (G_{sc}, G_{av}) .
2. By evaluating a spatial relationship $W_m, m = 1, \dots, M$ between geometries G_{sc} and G_{av} .

For the latter case, the process can be accompanied by numerical estimations or measurements, performed on a geometry domain G_{o2} and further mapped to the visual and the auditory feedback; or the optical A_{o2} and auditory As_{o2} model can be changed to highlight the ROI (see Fig. 4.8).

From overview in section 3.6.3 it follows that the evaluation of relationships W can be conveniently facilitated with ray-casting and SDF that allows fast evaluation of distance properties. For example, the basic pointing operation (see section 3.6.2) can be formulated as manual construction of G_{o2} from G_{sc} by iterative adding of cells to initially empty G_{o2} as a result of ray-casting based ray-cell intersection. We summarise, that the evaluation of relationship between geometries G_{sc} and G_{av} can be decomposed into the evaluation of

relationships between IC cells of $\langle I^{sc}, BV^{sc} \rangle$ and $\langle I^{av}, BV^{av} \rangle$. The bounding volume structures BV^{sc} and BV^{av} are used to accelerate the procedure.

Thus, the logic of the relationships evaluation on G_{sc} and G_{av} becomes very similar to accelerated rendering performed with ray-casting procedure. In section 5.3 we use these similarities to unify the design a both volume rendering and interactive exploration procedures on base of ray-tracing.

Moreover, in the complex cases G_{o2} is obtained as a result of combination of both geometric modelling and relationships evaluation two procedures:

1. On the first stage we select subsets of G_{cs} and G_{av} by evaluating the relationships between them $G_{cs1}, G_{av1} = W(G_{cs}, G_{av})$
2. On the second stage we perform the constructive modelling on the selected subsets G_{cs1} and G_{av1} $G_{o2} = \Phi(G_{cs1}, (G_{av1}))$

Such cases use a combination of geometric modelling and ray-casting. We will consider the example in section 4.6.3.

4.2.5.2 GUI extension

The GUI based interaction is conventional approach to manipulate the virtual scene in scientific visualisation.

As we have discussed in section 3.6.1 the extension of analysis with additional sensory output, in our case auditory model, conventionally leads to introduction of UI tools to manipulate this additional representation. We consider the task of ROI adjustment by manipulating ranges of visual and auditory properties from the UI. Within volume rendering framework the procedure is conventionally deployed as interactive adjustment of optical TF with GUI editors (see sections 3.6.1. In this work we extend the concept to adjustment of auditory TF, that takes advantage of principles introduces in music theory and deployed by musical systems (see section 3.5.4. This allows us deploying for user interaction a general type of input musical devices those input/output is based on MIDI format. Thus, we adjust the auditory TF directly via standard music device. We discuss the details in section 4.6.4.

4.3 Constructive geometry modelling

As we have discussed in section 4.2.3 the mapping procedure is performed through hybrid constructive modelling. The leaves of hybrid constructive tree are defined by representations of the explicit cells of 0D,1D,3D types from the input data. The nodes of the constructive

tree are various explicit and implicit operations over cells C_k and I_k to provide control over dynamic changes in shape and topology. The structure may also include nodes that perform conversion of different representations. In this work we focus the following types of conversion operations M that are the most common in the visualisation for mapping purposes and form a core of modelling of geometry:

1. Dynamic interpolation of geometry represented in the initial data. The mapping M_g is applied to two explicit cells and returns dynamic explicit cell:

$$M_g : \begin{cases} C_i(t_k), C_i(t_{k+1}) \Rightarrow C'_i(t) \\ g(t_k), g(t_{k+1}) \Rightarrow g'(t) \end{cases} \quad (4.8)$$

The input data $g(t_k), l(t_k), a(t_k)$ is computed at discrete key frames values t_0, \dots, t_N . Operations M_g that operate geometry data $g(t)$ are convenient for modelling dynamic changes as in-between points between two keyframes $g(t_k), g(t_{k+1})$ can be interpolated in time. The operation takes the explicit cells at key-frames t_k, t_{k+1} : $C_i(t_k), C_i(t_{k+1})$ and returns the dynamic other explicit cell $C'_i(t)$.

Dynamic or multi-scale interpolation of shape. The mapping M_s is applied to two implicit cells that model geometry in space E^n and returns implicit cell that represents a geometry in space E^{n+1} . For case of E^3 input data:

$$M_s : I_i(t_k), I_i(t_{k+1}) \Rightarrow I'_i(t)$$

This operation benefits from the flexibility of implicit modelling that allows to handle transitions in shape and level of representation as discussed in section 3.3.1.

$M_i : I_i(t) \Rightarrow I'_i(t)$ all other types of implicit modelling operations applied to implicit cell that do not change the dimension of the modelling space. In this work, we consider the SDF modelling operations that preserve the distance property of modelled cell geometry, such as set-theoretic operations, blending, metamorphosis and offsetting.

$M_m : C_i(t) \Rightarrow I_i(t)$ Functional mapping from the explicit cell C_i representation to the implicit SDF cell I_i . The M_m can be compared to conventional "glyph" mapping in scientific visualisation and can be a conversion of explicitly defined geometry to similar implicit representation. This a composite mapping that may include a set of various implicit modelling operations M_i (see below). For examples and details see section 4.3.1

$M_v : V_i(t) \Rightarrow I_i(t)$ Conversion procedures from voxel representation to SDF by using a signed distance transform. In this research we consider a basic case, when the multi-scale description can be a voxel representation that is associated with a small cellular structure. For rendering such structure within framework we apply a signed distance transform to discrete voxel data. We will provide the example of this technique application in the section 6.1.

In addition we separately discuss the following two complex cases of a combination of geometry modelling and ray-casting and consider their application areas:

1. In section 4.3.3 we detail the modelling of multi-scale features on cellular structure with the example of level-of-detail (LOD) dynamic molecular visualisation.
2. In section 4.3.4 we discuss cases of irregular geometry modelling and the case of secondary geometry modelling as "overlapping" geometry patches within initial spatial subdivision that visually form a large continuous volume.

4.3.1 From explicit to implicit cell

The conversion operation between explicit and implicit cells is one of the important in the proposed pipeline. This operation in a general case can have many various forms and interpretations. For the sake of being concise and driven by our case studies, here we concentrate on a mapping between point-based and cellular data. Consider the example of the pipeline with input data types that represent 0D case (points), 1D case (points and lines connecting them) and 3D case (volumes) where only scalar type of attribute defined. The first two cases are most common for molecular data CPK(0D) and Balls and Sticks (2D) models. Point-based data can map to SDF by using balls and beams approach, where the points are represented by signed distance function to sphere, the connectivity information for points is represented by signed distance function to cylinder. The primitives are connected by using distance-based set-theoretic operations over the distance primitives. See Fig. 4.9(a) for molecular data 1D case mapping example. The mapping M_m operates the input explicit cell C_i g, l values to specify the parameters of output SDF geometric primitives.

The other most common example of 3D cellular data, that is tetrahedron cell mapping in 3D meshes is presented in Fig. 4.9 (b). The mapping M_m is based on principles of conversion of explicit cell 3D polygonal representation to implicit cell I_i those basis is modelling through set-theoretic intersection of the implicitly defined planes.

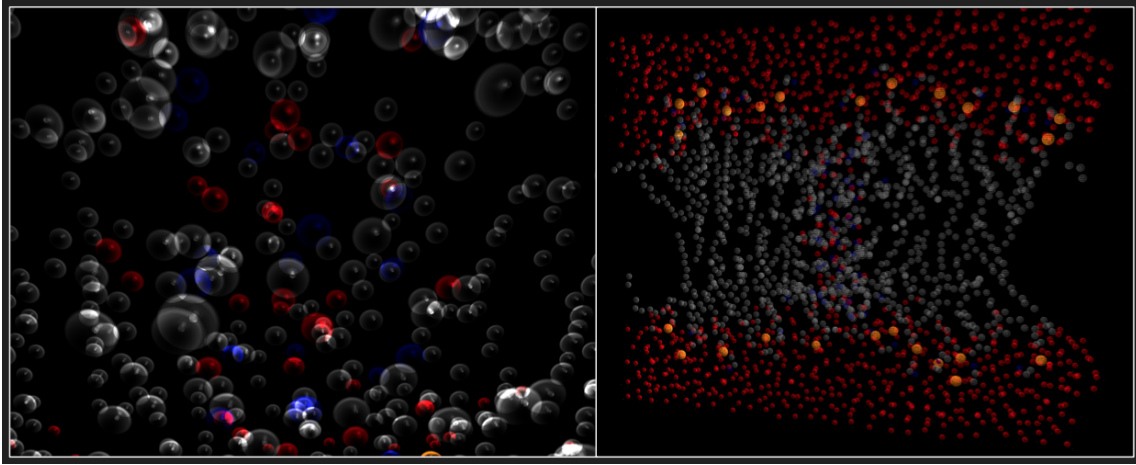


Figure 4.10: Dynamic changes in shape for 0D data.

4.3.2 Geometry, topology and shape dynamic changes

Compared to M_g , the interpolation of dynamic topological changes $l(t)$, when new points and lines are added or removed between two keyframes $l(t_k), l(t_{k+1})$ is not straightforward. However, those issues can be efficiently resolved as we go from explicit C_k to implicit I_k representation. The task can be addressed as a problem of modelling of dynamic implicit shape M_s . Additional control in modelling of shape transition that reflects topological change can be provided by combination with geometric operations M_g applied to explicit representations $C(t_k), C(t_{k+1})$ in constructive trees $M_g : C(t_k), C(t_{k+1}) \rightarrow C(t)$.

Each representation is modelled as explicit cell C_j for given time key frame t_j and mapped to implicit cell I_j (see Fig. 4.9). Explicit cells $C(t_k), C(t_{k+1})$ are defined by initial data at key frames t_k, t_{k+1} and may contain very different geometry and topology structures (see Fig. 4.11). In general case, new points or connections between points (change in topology) appear and dimension of topological dependencies may also change (see Fig. 4.11). The interpolation of dynamically changing geometry and topology representations within cells is controlled with hybrid nature of nodes.

In a basic case we continuously interpolate the transitions between cells $I(t_k), I(t_{k+1})$ with morphing operation (Liu & Sourin 2006, Adzhiev et al. 1999). To provide even more control in transition, both cells can be treated as E^{3+l} projections of cylinders in dynamic space E^{4+l} and space time blending union operation is applied (Pasko et al. 2004b). An arbitrary dynamic changes in shape and topology within cell can be modelled with such hybrid structures (see Fig. 4.11). As an example of 0D-1D dynamic changes, we use a crystal structure of quartz molecule (see details and problem description in Case studies section 6.2). The initial data defined the representation of explicit cells. With possibility of cells overlap a

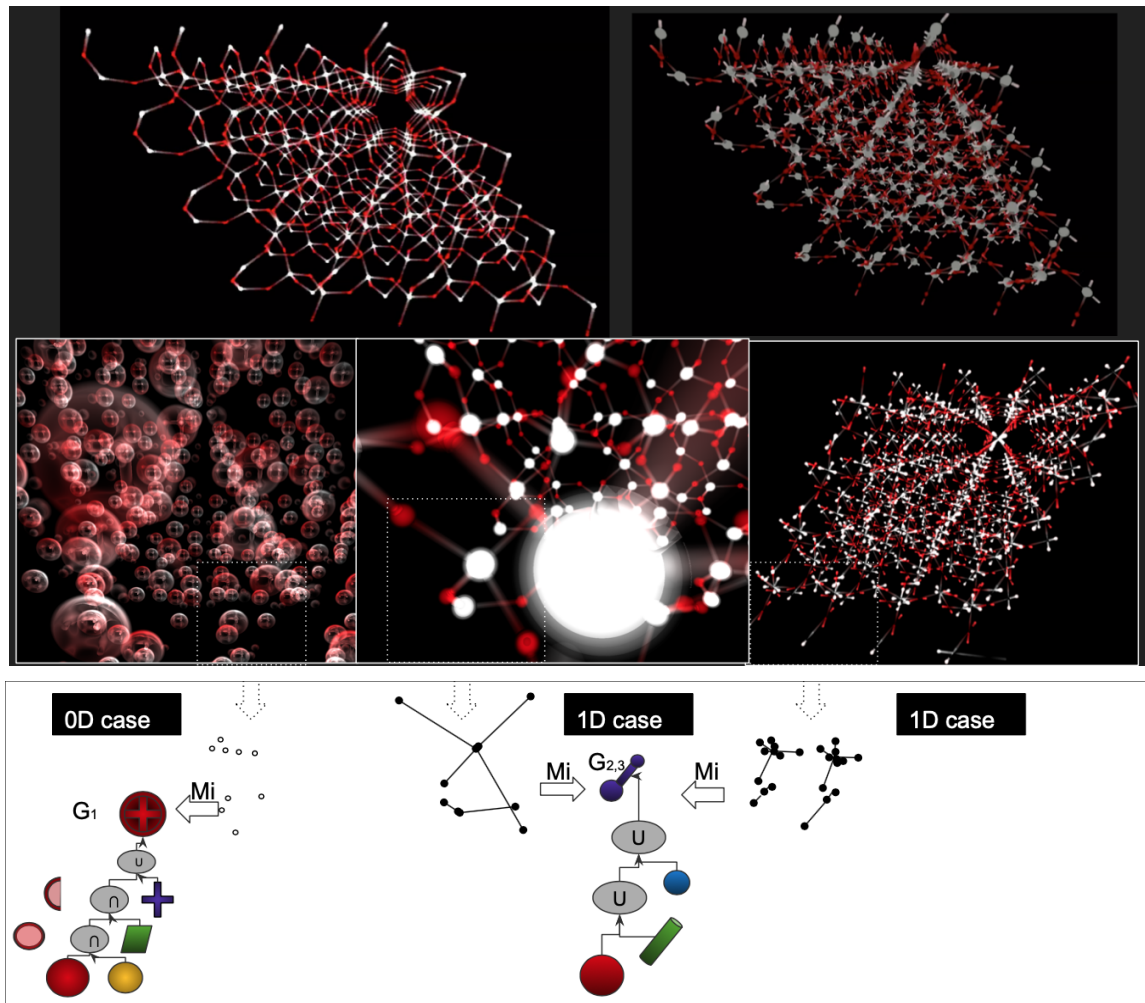


Figure 4.11: Various dynamic changes in shape and topology from 0D to 1D variations. (a) Microstructure type geometry G_1 mapping $M_{i1} : C_1- \rightarrow I_1$ (b,c) balls and sticks type geometries G_2, G_3 mappings M_{i2}, M_{i3} of 1D explicit cells with different topological structure. A transition between output implicit cells I_{i1}, I_{i2}, I_{i3} is modelled with geometry interpolation M_g and dynamic morphing of shapes M_s

various geometry of 0D to 1D type with changes of shape and topology can be constructively modelled on base of this information.

4.3.3 Modelling of multi-scale features with composite cells

The level of complexity of cells C_k in cellular structure is defined by the application. In this work the composite cell C_k is defined by modelling dynamic and multi-scale changes (see section 4.2.2). The examples of input data that require such representation are molecular clusters and lattice-based microstructures. Those geometry representations are problematic especially when dealing with dynamic and multi-scale features. For example, molecular clusters that are modelled as a set of molecules (see example for water cluster in Fig. 4.12), that in their turn are composed of atoms and microstructures lattice is modelled through notion of unit cell that also is composed of balls-and-beams notion. The composite cells are very convenient for such cases, where each C_k is composed of basic cells C_{k1}, \dots, C_{kn} .

To describe the dynamic multi-scale features, such cells are modelled in multidimensional space E^5 and we will further refer such cell as multi-scale cells for simplicity. Such multidimensional geometry can be processed with interactive camera-based level-of-detail (LOD) visualisation. The technique computes and renders the representation of the right scale depending on its proximity to the user (distance to the camera).

Let us consider a case of multi-scale modelling and visualisation of the dynamic water icosahedral cluster fluctuations from an extended low-density structure to more dense collapsed structure (Zhao et al. 2015) with simultaneous display of the general information on individual water molecule vibrations modes in Fig. 4.12).

The technique suggests that the user can zoom to get the visual insight into the molecular dynamic changes either on macro-level only (cluster fluctuations) or on both macro and micro-levels (cluster fluctuations and individual water molecule vibrations). For representation with the matrix spreadsheets (see Fig. 4.13), the lower row describes multi-scale change controlled with interactive LOD camera technique for final cluster configuration (ES) state and first column represents change of water cluster configuration on "macro" level.

Thus, we have a cellular complex with composite cells of 1D topology (H-O bonds), where each cell is modelled in E^5 and describes an individual water molecule on macro scale and its vibrations on micro scale. The constructive modelling of cell C_k is schematically presented in Fig. 4.14.

The change on macro level is described with input data and controlled with t_0 . Moreover, the micro-level representation is time dependent as well, as it depends on the value of t_0 . The parameter t_1 controls the transition between multi-scale representations. Moreover, different types of vibration of the water molecule are coloured differently. Thus, the constructive

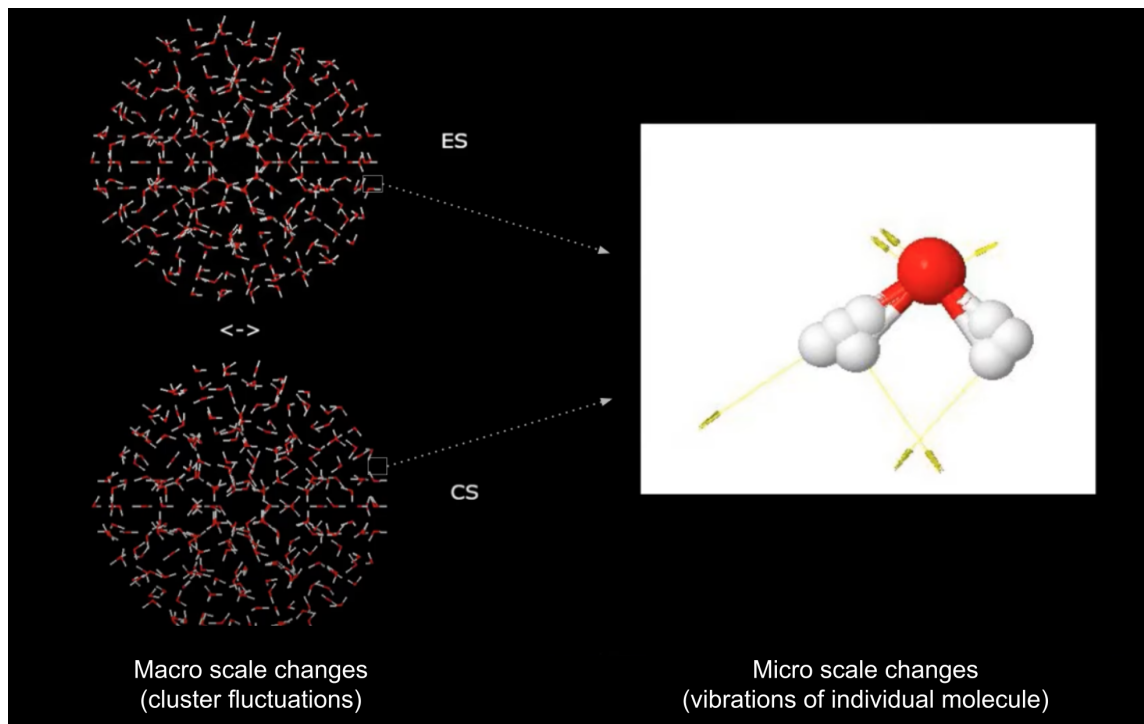


Figure 4.12: Macro and micro scale features for dynamic water cluster

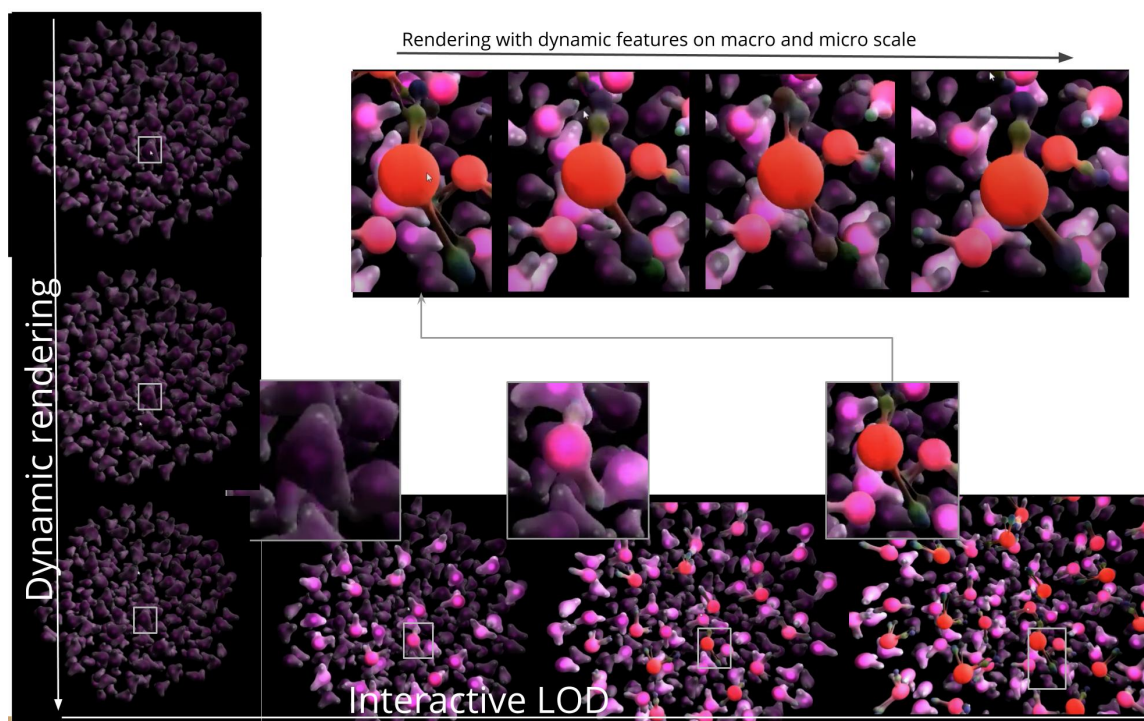


Figure 4.13: Visualisation of multi-dimensional geometry by a combination of interactive LOD and dynamic rendering techniques

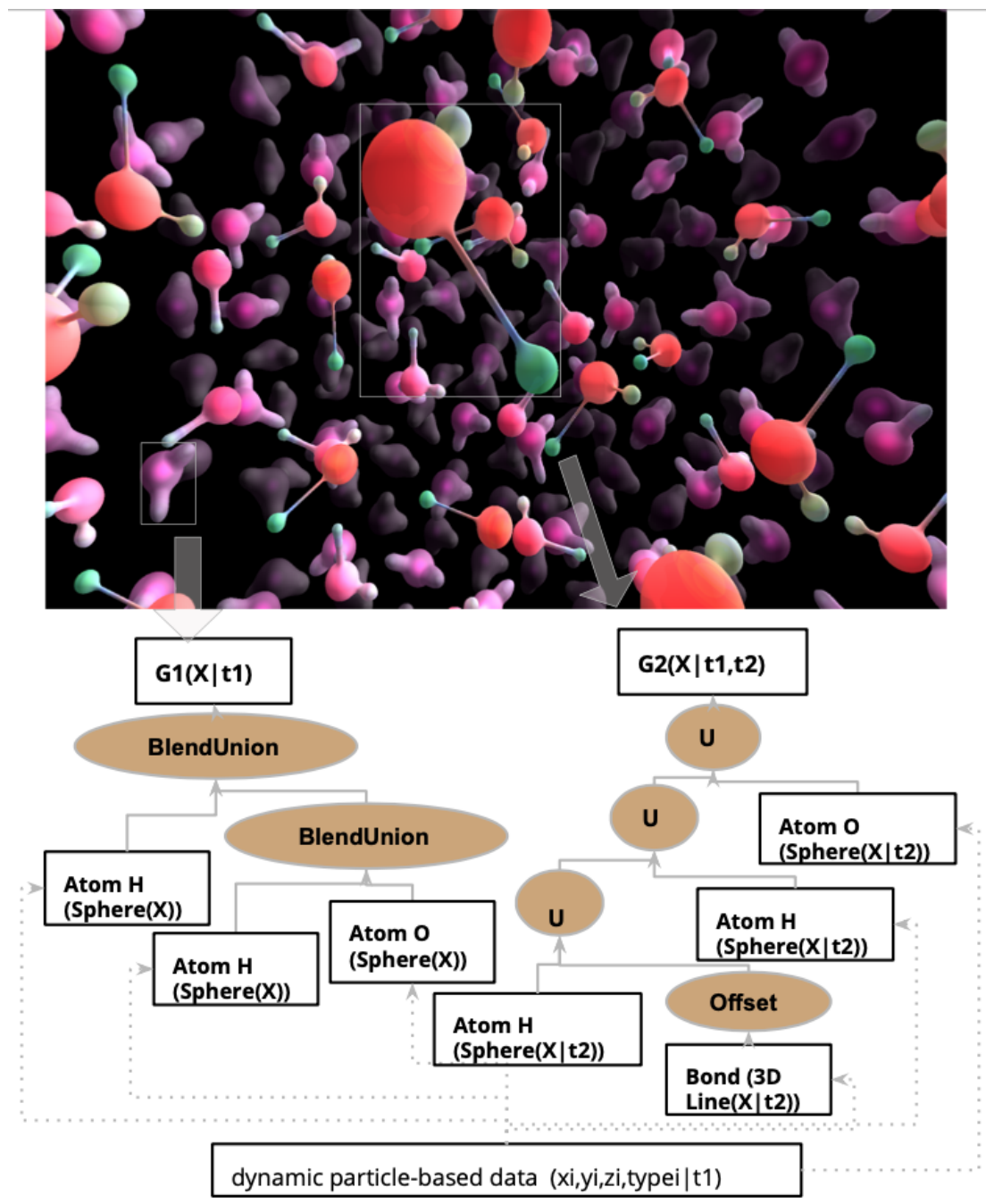


Figure 4.14: An example of constructive modelling of dynamic geometry on "macro" (cluster fluctuations) and "micro" (individual molecule vibrations) scales controlled with parameters t_1, t_2 for water cluster.

modelling operations are applied to both point-based data (dynamic change of position on various scale) and procedural continuous functions (dynamic change in shape and material).

The dynamic properties on "macro" and "micro" levels are modelled constructively as illustrated on the Fig. 4.14.

Such rendering procedure demands the computation of intersection of ray-cell in E^5 that takes advantage of direct projection of cell to E^3 space during ray-tracing. For this, the values of parameters t are defined during ray-tracing. Thus, both geometry and colour representations of multi-scale features are loaded from $G_i(t), A_{O_i}(t), A_{S_i}(t)$ during ray-tracing with further optical or auditory properties accumulation. As we use direct rendering approach, there are no intermediate representations for rendering and rendering itself is performed without any extra computations. This allows introduction of complex interactive visualisation techniques.

For example, in the considered LOD visualisation, several parameters can be changed interactively and in real-time:

- A number of loaded vibrations;
- The geometry and internal structure of each water molecule by changing the camera causing transition from "macro" scale to "micro" scale image of the given phenomena;
- Dynamic features on both "macro" and "micro" scale;

4.3.4 Lattices and irregular structure modelling on the sets of cells

Let us consider the case of lattice-based microstructures. The main specific of those objects is that they are modelled through the concept of a unit cell. A unit cell is the conventional basic construction element for the crystal structure. The representation of crystal structures is a basic inspiration for this task that assumes arbitrary modelling within initial crystal lattice representation. In this work we consider a core construction unit within the spatial subdivision, similarly to individual molecule in a cluster that was considered in section 4.3.3. The microstructures modelling assumes that cellular subdivision can be composed of unit cells of any geometry primitives. The most often examples are tetrahedra (see Fig. 4.15) or cubical crystal unit cell (see Fig. 4.16) inspired by input data from FEM or molecular simulation. The arbitrary structures are modelled within this subdivision (0D, 1D, 3D) with dynamic changes in topology of not only unit cells, but the entire structure.

In Fig. 4.15 we demonstrate the frames of a rendering of a dynamic structure modelled on a subdivision defined with the tetrahedral mesh with various dynamic changes of topology

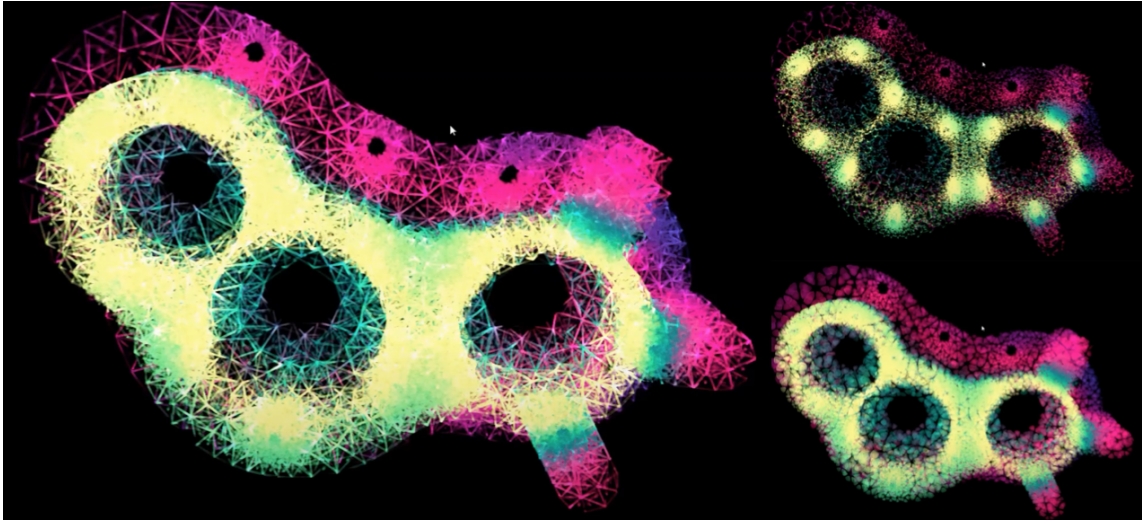


Figure 4.15: Using tetrahedral mesh subdivision as a basis for modelling of arbitrary geometry on set of cells

of 0D,3D,1D dimension. The information on neighbouring cells allows creating an effect of dynamical alteration of lattice structures with different typologies (see Fig. 4.15).

Moreover, the complex cases require the modelling of an irregular lattice structure. For example, in architecture the materials design is often inspired by crystal structures and uses the real crystal data as an input. A crystal cell is a basic construction unit for crystal-like mesostructures. They also use similar design concepts such as supercells allowing for more flexibility in terms of using purely arbitrary geometric modelling over data to create a hierarchical structure. The architected material is constructed through cellular domains that are filled with atomic crystal lattices of different types.

In terms of geometry modelling, the user is selecting on the lattice of such structure the several "meta" regions, or geometry subdomains of certain type. A new structure is injected inside each region while initial unit cell subdivision is still preserved. The new structure can be continuously modelled across several cells that this new region includes. See Fig. 4.17 for example of such modelling on initial crystal lattice presented in Fig. 4.16.

We define such "meta" regions boundaries with SDF geometries: $G_1 : F_1(X), G_2 : F_2(X), G_3 : F_3(X), G_4 : F_4(X)$ (in Fig. 4.17. We highlight the subsets of cells of initial lattice structures that belong to these regions with different colour: green,pink,violet,yellow).

On initial subdivision $\langle I, BV^{l_2} \rangle = \bigcup_{i=1}^N \langle I_i, BV_i^{l_2} \rangle$ 4 subsets of cells are selected: $\langle I_1, BV_1^{l_2} \rangle \subset G_1, \langle I_2, BV_2^{l_2} \rangle \subset G_2, \langle I_3, BV_3^{l_2} \rangle \subset G_3, \langle I_4, BV_4^{l_2} \rangle \subset G_4,$

A new type of geometry is modelled on base of crystal lattice initial data (explicit cell) and introduced subdivisions within each meta-region of defined type (see Fig. 4.16):

$$\langle I_1, BV_1^{l_2} \rangle \Rightarrow \langle I'_1, BV_1^{l_2} \rangle,$$

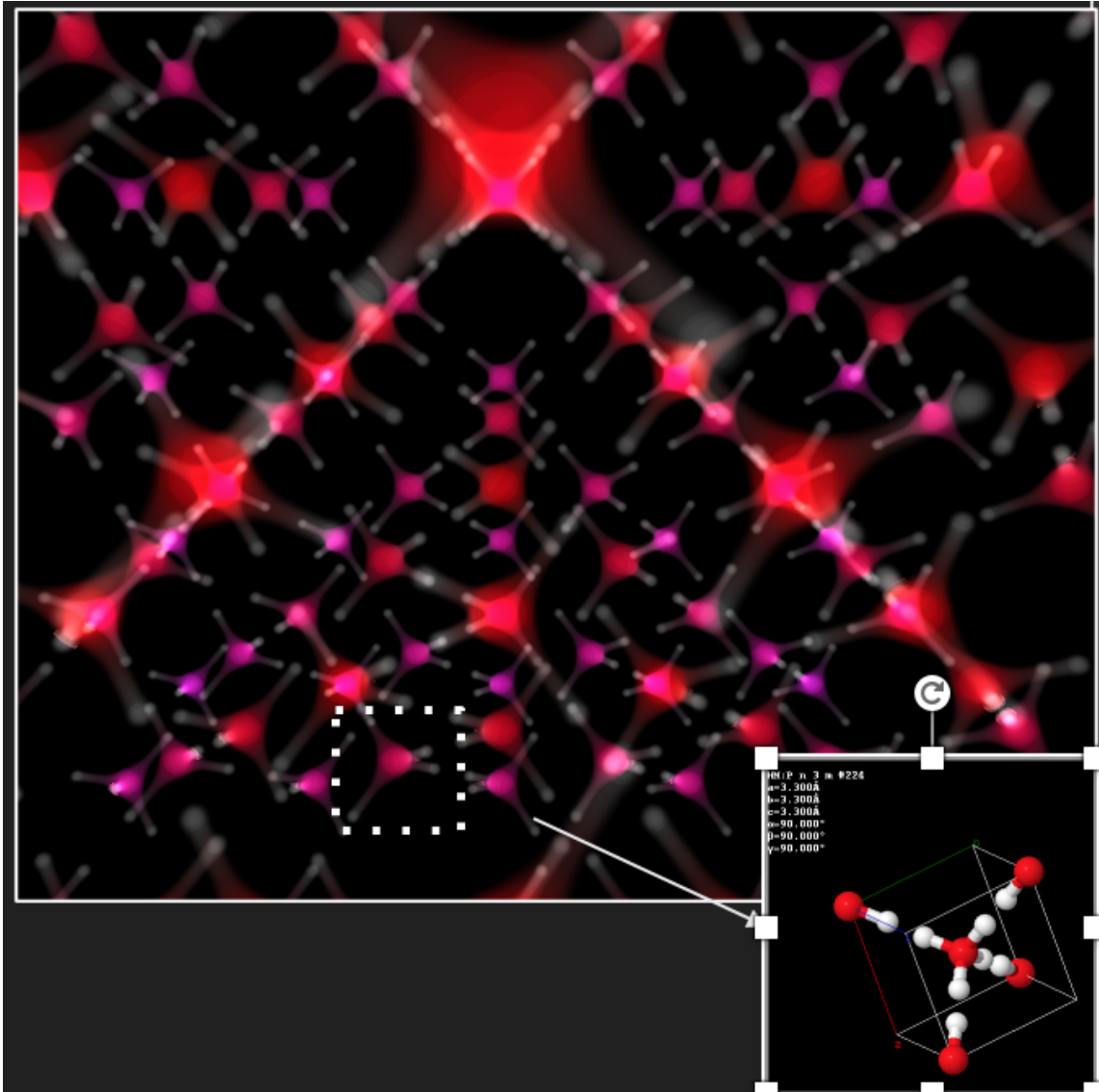


Figure 4.16: Ice crystal lattice-based microstructure a) Lattice b)Unit cell

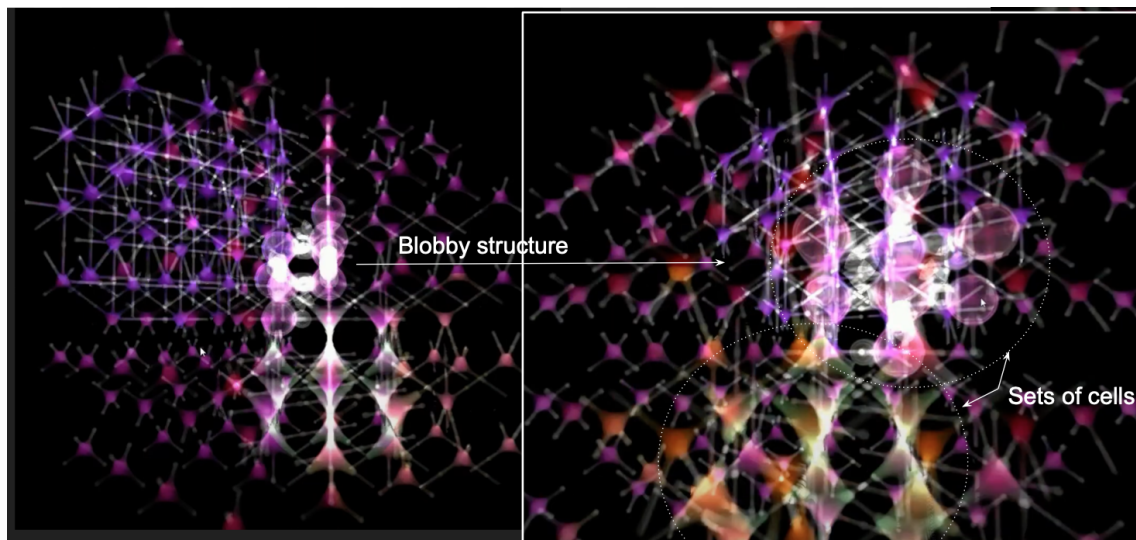


Figure 4.17: Modelling within the selection of unit cells. The lattice structure or "bloby" structure within each regions is highlighted with different colour (green, pink, violet, yellow)

...

$$\langle I_4, BV_4^{l_2} \rangle \Rightarrow \langle I'_4, BV_4^{l_2} \rangle$$

It should be noted that the area of digital fabrication demands injection of arbitrary geometry, not only balls and beams model and other simple primitives. In Fig. 4.17 we show the examples of different types of geometries modelled on sets of cells. This example also includes modelling of conventional "bloby" type structures as a continuous volume on initial subdivision $\langle I_4, BV_4^{l_2} \rangle$. The entire volume is modelled as union of local "bloby" overlapping patches that are assembled during volume ray-casting procedure. Each such patch is constructed during ray-casting as blob of currently intersected with ray cell $I_{i,j,k,l}$ and its cell neighbours $I_{i+1,j,k,l}, I_{i-1,j,k,l}, I_{i,j+1,k,l}$ and etc.

The overlap is handled during ray-casting procedure to render a continuous surface between neighbouring cells with overlapping bounding volumes. In section 5.3.2 we provide the details on design of complex ray-casting pipelines with post-processing stage to handle such cases.

We should note that the technique is very similar to (Gourmel et al. 2010b) and is quite common for modelling of secondary molecular surfaces (Parulek & Viola 2012) or fast reconstruction and rendering of arbitrary volumes with local features. In general case, to access the j -th cell neighbours and additional KD-structures are used. The crystal structure provide allow modelling of the entire lattice via unit cell and its symmetry and this information is sufficient to also construct the secondary volumes.

4.4 Visual-auditory materials modelling

4.4.1 Constructive material modelling

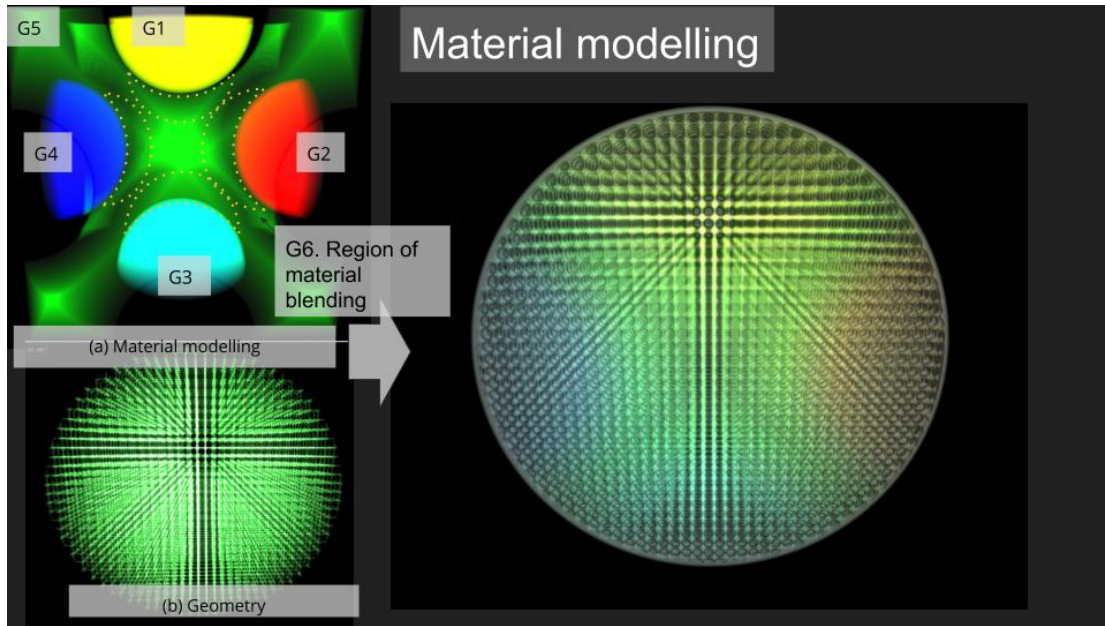


Figure 4.18: Material modelling and application scheme. a) G_1, G_2, G_3, G_4, G_5 are geometry regions of semitransparent homogeneous material. G_6 is computed as subtraction from cube of G_1, G_2, G_3, G_4, G_5 represents a region of homogeneous materials blending $f(x) = RGBW$ and blended material as blending function over two constant $f(X) = Blend(f_1(x), f_2(x))$ where f_1 and f_2 are functions returning material distribution within the bounding volume. b) Geometry c) Result of material application rendered with proposed sphere-traced sampling d) Comparison to regular volume sampling

The heterogeneous material distribution is a main feature that defines heterogeneous object. If we consider conventional optical material, it is defined by associated properties in geometric space that demonstrate a gradual change and need to be modelled continuously on geometric domain G_i . Given the initial data as dynamic tuple $g(t), l(t), a(t)$, the $a(t)$ are dynamic attributes that represent a heterogeneous object properties A'_1, \dots, A'_m in geometric space that are properties to be mapped to optical and auditory materials for further visual-auditory analysis. The continuous function representations of optical and auditory materials $(Ao_i, As_i) : So_i(X|t), Ss_i(X|t)$ is obtained as a result of mapping applied to each explicit cell discrete representations of attributes $M_a : (A'_{i1}(t), \dots, A'_{im}(t)) \rightarrow (Ao_i(t), As_i(t))$.

In digital fabrication a new material for the additive manufacturing process is often obtained with blending of existing materials, in simple case constant ones (Li, Jianzhong,

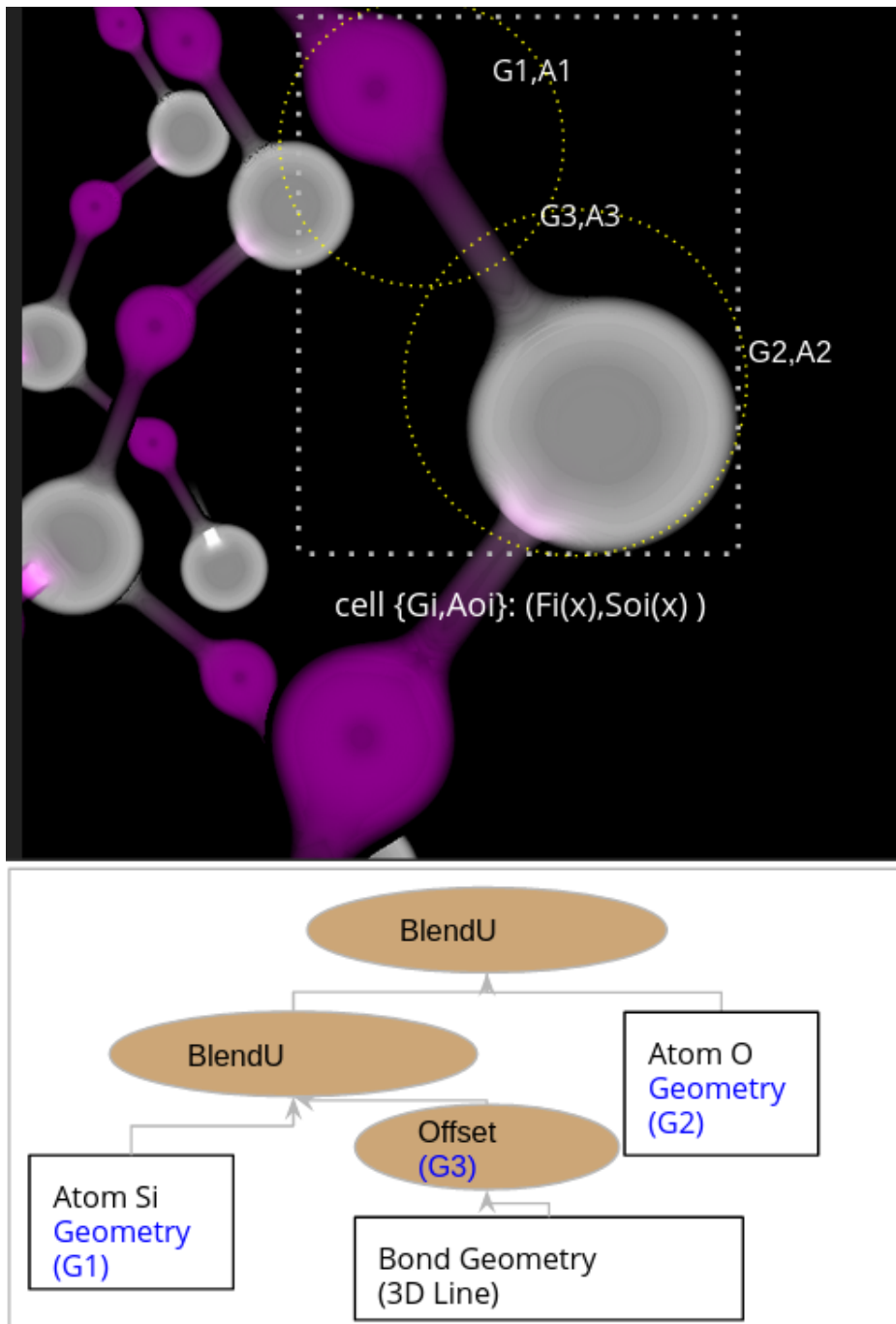


Figure 4.19: Geometry and material modelling within one cell with Si-O basic individual element. A1 and A2 are regions of homogeneous materials on geometries G1,G2 and A3 is defined as blending of A1,A2. Additional bounding subvolumes (yellow spheres) include blending of bond with one of its atoms

Feng, Shang & Lin 2020),(Jackson et al. 1999). Thus, the material modelling is unified and restricted to two techniques: specifying the geometry regions of constant semitransparent material and geometry regions of blending or interpolation between two or more materials (Samanta & Koc 2008),(Schmitt et al. 2008),(Adzhiev et al. 2002) (see Fig. 4.18 (a) for initial definition of geometry regions for material modelling and (c) for the result as material (a) is applied to geometry (b)). Such geometric methods allow flexible control of blend distribution (Adzhiev et al. 2002). We use these constructive modelling techniques to define geometric features of composite cells within subdivision control material composition inside the entire heterogeneous object (see Fig. 4.19) for optical materials. In this work the modelling of auditory properties is restricted to regions of constant material.

Further advantages can be obtained by combining this approach with volume ray-casting within the GPU programmable ray-tracing pipeline. Similarly to lightning techniques (Kulla & Fajardo 2012) the approach takes advantage of per-ray data structures and geometry and material representation within such structures controls sampling issues in evaluation of optical model (see section 4.5.3 for optical and auditory properties accumulation and sections 5.3.4,5.3.2 for implementation details of storage of constructively modelled material and geometry).

The mapping from attribute space of the initial data to space of optical or auditory properties assumes definition of transfer function (TF), which can conventionally be optical or auditory. The optical TF in volume rendering is defined as procedure that maps values of one or several attributes to vector $RGBW$ that describes colour and opacity. In heterogeneous objects the procedure assumes that:

1. Attributes are assigned and interpolated within explicit cell or voxel representation with further mapping to $RGBW$
2. The distribution on entire volume defined within parts of composite cell 4.2.2 and $RGBW$ is obtained as a result of material blending operation.

In this work we assume that TF can be defined in both explicit and implicit features. This means that TF can be defined within any subcomponent of hybrid constructive tree for I_j cell, which can be explicit or implicit cell representation. As TFs that returns $RGBW$ is defined in one or several components, the material distribution $So_i(X|t)$ over entire geometry domain I_j is constructively modelled with interpolation and/or blending operations. The $RGBW$ interpolation/blending modelling process takes as an input either explicit geometry and topology information of the cell, i.e. the leaves that model explicit cell and its lower dimension subcells, or implicit representation of subvolume.

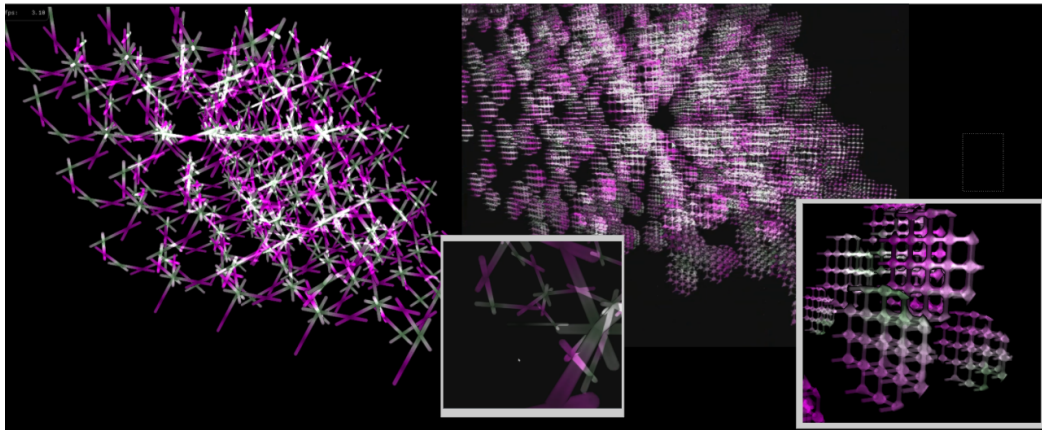


Figure 4.20: Examples of material blending modelling within various structures

Note, that both 1D and multidimensional TF can be integrated as a constructive tree nodes. In section 4.4.2 we provide the example of multi-dimensional TF constructive modelling. However, in this work we will consider mostly 1D TF constructive modelling and concentrate on the cases when the TF defined on subvolumes/implicit cells that represent a region of a constant material. In other words, the entire region is mapped to constant $RGBW$ value. Moreover, within this work we consider modelling of auditory properties only for regions of constant material and pay most attention to auditory TF. The constructive modelling of optical material combines regions of constant material and regions with interpolation/blending schemes applied. The last procedure includes the following types of operations:

1. $M_c : (C_i, A) \rightarrow RGBW$ mapping to $RGBW$ of explicit cell. It assumes TF defined on explicit cell and interpolation procedure that operates explicit cell geometry g .

Mappings are applied to explicit cell C_i and attribute data $a(t)$ defined within this cell. This suggest that a continuous representation of input attributes defined on explicit cell can be obtained. Attributes can be assigned to geometry, to explicit cell or its composing cells of lower dimension, e.g. 1D line segments that are 3D tetrahedron edges. Continuous representations $So_i(X|t), Ss_i(X|t)$ are conventionally obtained through data interpolation procedures.

For example, in visualisation of the tetrahedral meshes, the material description on tetrahedral domain is obtained as mapping of scalar attribute values defined in vertices to colour with further interpolation on tetrahedron volume domain using barycentric or mean value coordinates (Frank 2007), (Hormann & Floater 2006). The colour interpolation scheme is often formulated through weights that depend on distance to the points (vertices of polygon, tetrahedron). See Fig.4.16 for example of rendering of the results of heat transfer interpolation).

2. $M_i : (I_i, A) \rightarrow RGBW$ mapping to $RGBW$ of implicit cell. It assumes TF defined on implicit cells I'_{ij} that can be a subcells of a composite cell I_i (see section 4.2.2). The blending procedure operates the SDF-defined I'_{ij} with geometries G'_{ij} where homogeneous material is defined with TF.

Material at each sampled point is computed by using weighted sum of $RGBW_j$ defined in geometric regions I_{ij} . The modelling of gradual change in material distribution in many cases assumes that $S_{o_i}(X|t), S_{s_i}(X|t)$ are modelled through distance related properties of regions I_{ij} that use SDF representation. The procedure is often referenced as modelling of materials blending. The procedure is well studied in area of digital fabrication as a part of heterogeneous multi-material modelling (Pasko et al. 2001) is schematically presented in Fig. 4.18.

Note that the geometric regions of homogeneous constant and blended material may be different from those that are used in G_i constructive tree (see Fig. 4.18). However, in area of scientific data visualisation as materials reflect properties that are defined on geometry G_i (see the input data tuple definition), the G_i and A_{o_i} do share some geometries primitives in constructive trees. Simply speaking, material and geometry constructive trees correlate. Thus, the optical properties those are colour and opacity values change is modelled within this geometry domain as shown in Fig 4.19. We apply the same concepts to model material within lattice-based microstructures (see results on Fig. 4.20).

4.4.2 Multi-dimensional TF

As we have discussed in section 3.4.2 the multidimensional TFs are conventionally used in complex cases, when the user simultaneously analyses the distribution of several properties within the volume structure. In terms of constructive modelling 2D TF, that we consider in this work is a binary operation node, it takes two scalar fields/implicit representations as an input. For example in Fig. 4.21 we have considered the 2D TF that takes as input two molecular fields. The analysis problem requires the optical model to highlight the dynamic changes in both scalar fields that describe molecular phenomena (Electron density and Electrostatic potential scalar fields). To address the issue we use a 2D TF and different models of optical interaction those are emission-absorption and emission-absorption-scattering.

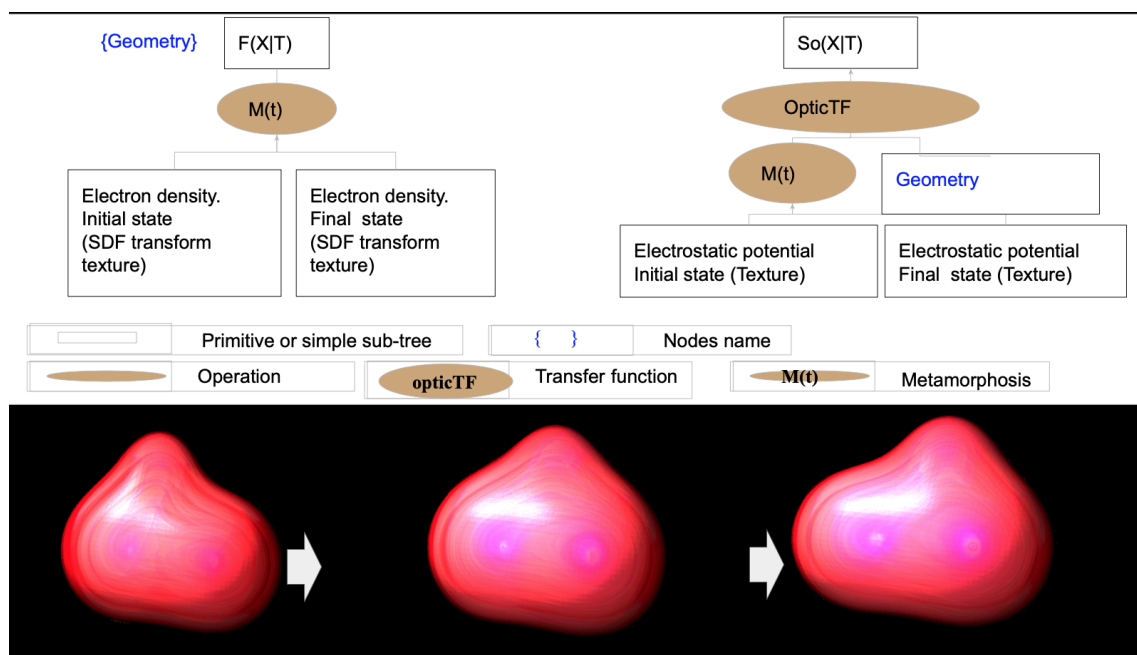


Figure 4.21: Constructive modelling of geometry and optical properties for dynamic HCN molecule

4.5 Visual-auditory rendering

4.5.1 Overview

As we have discussed in sections 3.4.2 and 3.4.4, the problem of volume rendering can be defined as solving the volume-rendering equation that describes a physical process of light transport. To solve the equation we use the ray-casting procedure that numerically approximates the solution to volume-rendering equation along each ray shot from the camera. The projected image is used for conventional visual stimuli based analysis. Solving volume-rendering equation for heterogeneous objects whose optical and auditory properties are modelled on spatial distribution, may be accelerated with empty space skipping as volume rendering equation is decomposed and solved only for each subvolume bounded with geometry G_i (see Background section 3.4.3 for details). We apply the general concepts introduced in optical rendering to define the visual-auditory rendering of heterogeneous objects with the procedures of two main types:

1. Finding the intersections along the ray for each 3D projected subvolume G_i obtained from multidimensional SDF $I_i(t0, t1)$ as a result of geometric modelling. In this

research it is a 3D slice $I_i(t_{0j}, t_{1k})$ for specified time and multi-scale parameters values t_{0j}, t_{1k}

2. Assembling optical Ao_i and auditory As_i properties as an impact of light/sound interaction within 3d subvolume G_i .

For conventional 3d subvolumes, bounded with convex geometry, the first step is simplified with computation of preliminary intersection with bounding volumes (see section 3.4.3). Those boundaries are refined with subvolume intersection and obtained ray segment is used further for the integration of optical properties in performed on per-voxel basis with discreet regular step sampling scheme (see section 3.4.4).

We consider the following adjustments to conventional procedure. Firstly, in general case we deal with multidimensional geometry $G_i : < I_i(t_0, t_1), BV_i^{l_2}(t_0) >$ with dynamic and multi-scale properties (see section 4.2.2). In this work we process multidimensional cells with dynamic LOD visualisation technique (see section 4.3.3) that deploys $BV_i^{l_2}(t_0)$ to obtain a projection into 3D space for final exact intersection evaluation. Secondly, we perform accumulation of optical and auditory properties not on conventional per-voxel basis with discreet regular step sampling scheme, but consider the light/sound interaction with ray-segment as basic visual and auditory properties accumulation unit (see section 3.4.4 for overview of optical integration principles). For this we use the constructive modelling of optical and auditory material scheme that we have proposed in section 4.4.

4.5.2 Intersection with multi-dimensional geometry

As discussed above, we use aim to avoid intermediate representations for rendering. The concept assumes that such procedures as geometry modelling or evaluation of relationships between IC cells are performed as a part of ray-casting procedure. In particular, the ray-casting becomes a basis of considered dynamic LOD visualisation technique that takes multi-dimensional geometry as input (see section 4.3.3). The parameters t_0, t_1 that control dynamic and multi-scale properties are defined/evaluated during ray-casting that operates $I_i, BV_i^{l_2}$ to slice and project the multi-dimensional geometry in E^5 space to E^3 space.

The basic scheme is presented in Fig. 4.22 as an adjustment to conventional volume integration scheme.

Step 1. For each currently rendered time frame we obtain a value of t_0 parameter t_{0j} . We shoot the rays from camera, where each ray is represented as augmented with time value parameter tuple $(o, -w, t_{0j})$, where o is the ray origin, and $-w$ is the ray direction.

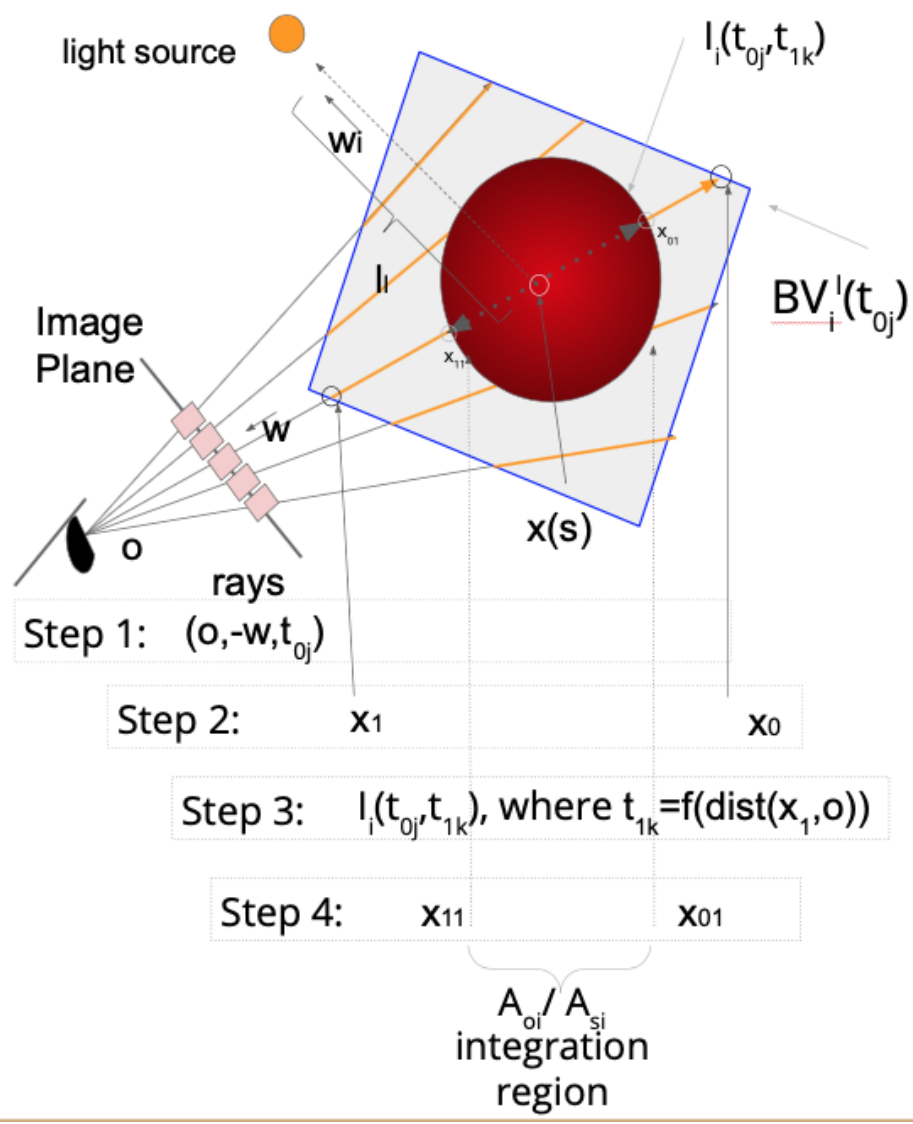


Figure 4.22: Intersection with multidimensional geometry for further optical and auditory properties integration.

Step 2. Bounding volumes $BV_i^I(t_0)$ are used to find the preliminary intersection points x_0, x_1 . As a result we can approximate a potential intersections distance d_j with 3D projection of $I_j(t_0, t_1)$ that we still have to compute.

Step 3. We use the value of d_j to estimate the parameter value t_1 and compute the 3D projected representation $I_j(t_0, t_{1k})$ defined by visualisation technique.

As in this work we use only two multi-scale representations (see section 4.2.2), we define d_{min}, d_{max} , where within segment (O, d_{min}) to render the first multi-scale representation (d_{max}, ∞) for the second. t_{1k} can be evaluated as:

$$t_{1k} = \begin{cases} 0, & \text{if } d_j < d_{min} \\ \frac{d_j - d_{min}}{(d_{max} - d_{min})}, & \text{if } d_{min} \leq d_j \leq d_{max} \\ 1, & \text{if } d_j > d_{max} \end{cases} \quad (4.9)$$

Step 4. We compute the ray intersection with 3D projected slice $I_i(t_0, t_{1k})$ and obtain the final intersection points x_{01}, x_{11} , that are used later for integration of optical and auditory properties.

Thus, the integration of optical and auditory properties can be performed on ray-segment basis on segment x_{01}, x_{11} .

4.5.3 Visual-auditory properties accumulation

4.5.3.1 General concepts

The auditory A_s and optical A_o material of HV model return the description of optical and auditory properties that are used by ray-casting. In this work, we take advantage of a musical systems approach to mapping to facilitate visual/auditory stimuli cross interpretation (see sections 3.5.4 and the spatial properties of sound for localisation of auditory object, the sources of sound. In sections 3.5.2, 3.5.3.1 we have discussed the basic principles how such auditory properties are "encoded" in generated digital sound wave representation and have discussed the ability of the human auditory system to automatically "decode", perceive and analyse such features in section 3.5.4. We take advantage of these principles to introduce an auditory TF and spatial sound rendering techniques for auditory stimuli generation with ray-casting similarly to visual. As a result of the auditory analysis, the human auditory system will "decompose" the generated sound waves properties and associate them with cells of a heterogeneous object that are treated auditory objects producing sound. The insight into heterogeneous phenomena is formed based on the auditory stimuli that can be combined and compared with visual stimuli based insight into a heterogeneous structure (see section 3.5.4.

The optical and auditory output of each i -th cell are computed as a result of light and auditory impulse propagation through optical Ao_i or auditory As_i material defined on cell within geometry regions G_i :

$$G_i, Ao_i \rightarrow RGBW_i \quad (4.10)$$

$$G_i, As_i \rightarrow S_i(d) \quad (4.11)$$

where $RGBW$ are colour and opacity and $S(d)$ is a time/distance-dependent sound wave, where d is normalised distance along ray from its origin o , that approximates sound front propagation and in this work takes into account only primary rays.

Ray-casting accumulates $RGBW_i$ and $S_i(d)$ to compute :

1. An output colour value RGB value for pixel of projected image, that listener sees.
2. Spatial auditory environment approximation that reaches the listener from a direction, defined by ray $S(d)$.

Conventionally, assembling of optical Ao_i properties on ray-segment defined with G_i , i.e. solving rendering equation for this ray-segment, is approximated numerically Riemann sum (see Background section 3.4.3 with volume sampling using the sufficiently small step. The constructive modelling of optical and auditory material allows introducing a more flexible integration scheme. We can compute/approximate the regions of constant and blended material along the ray and adjust our sampling and integration within G_i to provide more exact approximation of emission, absorption and scattering processes through subvolume G_i .

This scheme provides a unified approach to optical and auditory properties accumulation during ray-casting on per-ray segment basis that is an accumulation that is simplified by the nature of modelling of Ao_i and As_i .

4.5.3.2 Optical properties accumulation

For the subvolume G_i we can compute the ray-segments with:

1. Constant material properties, i.e. constant colour and opacity, s_c with length Δs_c
2. Distance-dependent change of colour and opacity that allows to subdivide the approximate the segment of length s_d into sub-segments with average colour and opacity values and consider approximately equal lengths Δs_{c_j}
3. Regions where only conventional volume sampling with regular sufficiently small step is applicable s_s

In this work, we do not use the latter case and focus on an adjusted ray-segment integration scheme, i.e. the first two cases.

The assumption provides the following simplifications for general volume integration scheme we have discussed in 3.4.3. Firstly, the integration is approximated by discrete sampling for constant transparency within region $s_d = \sum_{i=1}^N s_{ci}$ as:

$$T(s_d) = \exp\left(-\int_0^{s_d} \tau(t) dt\right) \approx \begin{cases} \prod_{j=1}^i \exp(\tau(s_j)\Delta s_{cj}) & \text{if } \Delta s_{cj} > \Delta s_{step} \\ \prod_{j=1}^i (1 - \tau(s_j)\Delta s_{cj}) & \text{if } \Delta s_{cj} \leq \Delta s_{step} \end{cases} \quad (4.12)$$

where Δs_{step} is a predefined minimum sampling step that is sufficiently small to further approximate the exponential Lambert-Beer's law.

Secondly, if we assume that in addition to each region s_{ci} we have a constant colour and transparency. Thus the approximation on each i^{th} segment will be defined through previous values as:

$$E_i = \int_{s_{ci}}^{s_{ci+1}} \tau_i c_i T(s) ds = T(s_{ci}) c_i (1 - \exp(-\tau_i \Delta s_{ci})) \quad (4.13)$$

Therefore, constructive modelling of the material allows adapting the sampling scheme from conventional small regular step sampling to blended material regions sampling and integration over regions of constant materials.

To find the optimal sampling $s_d = \sum_{i=1}^N s_{ci}$ for ray-based integration over regions of constant or averaged material, we consider sphere tracing algorithm (see section 5.2.4). The algorithm is based on the evaluation of distance properties of SDF and as we have discussed the same distance properties are applied to materials blending modelling. This allows us to use the sphere-tracing as a procedure that approximates the regions s_{ci} where we can consider the material colour and opacity to be constant or averaged.

4.5.3.3 Auditory properties accumulation

Similarly to optical material, integration of the auditory model is performed on a per-cell basis. For each cell the sound wave $S_j(d_j)$ evaluated as a result of backward sound propagation through a j th region of constant auditory material with length along the ray d_j . The perceived parameters of generated sound wave $S_j(d_j)$ are defined with auditory TF. Each ray-segment of constant auditory material acts like an activated by initial impulse sound source or an auditory object that is a cell in heterogeneous structure. Also, with applied HRTF convolution,

the user perceives a spatial position of cells (see example for molecular structure, where regions on constant material are defined within "atom" geometry in Fig. 4.23).

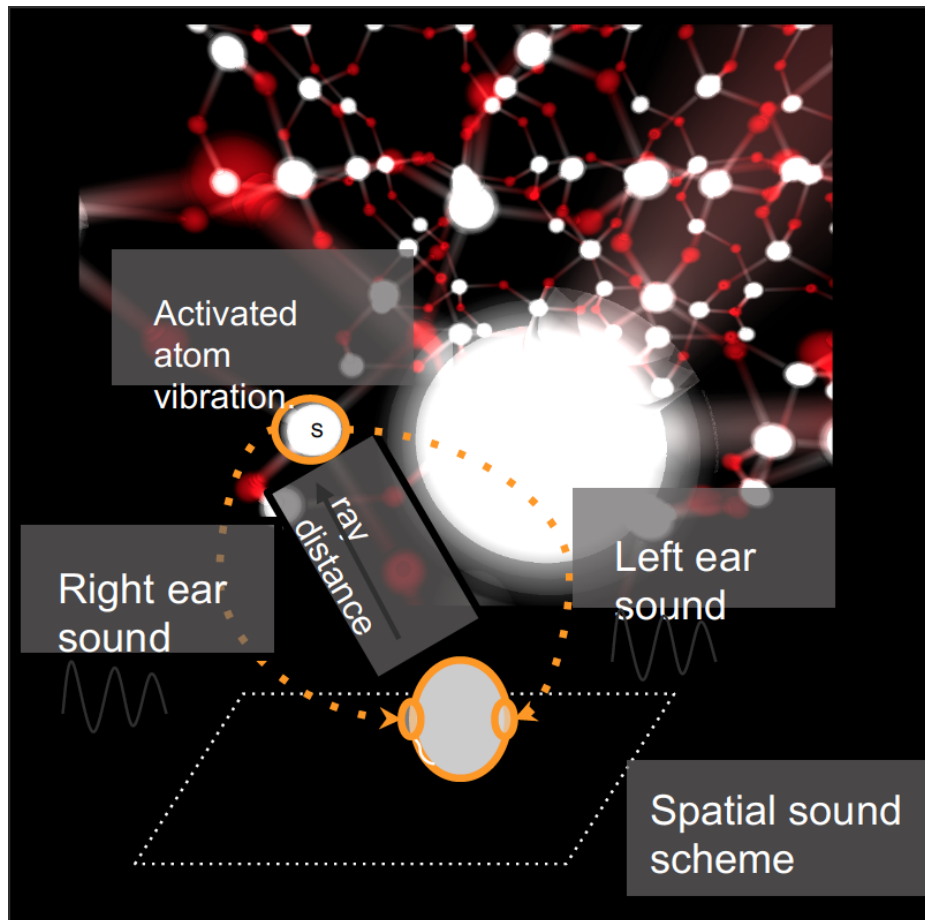


Figure 4.23: Auditory scene volume ray-casting for molecular structure where each region of constant acoustic material is defined on "atom" geometry.

As for large structures, we may have to deal with a large number of such auditory objects, we approximate the spatial sound by following two steps. The first part of auditory stimuli generation accumulates the results of interaction with auditory material of all cells along the ray with consideration of distance-based attenuation of initial impulse as it propagates backwards from a user into a scene (see Fig. 4.23). The second part approximates the spatial properties of sound/listener interaction with HRTF convolution applied on the per-ray basis for sound source position. Let us discuss the details.

The first part of auditory rendering procedure, that in this work considers only primary rays (see section 3.5.3.1), is similar to optic volume rendering. Let us consider the initial impulse propagating along the ray and attenuates exponentially. The auditory material A_{s_i} describes how each segment of region of constant auditory material with length s_{c_i} definition

along ray traversing i -th cell interacts with auditory impulse by producing a "modal" vibration that is a distance dependent sound wave representation $M_i(d)$. The output generated sound wave represents how the entire individual element described with geometry G_i within a cell (e.g., an individual atom or a molecule within subdividing) interacts with the sound impulse that propagates along a defined path. The accumulated along the ray auditory impulse represents an interaction of all intersected objects (cells) of an attenuating initial impulse.

Ray-casting through some geometry G_i with defined auditory material A_{si} interacts with propagating sound impulse and generates the individual modal sound with given frequency and amplitude as impulse "activates" it. As a result of the interaction, a "modal vibration" M_i is produced. The modes are activated in time and exponentially attenuated depending on the distance passed: $A(D_i) = A_{ini} * \exp^{-m*D_i}$, where D_i is a distance along the ray before intersecting i object, A_{ini} - initial amplitude and m is a coefficient that controls the speed of attenuation.

The contribution of each region G_i , its spatial position is perceived through time of "activation" and initial loudness: $A_{si} \rightarrow M_i(d)$. The final accumulated output signal can be described as:

$$I(d) = \sum_{i=0}^N A_i * M_i * \begin{cases} 0, & \text{if } D_i - d > 0 \\ e^{dur_i*(D_i-d)}, & \text{otherwise} \end{cases} \quad (4.14)$$

where d denotes the distance the ray passes, which is proportional to the time parameter of a spreading wave impulse; N is a total number of modes with the times they are activated/intersected as the ray travels; dur_i is a mode duration that can be computed as the difference in D_i of the current mode and the difference in D_k of the next mode $D_k = \min_{j=0}^{j=n} (D_j) > D_i$. M_i is a mode, and, finally, A_i denotes the initial amplitude of the mode, which describes the energy the impulse transmitted to the mode.

We use the sampled digital sound representation (see section 3.5.2) to describe the entire ray propagation path with a sampled buffer that is filled during ray-casting on base of current distance to ray origin along the ray interpreted as time and duration. For example, a digital representation of sound wave as sampled audio buffer with sampling rate FS will be represented with buffer of length L_b defined as $L_b = FS * T_r$, where T_r - duration time in seconds and is proportional to D_r , the approximate maximum passed distance of the initial auditory impulse propagation along ray. A contribution to total impulse of each auditory material A_{si} generated as interaction with each G_i with the passed distance along ray d (intersection with geometry G_i) relates to time t as $fractd = \frac{T_r}{D_r}$. Thus we can synchronise the visual effects, such as highlighting of "activated" atoms with sound. We use the total bounding box of current heterogeneous object to compute D_r and introduce a user defined

scaling coefficient $scale_{coeff}$: $D_r = \max(D_j) * scale_{coeff}$. $scale_{coeff}$ allows adjusting how long the resulting auditory output will be played (scale of an auditory track).

In this work, for the intersection with geometry G_i , the size of G_i that is the "atom size" in the case of molecular structure, is further neglected in the auditory sampling procedure. The duration dur_i of each mode along the i -th ray is defined by the distance between the intersected atoms (sound attenuation stage) and is scaled with user-defined scaling coefficient $scale_{coeff}$ that are introduced to D_r . Note, that the sampling buffer for the auditory track is filled during the ray-casting procedure for defined scales with no preprocessing/scaling directly of sampled buffers.

The second part of sound preprocessing enables binaural sound perception. Similar to (Chanda et al. 2006), (Adams & Wakefield 2005) that computes the "clusters" of sound sources and approximates their positions, we group the auditory objects on the per-ray basis (intersected with ray cells). Thus, we use the output sampled sound wave from equation 1) as the input for further HRTF convolution. We compute the ray intersection with a plane, parallel to the image plane in camera space that passes through the centre of the bounding box of the entire heterogeneous object BV and treats the normalised coordinates of this intersection as a position of the sound source that plays that wave. Each position is matched with HRTF coordinates and HRIR coefficients and all the delays are interpolated. The result of the procedure is the output sound pressures for left and right ears H_L and H_R (see details in on binaural rendering in section 3.5.3.2)).

Note that as large scale structures are considered, the area of future work is technique refinement in terms of potential issues related to arbitrary scaling variations with user-defined $scale_{coeff}$ and sampling issues. For example, it is highly unlikely that for large structures we can potentially expect imprecise auditory distance perception discussed in (Zahorik et al. 2005) (in general problem arises for simulated distances more than 1m). However, we consider the user-defined scaling of a scene with $scale_{coeff}$ as a potential adjustment to address the problems of auditory storage as spatial sound is used for object recognition, discussed in (Cowan 1984). Also, for large structures, we consider that regions of interest to be distributed relatively sparse to avoid the localisation blur effect (J. Blauert 1999). In total, the complex problems in the area of perfect localisation/ spatial sound quality related to HRTF customisation scaling or scene scaling issues in high-quality modelling of such binaural perception attributes as a sense of distance and direction (Pike 2019) are out of the scope of this research.

4.6 Interactive visual-auditory exploration

4.6.1 Constructive modelling with interaction avatar

Let us consider the interaction between two heterogeneous objects $h_{av}(t)$ and $h_{sc}(t)$ with geometries G_{av} and G_{sc} , where $h_{av}(t)$ is the representation of visual-auditory scene and $h_{sc}(t)$ is an interaction avatar. We model $h_{av}(t)$ similarly to $h_{sc}(t)$ with constructive hybrid modelling approach.

Let us consider the example of hand-based interaction (Phillips et al. 2010) (Hoell et al. 2018) with a gesture control device, such as Leap Motion.

We introduce the geometry G_{av} of interaction avatar $h_{av}(t)$ that represents a human hand with the following steps:

1. Positioning of the interaction device and getting input data for the virtual representation of the interaction avatar. In case of Leap Motion device is being used, the raw depth scan input data is pre-processed with SDK automatically. Thus, we obtain the initial data in a form of hand skeleton.

The hand skeleton describes the explicit structure composed of cells with 1D topology (see Fig.4.24). The basic geometry represents a palm and fingertips of virtual hand in scene. The entire structure is relatively small with five cells with a limited maximum distance between control points. Thus, the introduction of subdivision that we have considered for complex heterogeneous structures is not necessary as there will be not much increase in efficiency, and we can consider the entire structure as one dynamic explicit cell.

2. Mapping to interaction avatar with geometry G_{av} . For this, we use constructive SDF-based modelling as we have discussed in 4.3 and obtain an implicit cell (see Fig. 4.24).

After the G_{av} is defined, further constructive geometry modelling operations can be applied to G_{av} and G_{sc} after the user interaction.

In Fig.4.25 we show the example of blending geometry modelling procedure to notify users of distance based interaction between two objects $h_{av}(t)$ and $h_{sc}(t)$. Such operation can be modelled constructively with G_{av} and G_{sc} used as a part of constructive tree that is schematically presented in Fig.4.24. The $h_{sc}(t)$ represents the molecular object whose constructive modelling we have considered in Fig. 4.21 in section 4.4.2.

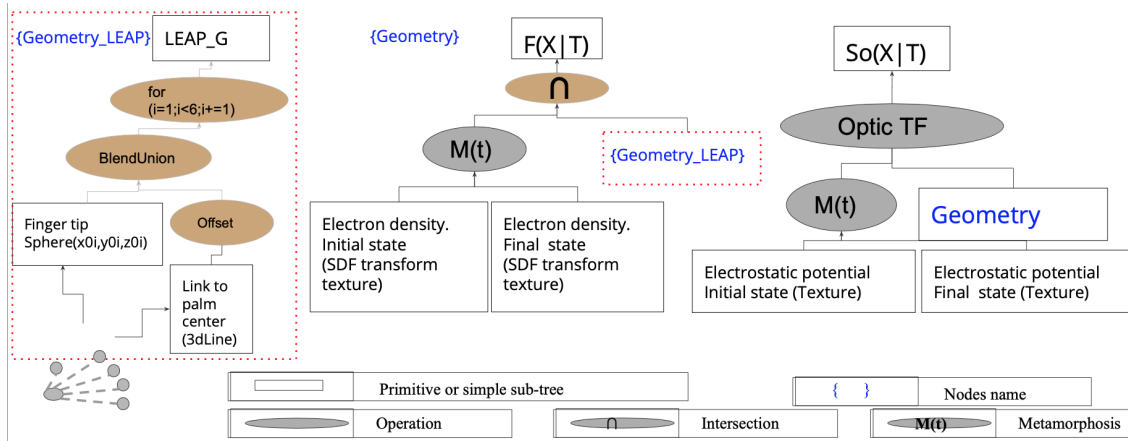


Figure 4.24: Constructive modelling of hand based of hand interaction with object that was considered in Fig. 4.21

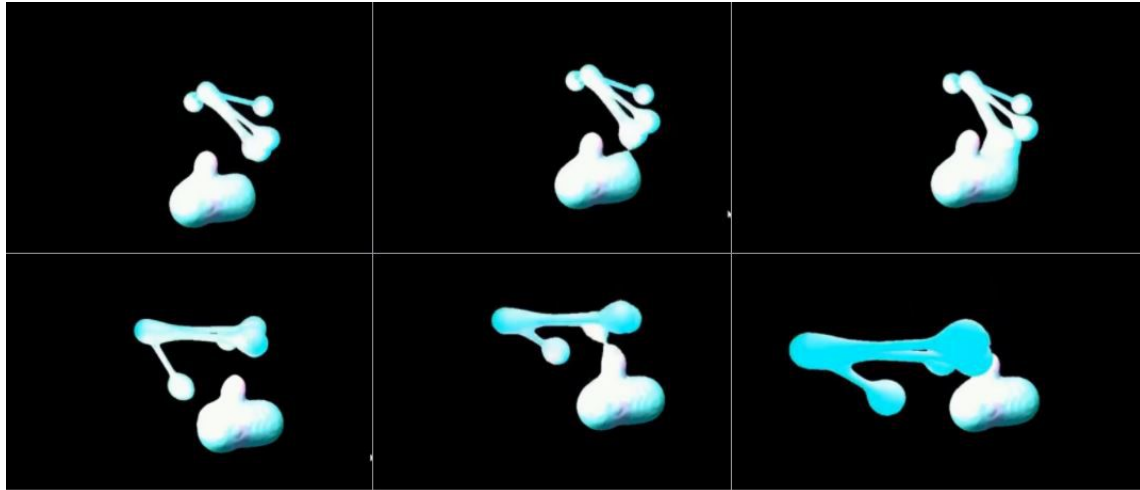


Figure 4.25: Frames of example of constructive modelling on base of hand interaction

The user interaction can also use more complex geometries of one of the interacting objects or both. The examples of such complex cases are the interactive modelling of lattice-based microstructures or modelling of the interaction between two molecular phenomena.

To accelerate the processing of such geometries the complex subdivisions $\langle I_{av}, BV_{av}^{l_2} \rangle = \bigcup_{i=1}^N \langle I_{avi}, BV_{avi}^{l_2} \rangle$ and $\langle I_{sc}, BV_{sc}^{l_2} \rangle = \bigcup_{i=1}^N \langle I_{sci}, BV_{sci}^{l_2} \rangle$ should be introduced for both geometries G_{av} and G_{sc} .

Furthermore, similarly to how accelerated ray-tracing uses the bounding volume subdivision BV_{l_2} within such structures to accelerate and facilitate intersection with I geometry, the modelling of user interaction for such cases employs the $BV_{av}^{l_2}$ and $BV_{sc}^{l_2}$ to evaluate the relationships between sets of cells $h_{av}(t)$ and $h_{sc}(t)$, and select a preliminary set of cells $\langle I'_{sc}, BV_{sc}^{l_2} \rangle \cup \langle I_{sc}, BV_{sc}^{l_2} \rangle$ and $\langle I'_{av}, BV_{av}^{l_2} \rangle \cup \langle I_{av}, BV_{av}^{l_2} \rangle$. $\langle I'_{sc}, BV_{sc}^{l_2} \rangle$ and $\langle I'_{av}, BV_{av}^{l_2} \rangle$ are further deployed for constructive modelling. We consider a basic case of such combination of evaluation of relationships on sets of cells and geometry modelling for accelerated interactive volume rendering in sections 4.6.3.

4.6.2 Measurement with auditory feedback

4.6.2.1 Auditory feedback generation as a part of ray-casting

Measurement procedures highly depend on fast evaluation of distance properties and often in context of ray-casting. We consider this feature to be a part of sound wave propagation within of ray-casting based measurements. Moreover, it makes very convenient to apply the waveguide synthesis that operates on sampled sound wave representations as a part of ray-casting. Consider a very basic measurement example, where we use a travelling wave solution for ideal plucked string as auditory model that can be automatically evaluated with ray-casting.

As mentioned above, as a result of initial impulse a plucked string travelling wave $y(x, t)$ can be represented as a sum of right going $y_r(xct)$ and left going $y_l(x + ct)$ waves. The travelling waves can be simulated through delay lines. Once initial waves are generated as a result of string picking, they travel along the string. Thus it can be said that the time impulse needs to pass till it is reflected (in other words, the distance) is aurally perceived through pitch. If we consider the case of sampled solution, where $SRate$ is sampling rate, string length l relates to the generated pitch p as $l = 2 * SRate / p$ (Smith 1992).

Thus a direct ray-casting based rendering of sampling solution to travelling wave: $y(t_n, x_m) = y^+(n - m) + y^-(n + m)$ will allow us to aurally judge about distance through pitch. As distance becomes smaller, the pitch changes from lower to higher values. The normalisation procedure should allow us to efficiently judge about distance through pitch

value. The auditory feedback rendering can be triggered at the end of user interaction or as a part of simultaneous visual-auditory rendering of dynamic structure with update of visual and auditory stimuli

In section 6.1 we discuss the case study for the analysis of molecular fields, where we use the introduced auditory model to judge on dynamic change of molecule properties that is the length of bond as the process is schematically presented in Fig. 4.26 .

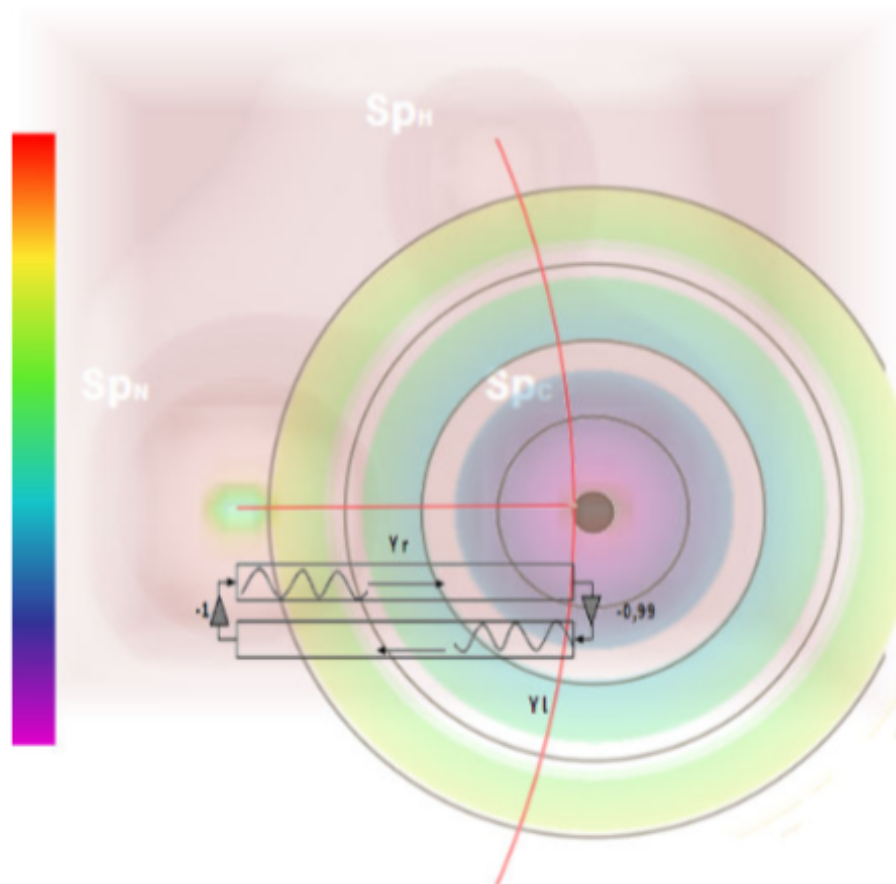


Figure 4.26: The scheme of auditory feedback generation with digital waveguide model of plucked string.

4.6.2.2 Numerical measurements with ray-casting

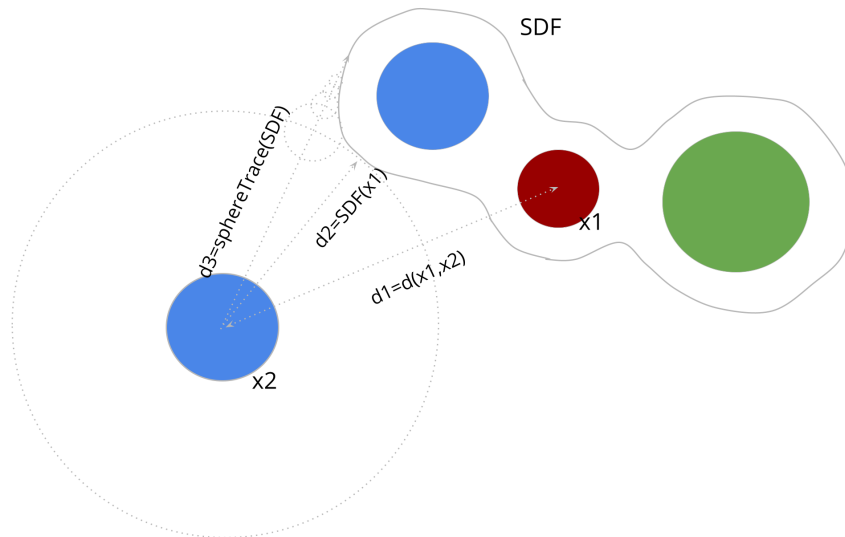


Figure 4.27: Examples of evaluation of distance properties on between cells and additionally modelled representations (SDF blobby structure) within proposed geometry model. $d1$ - euclidean distance between points that are centres of cells, $d2$ - distance from cell centre $x1$ to surface SDF, $d3$ - distance from cell centre to surface SDF along the ray computed with sphere tracing (general algorithm is discussed in section 5.2.4)

In general, the explicit representation $\langle C, BV^{l_2} \rangle$ and implicit representation in the form of SDF $\langle I, BV^{l_2} \rangle$ can be efficiently used for fast computation of distance related measurements. In Fig. 4.27 we provide a scheme of evaluation of distance properties for a basic case. Those can be applicable to the case when in addition to basic point-based representation we model a blobby surface within cellular subdivision. Those often a case of molecular structures when in addition to CPK representation the molecular surface is modelled with point-based data (Parulek & Viola 2012). The fast evaluation of distances between two atoms (cells with 0D data) or between atom and molecular surface (cell with 0D data and modelled surface) is required. Also, the evaluation of such basic distance properties is a core of arbitrary navigation and spatial positioning tasks. Such tasks also often deploy the auditory feedback to facilitate interaction with virtual objects, to coordinate the users movements and position as a part of collaborative spatial exploration or as additional source of information when visual system is fully engaged while performing complex task (Fishman et al. 1996, Song et al. 2011).

4.6.3 Modelling the region of two heterogeneous structures overlap

In conventional interpretation, the multisensory feedback from a user interaction demands evaluation of inside/outside properties between the geometries G_{av} and G_{sc} . Auditory feedback can be deployed only to notify the user that interaction took place, or can provide details on measured values such as: volume of overlap, distance from G_{av} to certain substructure in G_{sc} and etc.

The evaluation of relationships between geometries G_{sc} and G_{av} is split into evaluation of relationships between IC cells in equations 4.6 and 4.7. The process is facilitated by bounding volume structures $BV_{sc}^{l_2}$ and $BV_{av}^{l_2}$ and can be decomposed into two steps:

1. Preliminary evaluation of relationships between bounding volume structures $BV_{sc}^{l_2}$ and $BV_{av}^{l_2}$ and obtaining the subsets $\langle I'_{av}, BV_{av}^{l_2} \rangle$ and $\langle I'_{sc}, BV_{sc}^{l_2} \rangle$, where $\langle I'_{av}, BV_{av}^{l_2} \rangle \supset \langle I_{av}, BV_{av}^{l_2} \rangle$ and $\langle I'_{sc}, BV_{sc}^{l_2} \rangle \supset \langle I_{sc}, BV_{sc}^{l_2} \rangle$ that satisfy the relationship rules executed on bounding volumes

2. Refining the relationships evaluation with SDF representations I'_{av}, I'_{sc} from subsets $\langle I'_{av}, BV_{av}^{l_2} \rangle$ and $\langle I'_{sc}, BV_{sc}^{l_2} \rangle$. As a result we obtain the final subcomplexes with geometry $G_{cs1} : \langle I_{cs1}, BV_{cs1}^{l_2} \rangle$ and $G_{av1} : \langle I_{av1}, BV_{av1}^{l_2} \rangle$, where $\langle I_{av1}, BV_{av1}^{l_2} \rangle \supset \langle I'_{av}, BV_{av}^{l_2} \rangle \supset \langle I_{av}, BV_{av}^{l_2} \rangle$ and $\langle I_{cs1}, BV_{cs1}^{l_2} \rangle \supset \langle I'_{sc}, BV_{sc}^{l_2} \rangle \supset \langle I_{sc}, BV_{sc}^{l_2} \rangle$

For the obtained geometries G_{cs1} and G_{av1} we deploy the constructive modelling on this sets of cells to obtain a new geometry domain G_{o2} . The implementation of such procedures can be accelerated and facilitated with volume ray-casting. In Fig. 4.29 we consider an example of material modelling on region of intersection of two microstructures with evaluation of the overlap between cells. The case study is discussed in details in section 6.2.

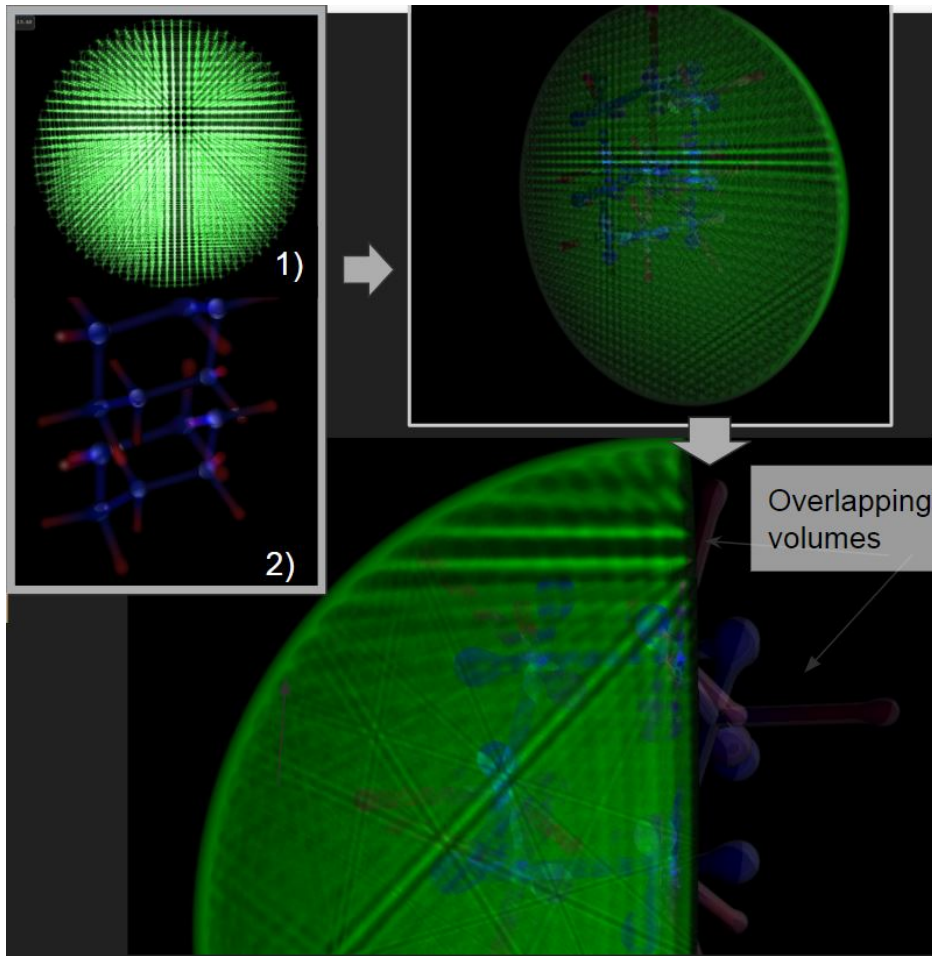


Figure 4.28: Example of volumes overlapping evaluation and complex modelling. Region of overlapping is modelled as “composite material injection” volumes

The implementation takes advantage of possibility to deploy constructive geometry modelling in combination with ray-casting procedures. We discuss the general principles of such ray-tracing pipelines design for heterogeneous objects in section 5.3. Implementation details for a particular case of composite material modelling for the microstructures case study are discussed in section 6.2.3.3.

4.6.4 User Interface for manipulating visual-auditory scene

The conventional GUI tools manipulate the ranges of visual properties (colour scale range and opacity) or additionally computed properties to perform the selection of ROI (see sections 3.6.1, 4.6)). In this research we consider possible extension in terms of visual-auditory interface and consider the interaction that directly manipulates auditory properties for this

purposes and considers the deployment of tools for music composing, such as the MIDI keyboard for interaction.

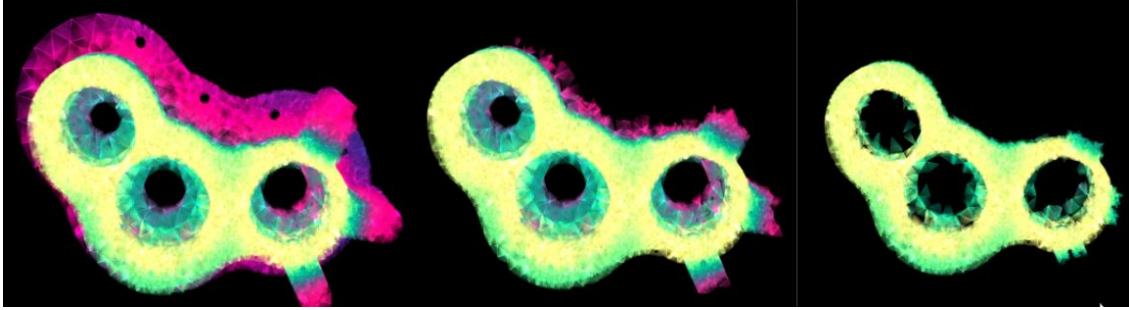


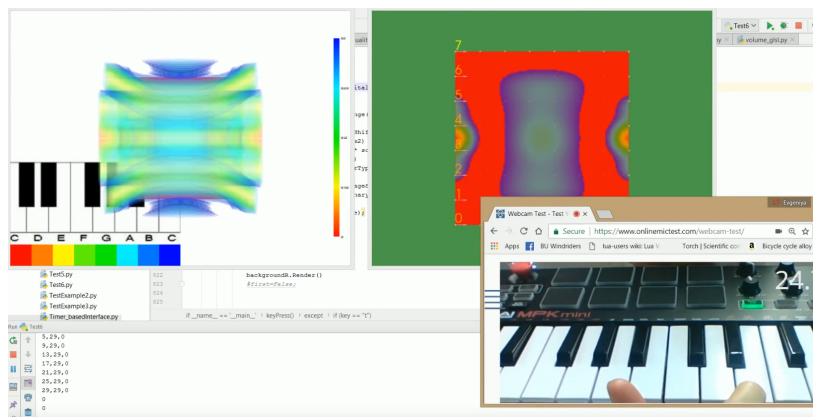
Figure 4.29: Isosurface extraction for tetrahedral mesh volume rendering

As we have discussed in sections 4.4, 4.2.3, the auditory TF $M : f- > w$ of scalar field values f to more pleasant "musical" sounds such as sequences of the specified musical pitches of frequencies w . In our approach, to specify these frequencies we are using MIDI (stands for Musical Instrument Digital Interface). In music, the MIDI format is widely used to formalise the sound representation, and the basic MIDI message tuple $(On/Off, MIDI_{Key}, MIDI_{KeyVelocity})$ can be used to find the wave duration, the frequency and the amplitude directly. Therefore, the auditory properties which we store in the HV model are mapped from MIDI message components as $M : f- > MIDI_{Key}$, where field $MIDI_{Key}$ represents frequencies, separate object modal areas and act like an auditory transfer function. Thus to establish the mapping $M : f- > w$, we select a musical scale with degree numbers $0, ..N$ within the specified range N . Whilst small range scales are easier to perceive, a bigger range gives a trained listener more options for judging about small data changes. Our experiments showed, that in most cases Cmaj of up to two-octave range is sufficient to auditory highlight areas the visual analysis might miss. The mapping, therefore, is described as follows:

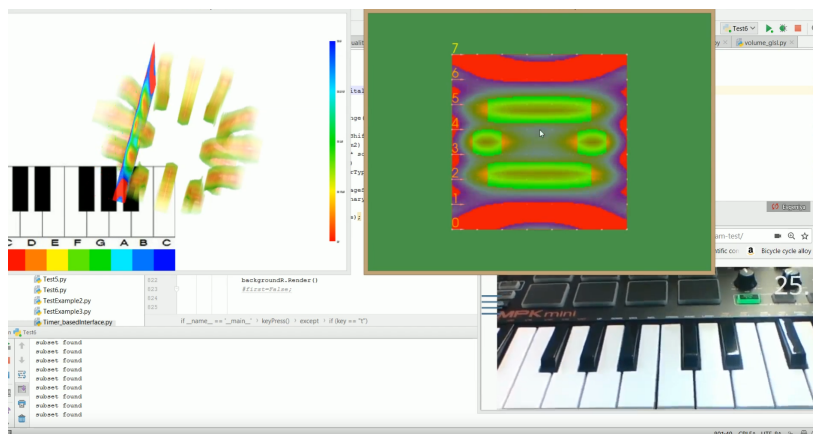
1. To establish the mapping $f- > 0, ..N$, we calculate the scale degree $n_i \in 0, ..N$ for each scalar field value $f(X)$ within the sub-range as $n_i = \lfloor \frac{f(X)}{\Delta d} \rfloor$, where $\Delta d = \frac{f_{max} - f_{min}}{N}$
2. $0, ..N- > MIDI_n$. The mapping for Cmaj scale of the defined range and the start key can easily be implemented on the basis of knowledge about the major scale structure of a combination of tones (T) and semi-tone (S) intervals between notes (TTSTTTS).
3. The mapping $MIDI_{Key}- > w$ can be obtained with well known MIDI keynote to the frequency conversion equation.

An approach to ROI selection via manipulating the values provided by auditory TF and musical scale is based on concept of defining "musical queries", the sequences on notes within the music scale, in this case Cmaj. To simplify the notion the interaction procedures operate MIDI field. For the musical query simplification, we neglect all the message components except the key number that defines a note.

Below we demonstrate a simple example of (Fig. 4.30 a,b) we use the MIDI keyboard for fast extraction of a particular part of field that demonstrates the musical pattern of interest (the scan is taken along y-axis).



(a)



(b)

Figure 4.30: Interaction via Midi keyboard a) Music pattern definition with Midi Keyboard b) Highlighting of scalar field areas, corresponding to defined pitch pattern

The music pattern is defined with Midi keyboard (Fig. 4.30 a). We can search and highlight the scalar field areas demonstrating the same pitch pattern (Fig. 4.30 b) via the defined field $MIDI_n$ and thus quickly define the area of interest in scalar field.

The technique may be used for search for smooth/fast gradient changes detection as well.

4.7 Summary

In this section, we have outlined the visual-auditory pipeline as an extension of conventional visualisation pipeline. We treat the problem of auditory modality introduction as a rendering problem and unify the approach to visual-auditory analysis with similarities in light and sound propagation through heterogeneous volume objects. We have discussed the following aspects of the introduced approach:

1. We have demonstrated the deployment of hybrid constructive modelling for explicit control over dynamic changes in both topology and shape for analysis of dynamic heterogeneous structures.
2. We have discussed a combination of geometry modelling with ray-casting for complex interactive visualisation techniques (LOD visualisation of dynamic multi-scale structures) and the modelling of a secondary volume structures within a heterogeneous subdivision, such as molecular surfaces or modelling of microstructures.
3. We have discussed the hybrid constructive modelling of optical and auditory properties within IC-based representation of a heterogeneous object
4. We have introduced the auditory model similar to optical one and consider the unified approach to the visual-auditory rendering of heterogeneous structures.
5. We have discussed how user interaction with visual-auditory feedback can be integrated as a part of the introduced model and can benefit from the flexibility of introduced techniques.

To summarise, the IC structure specifies the main rules for hybrid geometry modelling and computation of cells relationships. Those two features are essential part of visual-auditory pipeline modelling, parallelisation and efficient rendering with ray-casting. The introduced constructive approach to visual-auditory pipeline design can highly benefit of GPU implementation and combination with ray-tracing techniques.

In the next section, we will discuss the GPU implementation of our approach. The modern graphics hardware makes the introduced approach convenient for real-time visual-auditory analysis of heterogeneous objects. We discuss the design of a visual-auditory framework that facilitates the implementation of visual-auditory pipelines for heterogeneous objects.

Chapter 5

Algorithms and implementation

5.1 Overview

In previous sections, we have discussed challenges that appear in the visual-auditory analysis of heterogeneous objects due to different representations of multi-scale and dynamic features within a spatial subdivision. The complexity of multi-scale representation can be addressed by using a rich set of procedures for modelling of geometry and materials. However, the modern visualisation frameworks deal mainly with geometry modelling procedures with a main focus on surfaces not volumes. The visualisation of volume objects that is another essential property of heterogeneous structures, is often limited to volume rendering of structured grids.

As we focus on GPU-based implementation in line with relevant works discussed in the section 2.1.1 . The solutions in area use the techniques that allow real-time performance by using modern GPU hardware and algorithms to address bottlenecks and thus provide a solution for low budget graphic cards. The model of the visual-auditory scene which was presented in section 4.2.3 is convenient for GPU implementation as it treats rendering as a combination of constructive geometry modelling and volume ray-casting techniques to address the problem of heterogeneous objects visualisation. However, such approach requires revisiting of visualisation principles and algorithms in the context of a ray-tracing graphic pipeline.

Due to recent advances in GPU hardware, the ray-tracing APIs such as Nvidia Optix, DXR API or ray-tracing extensions for Vulkan, allow ray-tracing to become a part of the real-time graphics pipeline. At the same time modern graphics APIs provide more flexibility for GPU computations within graphic pipeline (Subtil 2018). Thus ray-tracing APIs provide an upper level of abstraction in the design of a ray-tracing application. The complex visualisation solutions often benefit from a combination of visualisation with ray-casting and interactive geometric modelling. In this work, we employ the flexibility of the

ray-tracing APIs to address the complex task of implementing visual-auditory pipeline for analysis of the heterogeneous objects.

Our visual-auditory pipeline is based on the principles of the GPU-accelerated ray-casting. The solution deploys the GPU computational features in implementation of pipeline that allow addressing the bottlenecks of visualisation of the heterogeneous objects as a part of volume ray-casting procedure.

Section 5.2 presents the main challenges and features of design of ray-casting inspired visualisation pipeline for heterogeneous objects analysis. We discuss the core aspects of accelerated volume ray-casting of GPU-based visual-auditory scene described in section 4.2.3, such as:

1. General pipeline structure and challenges that impose the deployment of acceleration structures (see section 5.2.3).
2. The unified approach with sphere-tracing for both ray-geometry primitive intersection and accumulation of optical and auditory properties (see section 5.2.4)
3. Deployment of constructive hybrid modelling within visual-auditory pipeline. We discuss the efficient evaluation of such constructively modelled pipelines as a part of ray-casting procedure (see section 5.2.5).

The introduced concept of ray-casting inspired interactive visual-auditory pipeline design provides a basis for implementation of the core procedures based on the ray-tracing API. In section 5.3 we discuss in detail the main blocks of modern ray-tracing APIs that are used for ray-casting inspired visual-auditory pipeline implementation. We explain how the model introduced in sections 4.2.2 and 4.2.3 is implemented within those blocks, the rules of introduction of acceleration structures, GPU modelling of constructive tree logic. Also we discuss the design of complex of volume ray-casting pipelines that allow dealing with arbitrary geometry within subdivision and combine geometry modelling with ray-casting that is an essential part of user interaction.

Finally, we take advantage of modern GPU hardware and algorithmic advances to design a framework that deploys a GPU accelerated visual pipeline design. In section 5.4 we introduce a flexible and extensible framework that deploys conventional principles of visualisation pipeline and data-flow (VTK) and reconsiders their application in terms of modern GPGPU implementation and flexibility that ray-tracing based computer graphics rendering pipeline provides.

The framework benefits from modern GPU hardware concepts to perform real-time interactive visualisation. This allows to design applications for low-budget hardware with

the API. Moreover, we demonstrate how the framework can be implemented as a flexible prototyping tool with C++ interfaces with further extensions for supporting Python interfaces. The framework main features are object oriented architecture and GPU data flow. Visual-auditory pipeline is constructed according to data-flow concept (see section 5.4).

Although implemented with the minimum of dependencies, the proposed framework allows flexible further extension for larger projects in scientific research area that take advantage of additional dependencies or are executed in Python environments.

5.2 Ray-casting inspired visual-auditory pipeline for dynamic heterogeneous objects

5.2.1 Overview

Visual pipeline optimisation often addresses the problem of the growing complexity of geometry. Dynamic heterogeneous object demands extensive modelling of dynamic multi-scale properties and real-time user interactive exploration. As a result, the pipeline evaluation time grows with the complexity of geometry and materials modelling procedures. The optimisation of evaluation of a pipeline for such complex objects is an essential requirement of real-time interactive visualisation.

The flexibility of the ray-tracing pipeline allows increasing the efficiency of visualisation of heterogeneous objects with multi-scale representation. We use various advantages that ray-tracing graphics pipeline provides, such as high transparency of the ray-object intersection, flexibility in terms of on-demand loading and rendering and programming flexibility.

5.2.2 General principles

Sections 4.2.3 and 4.2.4 present the unified approach to visual-auditory analysis as a result of the propagation of light and sound through heterogeneous volume object. The goal of visual-auditory visualisation is to get an insight into phenomena that is represented by the heterogeneous structure and is generated as a result of ray-casting of the sensory stimuli. Thus the issues of efficiency of visual-auditory pipeline and quality of visual-auditory analysis are related to optical and auditory models and their efficient evaluation with the ray-casting procedure (see section 4.4). In the similar way as the conventional techniques (Knoll et al. 2014) we apply the volume ray-casting accelerated with hierarchical structures for the integration of optical and auditory properties within tuple $HV = G, A_o, A_s$ to address the efficiency issues. Complex cases of ray-tracing often use multi-pass ray casting that can be

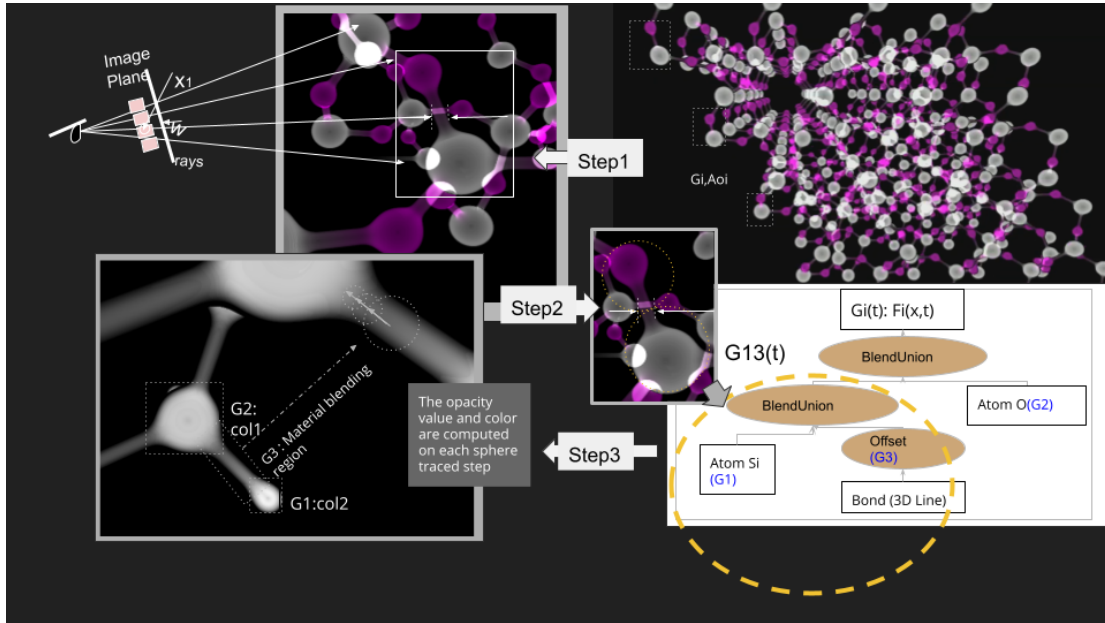


Figure 5.1: An approach to volume ray-casting of heterogeneous objects. Step1. intersection with bounding volume $BV_i^{l_2}$ - BVH acceleration. Step2. Intersection with "lower level" bounding volumes and decomposition of constructive tree. Sphere-tracing (Hahn et al. 1998) of SDF subtree for exact intersection with geometry domain G_i . Step3. Local volume integration of Ao_i and As_i with the ray-segment parameters for integration of constant and "blended" materials computed with sphere-tracing

executed in parallel. In this research, we use two different ray-passes for accumulation of optical properties Ao and auditory As properties that operate visual-auditory scene in the same way.

The optical Ao and auditory As properties are modelled on spatial subdivision $\langle I, BV^{l_2} \rangle = \bigcup_{i=1}^N \langle I_i, BV_i^{l_2} \rangle$, via continuous functions S_{oi} and S_{si} within each cell I_i , where I_i is represented as SDF.

Based on the existing volume ray-casting techniques as discussed in section 3.4.3, the ray-casting procedure is accelerated with hierarchical structure build on top of bounding volumes in subdivision $\langle I, BV^{l_2} \rangle$

The volume ray-casting operates the cellular structure $\langle I, BV^{l_2} \rangle$ by evaluating the intersections with SDF cells along the ray and integration of continuous functional representations S_{oi} and S_{si} to integrate the optical and auditory properties. .

Due to the constructive nature of modelling geometry, optical and auditory properties within subdivision $\langle I, BV^{l_2} \rangle$, the ray-casting of visual-auditory scene $h(t)$ that evaluates visual-auditory pipeline is summarised with following core procedures, that in basic case become a sequence of 3 steps (see Fig. 5.1):

1. Step 1. Shoot the rays and find preliminary intersection info along each ray.

Conventionally ray-tracing is accelerated with hierarchical structures (see section 3.4.3). In this research, we construct acceleration structures on top of bounding volumes in a subdivision in $\langle I, BV^{l_2} \rangle$. A hierarchical structure such as BVH allows preliminary finding of all geometry primitives G_j that ray intersect (see Fig. 5.1, Step 1). Thus for each ray an array of potential intersections is formed $\langle I', BV^{l_2} \rangle \subset \langle I, BV^{l_2} \rangle$. It should be noted that type of geometry specifies further processing steps for $\langle I', BV^{l_2} \rangle$.

2. Step 2. Find the exact intersections with all G_j geometries and reject the "false" ones from a set of $\langle I', BV^{l_2} \rangle$. As each cell is represented with SDF, the procedure evaluation is unified with well-proved for its efficiency sphere-tracing algorithm Hart (1996) (see Fig. 5.1, Step 2).

Moreover, on this step, we address the efficiency aspects in the constructively modelled visual-auditory pipeline. As discussed in section 4.2.3, the important aspect of that pipeline is the constructively modelled mapping operation. The constructive trees for geometry and material reflect the logic of visual pipeline. The trees evaluation can be optimised as a part of volume ray-casting. In many cases we "extract" a local geometry subdomain for j -th cell $G_{jk} \subset G_j$ and its constructively modelled SDF representation for sphere-tracing (see Fig. 5.1, Step 2)).

3. Step 3. Evaluate a contribution of optical Ao_j and auditory As_j materials on local geometry subdomain G_{jk} . In this research, we consider an emission-absorption interaction (see section 4.4). In cases of molecular structures, we also add to cells surfaces a basic Blinn-Phong shading to highlight the shape. We also use the sphere-tracing for the accelerated accumulation of optical and auditory properties (see Fig. 5.1, Step 3) by using the model discussed in the section 4.4.

Below we discuss the general aspects of implementing conventional ray-tracing structures within a visual-auditory pipeline.

5.2.3 Bounding volume hierarchy

The hierarchical structures are one of the key features of accelerated volume rendering of large scale heterogeneous structures. The bounding volume hierarchy (BVH) is introduced on top of the spatial subdivision in model $\langle I, BV^{l_2} \rangle$.

For efficiency of ray-geometry G_i intersection, we use the bounding volumes of the different level that were introduced as a part of pre-processing of the initial data with

dynamic and multi-scale features (see section 4.2.2) (Fig. 5.1, Step 1). However, the use of acceleration structures also sets restrictions on the design of the ray-tracing pipeline for volume ray-casting of heterogeneous objects. The main problem is that the cells in set $\langle I', BV'^{l_2} \rangle$ of preliminary computed with BVH intersections can be in arbitrary order. We discuss our approach to address the problem with the design of different ray-casting pipelines in section 5.3.1)). In addition to core procedures shown in Fig. 5.1, the post-processing step is applied for "proper" volume integral evaluation with empty space skipping. In basic case, it includes depth sorting of cells in $\langle I', BV'^{l_2} \rangle$. The other aspect of the procedure additional per-ray memory allocation for intermediate ray-cells intersection information $\langle I', BV'^{l_2} \rangle$ and associated visual and auditory properties. The post-processing step uses such per-ray arrays for further optical and auditory properties accumulation. We discuss the details of implementation on a base of ray-tracing API in section 5.3.2.

In the general case, the introduction of arbitrary post-processing stage provides additional flexibility in terms of a combination of accelerated ray-tracing with complex geometry modelling techniques. As we have discussed in section 3.6.3, the accelerated user interaction with multisensory feedback is based on a combination of accelerated ray-tracing and geometric modelling. The post-processing allows implementing various complex procedures such as the evaluation of the relationship between individual cells and process overlapping volume patches to overlaps" of surface patches. These procedures are part of user interactive modelling and geometry modelling that we will consider for a practical example of microstructures visualisation in section 6.2.

5.2.4 Sphere-tracing

5.2.4.1 Ray-geometry intersection

The possibility of fast evaluation of distance-dependent properties is a crucial feature of SDF representation that deploys real-time rendering (Hart 1996) and user interaction with multi-sensory feedback (Xu & Barbic 2017). In this research, we use sphere-tracing (Hart 1996) as a fast and unified algorithm for evaluation of the intersection of a ray with SDF represented IC cells.

Processing of such geometric objects is done automatically in a unified way and no preliminary information on the type of obtained geometry is required. Thus, all the constructively modelled cells within structures $\langle I, BV^l \rangle$ are processed similarly. BVH is deployed to compute the preliminary intersection (see Fig. 5.1 Step.1) and the exact intersection for any IC cell is evaluated with sphere-tracing of an entire constructive tree or one of its local subtrees (see Fig. 5.1 Step.2). Thus the ray-tracing operates each cell as a "black box".

The unified sphere-tracing based procedure for ray-geometry intersection allows introducing an object-oriented API with GPU data flow for the design of custom visual-auditory pipelines. In most of the cases, the user needs to specify only the SDF geometry and TF to introduce a custom heterogeneous object and visual-auditory mappings (see section 5.4.2 for details).

5.2.4.2 Local optical and auditory model integration

The distance-dependent materials modelling allow us further to facilitate the accumulation of optical and auditory properties in introduced model (see section 4.4) with sphere-tracing.

As we have discussed in section 4.4, for optical and auditory materials, we use constructive modelling by defining the geometry regions of constant and blended materials. The material blending is also evaluated as the distance to geometry regions of two or more materials. We use sphere-tracing to evaluate those distance properties and perform integration of optical and auditory properties as described in section 4.4 (see Fig. 5.1, Step.3 for a basic scheme of sphere-tracing of blending region). Moreover, the algorithm also allows additional space skipping for cell volumes with a lot of internal holes (sparse geometries). Such empty spaces within cell has to be skipped during optical and auditory properties integration(see section 6.2 for discussion on such case study). Such space skipping within sparse geometry is performed automatically as a part of optical and auditory model integration within a cell.

5.2.5 Visual-auditory pipeline optimisation and efficiency

We process in a unified way the arbitrary cell geometry in $\langle I, BV^{l_2} \rangle$ such as conventional tetrahedron and sphere (Knoll et al. 2009) or multidimensional geometry that was discussed in section 4.3. However, the evaluation of ray intersection with multidimensional geometry that represents dynamic and multi-scale features can be not straightforward, time-consuming and makes the volume ray-casting of entire $\langle I, BV^{l_2} \rangle$ structure more complex.

The efficiency of ray-cell geometry intersection is controlled by the tightness of deployed bounding volumes in BVH. The solution is straightforward for simple geometry, such as a sphere or tetrahedron (Knoll et al. 2014), but become complex for other geometries (Han et al. 2019). The dynamic deformations of shape demand more flexibility in adjusting the tightness of bounding volume (Nguyen 2006), so the "false" intersections are rejected before performing complex evaluations of the ray-cell intersection. The ray-casting of dynamically changing geometry in each cell G_j is challenging due to changes in topological structure, shape and size of G_j . Constructing the optimally tight bounding volume within BVH that

includes dynamic changes on a various scale is necessary to avoid significant increases of computational time.

The other problem comes from conventional visualisation area for the case of considered in this work dynamic multi-scale features. Due to modelling complexity of geometry and materials, a constructive tree evaluation during ray-primitive intersection slows down the rendering process. The constructive trees reflect the mapping logic of visualisation pipeline and optimisation of constructive tree evaluation is performed as a part of ray-casting. Like LOD techniques deployed in previous research in the area, we address issues of both memory and computational efficiency within a spatial subdivision. In the same way as related research in this area that works with on-demand data, in this work we execute on GPU only a necessary part of the visual-auditory mapping structure (see section 5.2.5).

The construction of IC due to rules discussed in section 4.2.2 allows efficient evaluation of composite cells. We implement bottom level bounding volumes to split the complex constructive tree into local subtrees. During ray-primitive intersection and materials evaluation, we load on-demand only the necessary part of the constructive tree (see Fig. 5.1, Step.2, where the bounding sphere for selected subtree is represented schematically with a yellow circle). For the details on the procedure for the dynamic multi-scale features see section 5.3.1.

5.3 Ray-tracing API for IC hybrid structure rendering

Initially aimed only for rasterisation purposes, GPUs evolved into processors not only for graphical applications. The GPGPU pipeline allow using GPUs to address a wide range of parallel computational problems, including simulation, computer vision and even generic data processing tasks. The recent research often takes those concepts further by combining GPU-accelerated parallel procedures such as image processing, reconstruction, geometric modelling with ray-tracing techniques (wu et al. 2018).

The modern GPU hardware and ray-tracing APIs provide programming flexibility and support for GPGPU to address the challenges in computer graphics and the research-intensive tasks (Alex Keller 2020),(Hoetzlein 2016),(Keller et al. 2018). Compared to rasterization pipeline with predefined set of shaders, ray-tracing GPU executed structure is more general and as a result more flexible. The programmers have an access to GPU compute facilities directly from rendering pipeline (*Vulkan compute pipelines* n.d.) that allows combining simulation and rendering tasks (Keller et al. 2018),(Chadzynski 2018).

In this work, we implement our approach with Optix ray-tracing API and deploy Cuda general-purpose GPU programming language. Below, we describe the implementation

structure with general ray-tracing terminology and provide references to structures deployed within context by both Optix and Vulkan, the new generation graphics and compute API that targets multiple platforms.

The ray-tracing APIs (DirectX, Optix, Vulkan extension) share the same execution model (Usher 2020). The key building blocks that deploy the modern ray-tracing APIs are:

1. Acceleration structures, the most common are BVH and KD-trees. In section 5.3.1 we discuss how we deploy BVH acceleration for composite cells and multi-scale feature ray-casting.
2. Programmable shaders for ray tracing. The real-time ray-tracing pipeline is constructed from shaders of various types. The functional features of shaders and introduced GPU memory structures to support the ray-tracing process correlate with core procedures presented in Fig. 5.1. We discuss the design of ray-tracing pipelines for heterogeneous objects depending in sections 5.3.2 and 5.3.3.
3. Shader Binding Table that brings together shader handles with associated data that they operate, i.e. the related to shaders information in Shader Storage Buffer Object (SSBO) structure. We actively use the structure for GPU implementation of the hybrid constructive modelling for heterogeneous objects representation. See details in section 5.3.4
4. A pipeline state object(PSO) handles the execution of ray tracing pipeline. In section 5.3.5 we discuss several ray-tracing passes deployment for visual and auditory properties rendering

Below we discuss the implementation of the core ray-tracing API structures in ray-casting inspired visual-auditory pipeline discussed in section 5.2.1.

5.3.1 Acceleration structures in visual-auditory pipeline

The acceleration structure (AS) within ray-tracing API is a two-level structure. The nodes of the bottom level AS contain geometry data and top-level AS nodes contain a list of references to bottom level nodes together with associated transform and shading information (see examples in Fig. 5.2).

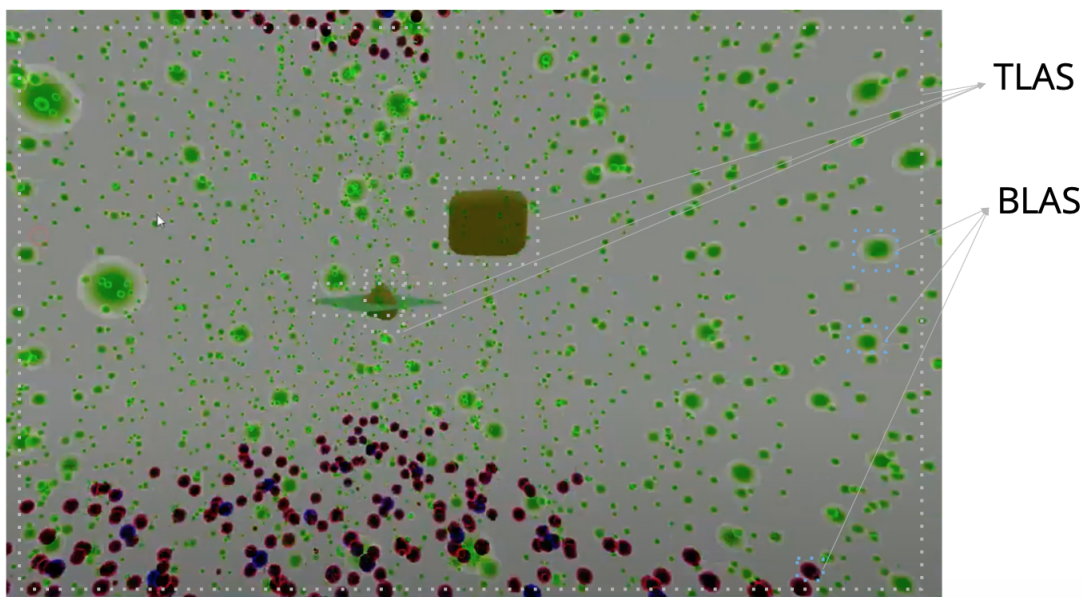


Figure 5.2: Examples of TLAS and BLAS for scene with different types of objects: polygonal plane composed of 2 triangles (BLAS), SDF primitives without BLAS acceleration and molecular structures those atoms are accelerated with BLAS

The ray-tracing APIs construct the acceleration structures on top of existing geometry as a two-step process: creating bottom level nodes first, then generating the top-level node. For the introduced visual-auditory scene with geometry modelled as $\langle I, BV^{l_2} \rangle$, the BLAS is constructed on top of the upper-level dynamic bounding volume structure BV^{l_3} and $BV^{l_2}(t_0)$ is deployed as a dynamic bounding sphere (see Fig. 5.3). $BV^{l_2}(t_0)$ is evaluated during ray-tracing for the currently rendered time frame. If BLAS is positive we testing the $BV^{l_2}(t_{0j})$, where t_{0j} is current time frame.

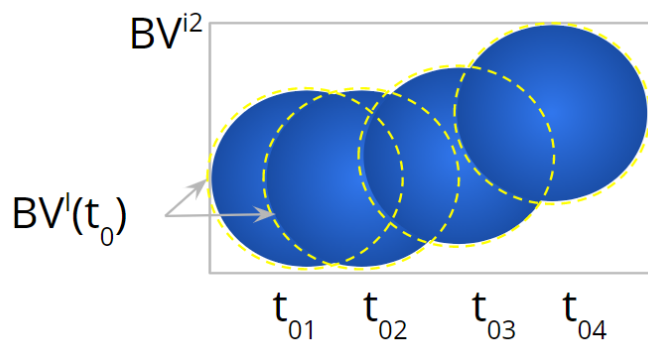


Figure 5.3: Bounding volumes deployment for basic dynamic geometry

$$BV^{l_2}(t_0) = \bigcup_{i=1}^N BV_i^{l_2}(t_0) \text{ that is modelled in } E^4.$$

BLAS is used to optimise ray-primitive intersection with each cell. The efficiency of the procedure is controlled by the tightness of bounding volume BV^{l_2} . Thus, for basic static geometry deployed within subdivision $\langle I, BV^{l_2} \rangle$, for example, CPK molecule those geometries are spheres, the upper-level acceleration is sufficient as optimal "tight" sphere-shaped bounding volume can be used. As a result, those structures are very fast to process compared to other types of geometry and even allow computing global illumination with Monte-Carlo technique for the case of surface rendering (see Fig. 5.4)

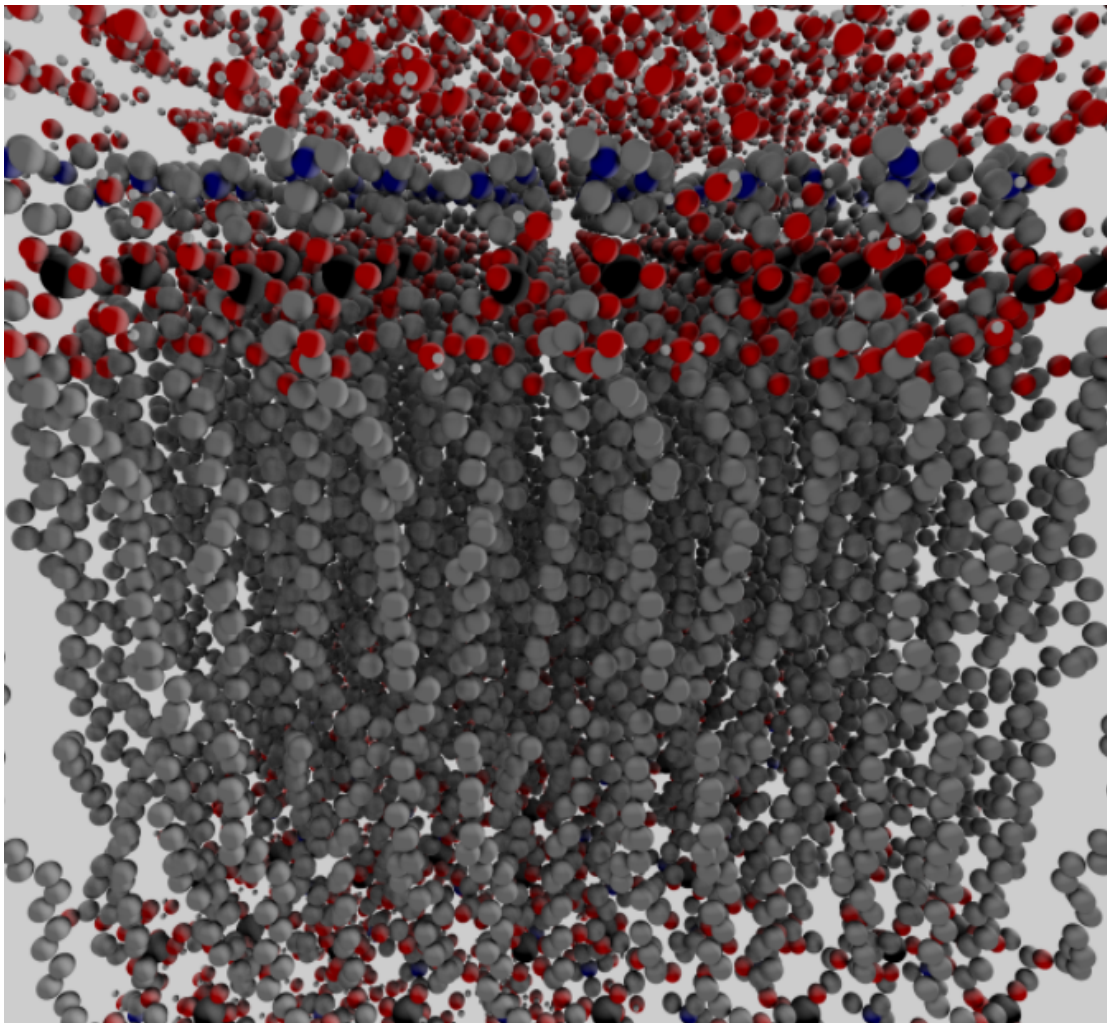


Figure 5.4: Monte-carlo ray-tracing of CPK molecular structure (surface)

However, volume ray-casting of heterogeneous objects is a more complex task. Also, dynamic deformations and multi-scale features the upper-level bounding volumes BV^{l_2} are hard to design as sufficiently tight. The research in area (Gournel et al. 2010b, Parulek & Viola 2012) often addresses the problem by the introduction of additional bounding volumes

that are evaluated in case of positive BLAS intersection. Such additional bounding volumes are used to optimise intersection and can be combined with evaluation of complex geometry within ray-casting for additional acceleration. The structure of layered bounding volumes allows fast rejection of "false" intersection before complex evaluations and reduce the number of computations as discussed in sections 3.4.3 and 3.6.3 for related research).

We use similar technique and consider two possible cases of composite and multi-scale cells (multidimensional composite) with per-cell bounding volume subdivision designed according to the nature of heterogeneous phenomena as discussed in sections 4.2.2 and 4.3.3.

The bounding volumes structure for complex general case (both composite and multi-scale) is :

$$BV_j^{l_0}(t_0, t_1) \subset BV_i^{l_1}(t_0, t_1) \subset BV^{l_2}(t_0) \quad (5.1)$$

Due to rules of $\langle I, BV^{l_2} \rangle$ construction for composite and/or multi-scale cells, we iteratively evaluate the bounding volumes in the cell that is available for these cases:

1. $BV_i^{l_1}(t_0, t_1) \subset BV_i^{l_2}(t_0)$ for the case of multi-scale dynamic geometry. The $BV_i^{l_1}(t_0, t_1)$ is used as additional acceleration subdivision to speed up dynamic multi-scale ray-primitive intersection within the context of LOD visualisation technique as discussed in the section 4.3.3.
2. $BV_i^{l_0}(t_0, t_1) \subset BV_i^{l_1}(t_0, t_1)$, where $BV_i^{l_0}(t_0, t_1) = \cup_{j=0}^N BV_{ij}^{l_0}(t_0, t_1)$ for further intersection acceleration with composite cells . In this work the technique is also used for complex geometric modelling such as construction of continuous surfaces, as discussed in the section 4.3.4.

The general algorithm of processing of bounding volumes is summarised in Fig. 5.5. We compute the time parameter t_{0k} and test the intersection with $BV_i^{l_2}(t_{0k})$ that is the top dynamic bounding volume deployed for BLAS acceleration. As the "preliminary" intersection is computed with BLAS, we further proceed with testing of intersections with lower level bounding volumes. The bounding volume hierarchy construction rules are specified by the cases of multi-scale and/or composite cells. If case of using LOD technique, we compute the parameter t_{1l} and test the additional intersections with $BV_i^{l_1}(t_{0k}, t_{1l}) \subset BV_i^{l_2}(t_{0k})$. Moreover, in case of composite cell we perform additional intersection query with each sub bounding volume of composite cell $BV_i^{l_0}(t_{0k}) = \cup_{j=0}^N BV_{ij}^{l_0}(t_{0k})$.

We can further use the bounding volume $BV_{ik}^{l_0}$ to evaluate the potential intersection in a composite cell as its ik subcell. We also deploy the bounding volume $BV_{ik}^{l_0}$ to extract only the necessary part of constructive tree for evaluation (see Fig.5.6 for example of multi-scale geometry subtree extraction. The full tree for the cell used in this heterogeneous structure

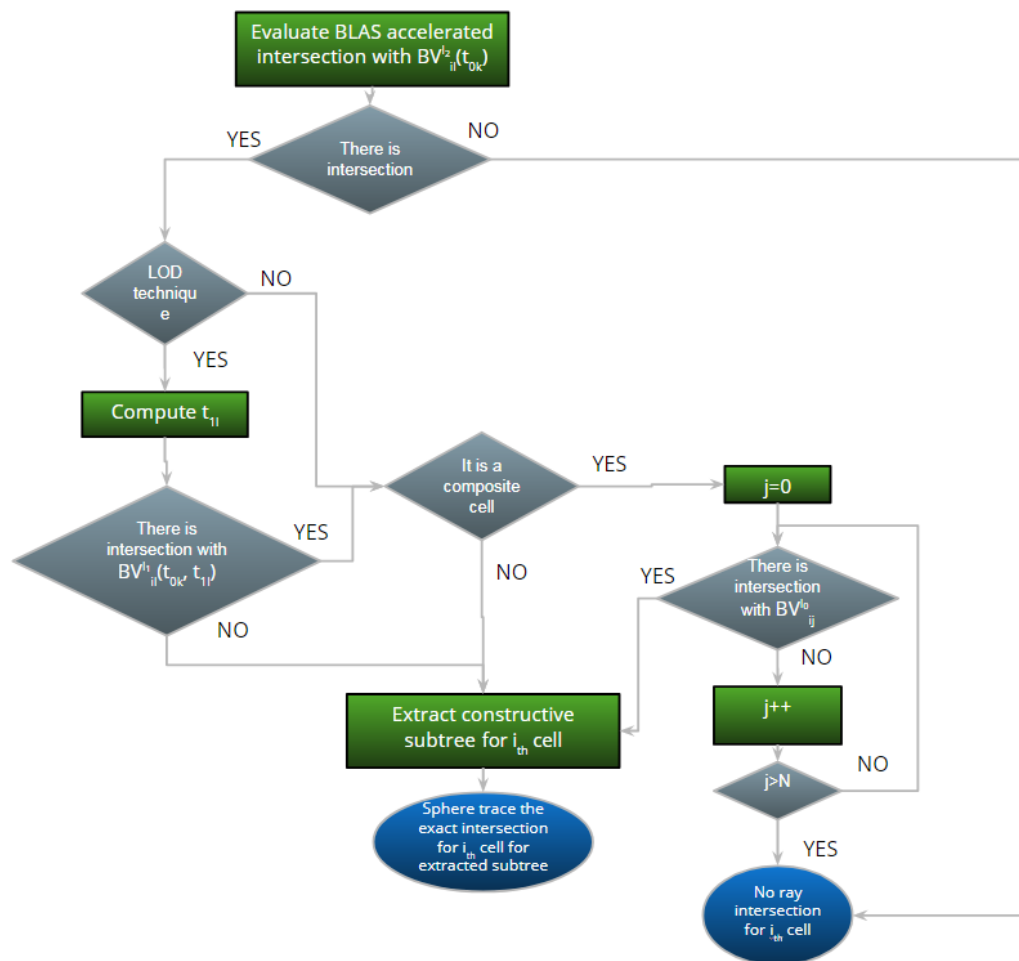


Figure 5.5: General scheme for testing and evaluation of intersection with i_{th} cell.

was presented in Fig. 4.14. Thus we automatically adjust the ray-primitive intersection evaluation according to dynamic and multi-scale nature of $\langle I, BV \rangle$ construction.

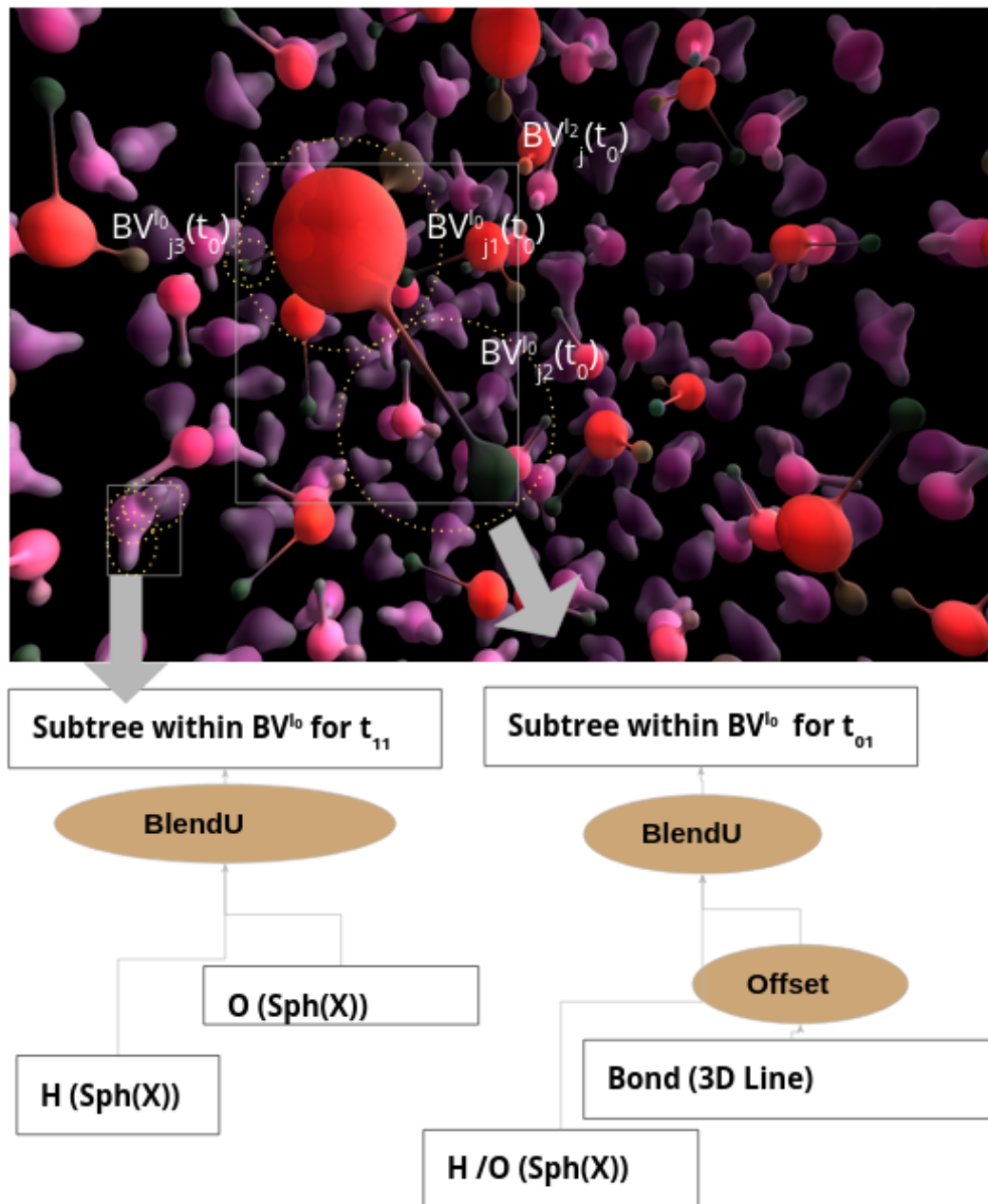


Figure 5.6: Splitting of constructive tree for composite cell with bounding volumes $BV_{ij}^{l_0}$ of dynamic and multi-scale nature. The technique suggests rendering of overlapping geometries.

We use the bounding volume structure to optimise the evaluation of constructively modelled visual-auditory pipeline. Due to unified ray-primitive intersection evaluation with sphere tracing, we can generalise the implementation of Step 2 procedure in Fig. 5.1 with execution of the following blocks that are custom defined for each heterogeneous object (see Fig. 5.7):

1. **GetTimeData**. Obtaining a bounding volume representation for current time frame t_{0k} : $BV^{l_2}(t_{0k})$
2. **GetSubtree**. Evaluation of intersection with lower-level bounding volumes that process the composite and/or multi-scale cell.
3. **SphereTraceForward/SphereTraceBackward**. Perform sphere-tracing in forwarding and backward directions to refine the ray input and output intersections with geometry G_j
4. Depending on the type of pipeline (see section 5.3.3) we proceed further to Step 3 that is an integration of optical and auditory properties or save $G_i(t)$ intersection info as per ray data

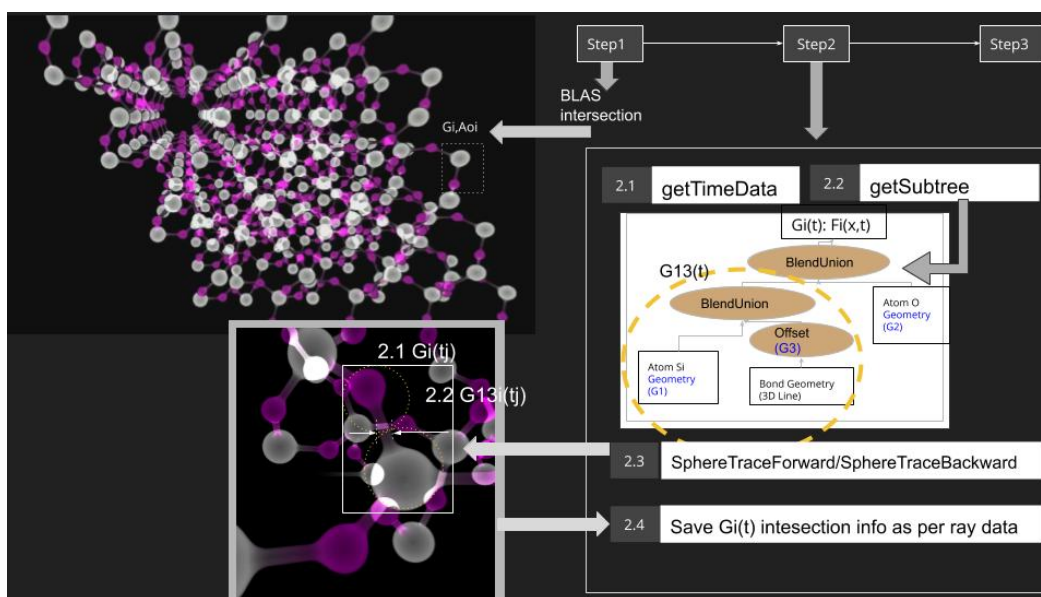


Figure 5.7: Decomposition of ray-cell intersection for constructively modelled heterogeneous structure.

The ray-tracing of heterogeneous objects follows the rules of object-oriented architecture. For each heterogeneous object, the procedures are redefined or inherited due to object-oriented architecture from parent heterogeneous object, including GPU-executed shaders. In

this work we implement entire constructive tree on GPU, as discussed later in the section 5.3.4. As the $\langle I, BV \rangle$ is constructed according to rules in section 4.2.2 the levels of bounding volumes provide a basis for the further GPU splitting to constructive subtrees within subdivision and reduction of SDF evaluation.

5.3.2 Data storage and intra-shader communication for various volume ray-casting strategies

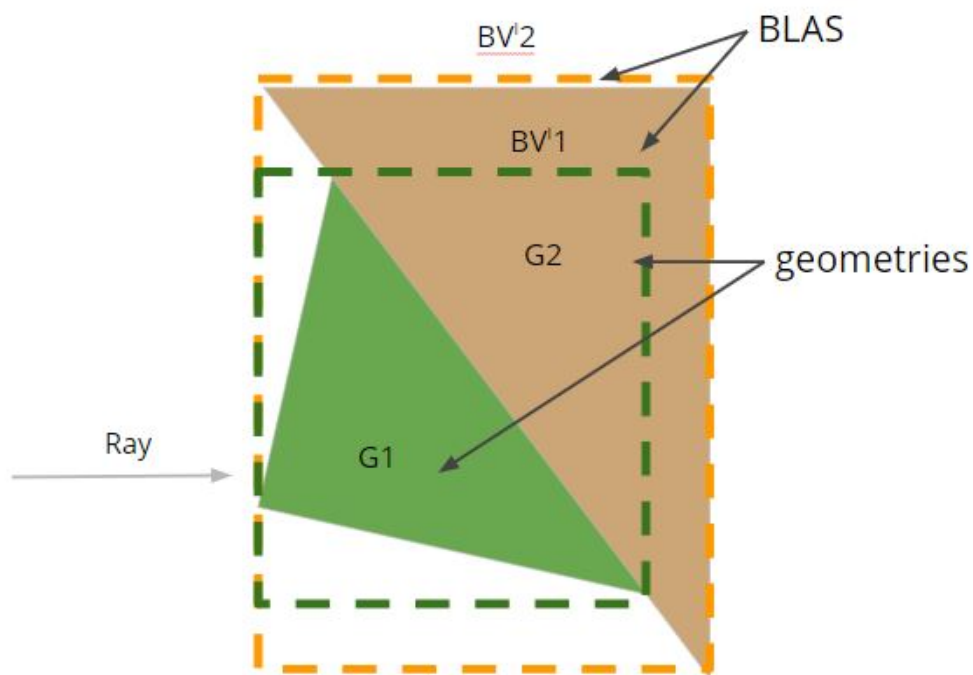


Figure 5.8: Example of complex BLAS accelerated intersection case. We do not know if intersection point computed with BLAS is the closest one for geometry G_1 .

The entire ray-tracing pipeline is organised as a set of GPU executed programmable shaders. Ray-tracing APIs provide a set of shaders of different type with predefined common logic of their execution (see Fig.5.9).

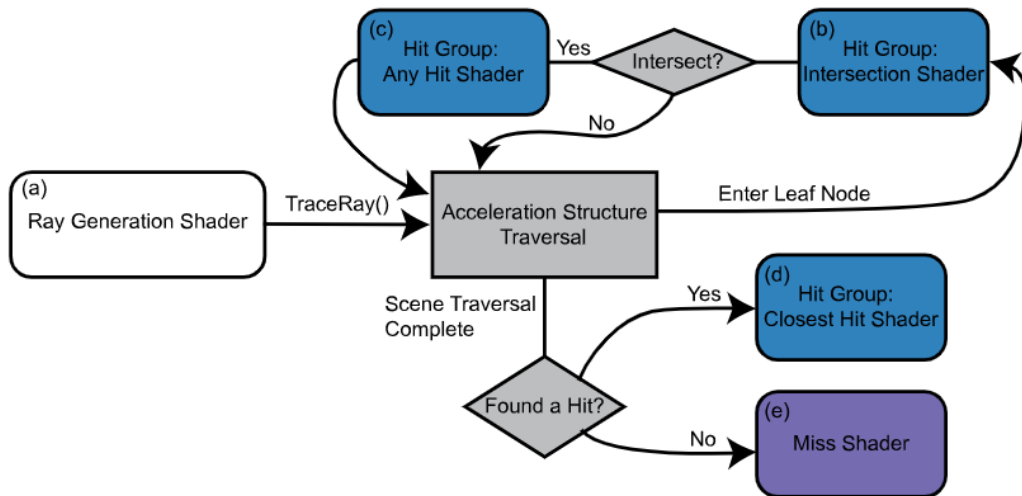


Figure 5.9: Ray-tracing APIs shaders and the execution logic (image from (Usher 2020)). During traversal, rays are tested against primitives in the leaf nodes (IC cells in our case) of the acceleration structure. (c) If an intersection is found the Any Hit Shader is called. After the traversal is complete (d) if defined the Closest Hit Shader of the hit geometry is called if a hit was found, otherwise (e) the Miss Shader is called. These shaders then return control to the caller of TraceRay, or can make recursive trace call.

In this research, we implement the different blocks of heterogeneous objects volume ray-casting pipeline that we have considered in section 5.2.2 in these shaders. In many cases, the functional features of those blocks correlate with initial application area of deployed shaders. For Step1 in Fig. 5.1, we specify with the ray-generation shaders the ray-shooting rules for visual and auditory rendering passes. For Step 2 in Fig.5.1, we deploy the Intersection shaders for the evaluation of the exact intersection with custom geometry that detailed decomposition with sphere-tracing of SDF and constructive tree splitting we have discussed in section 5.3.1). Finally, we compute integration of optical and auditory properties as a part of shading/material shaders or as a part of custom post-processing deployed at the end of ray generation shader or within miss shader.

The logic of distribution of the above procedures is defined by the following problem. In the basic case, the shaders for Step 2 in Fig. 5.1 that evaluate the exact intersection and shaders execution is assumed after detecting preliminary intersection with BLAS build on top of layered bounding volumes. However, for different types of cells with different geometries, the ray-tracing structure can be significantly different.

The case of tetrahedral meshes that are schematically presented in Fig. 5.8 shows that the "preliminary" intersection computed with BVH can be not the "closest" geometry intersection. In this example, two geometries have the same bounding volume and this leads to ambiguity

in intersection evaluation. In tetrahedral meshes rendering the problem is addressed with additional depth sorting of all computed preliminary geometries.

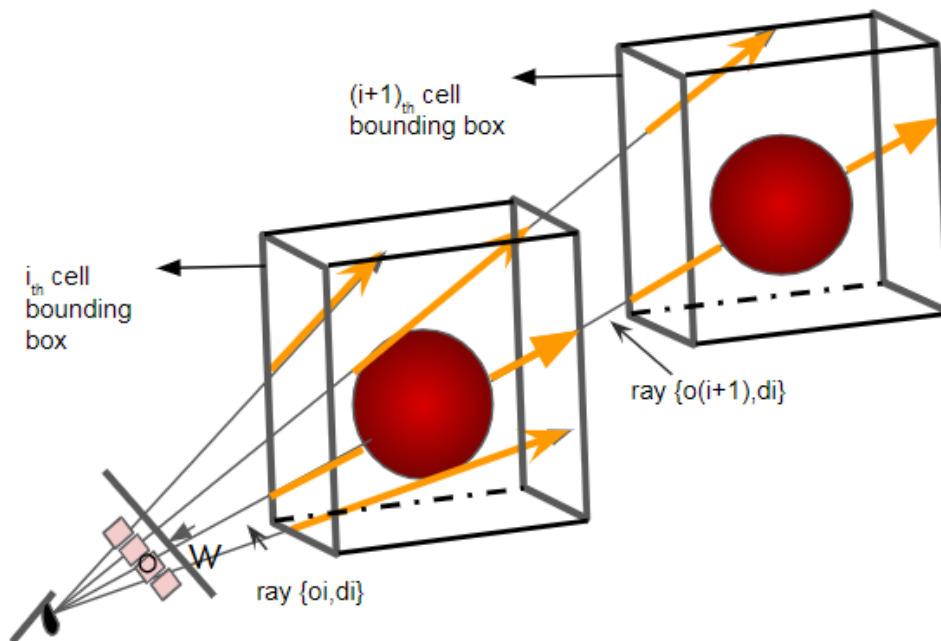


Figure 5.10: Iterative accumulation of optical and auditory properties for basic type of volume ray-casting pipeline

The ray-tracing API provides two types of shading approaches and allows allocating additional memory available on the per-ray basis (ray payload) to design various ray-tracing architectures. Applied to heterogeneous objects volume rendering, we consider two basic strategies for accelerated ray-geometry volume integral evaluation within volume ray-casting pipeline:

1. Implementation of Closest Hit shader after ray-cell intersection in the material shader. Conventionally the rendering of surface objects deploys this type of shader as the one where the closest intersection has to be found. For the volume rendering case, the assumed closest intersection approximated by bounding volumes might not provide the closest cell. However, this type of shader can be used for basic geometric objects modelled within the subdivision with 0D topology and significant space between the cells. The procedure assumes that secondary rays are used for processing further subvolumes along the ray. The basic scheme is presented in Fig. 5.10. For all objects along the ray, we iteratively find the closest ray-geometry intersection by relaunching

the ray shooting along the same direction but with new ray origin outside the bounding box of an intersected cell. This type of pipeline allows sequential evaluation of 3 types of procedures defined in Fig. 5.1.

The main advantage of the approach is an accumulation of optical or auditory properties during ray-casting without any need to allocate additional structures in memory per each ray.

The main disadvantage is its limited application in the case of volume rendering of heterogeneous objects. Thus, it is suitable for heterogeneous objects with significant space between sub geometries, for example some water clusters or simple molecular structures representations.

2. Implementation of Any Hit material shader for evaluation of all ray-cell intersection along ray segment. The approach assumes computation of all the intersections along the ray within defined ray length. Conventionally, further the post-processing procedure is executed that applies depth sorting and integration of optical and auditory properties (deferred shading (Eisenacher et al. 2013)).

The approach allocates the memory for GPU storage of a preliminary array of all positive BLAS intersections with approximate distances or an array of exact distances. Also, the information on materials distributed within such cells Ao_j, As_j and geometry descriptions G_j should be stored and later accessed from post-processing procedure as a part of volume integral evaluation. Various processing of these GPU arrays can be applied, such as depth sorting (case of tetrahedral meshes), removal of duplicate intersection points for the cases of overlapping surface patches for continuous surfaces modelling in section 4.3.4) and complex cases of user interaction that require evaluation of relationships between IC cells, for example, discussed in the section 4.6.3.

The advantages of this approach are: it is extremely flexible due to custom post-processing procedure; it handles any type of input sub geometries and complex cases of combining geometric modelling with ray-casting.

The disadvantage of this approach is that it can be less efficient due to computation of unnecessary intersections and also it requires storing ray payload information and, therefore, is less memory efficient.

Due to flexibility, we mainly use the second approach and construct volume ray-casting pipeline with post-processing procedure.

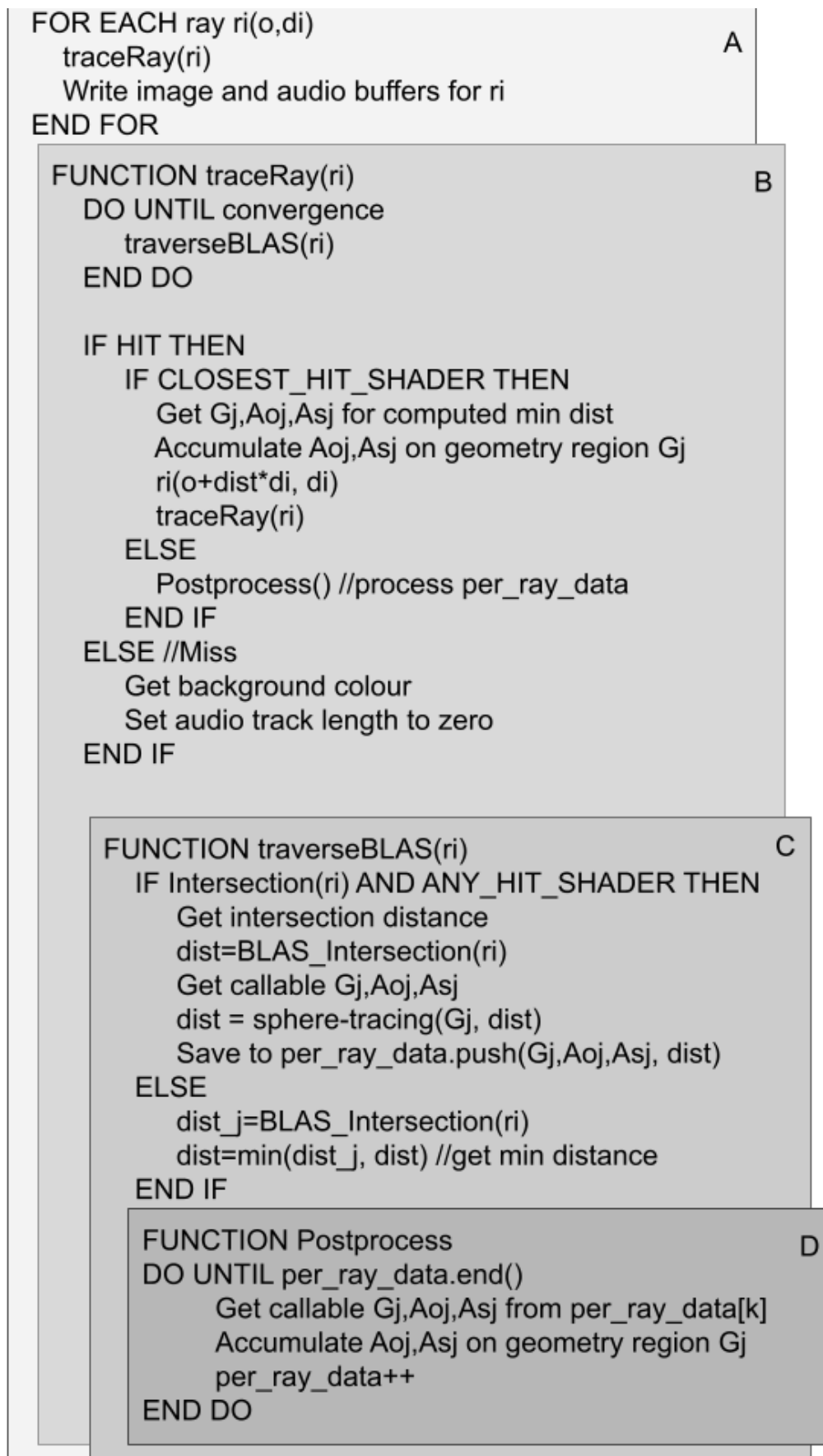


Figure 5.11: General optical and auditory volume ray-casting algorithm. Ray-tracing API shader domains and their augmentation with callable shaders accessed directly or from Per ray data array

In this work, the post-processing stage operates additional structures in GPU memory that are allocated during any-hit ray-cell intersection and preliminary evaluation of the material shader. The pre-processing of GPU arrays is followed by deferred evaluation of exact ray-geometry intersection and integration of optical and auditory properties.

Thus, the post-processing step assumes intra-shader communication. The constructive trees of each intersected primitive the G_i, A_{oi}, A_{si} that in the basic case are one-node SDF primitive and TFs are passed from conventional geometry and material evaluation shaders to post-processing shader. The post-processing shader is executed on the final stage, usually after the Miss shader execution (see Fig. 5.11). The procedure is handled via ray payload structure that is used in ray-tracing APIs. In this work, we use the Callable programs/shaders structure within ray-tracing APIs to describe, store and evaluate an arbitrary constructive tree for geometry and material (see more in section 5.3.4).

The ray payload is an arbitrary, application-defined data structure that stores information that is accumulated along the path of the ray. It is initialised by the shader that initiates a ray query operation. In our case, the structure is normally read and modified by any hit shaders. It is typically used to output material properties accumulated along the path of the ray, which the ray generation shader writes to the memory.

Also in ray-tracing APIs, the ray attributes are used to pass information from the intersection shader to the material hit shaders. We use the structure to transfer the intersection information G_i to a material shader. Overall, the data collected for each IC cell in ray-payload storage is represented with the following structure:

```
struct Per_cell_primitive_data
{
    enum type {avatar, scene}; //HV object for the scene or the interaction
    int G_i; //id of constructive tree for the geometry
    int Ao_i; //id of constructive tree for the optical property
    int As_i; //id of constructive tree for the auditory property
    float dist[2]; //first and last intersections of geometry with ray
};
```

As we discussed above, the type of pipeline is related to cell geometry, and implemented within a cellular subdivision.

5.3.3 Types of ray-tracing pipelines for heterogeneous objects

The conventional visualisation tools often design their pipelines based on all the possible geometry within the input data, topology descriptions with various dimensions and structure,

such as structured or unstructured grids. Similarly, we notice that in many cases the organisation structure of key pipeline procedures that we have discussed earlier in section 5.3.2 with post-processing depend on topological dimension used in explicit cell description. We use this assumption in the design of optimal class hierarchy presented in Fig. 5.12.

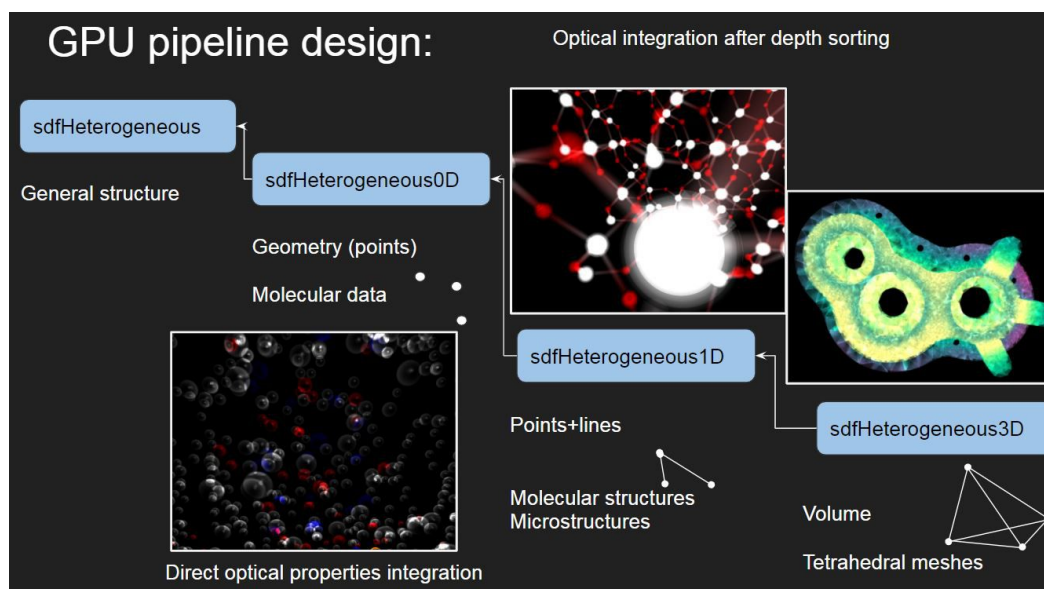


Figure 5.12: Heterogeneous objects architecture to define the logic of volume ray-casting

The topology dimension from the initial data that represents a heterogeneous object defines the architecture of ray-casting pipeline. In particular, it defines what intersection shaders are used, whether post-processing is required and what structures to store the per-ray data for post-processing are needed. Due to object-oriented architecture, the type of heterogeneous object (`sdfHeterogeneous0D`, `sdfHeterogeneous1D` or `sdfHeterogeneous3D`) is detected during visual-auditory pipeline execution. Accordingly, the structures in the GPU memory are allocated and used within post-processing that is a part of ray generation shader (see Fig. 5.9 and Fig. 5.11). The ray-tracing pipeline is executed according to the structure of ray-tracing pipeline. This concept is one of the essential parts of GPU data-flow implementation that we discuss in section 5.4.2.

In Fig. 5.13 we specify three different types of pipelines for the rendering of volume heterogeneous structures. In this work, we demonstrate those pipeline application for several cases of heterogeneous objects, such as:

1. molecular atomic structures (CPK representation case) (see Case study in section 6.1.3.1) that mainly uses the first type of pipeline.

2. Molecular structures (Ball-and- Stick representation) and lattice-based microstructures that are modelled as overlapping volumes and generally use the second type of pipeline (see Case study in sections 6.1.3.2, 6.2.1.2)
3. Microstructures modelled on tetrahedral meshes subdivision that use the third type of pipeline (see Case study in section 6.2.1.2).

5.3.4 GPU modelling and storage of hybrid constructive geometry

All the GPU-executed shaders which are introduced as a part of ray-tracing pipeline along with GPU-based arrays and embedded parameters are stored as a part of Shader Binding Table (SBT). The ray-tracing APIs allows allocating GPU Arrays in memory with user-defined structure and associates them with a particular type of shader. In Vulkan and Optix those are the VKBuffer and OptixBuffer respectively. Shader Storage Buffer Objects (or SSBO) can be seen as unlocked UBOs: they are accessible in reading and writing in a GLSL shader. The structure can be compared to conventional rasterisation bindless rendering that assumes the required data to be GPU-uploaded and accessed by ID in shader during execution.

However, because of greater flexibility in this implementation we use a particular type of GPU program called a callable shader. Callable shaders are custom user-defined programs that can be invoked from any other type of shader (Ray Generation, Closest Hit or Miss shader), including callable shaders. The structure allows reuse of GPU code across many different objects. That leads to both increase in productivity and effective use of GPU resources. Moreover, as such sharers can be called by a unique ID, a common trick is to build and store a GPU array of those IDs with associated additional information. We use the technique to support hybrid constructive modelling on GPU that we have discussed in section 4.3. In Fig. 5.14 we show the implementation of tetrahedral mesh as a set of OptixBuffers. All tetrahedra are stored as a set of GPU arrays with information about geometry and topology. The SDF representation is constructively modelled as IDs to Callable programs with associated input parameters (explicit cell description).

Similarly, we implement the geometry or material modelling as a result of user interaction as discussed above in the section 4.6.1. We simply need to pass the ID of other callable procedure to the callable shader of the constructive tree. See implementation example for geometry constructive modelling as a result of user interaction in Fig 5.15. The constructive tree for this example was presented in Fig. 4.24 in section 4.6.1.

The callable shaders allow flexible construction of different types of heterogeneous objects within ray-tracing pipelines, as each constructive tree for geometry and material is

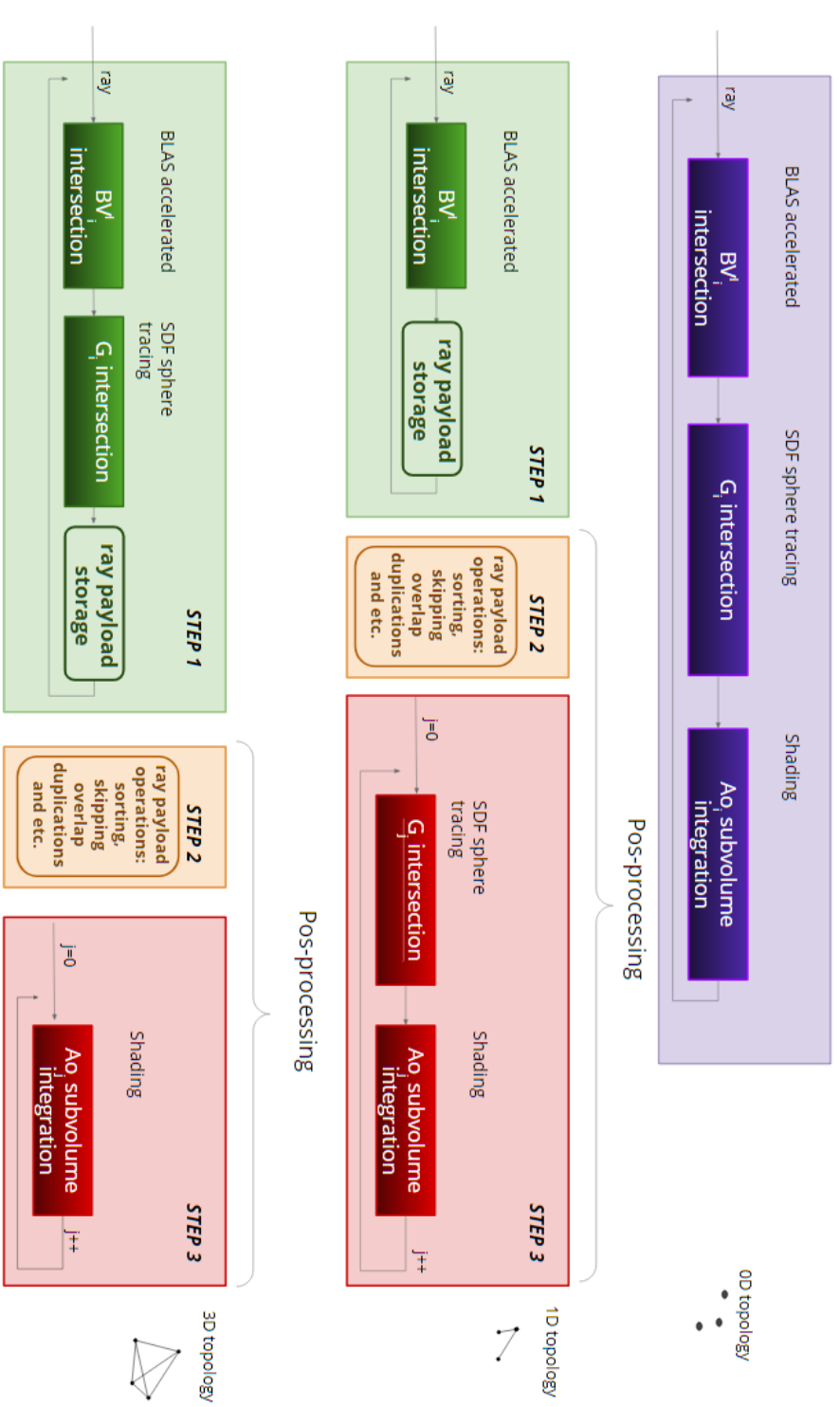


Figure 5.13: Types of volume ray-casting architectures

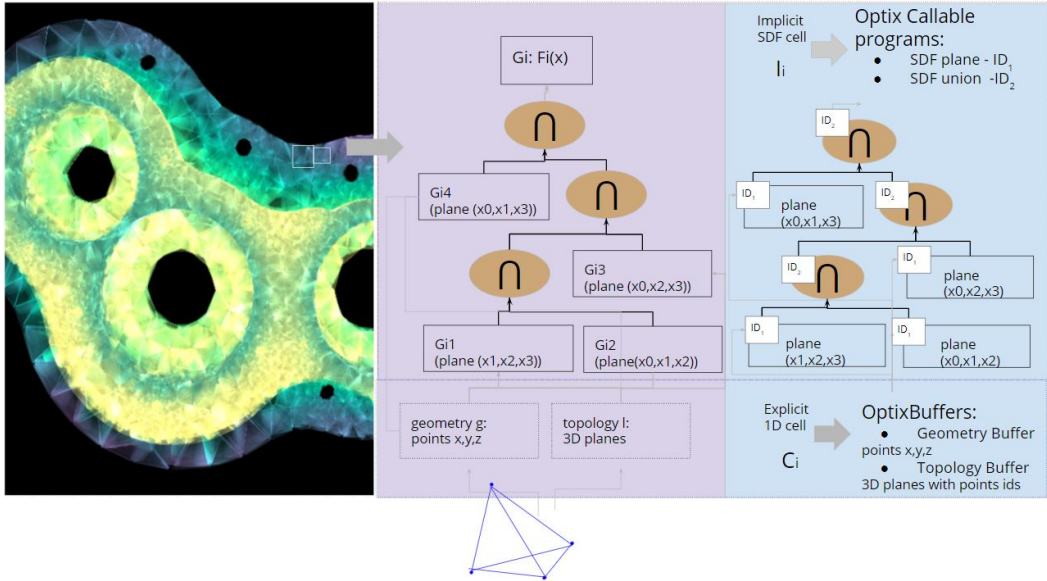


Figure 5.14: Hybrid constructive tree implemented as a set of Optix Buffers with explicit cell representation and Callable programs ids.

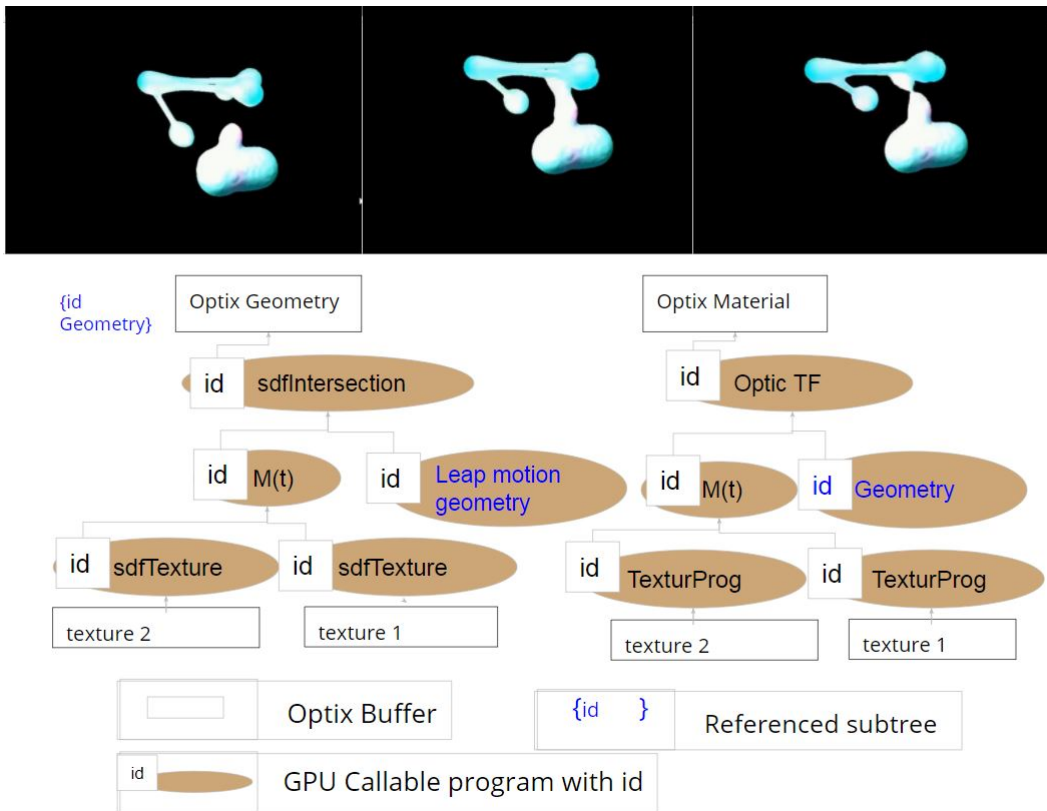


Figure 5.15: Interaction

evaluated as a "black box" procedure called by its ID. This structure is an essential part of GPU data-flow implementation that we discuss in section 5.4.2.

5.3.5 Visual and auditory rendering passes

The possibility to define the custom ray-shooting rules and several ray-tracing passes allows the design of complex ray-tracing shading techniques. In this work, we use this flexibility for simultaneous visual-auditory rendering that deploys visual and auditory rendering passes.

Let us consider the basic case, with A_s and A_o are distributed within spatial subdivision of the same geometry domain G . The visual-auditory ray-tracing scheme can be described as processing of two following steps:

1. Visual and auditory stimuli rendering stage.

We perform auditory rendering pass by using BVH and SDF to compute the input/output intersection distances of G_i and assemble all necessary for post-processing stage information on cells intersection, as discussed in sections 5.3.2 and 5.3.3. We refer to the array with intersection information resulted from visual ray-tracing as $RayArr1 = G_j, A_o_j, A_s_j$ and $RayArr2 = G'_j, A_o'_j, A_s'_j$ for auditory ray-tracing.

Thus, on post-processing stage we compute auditory image of the phenomena by integrating auditory properties. The auditory TF maps data to the modal frequency and the output's sound buffer updates for each ray-traced distance segment in $RayArr2$ according to equation until the end of the ray-casting along an individual ray. For each auditory ray, we generate sound wave $I'_j(d)$.

The outputs of procedures are the conventional visual stimuli 2D image buffer of RGB values and 2D buffer of sampled sound waves $I'_j(d)$.

We convolve all sound waves $I'_j(d)$ in auditory buffer with HRTF Wu & Yu (2016) according to shooted ray position to enable 3D sound. The result is a sampled wave $I(d)$ played with the selected sample rate for each time t value. That is a representation of the 3D sound that allows the listener to perceive the auditory impulse propagation along with the ray path heterogeneous object and highlight with auditory stimuli its internal structure.

2. Visual rendering loop with synchronisation of the auditory soundtrack played in time.

We perform simultaneous visual-auditory image generation by playing in real-time the obtained sampled wave $I(d)$ and for each time parameter t . At the same time, we perform the visual stimuli rendering pass to compute individual pixel of a projected

visual image (visual stimuli buffer). We use the *RayArr2* data during visual rendering pass to dynamically highlight the region of auditory ray propagation as the sound is played. With *RayArr2* distance-based data, for current time parameter t we evaluate if the current cell was activated by auditory ray and change its optical properties to highlight it in case of activation.

5.4 Visual-auditory API

5.4.1 Overview

The syntax and architecture of API are very similar to Visualization Toolkit. Since it has been developed (Schroeder et al. 1998) the tool has become a core of many open-source scientific visualisation tools (Ayachit 2015), (Kikinis et al. 2014). As VTK natively supports terminology and concepts used by visualisation specialists we consider it as a reference and design an API with structure and syntax similar to VTK. To perform the conventional visualisation pipeline transformation from input data to a rendered image, the VTK deploys a CPU-implemented data flow approach.

Currently, the modern GPU architectures allow introducing the GPU-implemented dataflow paradigm that is being used in GPU-computational APIs where computations are described using the data flow graph (Abadi et al. 2015). This allows for example to address the dataflow optimisation tasks by removing the unnecessary CPU/GPU data exchange (Team 2018b) that is often a result of outdated architectures.

Possibility to implement data flow concept on GPU provides an opportunity to design user-friendly visualisation solutions with an efficient GPU accelerated pipeline execution. The proposed API targets establishing the main features of the design of pipeline for the visual-auditory analysis of heterogeneous objects. Very similar to how VTK implements and uses in its architecture the standard visualisation concepts, such as visualisation pipeline, we introduce a concept of the visual-auditory pipeline, unified on a basis of the ray-casting procedure. The API targets to provide high-level access to hybrid constructive geometry and materials modelling and rendering that is essential for heterogeneous objects visualisation. It allows users to operate familiar visualisation concepts and terminology. At the same time, it is very lightweight and fast as all core procedures are CUDA kernels running on NVIDIA GPU card.

The API not only provides the users the easy access to the basic procedures of a pipeline, but considers further extension possibility with C++/CUDA and Python bindings.

5.4.1.1 Naming structure

Most of the API classes have prefix "va" (for example vaBasicRenderer). The data Readers names are formed with a prefix of file format, for example, xyzReader. All SDF primitives and operations that can be directly used within the FRep modelling pipeline have "sdf" prefix. For example sdfSphere, sdfBox, sdfTextureReader, etc.

5.4.1.2 Prerequisites

The API is based on Optix engine. The visual and auditory rendering is performed through the use of OpenGL and OpenAL accordingly. For details on visual-auditory rendering, interoperability sees the implementation of optical model class: for optical model and auditory model class: for 3D sound rendering. Additionally, some of the API classes use the following open source libraries (those procedures might be not used and libraries excluded from the project):

- Readers: ITK for data preprocessing
- stkSound class: STK for sound synthesis
- Leap Motion SDK for interaction
- Pybind for python bindings.

For detailed requirements, compiling source codes on Windows and Linux and other relevant information, please, see README document in github repository (E.Malikova 2020)

5.4.2 Data-flow in GPU-accelerated visual-auditory analysis

The ray-tracing APIs facilitate procedures related to the low-level ray-tracing, such as memory allocation, handles optimisation for GPU implementation (Wald & Parker 2019) and provides the possibility of GPGPU programming in a pipeline. This allows to design upper-level GPU solutions. In this work, we consider the design of visualisation API for heterogeneous objects analysis that is based on Optix ray-tracing API and uses a GPU data-flow structure allocation and execution that is a core of conventional CPU visualisation frameworks.

Moreover, we consider the conventional advantages of the object-oriented approach to such GPU data-flow visual-auditory pipeline design. We combine GPU hybrid constructive modelling and ray-casting within IC structure for outline the unified implementation based on ray-tracing API (see section 5.3). This allows us to use object-oriented architecture and GPU data-flow in design visualisation pipeline and extend it further to the visual-auditory case.

The API core functionality is designed based on functional features similar to VTK and considers the following similar to VTK classes, such as Reader, Mapper, Actor, Renderer, Window, Interactor and Widget.

Similarly to VTK, we construct the visual-auditory pipeline with "input-output" concept from core object-oriented blocks that invoke the ray-tracing shaders, such as Miss, Ray Generation, Hit, etc. (see Fig 5.11 in section 5.3.2) and introduced set of callable shaders. The shaders can be executed on various stages with an execution structure defined by the type of heterogeneous object (see Fig. 5.13 in section 5.3.3). This allows us to create a data-flow structure that is stored and executed in GPU memory (see Fig. 5.16 for a basic scheme of classes communication structure and shaders management).

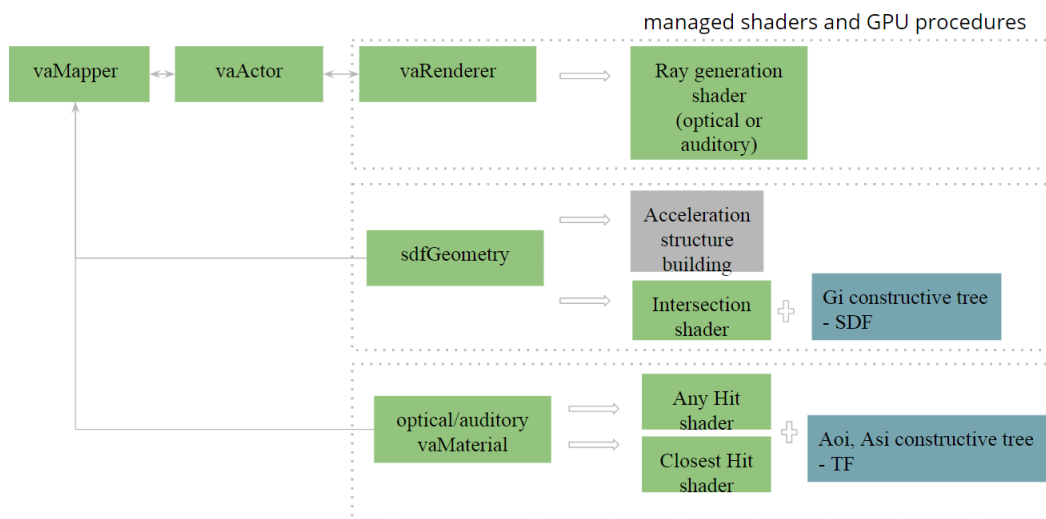


Figure 5.16: The structure of communication between classes and shaders management

Combined with object-oriented principles, the GPU data-flow paradigm provides the user with the possibility of building a visual pipeline as building blocks similar to conventional visualisation frameworks (see Fig. 5.17). The core of such visual pipeline design for heterogeneous objects is the ray-casting pipeline that operates the GPU implemented $\langle I, BV^{l_2} \rangle$ structure. The manipulations include queries/intersections with the nodes of constructive trees and operating a different levels of BVH structure (see section 5.3.1), configuring type of pipeline depending on type of used heterogeneous object (see section 5.3.3), user interactive procedures or LOD techniques that involve projection of multidimensional structure $\langle I, BV^{l_2} \rangle$ to 3D space (see sections 4.3.3 and 5.3.1). All the necessary configuration is done as the pipeline is constructed from object-oriented building blocks due that handle the procedures on both CPU and GPU.

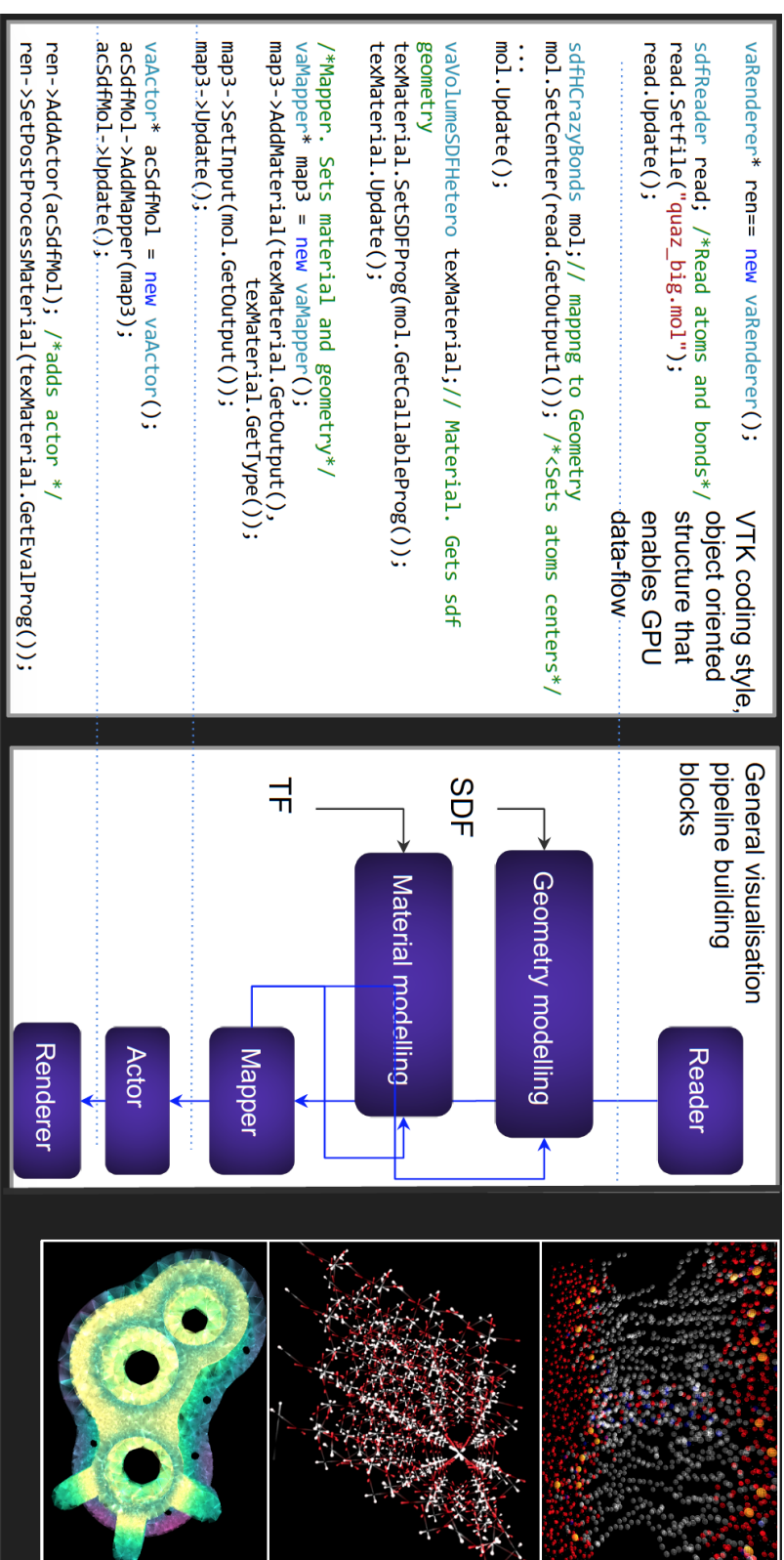


Figure 5.17: A structure of proposed framework for volume rendering of heterogeneous objects. Visual-auditory pipeline is constructed according to data-flow concept with two main procedures to be user defined: mapping geometry primitive (SDF) and TF

As a result of such object-oriented programming, the ray-tracing pipeline is built with ray-tracing API and is executed on GPU in a rendering loop (see section 5.3). As the ray-tracing context is launched to obtain a visual and auditory image for further analysis, the shaders defined within Geometry, visual and auditory Materials are executed within the ray-tracing pipeline as it was described in section 5.3.2. To facilitate the visual-auditory scene management, handle different rendering passes for visual-auditory properties rendering and interaction the `vaActor` and `vaMapper` are implemented similarly to VTK Actor and Mapper.

The pipeline was implemented in C++ (see Fig. 5.17). As a proof of concept for some cases the Python bindings were provided with pyBind (Jakob et al. 2016) to read NumPy arrays as an input data (see Fig. 5.18)

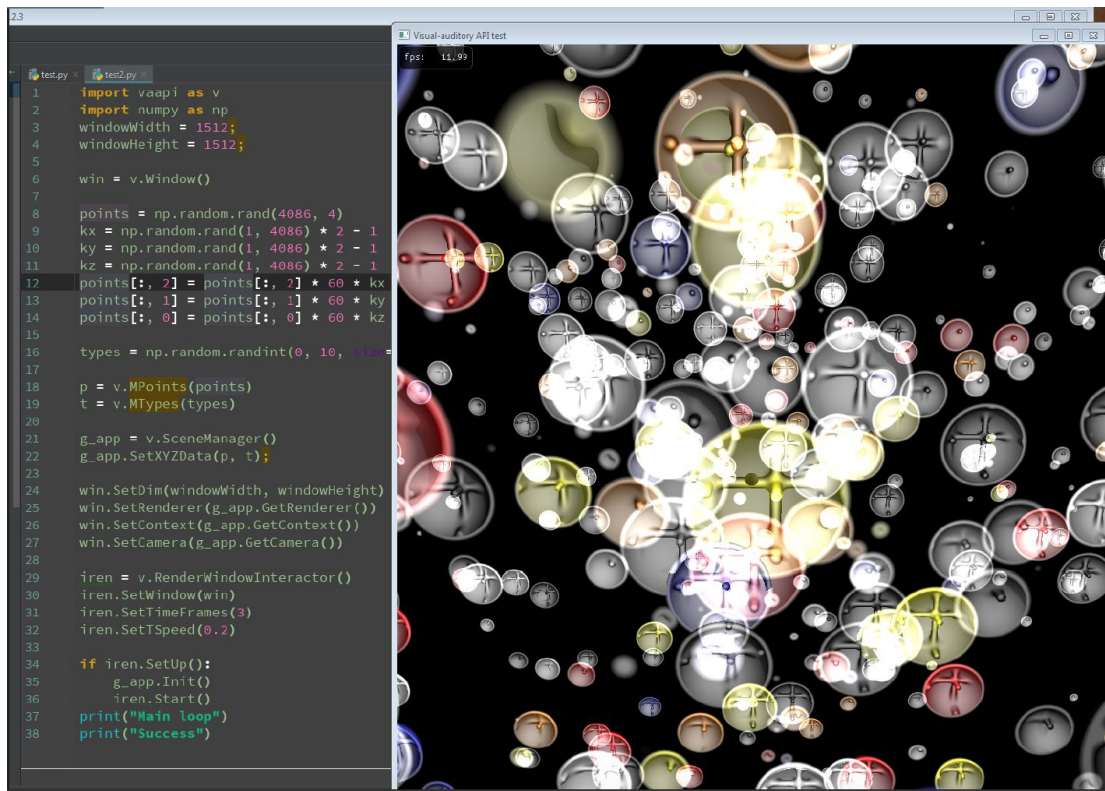


Figure 5.18: An example of calling GPU accelerated API from Python

The execution within Python-based scientific environment demonstrates the main advantages of the proposed GPU-accelerated approach to construction of visualisation pipeline. In Fig. 5.19 we have provided the comparison of the conventional CPU implemented visualisation pipeline execution scheme (VTK can be an example of such API) as it is executed from Python-based scientific environment and for the proposed API with Python bindings.

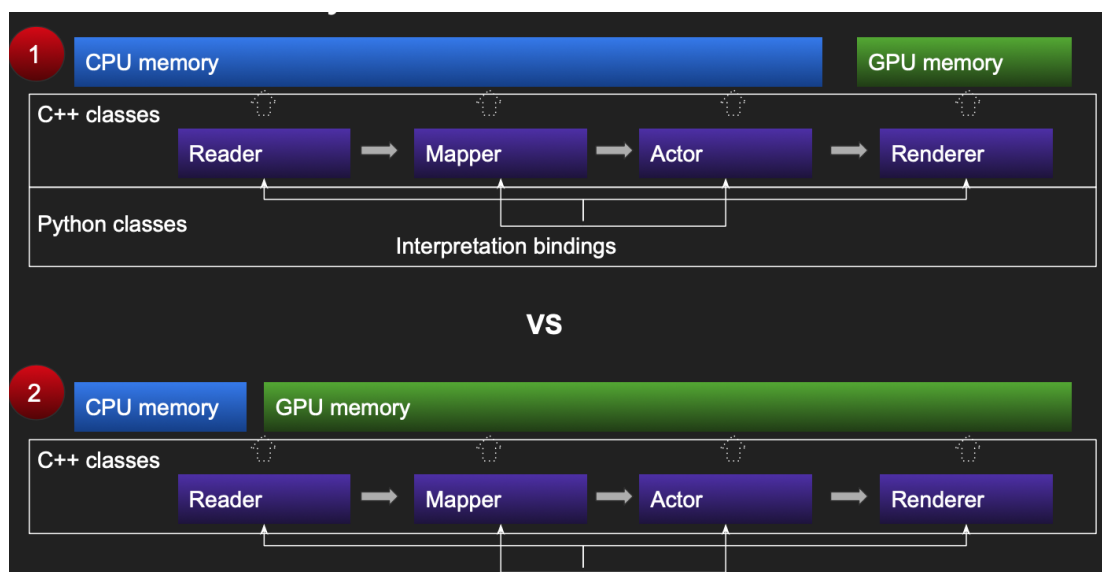


Figure 5.19: Execution in Python based scientific environment for conventional visualisation APIs (1) and the proposed API (2) that minimises CPU-GPU data exchange

5.4.3 Handling GPU programs

As the API was designed based on the Optix Engine, it takes advantage of its architecture and functional features that facilitate management and execution of the ray-tracing shaders (GPU programs). In many cases, the inputs and outputs of the proposed API are the references to Optix objects, such as `optix::Geometry`, `optix::Material`, `optix::GeometryInstance`, Optix callable programs. Most of Optix objects are created and handled in Optix API and the process uses `optix::Context`. This structure is necessary for most of the classes, except some readers and is set with `SetContext` procedure. We create a `ContextManager` class that facilitates the process of content creation and further management.

Below is the typical example of Optix context creation:

```
contextManager m;
m.Update(); //creates context

...

sdfCPKMol mol; //
→ mol.SetContext(m.GetOutput()); //passing the reference to context
→ before calling any further procedures associated with GPU
```

`vaBasicObject` implements the general procedures on operating the Context and handling a set of executed ray-tracing shaders of any type. For each class we specify the shaders of a

certain type and custom callable shaders depending on the functionality. The examples of such classes are `vaAuditoryMaterial`, `sdfGeometry`, `vaWidgetHandles` or `vaBasicRenderer`. Those classes take advantage of `vaBasicObject` implemented procedures for handling their GPU programs (see Fig. 5.20 for the hierarchy of core classes).

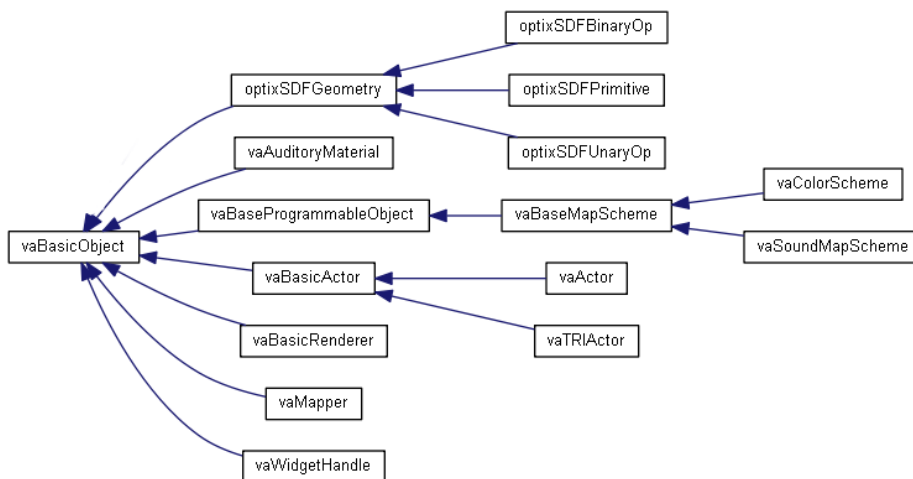


Figure 5.20: Core classes

5.4.4 Data readers and SDF geometry mapping

This work considers the following file formats for input data representation (see Fig. 5.21) :

1. molecular particle-based data: MOL, SDF, XYZ.
2. tetrahedral meshes: vtk unstructured grids
3. voxel data: txt

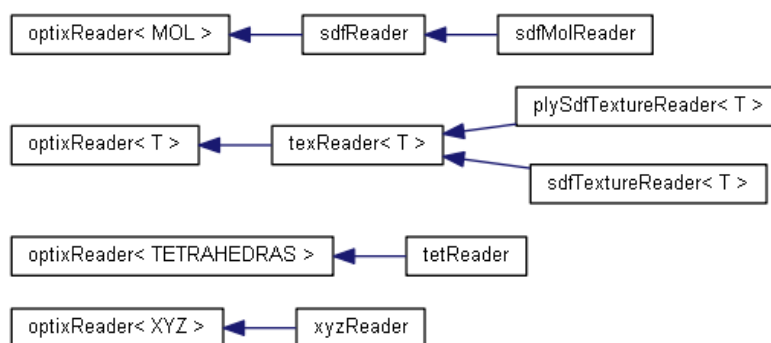


Figure 5.21: Reading classes

Below is the example for molecular data described in XYZ file format. The code reads the data and creates a procedural CPK molecule representation on GPU as a set of SDF spheres, representing atoms. All necessary GPU structures (BVH acceleration, GPU hybrid constructive trees) are handled within the pipeline and used later on the rendering stage:

```
contextManager m;
m.Update();//creates context

xyzReader read; //reads data
read.Setfile("molecule.xyz");
read.Update();

sdfCPKMol mol; //
mol.SetContext(m.GetOutput());
→ mol.SetCenter(read.GetOutput1()); //centers, data stored in std::vector
→ mol.SetTypes(read.GetOutput2()); //set types of atoms, data stored
→ in std::vector
mol.SetMaterialType(0);
mol.Update();
```

In the other example below, the Reader performs signed distance transform (ITK is deployed for implementation) and allocates the necessary GPU Buffers and Textures Samplers:

```
contextManager m;
m.Update();//creates context

sdfTextureReader<float> readSDFTex1;
readSDFTex1.SetContext(m.GetOutput());
readSDFTex1.SetSize(139, 150, 160); //data dimensions

readSDFTex1.SetThreshold(0.1); //isolevel of scalar field
readSDFTex1.Setfile("ed1.txt");
readSDFTex1.Update();

sdfTextureReader<float> readSDFTex2;
readSDFTex2.SetContext(m.GetOutput());
readSDFTex2.SetSize(138, 150, 160);
```

```

readSDFTex2.SetThreshold(0.1);
readSDFTex2.Setfile("ed2.txt");
readSDFTex2.Update();

sdfTexture tex; //dynamic SDF object creation
tex.SetContext(m.GetOutput());
→ tex.SetTexture(readSDFTex1.GetTexture(), readSDFTex1.GetParam());
→ tex.SetTexture(readSDFTex2.GetTexture(), readSDFTex1.GetParam());
tex.Update();

```

5.4.5 Setting up Mapper and Actor for visual-auditory Rendering

vaMapper, vaActor and vaRenderer are implemented similarly to VTK classes. The vaMapper collects and manages the geometry and material representation within a pipeline, in current implementation with optical or auditory properties. The vaMapper activates optical or auditory material, depending on visual or auditory volume ray-casting pass. Within a pipeline, we implement optical and auditory materials similarly with the closest hit and any hit shaders. The shader type is configured depending on the type of heterogeneous object (see section 5.3.3).

The vaRenderer is responsible for rendering of visual and auditory properties. We consider several rendering modes that can specify optical or auditory rendering passes, rendering in an interactive camera mode, user interaction mode or visual-auditory animation (for more details and example see section 5.4.8). vaRenderer operates the vaActors that in its turn handle vaMapper to configure the pipeline for specified ray-casting mode.

The code below demonstrates the use of Mapper, Actor and Renderer classes:

```

vaMaterial mSdf;
mSdf.SetContext(m.GetOutput());
mSdf.Update();

vaMapper map21;
map21.SetContext(m.GetOutput());
map21.SetInput(sdf.GetOutput());
map21.AddMaterial(mSdf.GetOutput(), mSdf.GetType());
map21.Update();

```

```

vaActor acSdf1;
acSdf1.SetContext(m.GetOutput());
acSdf1.AddMapper(&map21);
acSdf1.Update();

ren.AddActor(&acSdf1);

....
ren.LaunchAuditoryContext(); //compute auditory ray-tracing

...
ren.LaunchOpticContext(); // compute optical ray-tracing

```

5.4.6 Window, GUI and Interactor

Ray tracing generates an image with each pixel computed with the ray-casting from the camera. The entire procedure is implemented with CUDA with the 2D image submitted to OpenGL as a texture. OpenGL sends to windowing API a textured quad. Thus we have a relatively fixed OpenGL/window rendering part that we implement with vaWindow. We use GLFW and ImGui (O. n.d.) libraries to design a custom GUI.

The API provides a basic Renderer, GLFW window and Interactor. Below is a simple code to set up Renderer, Window and Interactor for default interactive camera rendering mode:

```

contextManager m;
m.Update(); //creates context

PinholeCamera pinholeCamera; //basic camera

vaBasicRenderer ren;
ren.SetValid(m.GetValid());
ren.SetContext(m.GetOutput());

ren.SetOpticalDims(windowWidth, windowHeight);

```

```
ren.SetCamera(&pinholeCamera);

//set not dynamic
ren.SetDynamic(false);
ren.SetAuditory(false);

//window procedure

vaWindow vaWindowProc;

vaWindowProc.SetDim(windowWidth, windowHeight);
vaWindowProc.SetRenderer(&ren);
vaWindowProc.SetContext(m.GetOutput()); //returns context
vaWindowProc.SetCamera(&pinholeCamera);

→ vaRenderWindowInteractor iren; //TODO always check that basic still
→ works
iren.SetWindow(&optixWindowProc);
```

5.4.7 Constructive modelling

As we have discussed in section 5.3.4 we implement constructive modelling principles on GPU. Below in Fig. 5.22 is the class hierarchy for some SDF primitives and operations available within the API.

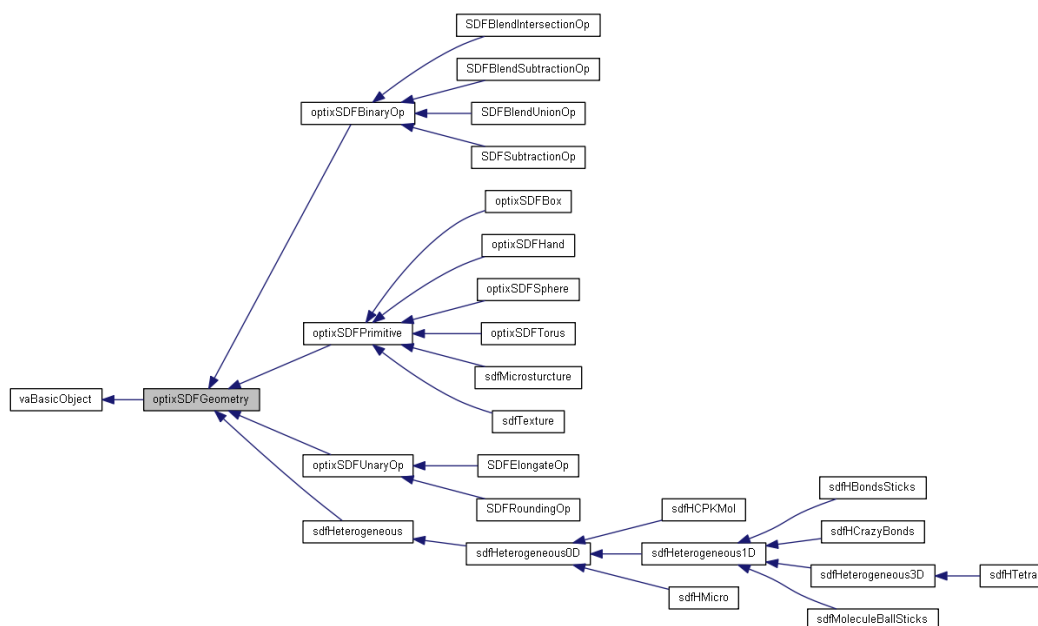


Figure 5.22: Constructive geometry modelling classes, including heterogeneous objects modelling framework

Below we consider the example that constructively models on GPU a geometry via a set of available SDF primitives and operations:

```

1  sdfBox sdf;
2  sdf.SetContext(m.GetOutput());
3  sdf.SetCenter1(optix::make_float3(1.0));
4  sdf.SetDims(optix::make_float3(0.3));
5  sdf.Update();
6
7  sdfRoundingOp round;
8  round.SetContext(m.GetOutput());
9  round.AddOperand(&sdf);
10 round.SetKoeff(0.01);
11 round.Update();
12
13 sdfTorus sdfT;
14 sdfT.SetContext(m.GetOutput());
15 sdfT.SetCenter1(optix::make_float3(0.0));
16 sdfT.SetRadius1(optix::make_float2(0.4, 0.1));

```

```
17     sdfT.Update();
18
19     SDFElongateOp el;
20
21     el.SetContext(m.GetOutput());
22     el.AddOpoperand(&sdfT);
23     el.SetHKoeff(optix::make_float3(0.0, 1.0, 2.1));
24     el.Update();
25
26
27     sdfBlendUnionOp opBlend;
28     opBlend.SetContext(m.GetOutput());
29     opBlend.AddOpoperand1(&sdf);
30     opBlend.AddOpoperand2(el.GetOutputSdfObject());
31     opBlend.SetKoeff(0.3);
32     opBlend.Update();
33
34
35     vaBasicMaterial mSdf;
36     mSdf.SetContext(m.GetOutput());
37     mSdf.Update();
38
39     vaMapper map21;
40     map21.SetContext(m.GetOutput());
41     map21.SetInput(sdf.GetOutput());
42     map21.AddMaterial(mSdf.GetOutput(), mSdf.GetType());
43     map21.Update();
```

The modelled geometry is presented in Fig. 5.23.



Figure 5.23: A example of constructively modelled geometry

5.4.8 Rendering

In the same way we implement the visual-auditory rendering, user interaction and dynamic rendering by specifying the different rendering modes in vaBasic Renderer:

```
enum vaBasicRenderer::RenderModes {  
    INTERACTIVE_CAMERA,  
    → /*<Mode by default. Rendering through defined camera with interactive  
    → manipulation of its parameter (pan, zoom, etc.). In this mode the Optix  
    → context launches rendering of optical model. In this mode only scene  
    → geometry and optic materials are rendered.  
    See vaBasicRenderer::LaunchOpticContext() function*/
```

```

        COMPUTE_SOUND,
        → /*<Auditory ray-casting. In this mode the Optix context launches rendering
of optical model. See vaBasicRenderer::LaunchAudioContext() function.
        → The result of procedure are the computed with ray-casting auditory properties
        → that are defined with auditory material distribution on scene geometry.
        → OpenAl is used for auditory scene representation ready for playing :
        → set of sound sources, sampled sound waves, configured HRTF and etc.

        → If the auditory scene was computed, it would be automatically played if
        → the RenderModes::PLAY_ANIMATION is activated
*/

        PLAY_ANIMATION,
        /*<Rendering of visual-auditory dynamic scene. */

        INTERACTIVE_WIDGET
        → /*<Interactive manipulation through assigned widget. The widgets are similar
        → to VTK widgets and are used for
        → interactive definition of various optical/geometry/auditory parameters,
        → that are considered once the renderer
*/
};

```

The default interactive camera manipulation mode

vaBasicRenderer::RenderModes::INTERACTIVE_CAMERA is activated by default. To render, for example, the animation represented within dynamic scene we just need to activate the **vaBasicRenderer::RenderModes::PLAY_ANIMATION** mode. Similarly the **vaBasicRenderer::RenderModes::COMPUTE_SOUND** and

vaBasicRenderer::RenderModes::PLAY_ANIMATION should be activated one after another for 2 steps of visual-auditory rendering that has been described in section 5.3.5 accordingly.

The **vaInteractor** will read **vaRenderer** modes and initiate according procedures of the renderer to perform visual/auditory or dynamic scene ray-casting.

In the example below, we implement this part within a conventional interactive key callback procedure:

```

namespace Render {
    struct CallbackData

```

```

    {
        vaRenderer* ren;

    };
}

→ void keyCallback(GLFWwindow* window, int key, int scancode, int action,
→ int mods)
{
    bool handled = false;

    if (action == GLFW_PRESS)
    {
        switch (key)
        {
            case(GLFW_KEY_S):
            {
                Render::CallbackData* cab =
→                 static_cast<Render::CallbackData*>(glfwGetWindowUserPointer(window));
                if(cab->ren->isDynamic()){
                    std::cout << "Playing the dynamic scene" << std::endl;

→                 cab->ren->SetMode(vaBasicRenderer::RenderModes::PLAY_ANIMATION);
                    cab->ren->SetTime(0.0); /*<Set initial time to 0*/
                    break;

                }

            }

        }

        if (!handled) {
            // forward key event to imgui
→            ImGui_ImplGlfw_KeyCallback(window, key, scancode, action, mods);
        }
    }
}

```

The vaRenderer deploys optical and auditory models that specify the necessary procedures for optical and auditory ray-tracing. The core functionality is implemented in abstract class vaBasicModel for both optical and auditory modes (see Fig: 5.24):

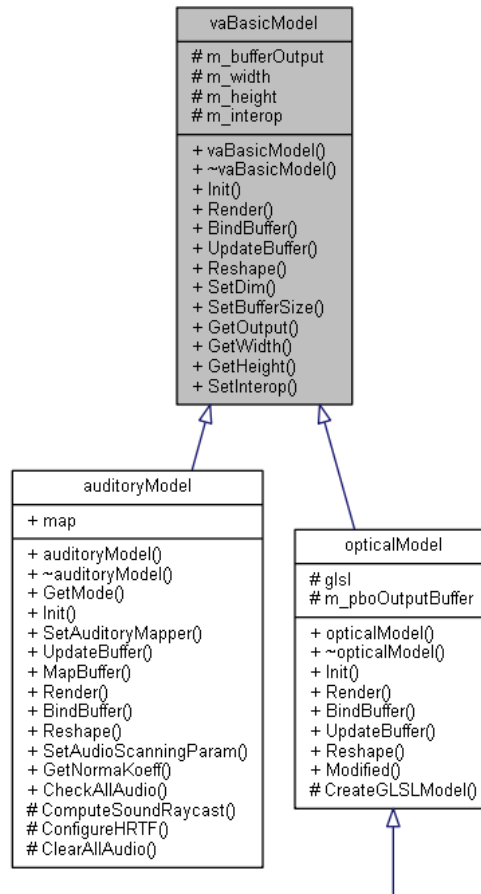


Figure 5.24: Optical and auditory models

5.4.9 Interactive widgets

The interactive widgets concept is similar to conventional interactive rendering in such toolkits as VTK, where the user performs an interactive exploration and scene manipulation through using cameras and 3D interactive widgets. Those widgets define custom ray-shooting procedures to compute various procedures with ray-tracing, like collision detection, volume computation, etc. with further auditory feedback.

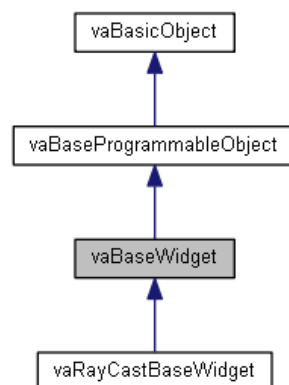


Figure 5.25: Widgets

In this work we consider how the user interactive exploration can benefit of ray-casting and constructive modelling (see sections 3.6.3 and 4.6). Thus, the core features of deployed in this work interactive widgets are:

1. constructively modelled geometry for handle/avatar representation. This representation can be directly deployed as a part of interactive geometry modelling (see the example in sections 4.6.1 and 5.3.4).
2. widgets can define their ray-casting procedures. Those may be procedures for custom measurements that can be followed by mapping the results of those measurements into auditory feedback (section 4.6.2) or other procedures. For example, in this work, we have experimented with a registration procedure that is conventional for the image processing area. The procedure aligns two objects by minimising the distance between points on surfaces of two objects (see Fig.5.26).

Let us consider the examples of programming of various aspects related to widget-based user interaction. Widget creation and adding it to 3D scene:

```

//widget creation
→ std::shared_ptr<vaBaseWidget> m_widget = std::shared_ptr<vaBaseWidget>(new
→ vaRayCastBaseWidget());
   m_widget->SetContext(m.GetOutput());

→ //Create geometry handle for specified widget and widget to interactive
→ scene with vaRenderer method SetWidget
   m_widget->CreateGeometryHandle();
   ren->SetWidget(m_widget);
  
```

The example of assigning a ray-casting widget a plucked string model for auditory feedback generation (see section 4.6.2):

```

1  → //Setting auditory model (plucked string in this case) for widget feedback
2  if (m_widget->isRayCast()) {
3      ren->SetAuditoryRayGenerationFromWidget("widget_ray_cast",
4  →      dynamic_cast<vaRayCastBaseWidget*>(m_widget.get())->GetRayCastProg());
5
6      ren->SetAuditoryMapModel(new auditoryMapperPlucked());
7  }

```

The code below demonstrates the use of widget geometry as a part of a constructive tree to enable interactive geometry modelling. See sections 4.6.1 for technique details.



Figure 5.26: Registration of widget geometry (sphere) and molecular surface object. (a) The ray-casting based scanning of local surface patch for assumed local registration area. For this the user interactively moves widget in specified direction (b) Result of least-squares registration of two defined point sets.

```

1  optixSDFBox sdf;
2      sdf.SetContext(m.GetOutput());
3      sdf.SetCenter1(optix::make_float3(1.5));
4      sdf.SetDims(optix::make_float3(0.3));
5      sdf.Update();
6
7  SDFBlendUnionOp opBlend2;
8      opBlend2.SetContext(m.GetOutput());
9      opBlend2.AddOpperand1(&sdf);

```

```
10     opBlend2.AddOpperand2(m_widget->GetHandle());  
11     opBlend2.SetKoeff(0.5);  
12     opBlend2.Update();
```

Similarly to conventional toolkits, the widgets in this API are an entry point for user interaction and introduce changes into the visualisation pipeline as a result of an interaction. Together with the other core components, such as Readers, Mappers, Renderers they shape a framework for the development of a wide variety of interactive visualisation applications for the analysis of heterogeneous objects powered by ray-tracing API. The object-oriented structure facilitates the creation of GPU procedures for execution and the ray-tracing is an entry point for the evaluation of visualisation techniques. In this context, we are interested in the performance of such visualisation procedures and relative timings depending on the complexity of mappings and visualisation techniques, size and spatial dimension virtual scene. We discuss the main features and provide the approximate timings in the next section.

5.4.10 Timings

Compared to rasterization, the ray-tracing algorithm most often emphasises the efficiency problem in the context of maximising rendering quality (Beets 2020). Due to differences in procedures design, the efficiency metrics of graphic pipelines are also addressed differently (Vasiou et al. 2018),(Beets 2020).

Firstly, the acceleration structure building, such as the BVH, which is the most expensive part of the ray-tracing based graphics pipeline (Deng et al. 2017), (Kopta 2016),(Hendrich et al. 2017) is considered. If it is possible, the rendering pipeline is programmed to execute it only once, although it is not always can be done for dynamic objects and in case of user interaction or dynamic scenes (Wald 2007).

Secondly, the performance on the ray-tracing stage is much justified by ray coherence, and the ability to balance the computational load between shooted rays. The procedures executed per GPU unit may require different execution time. Also, the process can be affected by non-coherent data access (Beets 2020),(Sommefeldt 2020). Ray-tracing the performance timing highly dependent on data access/movements (Kopta 2016) as those are often the main consumers of time (Vasiou et al. 2018). Although no secondary rays are often considered, the case of volume ray-casting can be as difficult as surface rendering in terms of coherency. The process similarly deals with the balancing of computational load on a per-ray basis as the rays travel inside a BVH-accelerated volumetric structure. The ratio of BVH accelerated space skipping regions and computationally expensive volume sampled regions is hard to predict as it can vary even for the ray paths of similar length. The large difference in the rays

traversal time per GPU unit affects the total GPU executed ray-tracing time that may depend on viewing direction and how dense the material distribution in the heterogeneous object.

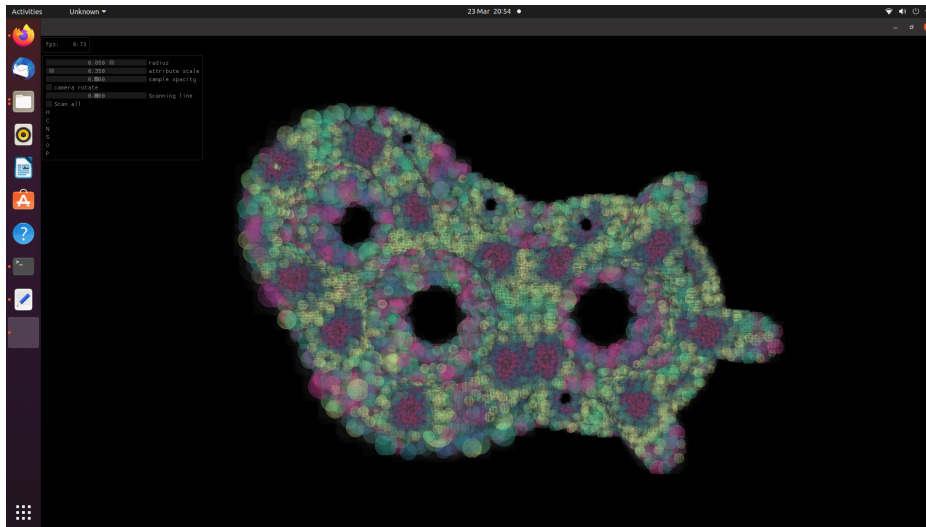
The data movement-related issues are of particular importance as ray-tracing based visualisation of dynamic and multi-scale properties is considered. We consider the volume ray-casting performance aspects in terms of visualisation pipeline efficiency, as conventional solutions often consider the two main metrics: the time for entire visualisation pipeline evaluation and the time directly for interactive rendering once the pipeline has been evaluated. In this work, the visualisation pipeline evaluation includes the conventional for ray-tracing pipeline virtual scene BVH tree building. We avoid the cases of dynamism or user interaction that lead to BVH rebuilding. The data is loaded directly on GPU and access it minimising CPU/GPU communication in interaction and limiting control only to GPU memory issues in computation, such as the amount of data accessed by computing units (Chatterjee et al. 2017).

Thus, most of the dynamic/interactive visualisation efficiency are defined on rendering stage where ray-tracing is considered in terms of ray coherency and memory-access (Moon et al. 2010),(Kopta et al. 2015). We expect that stored on GPU as callable procedures the constructive trees for complex dynamic and multi-scale geometry and material will increase ray-tracing time, compared to ray-tracing of simple geometries, such as spheres. Also, the per-ray data structures required additional memory use.

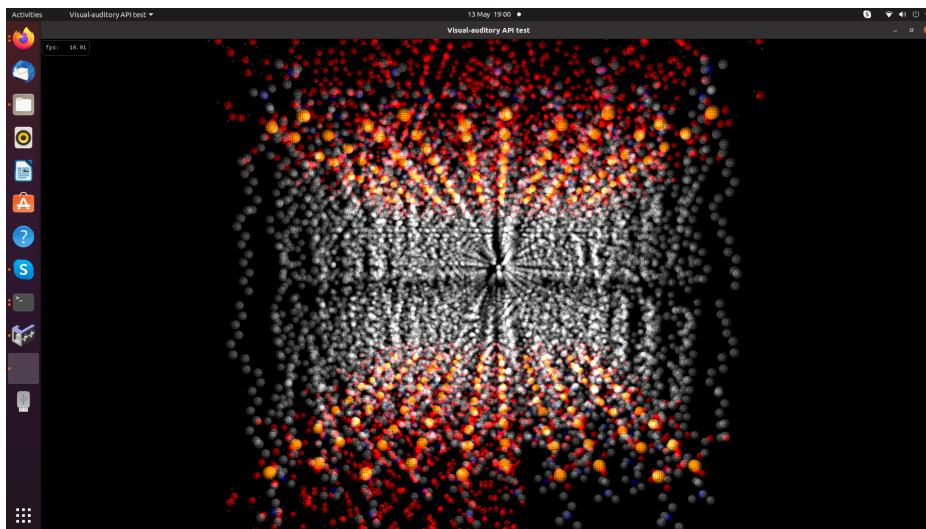
To get a basic idea of how the performance parameters are affected in ray-tracing based visualisation, we evaluate the performance for conventional particle splatting described in (Knoll et al. 2014). Compared to more universal cases of volume visualisation of arbitrary geometry within a subdivision, the conventional splatting approach benefits from the following simplifications:

1. no sampling inside volume is needed as a material is homogeneous within a subdivision
2. the intersection can be computed with sphere can be fastly computed and bounding volume is optimal (sphere-shaped)

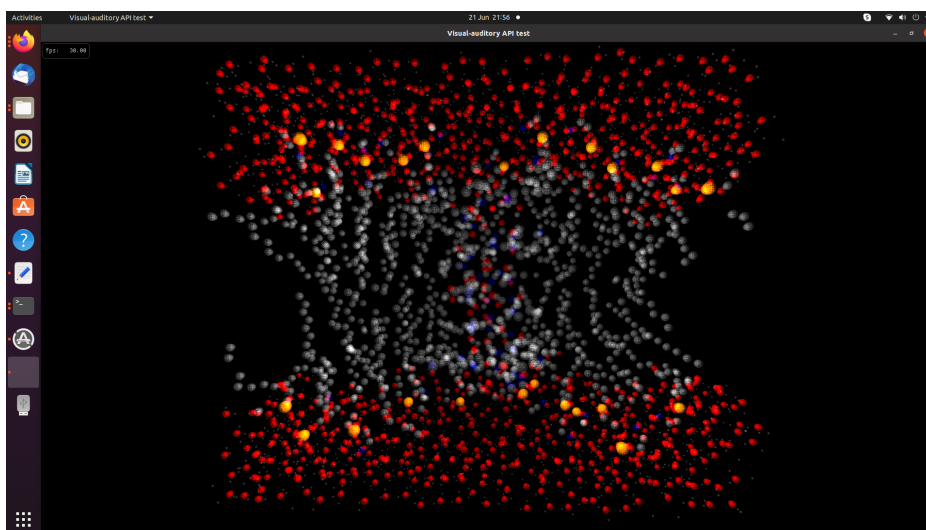
Depending on camera parameters defined with user interaction (zoom in/out, rotation) the FPS ranges obtained for different types of data are presented in table 5.1 (see also Fig. 5.27 for example of heterogeneous representation modelled on three types on input data). The input data differ in the number of cells and "density" of volume structure. The tetrahedral mesh-based structure (model 1) is an example of dense volume, while molecular data (models 2,3) are examples of "sparse" volumes. Moreover, model 3 is also a thin, slice-like volume and thus in most cases, rays will be relatively short in length. As we have to use more complex geometry, the evaluation time increases. Those are the case of basic dynamic



(a)



(b)



(c)

Figure 5.27: Examples of input data with dynamic microstructure shape modelled within defined heterogeneous subdivision a) Heat equation mesh; b) Diffuse membrane (molecular data) d) Slice of diffuse membrane

(shape deformation with morphing) and dynamic microstructure primitives (see Fig. 5.27) and dynamic microstructure primitives (see Fig. 5.27 in table 5.1). The results for both pipeline evaluation performance and averaged FPS are summarised in graphs presented in Fig. 5.28 and Fig. 5.29.

Table 5.1: Performance for volume splatting for structures of different size and complexity

Model	Cells num	Pipeline evaluation	Sphere geometry	Basic dynamic	Microstructure dynamic
1)Heat equation mesh	34444	0.18 sec	30-32	11-15	0.73-0.9
2)Diffuse membrane	15848	0.031 sec	40-61	30-60	8-15
3)Slice of membrane	4000	0.019 sec	59-64	49-60	19-30

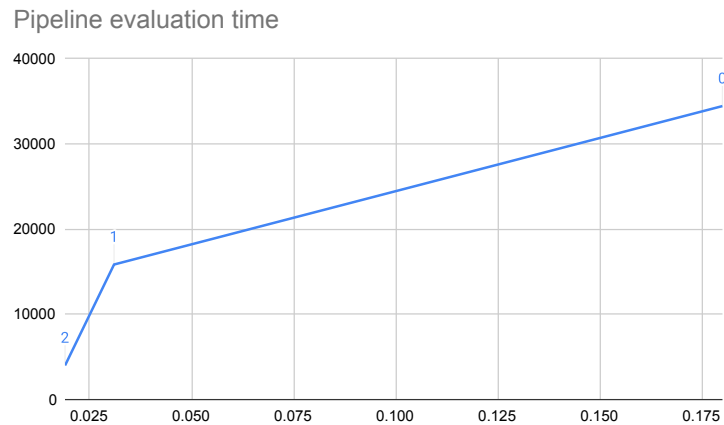


Figure 5.28: Pipeline evaluation time depending on number of cells for models 1,2,3

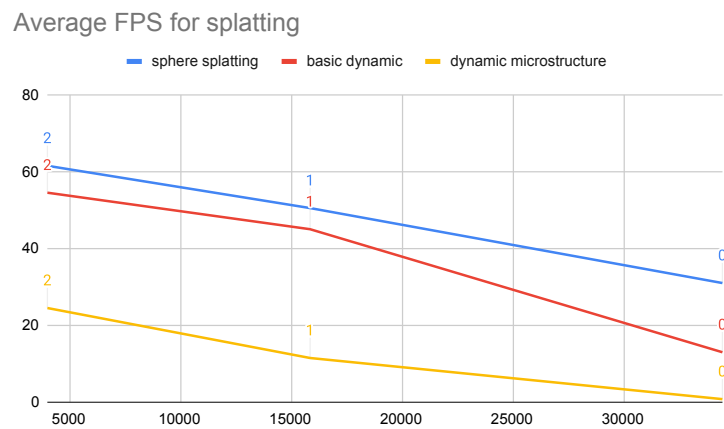


Figure 5.29: Averaged FPS depending on number of cells for models 1,2,3

Thus, it can be concluded that performance decreases with the size of construction tree for modelling geometry. For geometry with dynamic and multi-scale features, such complexity is usually proportional to considered dimension: dynamic shape deformations can require non-trivial operations within constructive trees (Pasko et al. 2004b, Adzhiev et al. 2002) and multi-scale features introduce even more complex geometry (Liu & Shapiro 2018), (Wang et al. 2011), (Wahle & Wriggers 2015), such as microstructures (Pasko et al. 2011b), (Putanowicz 2015), those efficient sphere-tracing maybe not straight forward (Bálint & Valasek 2018, Keinert et al. 2014). In addition, the consideration of non-homogeneous material distribution leads to the necessity for sampling inside volume and thus increases the number of constructive trees evaluation. As an example of a particular case study, below in table 5.2, we have considered how ray-tracing time grows with the complexity of representation for dynamic and multi-scale features space, for a molecular water cluster of 840 atoms with 560 bonds that are used to model 280 water molecules in total (see details on a case study in section 6.1.3).

Table 5.2: Molecular cluster

CPK dynamic	Balls and Sticks dynamic	Multi-scale representation
60-64	20-15	15-13

Chapter 6

Case studies

While the proposed visual-auditory approach can be used in many areas, in this work we are focusing on two case studies that highly depend on efficient scientific visualisation and geometric modelling. We consider the areas of molecular structures visualisation and microstructures modelling and rendering in digital fabrication. Those areas highlight different challenges related to heterogeneous objects modelling and visualisation. We demonstrate how the proposed approach can address such challenges and provide examples of real-time visualisation of such structures.

6.1 Molecular simulation case study

The molecular phenomena analysis is an area of active research that connects simulation and experiment to get a correct insight into the compound dynamic structure (Miao, Klein, Kouřil, Mindek, Schatz, Gröller, Kozlíková, Isenberg & Viola 2019). The molecular visualisation is a challenging task due to a large amount of data and a wide range of complex data representations (Kozlikova et al. 2017). Conveying information about the properties of dynamic multi-scale molecular structures demands consideration of various visualisation techniques (Miao, Klein, Kouřil, Mindek, Schatz, Gröller, Kozlíková, Isenberg & Viola 2019) and multimodal exploration (Kozlikova et al. 2017). Multimodal systems facilitate the analysis of complex molecular phenomena. Often the techniques use the interactive exploration with such gesture control and eye gaze devices (Hoell et al. 2018),(Silva et al. 2019) or introduce various sensory modalities such as visual, auditory, tactile that complement each other and can highlight features of interest (Silva et al. 2019).

The design of interactive visualisation and multimodal interfaces for molecular phenomena analysis is a challenging task. There is no universal approach to support various output modalities and multi-scale visualisation techniques. Most of the techniques in the area

restrict the geometry type to increase rendering efficiency. However, such restrictions can not be applied to the case of analysis of multi-scale molecular phenomena that combines both experimental data and simulation results. The use of various representations of molecular phenomena demands flexibility in the modelling of the geometry and materials within the introduced subdivision.

Below, we consider the problem of modelling, accelerated rendering and visual-auditory analysis of dynamic multi-scale molecular structures. Such structures appear in molecular biology, chemistry, new materials design (Norman 2016). Such heterogeneous objects are an important representation of the real-world phenomena on various levels. We discuss our approach application for flexible modelling of dynamic multi-scale molecular representation and unified approach to visual-auditory volume rendering and analysis. Below we outline the representations of molecular phenomena and related to complex structure analysis challenges. We consider the ray-casting and GPU accelerated geometry modelling techniques deployed to address some of these challenges.

6.1.1 Molecular phenomena representation and visual analysis

The modern research in the area of molecular phenomena analysis deals with large scale data (Chavent et al. 2011). Moreover, the problem brings together the necessity of simultaneous analysis of both experimental and numerical simulation data to understand complex molecular phenomena (Luck 1991). As a dynamic nature of multi-scale molecular phenomena is considered, in addition to "macro" changes in molecular structure such "micro" level dynamic changes as molecular vibrations can be displayed (Ojha et al. 2018). There is a need for a hybrid representation that allows simultaneous modelling of molecular structures on "macro" and "micro" levels and can combine various data types. Below we consider the two common types of molecular data representations those are voxel and point-based data.

Representation on a macro level with particle-based data The concept of "atoms and "bonds" is the easiest way to describe the molecular phenomena. The most common graphical representation of molecular structures is a space-filling or CPK models (Berg et al. 2002) or more complex "Ball-and-Stick" model (Berg et al. 2002). With GPU acceleration, this representation can be used for rendering of large scale molecular structures obtained from molecular dynamics (Muzic et al. 2015),(Grottel et al. 2015). While being simplistic, the Ball-and-Stick model is good for measurements and monitoring of distance-related parameters and can be used for visualisation of large dynamic structures (Chavent et al. 2011) with detailed analysis of the bonding process.

Space-filling and "Balls and Sticks" models are particle-based data representation (Grottel et al. 2015) which generally operates on a macro level. The representation is applied on a

"macro" level model. The additional "micro" level properties are often represented with other computational data, that is associated with the cellular subdivision defined on a particle-based data.

The "macro" level representation often uses implicit geometric modelling to improve rendering performance and often in the context of ray-tracing (Muzic et al. 2015). The (Chavent et al. 2011) introduces quadric surfaces for real-time modelling and rendering of the dynamic molecular structures on GPU. Similarly, Parulek & Viola (2012) constructs exact solvent-accessible surfaces.

The research in the visualisation of the molecular structures generally restricts a type of the geometry and, therefore, the visualisation process is often based on ray-casting of surface objects, which is much faster than volume rendering. Modern GPU hardware allows for efficient visualisation of large scale molecular data (Grottel et al. 2015), (Muzic et al. 2015) through implicit representation allowing for real-time modelling and rendering of the dynamic molecular structures (Chavent et al. 2011) or constructing exact molecular surfaces (Parulek & Viola 2012).

Micro level representation with scalar fields obtained with quantum chemistry. A more sophisticated abstraction of molecular phenomena is the concept of the "boundary" of the molecule and its internal properties (Shusterman & Strauss 2001). Based on the electron density field, the "quantum model" of the molecular phenomena provides the detailed picture on its properties like bonding (Wang et al. 2016). The representations are obtained with a scanning device or a numerical simulation. The later is often used as a theoretical explanation for molecular properties that are observed experimentally (Luck 1991). The representation may demand a simultaneous analysis of two scalar fields (Shusterman & Shusterman 1997). The shape of the electron density field is treated like a molecule's interaction boundary as it defines a probability of an electron occupying an infinitesimal element of space surrounding any given point. At the same time, its topological analysis provides a deeper understanding of bonding. The electrostatic potential field represents a charge distribution, a property that allows predicting the behaviour of complex molecules.

The consideration of the "quantum" nature of the molecular phenomena allows for an accurate analysis of their properties such as bonding, but computation is expensive and problematic for big structures. The initial data typically is a voxel representation. Volume rendering is a conventional framework to address issues of getting insight into complex phenomena represented with voxel data (Kniss et al. 2003). The technique exploits the physical process of light transport to obtain a well-structured framework that allows addressing the issue of getting a correct insight into phenomena. Flexible control over visual analysis quality issues is obtained as only two components are adjusted: optical model and multi-dimensional

transfer function (TF). The user designs the custom TFs to address the needs of the specific practical problem without changing the entire approach.

Overall, molecular phenomena take advantage of two geometry representations: implicit modelling on a base of particle-based data and voxel representation for molecular fields obtained as a result of computer simulation or experimental study. In section 2.1.2 we have provided a summary of the advantages and limitations of the most often used in rendering geometry representations, that include voxel and implicit. Both implicit and voxel-based geometry representation is convenient for GPU accelerated volume ray-tracing that allows conveying information about the internal structure of complex phenomena.

In many cases, the GPU modelling of dynamic multi-scale molecular phenomena requires procedural modelling with control over topology and shape of dynamically changing structure. Such representations can highly benefit from implicit modelling on subdivision defined with particle-based data. The space partitioning is used as a part of GPU modelling and ray-casting of both discrete geometry and continuous molecular surfaces (Parulek & Viola 2012).

Often, the molecular scalar fields are computed or obtained as a result of an experiment in addition to particle-based data representation. Such molecular fields are stored as voxel representation. A more efficient representation of such structures is hierarchical sparse voxel octree representation (SVO) that was introduced as an alternative to meshes for rendering surface objects (Crassin et al. 2011). However, this geometric representation does not have the flexibility of procedural techniques. As a result, they cannot be applicable for practical modelling of multi-scale features that display dynamic properties on both macro and micro-level. To deal with the latter, more complex visualisation techniques for molecular phenomena study are required (Kozlikova et al. 2017). We discuss some of these examples below in section 6.1.3.2.

6.1.2 An overview of multi-modal visualisation of molecular data

In general, the visualisation of large-scale molecular structures requires modelling and rendering of dense semi-transparent geometry, sparse volume data, an implicit surface representations with unified data structure (Kauker et al. 2016). The main requirements for GPU-assisted geometry and material modelling for dynamic multi-scale molecular structures are as follows. Firstly, geometry representation should be convenient and efficient for fast ray-tracing. In case of dynamic and multi-scale features, the representation should also support optimisation of LOD-like algorithms within a ray-casting, such as ray-based techniques considered in (Silva et al. 2005), (Beyer et al. 2015). Secondly, the geometric representation should be flexible enough to provide procedural modelling procedure with control over topology and shape of dynamically changing structure and control over transitions between

multi-scale representations. Also, the visualisation of molecular structures requires volume rendering to highlight internal properties of large-scale structure.

6.1.2.1 Constructive modelling of visual-auditory molecular scene

The theoretical aspects in sections 4.2.3, 4.2.2 establish the principles of constructive hybrid modelling of dynamic multi-scale molecular phenomena described with particle-based and voxel representations. We use a multidimensional HyperVolume (HV) model for visual-auditory molecular scene representation with geometry G , optical (A_o) and auditory (A_s) models as considered in section 4.2.3. The representation employs hybrid constructive modelling of geometry and material within IC structure (see sections 4.3 and 4.4). The particle-based data, that in complex case provides the description of both atoms and bonds, defines the spatial subdivision with 0D or 1D topology (see Fig. 6.1). Within cellular space partitioning (see section 4.2.2), each cell is represented with a tuple $\{G_i, A_{oi}, A_{si}\}$, where G_i is SDF-defined geometry and A_{oi}, A_{si} represent respectively optical and auditory properties within a geometry domain. The signed distance field G_i can be modelled either procedurally from particle-based data by using distance-based primitives and operations, or obtained directly from voxel data with the signed distance transform.

For example, in the Ball-and-stick representation the points are represented by spheres, the connectivity information for points is represented by cylinders and the SDF geometry is obtained as an SDF union of distance-to-sphere and distance-to-cylinder primitives (see Fig. 6.1). The material is modelled constructively with a complex multi-dimensional volume rendering transfer functions deployed as "operation nodes" of the tree (see the example in section 6.1.3.3). The more complex cases of multi-scale representations are handled with composite cells with multi-dimensional geometry modelling (see section 6.1.3.2).

6.1.2.2 Visual-auditory analysis of molecular structures

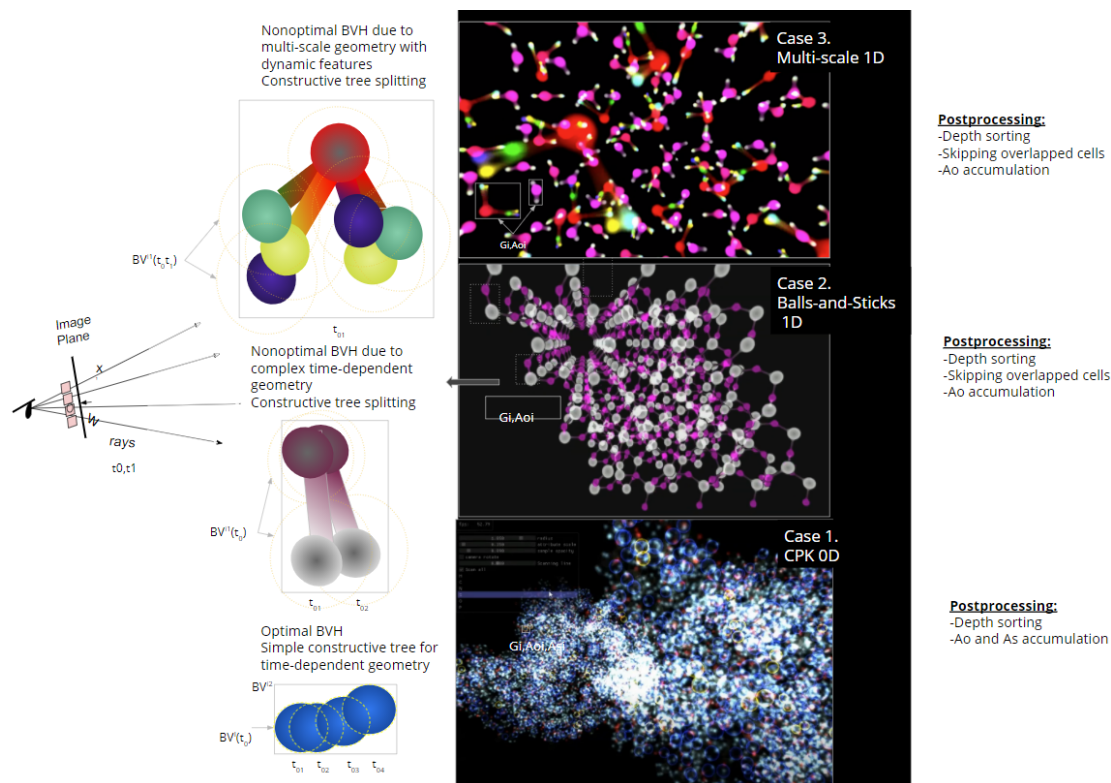


Figure 6.1: Volume ray-casting of various representations of molecular phenomena that is a result of molecular dynamics simulation

The approach to GPU-accelerated ray-casting based visualisation of heterogeneous structures was presented in section 5.2.2. We apply it for the case of molecular phenomena representations that is modelled on GPU with hybrid constructive trees within cellular structure. We introduce a BLAS for cellular subdivision $\{G_i, A_{oi}, A_{si}\}$. For each ray, we compute all cells intersections. Secondly, we refine intersections with cells by sphere-tracing to geometry G_i . On the last stage, we apply post-processing, that depending on the type of molecular representation (CPK, Ball-and-Stick) includes depth sorting and skipping repeated geometry segments. On a final step, we perform volume integration for computed ray-segments in geometries G_i , in other words, accumulate optical and auditory properties A_{oi} and A_{si} on each i -th segment.

Note, that each cell G_i that can be basic or a composite is evaluated during ray-casting as a "black box" in a unified way (see section 5.3.1). The various modalities, such as visual A_o and auditory A_s , are introduced as constructive trees and rendered in a unified way with the

ray-casting procedure. This also allows designing quite different visualisation techniques for molecular phenomena analysis in a similar way as a part of volume ray-casting.

Let us we start from conventional representations of large-scale molecular phenomena that is a result of molecular dynamic simulation and is represented with particle-based data (see examples in section 6.1.3.1). Both CPK and Ball-and-sticks representations are constructively modelled as cells with 0D and 1D topology. The structures are processed differently within ray-casting pipelines with a type of pipeline automatically decoded from topology dimension of the heterogeneous cell(see details in sections 5.2.1. See Fig. 6.1 for summary on main differences within pipeline (Case 1,2). Moreover, both the optical A_o and auditory A_s properties are accumulated in a similar way within the pipeline (see Fig. 6.1). This allows a further extension to the case of visual-auditory analysis.

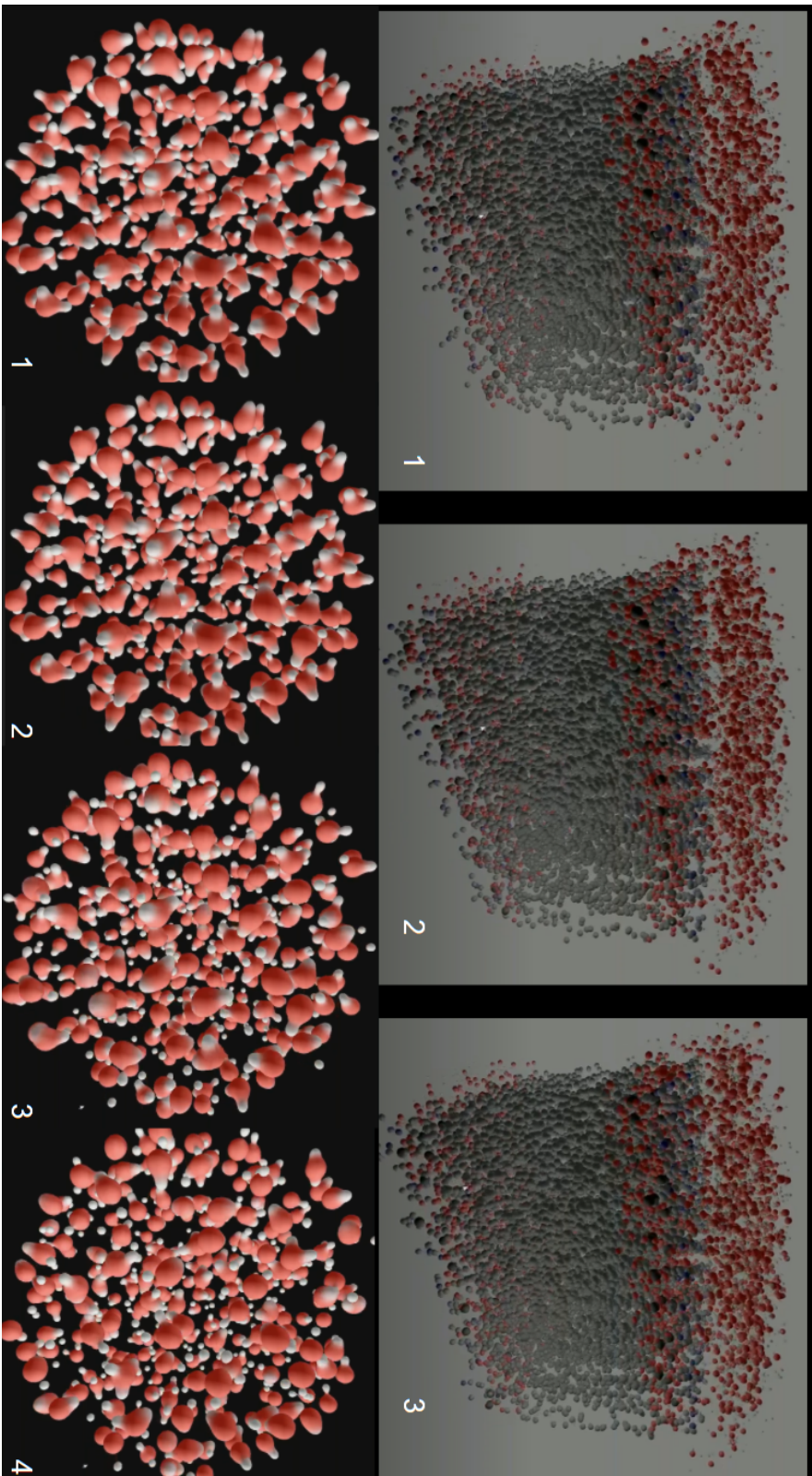
In a similar way we handle more complex cases of dynamic multi-dimensional molecular geometry modelling, for example the case when micro-level attributes are defined on particle-based data in addition to molecular dynamic simulation results. The interactive multi-scale visualisation techniques introduced similarly to techniques in Case 1 and Case 2 are essential for molecular phenomena exploration. An arbitrary set of parameters t provides simultaneous and unified control over dynamic and multi-scale features. The values of parameters are defined during volume ray-casting. The values of these parameters define how we split the complex constructive trees to optimise the visual-auditory pipeline evaluation (see section 5.3.1).

6.1.3 Case studies

6.1.3.1 CPK and Ball-and-Stick representations for molecular dynamics results visual-auditory study

Let we provide the examples of visualisation of most common representations of the results of molecular dynamics simulation. Those are CPK and Ball-and-Stick representations, see Fig. 6.2 for examples of dynamic surface ray-casting and Fig. 6.3 for volume ray-casting. For Ball-and-Stick representation that are often modelled with blending union, the computational time for ray-casting slightly higher than for simple and static geometries such as sphere Knoll et al. (2014). In general, the surface ray-casting for molecular structures is approximately 2-3 times faster than volume rendering.

The modern graphics hardware allows to extend to the case of simultaneous visual-auditory rendering (see Fig. 6.4) where visual and auditory stimuli are generated in a unified way (see details in section 5.3.5).



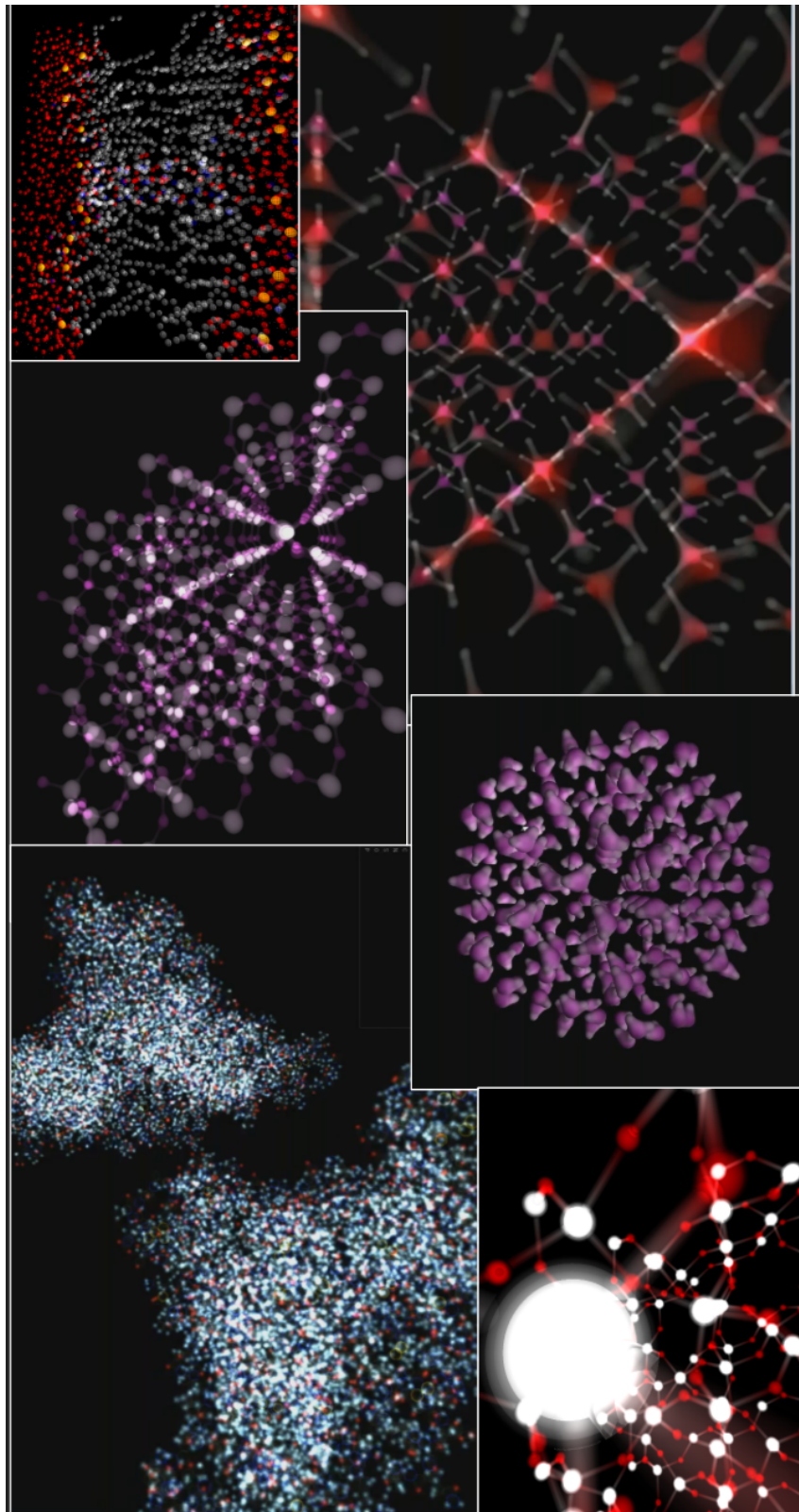


Figure 6.3: Volume ray-casting of various molecular structures

Both optic and auditory model follows similar principles and rendered in a unified way with GPU accelerated ray-casting. Similarly to the computation of a pixel colour in volume rendering, the final acoustic impulse is a weighted sum of all the vibrations produced by activated acoustic regions those are cells with geometry G_i and auditory material As_i , along the ray. In the visual-auditory scene, each geometry G_i represents an atom within the molecular structure. The simultaneous visual-auditory rendering assumes the visual highlighting of the activated as a result of acoustic ray intersection atoms as generated with material As_i vibration is played in time.

Thus, similarly to visual stimuli interpretation, the selected region of interest of the molecular structure is characterised by the specific sound generated as a result of initial impulse propagation through this region that we compute with the rays from the camera (listener position). The atomic structure is perceived through the pitches of sounds produced by activated atoms (auditory objects), the "activation" time delays as each ray propagates and the spatial position of activated atom perceived through binaural perception of 3D sound properties. The final insight on the phenomena is formed by its graphical and generated auditory image.

6.1.3.2 Visualisation of dynamic multi-scale molecular structures example

The example of water clusters reflects the complexity of the multi-scale molecular phenomena study. The microscopic properties defines the macroscopic properties and functions of entire structure (Zhao et al. 2015). Study of the water is key to understanding the complex proteins behaviour (Luck 1991). The understanding of the water phenomena depends on the study of the dynamic cluster structures and the corresponding hydrogen bonding changes. Also, an individual water molecule displays different kinds of motions simultaneously, the molecular vibrations provide an example of that (Ojha et al. 2018).

In this case study, we explore possibilities to visualise simultaneously both macro- and micro-level dynamic properties. We consider an educational example of the dynamic water icosahedral cluster fluctuations (*Icosahedral water clusters* 2018),(Loboda et al. 2009) from extended low-density to the more dense collapsed structure (Zhao et al. 2015) and simultaneously display the general information on individual water molecule vibrations modes with a level-of-detail visualisation technique (see details in section 4.3.3).

Below in Fig. 6.5 we provide the frames of interactive and dynamic volume rendering of such multi-scale molecular structure. We display all three types of water vibrations simultaneously, we highlight then with red, green or yellow colour. The geometry and internal structure of each water molecule change as the camera approach to it. The user can zoom for the analysis

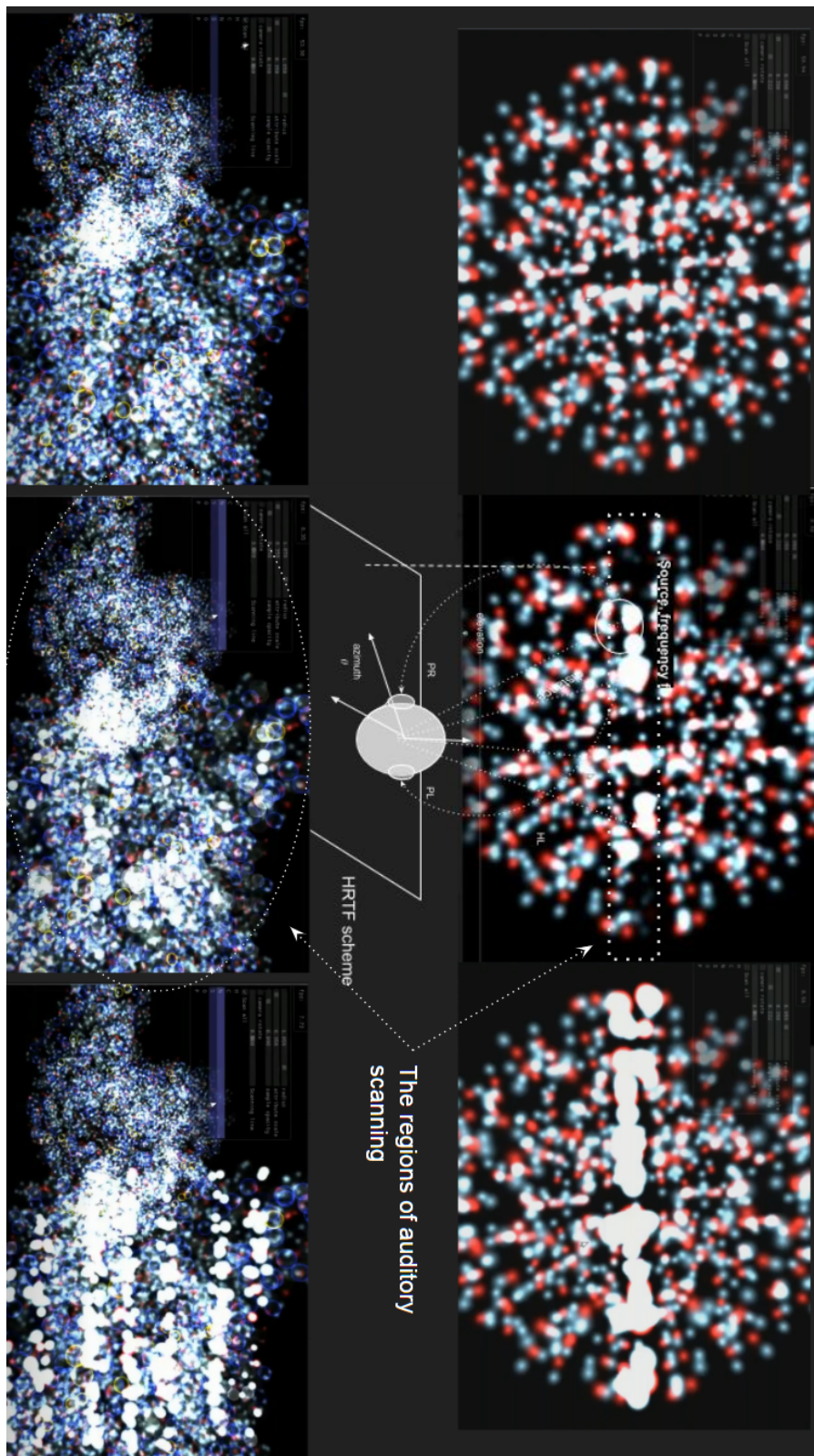


Figure 6.4: Visual-auditory volume ray-casting of various molecular structures

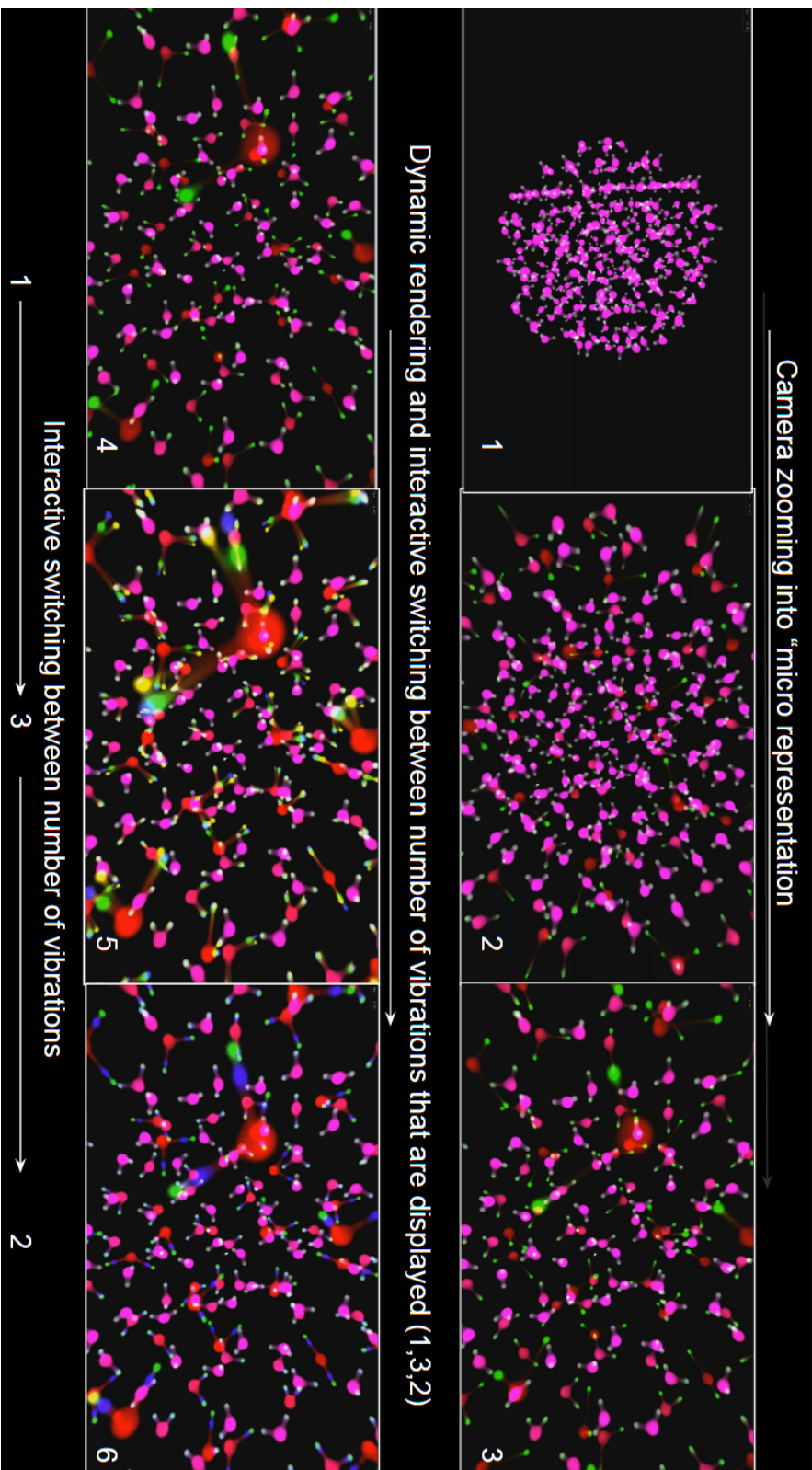


Figure 6.5: Visualisation of molecular structure with dynamic features on both macro and micro scale

of the molecular dynamic changes only on macro-level (cluster fluctuations) or both macro and micro-level (cluster fluctuations and individual water molecule vibrations).

6.1.3.3 Quantum chemistry example

Here we use the molecular structure that is the result of the quantum simulation using GAMESS software (M.S.Gordon & M.W.Schmidt 2005). Being computationally expensive, the visualisation is done using rendering of the dynamic scalar fields, which usually describe small molecular phenomena. As a case study, we analyse the dynamic chemical reaction of the transformation of HCN to HNC isomer. In our visual-auditory approach, we are employing both models in the analysis process keeping in mind the dynamic nature of the phenomena. We use the volume rendering techniques that highlight changes in both scalar fields for visual analysis of the quantum chemistry model. To implement our approach, we firstly perform the conversion of initial voxel data to SDF representation.

Signed distance transform within constructive modelling

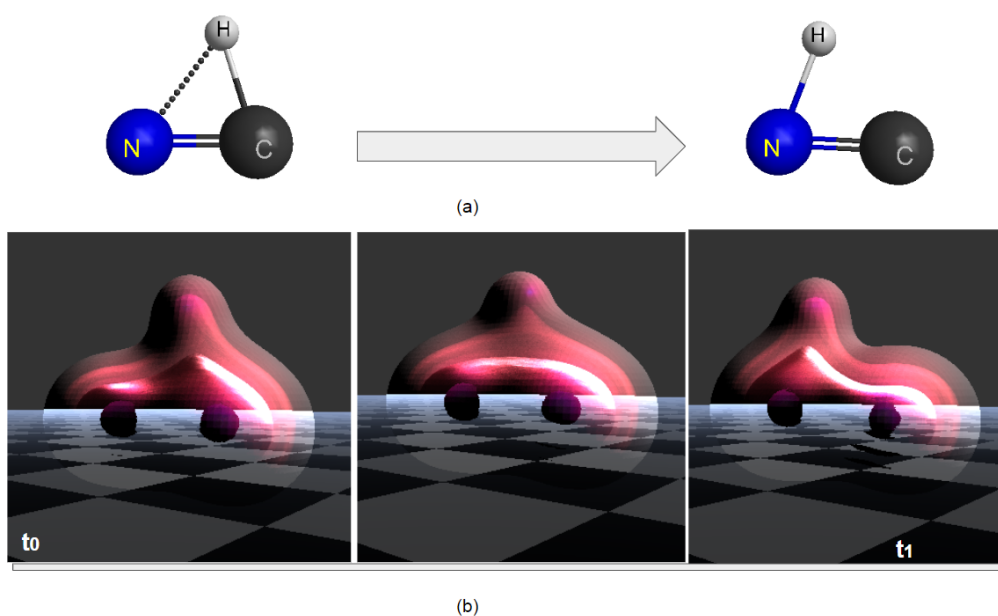


Figure 6.6: Selected frames of dynamic Volume Rendering of the chemical transformation from HCN to the HNC isomer. Ball-and-Stick model (a) and quantum chemistry model (b)

The conversion between different representations can be done by using state-of-the-art techniques, which are very often supported on the graphics hardware. The modern GPU supports a direct interpolation from SDF to voxel representation and back by storing the data in texture memory and employing hardware-accelerated trilinear or cubic interpolation. In our work we (Malikova et al. 2020) we use a signed distance transform for conversion from

voxel representation to SDF for rendering small multi-scale molecular structure (see Fig. 6.6).

The conventional type of micro level representation for molecular structures is a set of two or one scalar field obtained as a result of quantum simulation or experimentally (see discussion on problem in section 6.1). The scalar fields are stored in general case as voxel representation and have conventional interpretations as representation of molecular interaction boundary and internal property. We convert the voxel representation to SDF for initial and final molecular structure configuration and constructively model the dynamic changes of geometry for molecular structure for quantum chemistry representation (see Fig.6.6).

Multidimensional TF

The case study of quantum chemistry representation demonstrates the simultaneously analysis of the distribution of several properties within the volume structure. The molecular phenomena is represented with two scalar fields those are Electron density and Electrostatic potential. The main target of the optical model is to allow the user getting insight into the molecular phenomena through colour and opacity. To address the problem, we propose a custom distance-based TF. This TF takes advantage of both distance properties of SDF representation of Electron density field (for this task we use signed distance transform) and Electrostatic Potential Field. We consider Blinn-Phong model as base and deploy the specular and diffuse shading to provide highlights of both scalar fields and especially closer to the "atom" regions.

As described in Levoy (1988), a numerical optical model for colour at i -th voxel $C_i = C(x_i)$ for a parallel light source is:

$$C_i = c_p \cdot k_a + \frac{c_p}{k_1 + k_2 \cdot d(x_i)} \cdot [k_d(N(\vec{x}_i) \cdot \vec{L}) + k_s(N(\vec{x}_i) \cdot \vec{H})^n] \quad (6.1)$$

where $N(\vec{x}_i)$ is a surface normal at voxel x_i location, \vec{L} is a normalised vector in the direction of the light source, \vec{H} is a normalised vector in the direction of maximum highlight; c_p is a component of colour parallel to the light source; k_1, k_2 are constants used in a linear approximation of the depth-queuing; $d(x_i)$ is perpendicular distance from the picture plane to the voxel location x_i .

The ambient, diffuse, specular coefficients k_a, k_d, k_s are vary at different parts of the volume and are controlled by the SDF value of the Electron Density Field in order to highlight how colour is distributed on selected isosurfaces. We multiply the opacity value of the TF by the coefficient controlling the isosurface highlight o_h : $o_h = o_0^{\frac{d(x_i)}{d_{max}}} \cdot |\frac{d(x_i)}{d_{max}} \cdot \pi \cdot f|$, where f is a number of isosurfaces; d_{max} is a maximum value of the distance field; o_0 is a basic coefficient

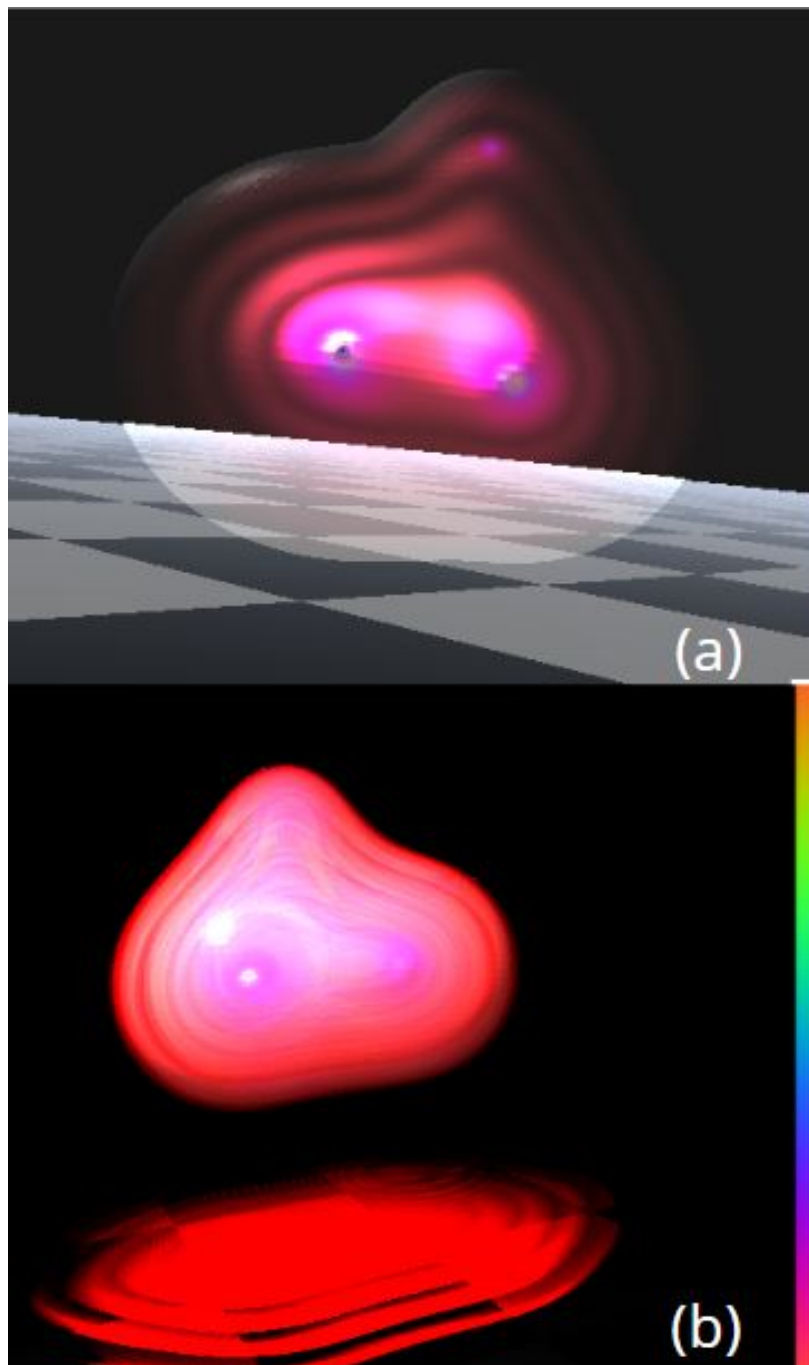


Figure 6.7: Volume Rendering of the HCN molecule. Rendering with introduced TF and the following optical models: a) without scattering; b) with basic single scattering.

that is the maximum o_h value can take. If o_h is greater than a certain threshold value we apply surface shading with k_s and k_d values equal to o_h .

The results of volume rendering for emission-absorption and single scattering optical models is presented in Fig. 6.7. In this case we have used SDF as well as acceleration techniques for computation of the optical model.

Visual-auditory analysis of dynamic multi-scale phenomena and interactive exploration

The ray-casting based visual-auditory pipeline allows designing in a unified way and combines various modalities. For example, we can simultaneously deploy both user interactive geometry modelling and dynamic rendering, or visual-auditory rendering in a unified way. The dynamic structure or results or user interaction are updated automatically within a rendering loop as a result of ray-casting (for details see implementation of different modes in `Renderer` class in section 5.4).

In this example, we perform simultaneous visual and auditory analysis of dynamic molecular phenomena. We consider the plucked string model for auditory measurements of dynamic changes of NC bond length through changes in sound property "pitch" (see details on auditory model deployed for measurement of molecular phenomena properties in section 4.6.2). We also deploy constructive modelling for hand-based interaction with the leap-motion device. See details on construction tree structure in section 4.6.1. The user's hand fingertips those positions obtained with leap motion automatically update the representation of "hand geometry" in a scene. The geometry representation in constructive trees is updated in real-time as a result of ray-casting based user interaction and volume rendering.

6.2 Microstructures in digital fabrication

The modelling of microstructures for digital fabrication is a rapidly developing area of shape modelling which deals with representations of the volume objects with their internal spatial variations of single or multiple materials. Rapid progress in digital fabrication boosts the need in methods which allow representing multi-material volume objects efficiently. On the other hand, the development in some areas of additive manufacturing, such as bio-printing, requires increased complexity and precision of the volume models. Modelling and analysis of volume microstructures require significant computational resources. Moreover, the tools for heterogeneous volume modelling are very often limited by the lack of methods for real-time visualisation of the multi-material objects. The parametric or mesh-based models conventionally used in the computer-aided design are not ideal for complex topological structures (Feng et al. 2018). Moreover, the digital fabrication area does not allow neglecting the volume

nature of the phenomena, the assumption that often simplifies the visualisation of large-scale structures via deploying of surface rendering techniques. From the visualisation point of view, the deployment of accelerated volume ray-casting of heterogeneous structures can be not the straightforward process as the material distribution is modelled on complex geometry domain. The visualisation of such microstructures is challenging as demands volume ray-casting of material distribution of complex "sparse" geometry subdivision. Moreover, similarly to the case of dynamic modelling and rendering of molecular structures the consideration of dynamic changes in microstructures geometry requires control over topology and shape. Inspired by natural phenomena, the microstructures are often modelled on a base of scientific data. The heterogeneous objects represented by this data are described by the results of FEM simulations or by crystal / molecular structure. We believe the accelerated rendering techniques for such data can be successfully applied for microstructures real-time modelling and visualisation and overview the core features of these techniques (sections 6.2.1.1 and 6.2.1.2).

Our approach of accelerated visualisation of heterogeneous structures can be deployed for modelling and rendering of microstructures. The microstructures impose a challenge of interactive modelling of large-scale and complex volume objects. The case of microstructures is an area of interest in this research because we consider digital fabrication as one of the output modalities. Moreover, we consider the interactive modelling of microstructures as an area that can benefit from the proposed in this work approach to GPU accelerated interactive geometry and material modelling on heterogeneous objects. The core of the technique is the evaluation of relationships between two IC structures that is followed by constructive modelling on selected subcomplex (see section 4.6.3). As we have discussed in section 6.2.3.3 procedure can benefit from GPU implementation. Here we consider the aspects and challenges of modelling and visualisation of the injection of a semi-transparent material into the microstructure geometry (see section 6.2.2).

6.2.1 Problem overview

6.2.1.1 Modelling of multimaterial microstructures

Recent attention to modelling and interactive visualisation of multimaterial microstructures is demanded by the digital fabrication area (Schaedler & Carter 2016). Designers and users need to get the accurate image of how the 3D printed objects will look like (Luongo et al. 2020) and what properties they will have (Pham et al. 2019). In this work, we will concentrate on aspects of multimaterial microstructures modelling and the closely related area of molecular structures modelling based on mainly lattice-based structures. To provide

a lightweight property and optimise 3D printing material consuming the uniform procedural generation of microstructure geometry and material for filling the object shape is an effective solution to address modern challenges (Lin Lu 2014),(Pasko et al. 2011*a*),(Wang et al. 2013). However, the recent research that addresses the problem of new material design and takes advantage of natural objects topological structure (Feng et al. 2018).

The lattice-based microstructure is modelled through common for crystal structures notion of the unit cell with certain topology Deshpande et al. (2001) to design materials with certain properties, such as acoustic (Syam et al. 2018) or mechanical (Pham et al. 2019). Often the microstructure modelling demands the control over shape and topology within the subdivision is required as a part of user interactive modelling (Schaedler & Carter 2016).

The real-time modelling of the microstructure is generally computationally expensive due to its possible large scale. However, similarly to molecular structures, it can highly benefit from the use of modern GPU architecture and advanced ray-casting algorithms for both modelling and rendering. Also, considering the areas where these data types are used (Grottel et al. 2015), (Muzic et al. 2015), the modelling of microstructures can highly benefit of lightweight representations for real-time GPU modelling. Similarly to molecular structures, the research in an area mostly constrained to basic geometric primitives such as spheres and cylinders to model the lattice (Kurzeja & Rossignac 2019) and can potentially benefit from similar GPU techniques and the geometry restriction.

6.2.1.2 Rendering multimaterial volume objects

The volume rendering technique is required to pre-visualise the appearance of a digitally fabricated object with semitransparent material distribution. If we want to achieve visualisation with interactive or real-time speed, the accelerated volume ray-casting of the large heterogeneous structure should be used. The volume ray-casting procedure is an area of additional active research in terms of both quality and minimisation of the computation cost. The problem is addressed with space skipping technique, early ray termination and optimisation of volume sampling and active deployment of acceleration structures.

In digital fabrication, the complex material distribution is often modelled by using spatial partitioning, where each region has a constant material assigned with smooth material transitions between regions. That allows application of techniques such as bricks (Ruijters & Vilanova 2006),(Beyer et al. 2015) or ray-segmentsMax & Chen (2010) of volume integration. Moreover, the works demonstrate the accelerated volume ray-casting of a constant material distribution defined within a set of simple, convex geometric domains (Knoll et al. 2014),(Weiler et al. 2003) that is a case of a rendering of molecular point-based data. The

ray-object intersection is conventionally accelerated by using GPU acceleration structures (Beyer et al. 2015).

However, as we have discussed in section 5.2.1 the volume ray-casting of dynamic multimaterial objects on arbitrary geometry domain is a more complex problem. Accelerated volume ray-tracing of multimaterial concave shapes, for example, is not straightforward Meibner et al. (2000), (Silva et al. 2005). Certain difficulties also arise after rendering of multiple volumes Kainz et al. (2009), Brecheisen et al. (2008) that can appear during the process of interactive modelling of multimaterial microstructures. Overlapped volumes create ambiguities in a volume ray-casting procedure (Schmidt & Budge 2002) that should be addressed in real-time.

6.2.2 Case study overview

Our approach is based on GPU implicit modelling within spatial subdivisions and accelerated volume ray-casting techniques. As we have discussed above those techniques have proved to be efficient in relevant to problem areas of GPU-accelerated modelling and visualisation of the geometry of the molecular structures and volume rendering of tetrahedral meshes.

However, comparing with basic cases of molecular data, the microstructure data poses extra requirements such as arbitrary geometry and material modelling within individual unit cell Schaedler & Carter (2016). Moreover, these two requirements are considered in the context of the analysis and interactive modelling of large scale microstructures. The problem of modelling and visualisation of semitransparent multimaterial microstructures requires the efficient way to represent and render the "sparse" dynamic geometry with its material properties within a spatial subdivision. Combined with accelerated volume ray-casting, the hybrid constructive modelling of geometry and material within heterogeneous microstructure can address these challenges.

6.2.2.1 GPU modelling geometry and material

Let us consider a basic case of lattice-based microstructure modelling. The initial inspiration is crystal lattice data that is a cellular subdivision $(G, Ao) = \bigcup_{i=1}^N (G_i, Ao_i)$, where each cell includes Si and O atoms and bond connecting them (we have considered the example of a lattice structure in Fig. 4.19). Both geometry G_i and material Ao_i within a cell G_i, Ao_i are modelled with constructive trees. The constructive tree defining G_i returns the value of the signed distance function which is used for sphere tracing algorithm.

We use the hybrid constructive modelling of arbitrary material distribution that we have discussed in section 4.4. However, unlike the molecular structures, the geometric regions of homogeneous and blended material for microstructures may be different from those that

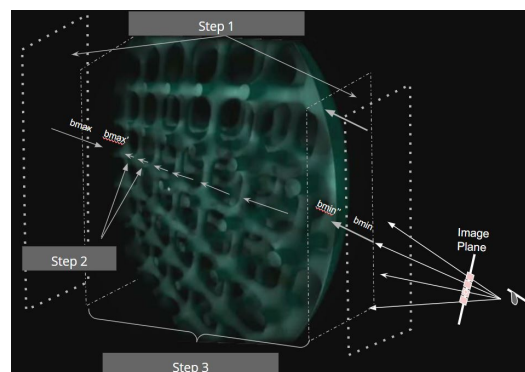


Figure 6.8: Sphere-tracing of cell with sparse geometry within lattice microstructure. The shape is a part of representation of dynamic cell within microstructure presented in Fig. 6.11

are used in G_i constructive tree, see discussion in section 4.4 and Fig. 4.20 for examples of arbitrary material modelling within microstructures modelled on a base of initial Si-O lattice that does not depend on cell geometry G_i constructive tree.

6.2.2.2 Accelerated volume ray-casting of semitransparent multimaterial microstructures

A general scheme for volume ray-casting shown in section 5.2.1 and its application for microstructures case are very similar to the case of molecular structures visualisation. However, compared to molecular structures, the microstructures modelling often deals with more complex geometries, there might be a lot of "empty" space to skip directly within cell G_i . These space "inside" complex geometries not always can be handled with a complex hierarchy of bounding volumes that we have discussed in sections 5.3.1. In the case of microstructures, geometry within the subdivision is often modelled with primitives and operations that are fast for evaluation (Fryazinov et al. 2013). Thus compared to the case of molecular structures, there is no need to model cells within microstructure lattice as composite ones or the process can be not straightforward.

In this case, the entire cell volume structure with empty spaces inside is processed on the stage of optical properties integration. In this case, we represent each primitive G_j by a signed distance field (SDF) and constructive material A_{O_j} modelling as regions of constant and distance-dependent blended material. Thus, the accelerated volume ray-casting of semitransparent multimaterial within a cell is facilitated with a sphere-tracing technique (Hart 1996) that is applied at various stages of accelerated volume ray-casting, such as additional space skipping and constructively modelled optical properties integration (section 4.4).

In Fig. 6.8 we show the scheme of space skipping within primitive G_J with "sparse" geometry, like in Fig. 4.20.

In cases of complex geometry, all the ray-structure intersection points in $G_i(t)$ are found with sphere tracing in the positive direction, given an offset from the found roots, which allows to "skip space" within the complex shape of microstructure and to compute areas of further ray-segment volume integration scheme within volume ray-casting (see Fig. 6.8, step 2). The volume integral is evaluated only for precomputed semitransparent regions (see Fig. 6.8, step 3). The optical model introduced in section 4.4 and its sphere-tracing based integration scheme (see section 5.2.4 allows combining additional space skipping (step 2) and optical properties integration (step 3). For the case of microstructures, this approach can be applied due to the core assumption in digital fabrication that materials are modelled with regions of constant material and "blended" material. We specify those regions and model the entire structure with a constructive tree that we actively use during sphere-tracing. The technique provides a better rendering quality (see Fig 6.9) compared to regular volume sampling. That is due to core optical model integration principles highlighted in (Max & Chen 2010) that we have considered in the design of optical and auditory models in section 4.4.

6.2.3 Examples

6.2.3.1 Multimaterial lattice-type microstructures

Consider the lattice-based microstructure inspired by crystal lattices and tetrahedral meshes. The core principles of modelling such microstructures were described in 4.3.4 and 4.3.

Fig. 6.10 and Fig. 6.11 show the frames of dynamic microstructures modelling, as a transition from one geometry representation within the cell to the other occur. The dynamic control over topology and shape within the cellular subdivision is possible due to hybrid constructive modelling within the cellular subdivision.

The core idea of crystal lattice construction for molecular objects is based on the notion of a crystal unit cell. The lattice-based microstructures consider an arbitrary material and geometry modelling within such cellular subdivision. Within each cell $\{G_i, A_{oi}\}$ the geometry G_i and optical material A_{oi} are modelled with dynamic constructive trees. The heterogeneous structure deployed as inspiration, can be tetrahedra (see Fig. 6.10) or crystal unit cell (see Fig. 6.11). The arbitrary structures are modelled within this subdivision (0D, 1D, 3D) with dynamic changes in the topology of not only unit cells, but the entire structure.

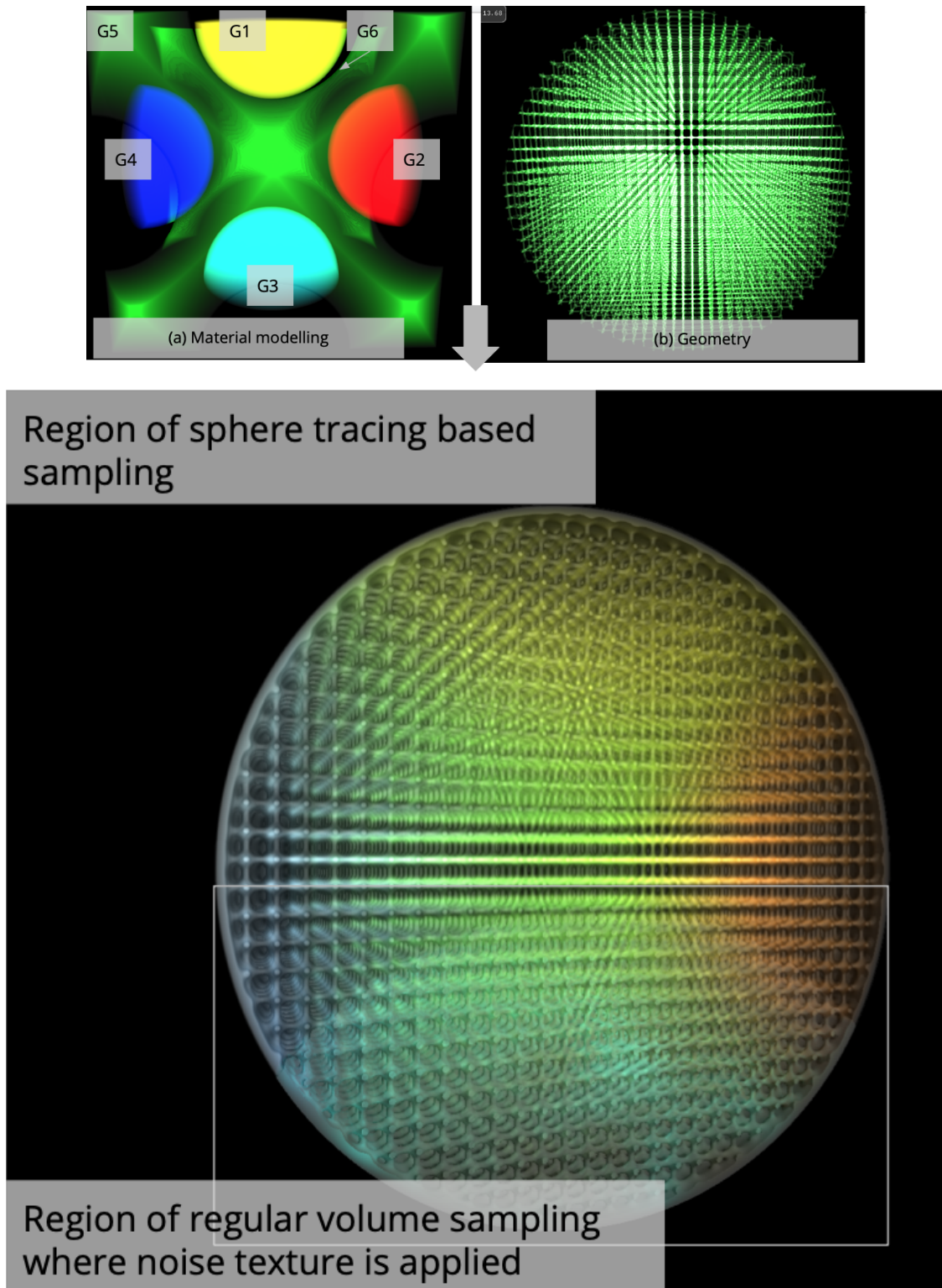


Figure 6.9: Comparison of regular volume sampling and ray-segment integration (Max & Chen 2010) where ray-segments are computed with sphere-tracing for constant and blended material regions

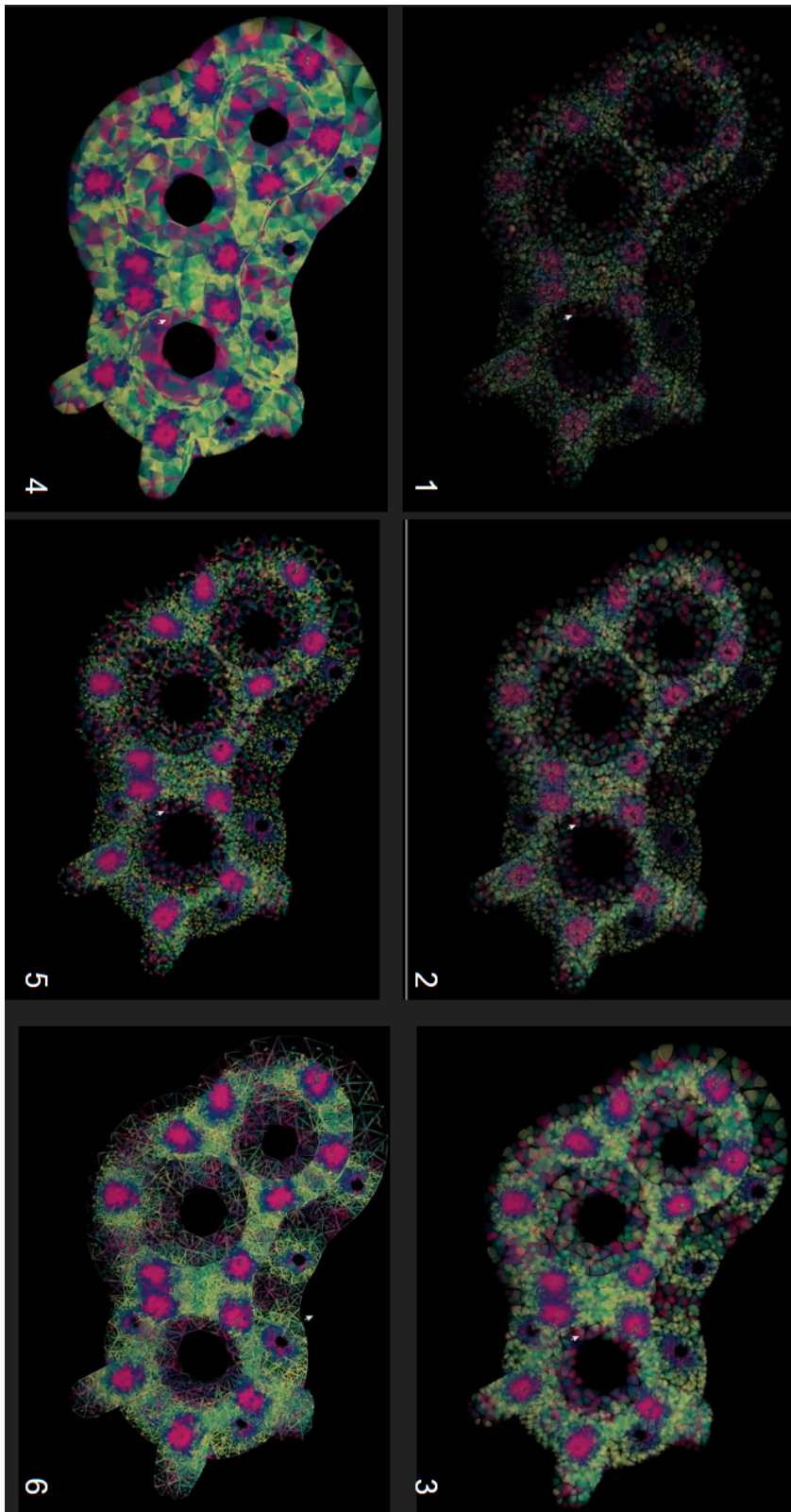


Figure 6.10: The frames from the animation that demonstrates the dynamic changes of shape and topology within subdivision defined by tetrahedral mesh

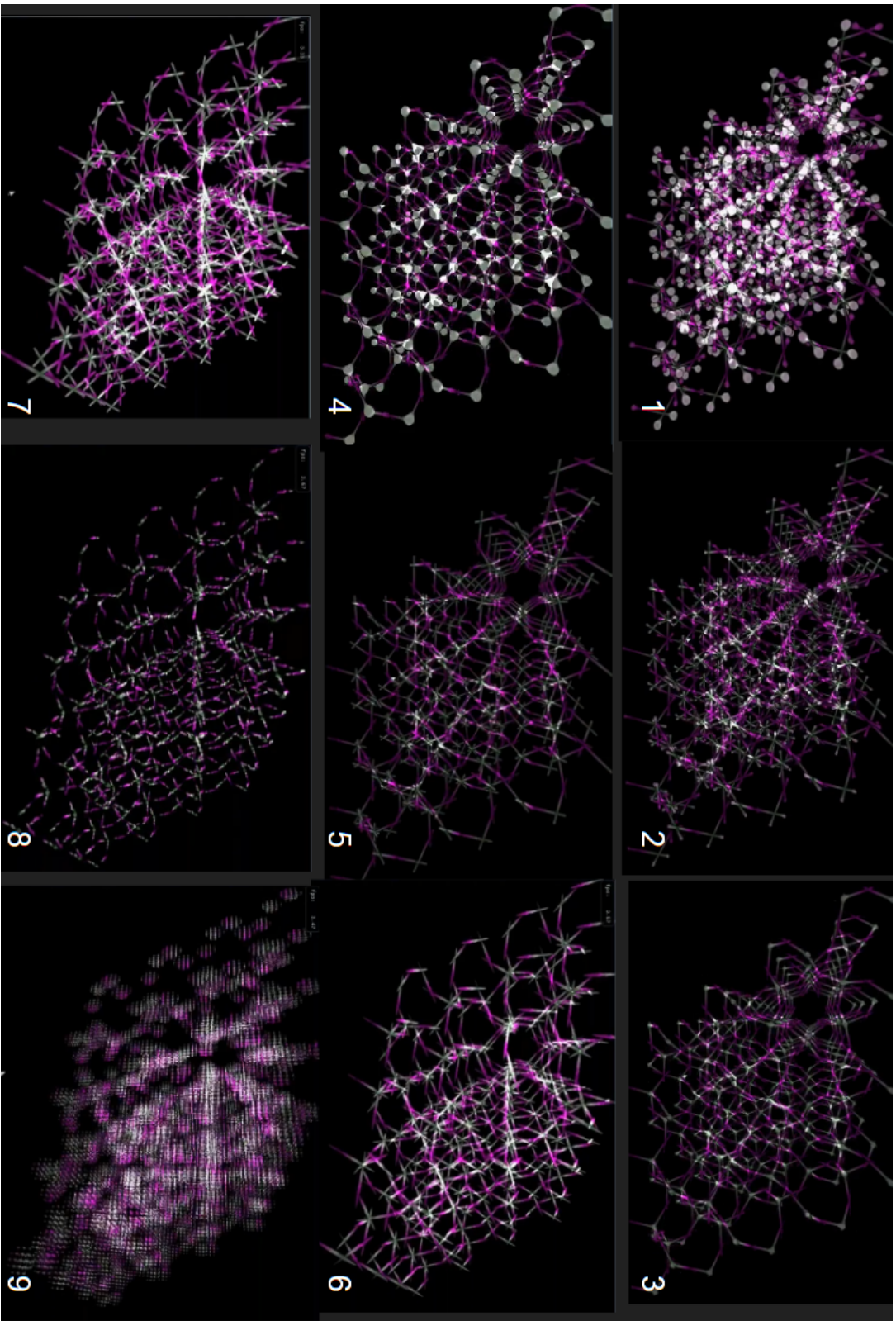


Figure 6.11: The frames from the animation that demonstrates the dynamic changes of shape and topology within subdivision defined by crystal lattice

6.2.3.2 Modelling on the sets of cells within lattice microstructures

The crystal structures demonstrate the lattice of regular nature. However, the modelling of microstructures assumes modelling of irregular structures on such subdivision as well. As we have discussed in section 4.3.4 such cases may demand an interactive definition of subregions within the lattice, that is composed of several unit cells and may have custom geometry and material representation much different from entire lattice structure.

Inspired by the architectural design of the materials (Pham et al. 2019) where the architected material is constructed through cellular domains that are filled with atomic crystal lattices of different types, we apply such techniques of GPU accelerated modelling on irregular structures on crystal cell. We take ice crystal lattice as a reference (see Fig. 6.12) for modelling of irregular structure. Fig. 6.13 shows the frames from the video that is a dynamic rendering of the results of modelling of such microstructures. The positions and size of regions of irregular structure definition change in time.

6.2.3.3 Composite material modelling on microstructures

Let us consider another class of a modelling performed on dynamic microstructures that can be obtained after user interaction.

Compared to the accelerated ray-casting of a single heterogeneous volume, the ray-casting of multiple heterogeneous volumes in a scene, especially when they overlap as a result of user interaction, is a more complex problem (Fong et al. 2017). The problem of ray-casting of overlapping or "nested" volumes impose certain challenges (Wächter & Raab 2019). The problem can be addressed with additional geometric modelling over the scene to optimise it for ray-casting procedure (Schmidt & Budge 2002) or decomposition to convex regions. Other solutions demand consideration of in general case complex ray traversal procedure that is combined with geometric modelling techniques. Overlapping volumes create many short integration intervals as volume boundaries are tracked explicitly. The ray-tracing procedure stores a list of intersections that allow identifying the object that ray is travelling through with additional information on intersections type (Schmidt & Budge 2002). As we have discussed in sections 5.2.1, 5.3.1 such techniques highly rely on post-processing stage that evaluates the relationships between cells on IC structure and use geometry or material modelling based on results of the evaluation of this relationship.

In this work we let us consider the problem of material modelling on microstructures as a result of two overlapping heterogeneous volumes. We have the initial microstructure with a material distribution that is a heterogeneous object h_{sc} . The new material that is to be injected into some part of this microstructures is modelled on complex geometry domain and the entire

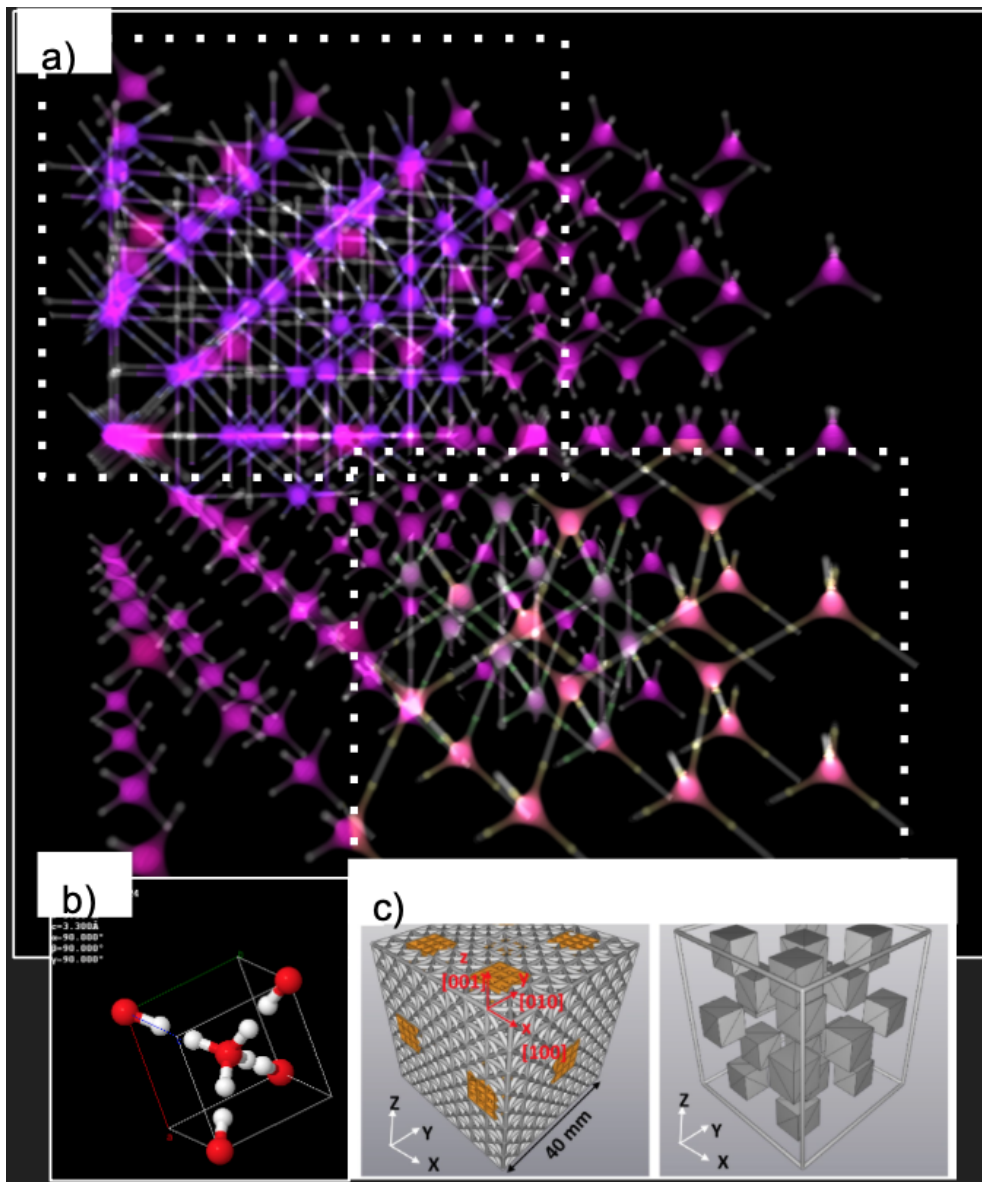


Figure 6.12: (a) irregular lattice structure modelling scheme (b) initial ice cell (c) The scheme of "meta" regions modelling on crystal lattices from paper (Pham et al. 2019)

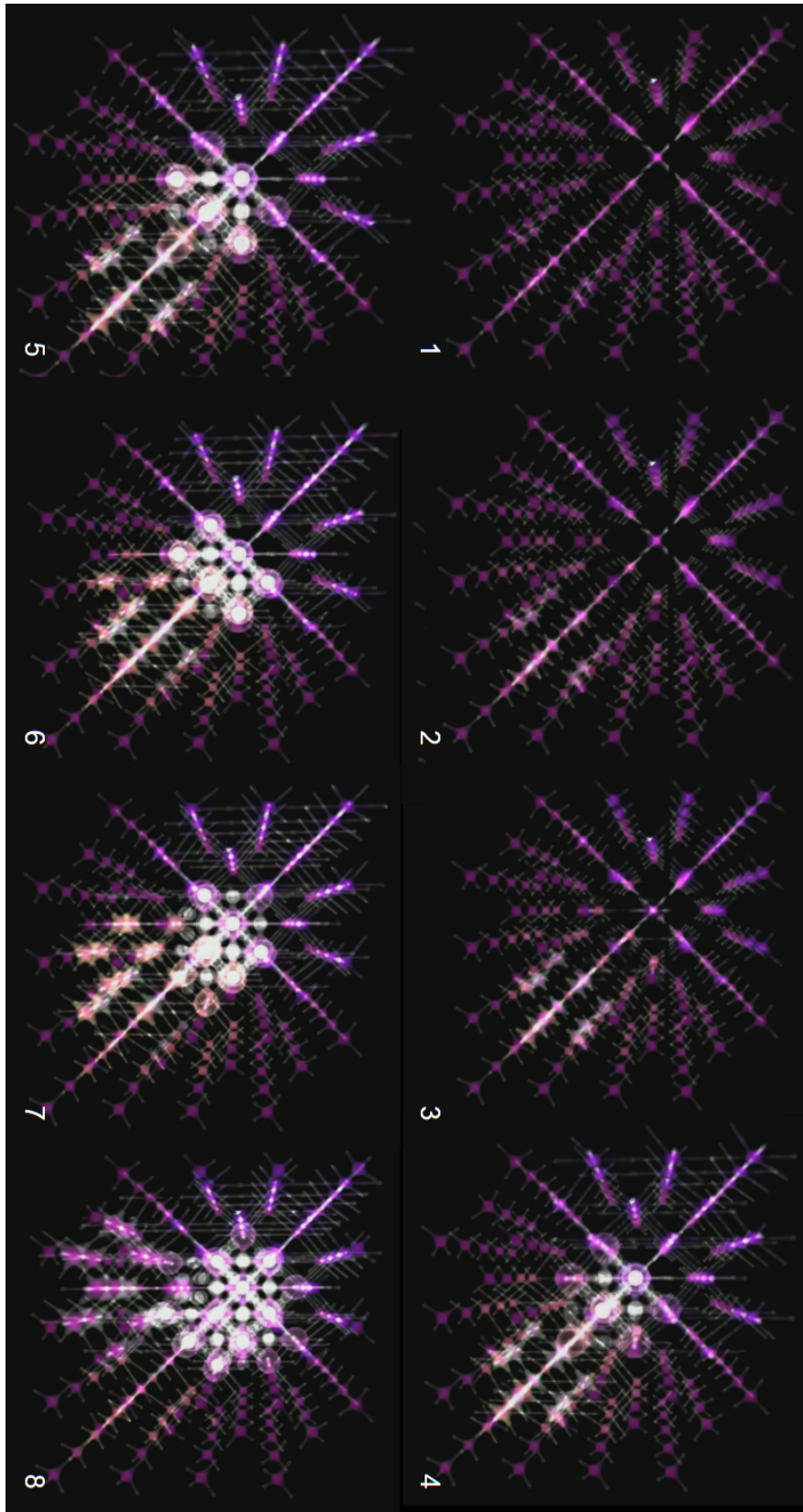


Figure 6.13: Frames of dynamic modelling within the selection of unit cells. The lattice structure within each region is highlighted with different colour (green, pink, violet, yellow)

structure also is a heterogeneous object h_{sc} . The region of material injection is computed with the intersection of geometries of complexes G_{sc} and G_{av} that can be obtained as a result of user interaction. See Fig. 6.15 (a,b). We model a new composite material distributed on initial microstructure domain in a form of some "injections" of Ao_{av} made to the main material Ao_{sc} . Ao_{av} is defined on heterogeneous subdomain G_{av} that is interacting with initial microstructure geometry domain G_{sc} and the result of this interaction is modelled as a subdomain domain $G_{o2} = G_{sc} \cap G_{av}$. The visualisation process has to simultaneously operate two geometry domains G_{sc} and G_{av} with two materials, detect the regions of composite material modelling and perform the volume integration for those regions.

To model and render the distribution of new composite material, we evaluate the relationships of cells within the subdivision of geometries G_{sc} and G_{av} and constructively model material on an obtained geometry domain as a result of user interaction directly during the ray-casting procedure.

In section 4.6.3 we discussed the main scheme of GPU accelerated evaluation of cells relationships. To summarise the situation for material modelling from a rendering point of view, as a result of a combination of constructive modelling and ray-casting procedures deployed on the post-processing stage. Depending on the cell distribution and the shapes, we can distinguish different cases of ray-cell intersection (see Fig. 6.14). In case two cells are either non-adjacent or adjacent, we can deal only with ray-cells intersection (see b,c in Fig. 6.14).

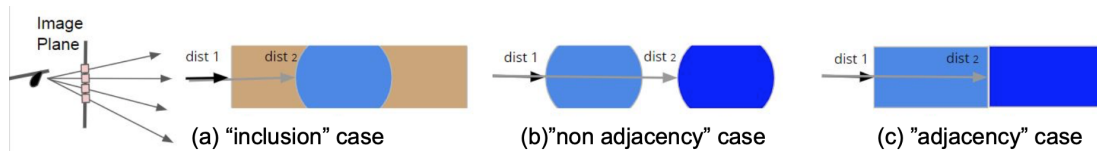


Figure 6.14: Various cases of cells ray-casting

In this particular case, we detect the inclusion of cells, meaning that some cells can be of a concave shape and can be "inside" each other (see Fig. 6.14(a)) that in terms of modelling means that intersection of cells of G_{sc} and G_{av} is not empty.

In this work, the material modelling on overlapped regions will include the following procedures. Firstly, much similar to other ray-tracing pipeline (see section 5.3.3, we select a bounding volume composed of cells of $\langle I_{sc}, BV_{sc}^{l2} \rangle$ and $\langle I_{av}, BV_{av}^{l2} \rangle$ that intersect with the current ray. Then, we go to a post-processing stage where in terms of ray-tracing we are searching for "inclusion" cellular regions (see Fig. 6.14). As a part of post-processing we apply depth sorting, evaluate the relationships between cells $\langle I_{sc}, BV_{sc}^{l2} \rangle$ and $\langle I_{av}, BV_{av}^{l2} \rangle$ and perform material modelling of selected subset of cell.

Thus constructive modelling is performed on a post-processing stage and followed by a sphere-tracing for a new material evaluation. We refine the intersection distance values with each cell with sphere-tracing for performing depth sorting and also deploy it as a part of cell relationships evaluation procedure. We detect types of cell relationships from the ray-tracing point of view as it was classified in Fig. 6.14. Finally, we perform ray-segment volume integration with computing the material based on relationships between cells evaluated. In Fig. 6.15 we provide the frames from the animation of the result of material injection as both objects h_{sc} and h_{av} are dynamic.

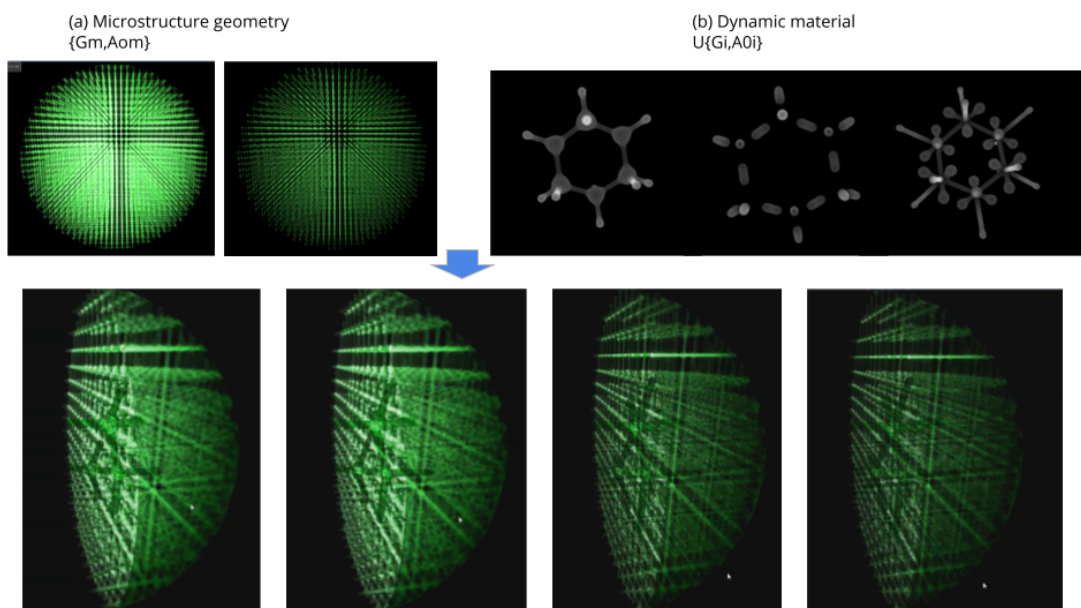


Figure 6.15: The frames of volume rendering of the multimaterial microstructure

Chapter 7

Preliminary evaluation

The conventional volume visualisation enhances quality of the heterogeneous structures analysis by choosing more precise light/volume object interaction models or by refining those interactions on the level of individual components within a spatial subdivision. We extend the technique to visual-auditory case by taking advantage of well established in various areas similarities in light and sound propagation modelling (section 3.5.4) to propose a unified framework for visual-auditory analysis of heterogeneous objects. Moreover, the human auditory system directly imposes the perception of spatial sound properties that are a result of auditory propagation that allows us to assume that the proposed approach is not only efficient and unifies the analysis procedure, but can facilitate the cross-interpretation of visual and auditory cues for analysis of various aspects of complex heterogeneous phenomena. Our main assumptions in the simultaneous deployment of a combination of both visual and auditory interpretations:

1. Similarities in light and sound propagation. We assume that the analysis of heterogeneous phenomena with visual and auditory stimuli generated through the concept of light and sound propagation lead to the simultaneous perceptions and interpretation of visual-auditory stimuli (see discussion in section 3.5.4)
2. Well-proven efficiency of the application of musical systems mappings in combination with visual stimuli. The previous research in the area (see details in section 3.5.4) highlights the aspects of successful application of cross interpretations of visual-auditory stimuli through colour and pitch mappings. We consider this as a basis in the design of auditory TF (see section 4.2.3, 4.4) and its use with optical TF.

The presented approach implies the user is a main part of the interaction. To strengthen the value of this research as well as to evaluate the vision of the application of the techniques described above, we carry out a preliminary user study that aims to define the full user study

when it will be possible. The presented in section 6.1.1 case studies, become a basis for this user study that aims to compare our expectations on the visual-auditory approach with the views of the potential users of this system if it is implemented as a software product beyond this research and identify the key factors for further enhancement, the possible future directions of approach enhancement and development.

The preliminary evaluation targets providing the insight into the following main questions about the proposed visual-auditory approach :

1. How well the proposed methods and techniques correlate with the needs of target users of the specified two groups of potential users.
2. How robust the proposed techniques are?
3. What are the core factors that affect the usability/user vision of application of the visual-auditory techniques.

7.1 Design

7.1.1 Introduction

Evaluation of both scientific visualisation (Seyb et al. 2019b) ,(Plaisant 2004) and sonification techniques (Bonebright & Flowers 2011) is not straightforward. The results highly depend on visual and auditory stimuli perceptual aspects, user ability to judge about properties of physical phenomena and how complex the data that it describes (North 2006).

The design of relevant quantitative metrics is difficult (Tory & Moller 2005) due to the differences among participants in understanding visual (Heer & Bostock 2010) and auditory (Bonebright & Flowers 2011) representations and background knowledge in area (Ziemkiewicz et al. 2012),(Peck et al. 2012). The latter is particularly challenging when it comes to the perception of 3D spatial scenes and user interaction within such scenes (Ziemkiewicz et al. 2012),(Peck et al. 2012).

To facilitate the task and reduce the potential bias the conventional evaluation of visualisation often considers the aspects of graphical perception (Heer & Bostock 2010), or takes advantage of comparison-based techniques for the low-biased control of the effectiveness measurement (Huang et al. 2009). In this work, we compare results of visual and visual-auditory analysis to facilitate and reduce the potential bias in the evaluation results measurement (Huang et al. 2009). We use the controlled experiment for easier and more convenient evaluation in a relatively new area of visual-auditory analysis(North 2006). Also, to address the bias in results, we design a questionnaire (see section 7.1.5) with consideration of a problem

of potentially long training and trial times depending on data and knowledge of users in specified domain. We discuss our evaluation sample (see section 7.1.2) and specify our set of dependent and independent variables (see details in section 7.1.3) with consideration of such significant usability aspects of visualisation techniques as the user experience in multi-sensory analysis and analysis of complex physical phenomena.

7.1.2 Sample population description

This research considers a niche area, where the potential users are aware of heterogeneous phenomena related problems. The conventional visual analysis of heterogeneous objects is an area of interest for specialists in physics, chemistry, digital fabrication who work with heterogeneous objects as a part of their engineering and research practices. Also, the VR and multi-sensory analysis specialists deal with the design of GUI and interactive techniques or use heterogeneous objects as a part of VR simulation tasks.

Thus, our preliminary evaluation targets the specialists of the above two groups that deal with heterogeneous phenomena as a part of their research or aware of the analysis techniques used for this task. In total, we have a sample of 13 people with 6 people from the first group and 7 people from the second group. The age and gender distribution vary in two groups. There are mostly representatives of the elder generation and only one female in the first group and younger generation with equal gender diversity in the second group.

We expect the independent variables for the user estimated usability of visual-auditory heterogeneous phenomena analysis, will correlate with the description of the sample population. The latter characterise users' experience in the area of visualisation of complex physical phenomena and experience in multi-sensory feedback. Let us consider the details below.

7.1.3 Independent and dependent variables

Quantitative experiments as controlled experiments often involve comparisons of performance or estimated usability of different techniques/tasks between different participants. Experimental conditions for each visualisation technique include a complete set of values for the factors or independent variables that are believed to affect performance or, in the case of this research, a technique usability estimation.

In this work, the dependent variables characterise the user expectations in the general areas of visual-auditory techniques application. Those are such problems as highlighting visual perception errors, an extension of spatial interactive exploration or introduction of non-conventional types of user interaction (see details in section 7.1.4). The dependent variables are defined by user experience/training. Similarly to related works in the evaluation of

conventional visual analysis of physical phenomena (North 2006), we consider that the heterogeneous objects analysis demand users to have specific knowledge and experience in the area, such as awareness of conventional principles of scientific data analysis, specific knowledge on physical phenomena that the heterogeneous structures represent, interactive and visualisation techniques. Also, the explored visual-auditory analysis efficiency and usability aspects can be influenced by the awareness or certain experience in multi-sensory analysis area that the users may have (Ziemkiewicz et al. 2012),(Peck et al. 2012).

The auditory techniques are designed bearing in mind the possible limitations of an auditory analysis Hermann et al. (2011) such as memory-related issues, the necessity of training for complex auditory mappings, overload with auditory information etc. We have tried to mitigate the problems of auditory analysis of heterogeneous phenomena and, in particular, ask users to compare two visual-auditory techniques that minimise either time or memory issues (see section 7.2.1). We introduce additional independent variables that affect the final decision on auditory approach application strategy, those are the user estimated aspects of visual-auditory techniques application and usability, such as the difficulty of the technique, how easy the technique was to understand and use.

7.1.4 Data analysis structure

We evaluate various aspects of approach application, such as basic cases of 3D volumes analysis, exploration of heterogeneous molecular structures, user interaction with auditory information to explore heterogeneous phenomena. Our preliminary evaluation targets understanding if depending on the user experience they believe that volume rendering should be extended with the proposed techniques for visual-auditory analysis as well as identifying the key factors of this vision. Thus, we have considered the following successful problem areas of auditory stimuli deployment Hermann et al. (2011) where we run the visual-auditory evaluation study to address those questions:

1. Ability to detect small changes. We consider the scalar fields that are results of physical simulation and have symmetrical features that reflect the nature of phenomena. The properties of such volume data structures are conventionally highlighted with optical TF. We use auditory feedback for tracking small changes in symmetrical properties of this fields with auditory TF (see section 7.2.1)
2. Data exploration of spatial distribution structures. The area exploits an auditory ability to encode and convey information about the entire data set or its aspects with soundscapes that provide an auditory image of complex spatial phenomena. We

consider a visual-auditory exploration of heterogeneous molecular structures that are results of molecular dynamics (see section 7.2.2).

3. Human perception and identification of auditory objects Hermann et al. (2011) that produce the sound. To facilitate the heterogeneous data exploration through both visual and auditory information, we consider a MIDI-based user interaction (see section 4.6.4) and get a preliminary opinion of users on this technique in section 7.2.3.

For analysis of the results of the user evaluation in the above areas, we carried linear regression, t-test and power analysis with Analysis ToolPack (Microsoft 2020) and G*Power (UCLA 2020) software.

To estimate what variables define the usability/performance/user vision of the visual-auditory technique of each group, we carried out a linear regression analysis with specified independent and dependent variables for each technique (see section 7.1.3). We also carried out the analysis to get a basic idea of how well the sample represents the considered population. The users of two groups have different experience that can affect their vision of auditory technique application and the vision of volume rendering extension with auditory stimuli (see section 7.1.3).

We use hypothesis testing (t-test) to make inference about the properties of our population of the above two groups. We will perform the analysis with a two-tailed estimation of a p-value. In case, when p-value more than the significance level, the difference between the estimated mean values for the two groups is statistically insignificant. However, there is a chance that there is still a difference between the two groups of users as we are dealing with II-type error when the test fails the rejection of null hypothesis due to false negatives. As we discuss in section 7.1.5 for such cases the correct estimation of sample size is important.

7.1.5 Questionnaire structure and limitations of the procedure

To answer the above questions, we have run an evaluation in a form of a semi-structural interview (questionnaire). For each visual-auditory analysis technique from the above three groups (see section 7.1.4), we ask the questions related to their performance, usability and further enhancement.

Because of the restrictions caused by the ongoing pandemic situation of 2020, we were not able to implement the evaluation set-up as it was planned from the start. We had to deal with a relatively small number of participants, could not implement the case of real-time user interaction or provide real-time guidance on how to perform procedures or user training. The entire online questionnaire was implemented as a Google Form that was available online to facilitate access. The users were asked to preview the online video materials of a recorded

screen of the visual-auditory feedback that occurs as a result of user interaction in each specific visualisation scenario (controlled experiment set up). Then, a set of questions on the demonstrated experimental set up is asked. The goals are to collect user feedback on technique in total, to understand what could lead users to such conclusion, to understand the limitations and possible direction of further enhancement. To unify the process, in most of the cases the users were asked a set of statements which they could rate as [fully agree, agree, neither agree nor disagree, disagree, fully disagree]. Such statements were further transformed into values of independent and dependent variables with values [2,1,0,-1,-2] accordingly (see section 7.1.3).

As it is discussed in section 7.1.1, in the case of visual-auditory analysis it can be particularly difficult for users to learn, adapt and deploy the auditory analysis tools that are an extension of visualisation techniques for complex partial phenomena analysis. Moreover, due to the online form of a questionnaire, we were limited in terms of conventional guidance and users training that usually is provided during non-conventional visualisation techniques evaluation. In this work, we address the problem with introducing our visual-auditory approach to users on the more simple 2D cases before asking them to perform visual-auditory analysis tasks of 3D spatial structures.

Our desired outcomes of t-test analysis is to get probability of type I error less than 5% and of type II error less than 20%. However, due to current limitations, we were able to obtain a relatively small sample size for analysis. As a result, there is a high risk of population misrepresentation that results in hypothesis test errors (t-test failure with type II error). To address the problem in necessary cases, we compute the effect size (for t-test it is 0.2 – small, 0.5-medium, 0.8 – large) and perform the power analysis to estimate the sample size that is sufficient to conclude that the studied effect exists in a population.

7.2 Analysis of the results

7.2.1 2D scanning for volume rendering to highlight visual perception issues in superconductor field

The first topic of the user study was the ability of auditory feedback to highlight small changes in symmetry feature of scalar fields.

This problem arises in various application domains (Sachin & Khairnar 2014, Santosh & Antani 2017, Liu 2009, Im et al. 2012), where small local changes in the field isosurfaces should be detected to highlight areas of potential physical properties change such as small

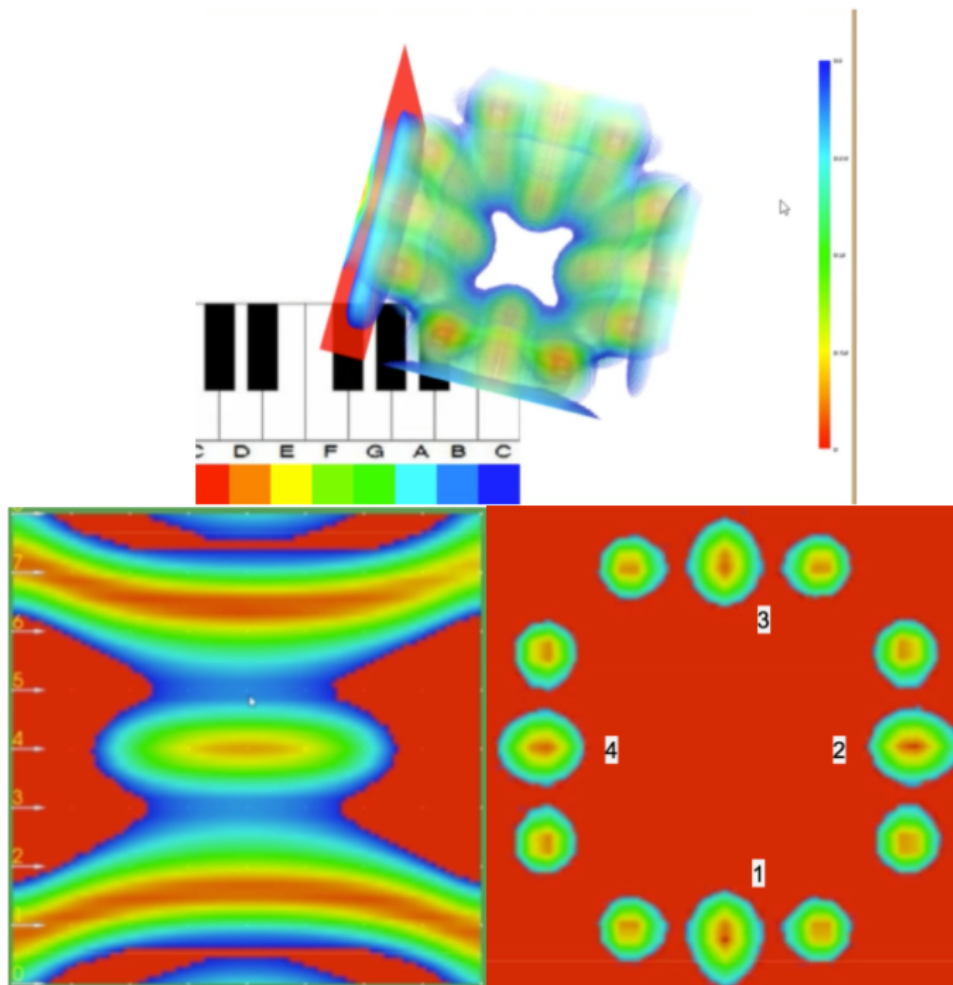


Figure 7.1: The screenshots of the results obtained with implemented visual-auditory techniques used for the analysis of superconductor field symmetry features

defects in crystal or vortex lattice. Tracking of the small changes in the dynamic scalar fields can be solved with additional numerical methods, which makes the whole process inefficient. For this user study we used a superconductor field analysis as a case study, in particular the analysis so-called Abrikosov vortex, which is one of the particular geometric features of the field (Suderow et al. 2014) (Fig. 7.1 a)). The structure represents isosurfaces of the circulating supercurrents. The analysis of the vortex arrangements is applied to carry out judgements on the material properties (Dachuan et al. 2017).

The area can be an application of our visual-auditory approach in the analysis of symmetry and geometrical changes/features detection. The dynamic changes can be observed and analysed visually with scanning microscopy or with computer simulations. In this case, we consider the similar optical and auditory models deployment with similar 1D TFs and deploy simultaneous visual-auditory rendering, where auditory TF is assumed to enhance visual one as it leverages conventional visual perception limitations. The evaluation should allow us to assess the advantages, limitations and possible adjustments to the technique.

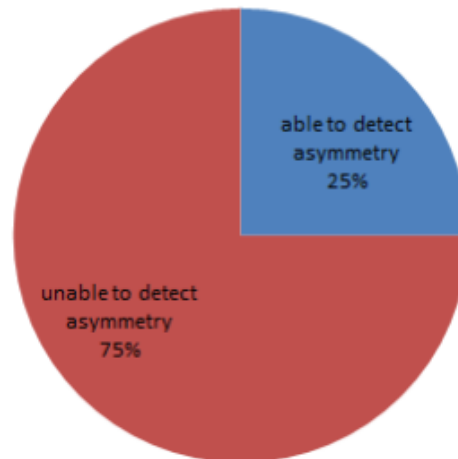
First, we asked the users to detect small changes in the scalar field that initially assumed to be symmetrical and without any distortion created as a result of external influence solely with conventional visual analysis. The users were struggling with both of the tasks (see Fig. 7.2). In the second case, as a result of image processing, the additional helping 2D hints were added to an image to localise and attract user attention to areas of potential problems. For most of the users, the introduction of such structures has facilitated the task. However, some users were still struggling.

Second, we asked the users to repeat the analysis with the deployment of both visual and auditory stimuli. We assume that auditory TF will be more sensitive to small changes in scalar field values compared to similar optical TF. Thus, both visual and auditory image will correlate if there are no visual perception issues or auditory stimuli will highlight the problem areas otherwise. As the same time, we had to minimise issues related to auditory stimuli overload and memory issues as several different sound waves should be memorised and compared by the user. We consider two slightly different techniques for two slightly different cases (see Fig. 7.1).

In the first case we concentrate on analysis of field symmetry. We simultaneously scan the field areas that are supposed to be equal. Thus, the small differences in the field symmetry will sound like a non-perfect unison musical interval that can be aurally distinguished by the untrained user (see Fig. 7.1 (a)).

The second case we track both symmetry and shape distortion of vortices in scalar field combines auditory feedback generation with image processing techniques. To reduce the number of sound waves generation and handle the overload with auditory information we

Visual detection of asymmetrical features in scalar field



Distortion in vortex shape and symmetry of the field

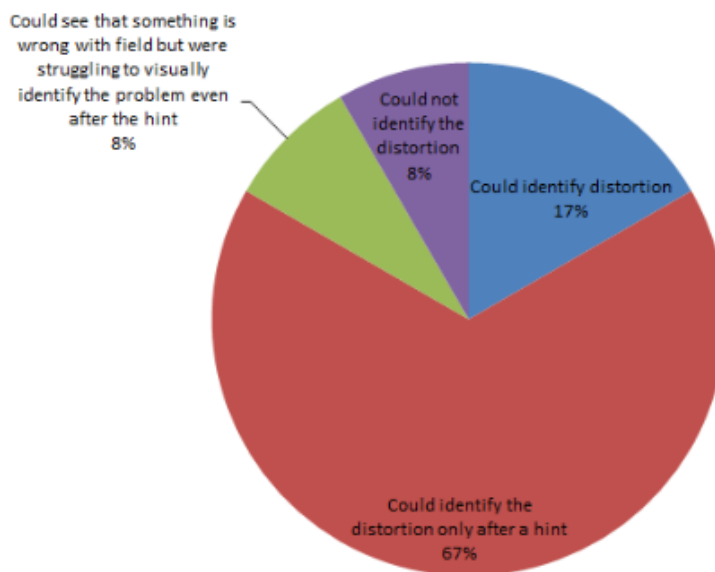


Figure 7.2: Visual detection of small geometric features (changes in symmetry and distortion) in a scalar field. (a) Simultaneous scan the field areas that are supposed to be equal due to symmetrical field properties, for example, lines $\langle 0, 8 \rangle, \langle 1, 7 \rangle \dots \langle 3, 5 \rangle$, in Fig. 7.1 a) (b) Tracking the possible vortex distortion due to external influence applied to a field that changes its symmetrical properties and shapes of vortices. The scanning vortices 1, 2, 3, 4 and) is a centre of symmetry in Fig. 7.1 b).

specify the potential region of interest (ROI) for auditory scanning (see Fig. 7.1 (b)). In this case of the superconductor analysis, we examine an area around a vortex. The technique highlights the possible distortions in the shapes of vortices and symmetry changes.

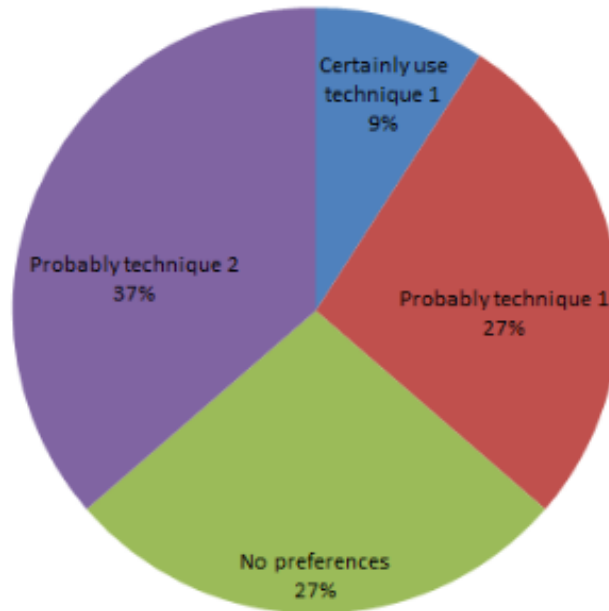
7.2.1.1 Comparison of two different visual-auditory techniques

Most of the users found both techniques easy to use and quickly understood the main idea of the application. The approach was mainly characterised by users as easy to understand and implement (see Fig.7.3 (b)), with a slight preference for first technique (see Fig.7.3 (a)).

The first type of auditory interface design uses an instant comparison of two soundtracks and reduces the necessity to memorise sounds. As a result, the technique demands more time for listening to audio tracks (less time-efficient). The second technique was introduced to address the main disadvantages of the first technique that are finite sampling resolution of rays casting and possible overload with auditory stimuli as a large number of auditory tracks may be generated and perceived. However, it may be more difficult for users with little experience in the area of multi-sensory analysis due to the necessity of memorising and comparing 4 different soundtracks (memory issues).

To estimate the variables that define the user preference of visual-auditory technique, we carried out a linear regression analysis. The results are presented in Fig. 7.4. The obtained linear model approximates quite well the experimental results (r square value of 0.87) with 4 significant coefficients values. As it can be seen, the user experience in volume rendering and experience of work with complex data much define the user's preferences (p -values of 0.04,0.05), including cases when no technique was chosen. The estimated user impression on the technique's difficulty and ability to correct the visual perception issues are also important parameters (p values 0.004, 0.06), as well as user estimated difficulty of the technique-competitor (p -value 0.007).

What technique will you prefer



The technique is clear and its logic is easy to understand and deploy

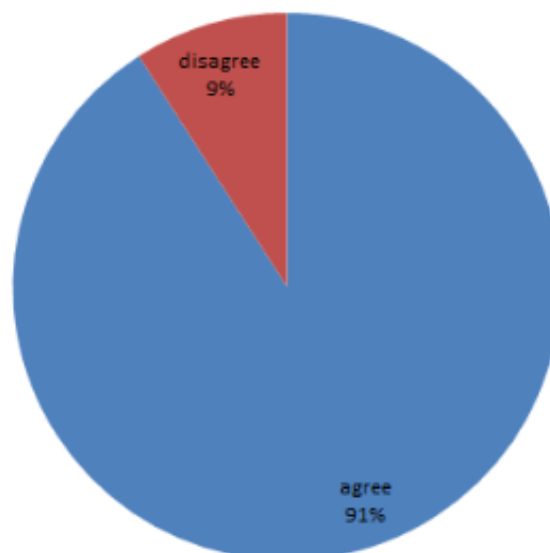


Figure 7.3: Overall experience on two considered visual-auditory techniques that were applied to superconductor fields analysis problem

SUMMARY OUTPUT								
<i>Regression Statistics</i>								
Multiple R	0.93294281							
R Square	0.87038229							
Adjusted R Square	0.68891749							
Standard Error	0.70039503							
Observations	13							
<i>ANOVA</i>								
	<i>df</i>	<i>SS</i>	<i>MS</i>	<i>F</i>	<i>Significance F</i>			
Regression	7	16.4703109	2.35290156	4.79642491	0.05163704			
Residual	5	2.45276598	0.4905532					
Total	12	18.9230769						
	<i>Coefficients</i>	<i>Standard Error</i>	<i>t Stat</i>	<i>P-value</i>	<i>Lower 95%</i>	<i>Upper 95%</i>	<i>Lower 95.0%</i>	<i>Upper 95.0%</i>
Intercept	-0.0412218	0.65139382	-0.0632824	0.95199357	-1.7156829	1.63323934	-1.7156829	1.63323934
work with physical phenomena and	-2.653151	0.96976898	-2.7358588	0.04099346	-5.1460215	-0.1602805	-5.1460215	-0.1602805
volume rendering experience	2.44183176	0.96915997	2.51953428	0.0532049	-0.0494732	4.93313677	-0.0494732	4.93313677
multisensory interaction experience	-0.3619593	0.23593494	-1.5341486	0.18557772	-0.9684493	0.24453082	-0.9684493	0.24453082
Impression of correction of wrong v	1.53592672	0.30674718	5.00714212	0.0040797	0.74740799	2.32444545	0.74740799	2.32444545
Difficulty of technique	0.68888582	0.29634351	2.32461926	0.06766309	-0.0728894	1.45066105	-0.0728894	1.45066105
Concurant impression	0.51256201	0.29118675	1.7602518	0.13867833	-0.2359574	1.26108139	-0.2359574	1.26108139
Concurant difficulty	1.35092638	0.31586612	4.27689546	0.00788679	0.53896667	2.1628861	0.53896667	2.1628861

Figure 7.4: Screenshot of Analysis ToolPack linear regression results for the analysis of user preference of the visual-auditory techniques that minimise either memory or time issues

t-Test: Two-Sample Assuming Unequal Variances		
	<i>Variable 1</i>	<i>Variable 2</i>
Mean	-0.5714286	0.5
Variance	1.61904762	1.1
Observations	7	6
Hypothesized Mean Difference	0	
df	11	
t Stat	-1.6639299	
P(T<=t) one-tail	0.06216148	
t Critical one-tail	1.79588482	
P(T<=t) two-tail	0.12432295	
t Critical two-tail	2.20098516	

Figure 7.5: T-test on sample for preference of the visual-auditory analysis technique

The results of population analysis are presented in Fig. 7.5. With the mean of 0.57, the second visual-auditory technique is preferred by the second group of users and with the mean of 0.5, the users of the first group preferred the first technique. However, the p-value is higher than significance level 0.05 (see Fig.7.5), the difference between those means is statistically insignificant and the effect size is still informative. We conducted the power analysis to compute the sample size for II-type error less than 20% . The computed effect size for two independent groups is 0.78 (medium) (see an illustrative graph for sample size required for specified type II error amount in Fig. 7.6). To make judgements with at least

80% certainty that there is no difference between these two groups we have to have a sample of at least 54 people in total.

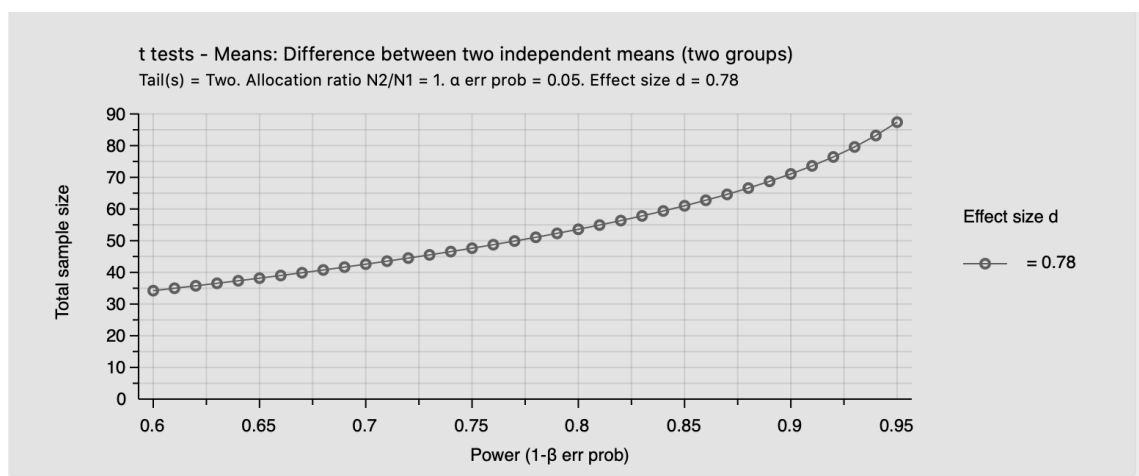


Figure 7.6: Power analysis. Estimation of sample size for defined II-type error with effects size of 0.78.

7.2.1.2 Impression on visual-auditory volume rendering across population

Similarly, we carried out the regression and t-test analysis to estimate important variables (see Fig.7.19 and Fig. 7.8) and how well the sample represents the population (see Fig.7.9).

SUMMARY OUTPUT							
Regression Statistics							
Multiple R	0.9634286						
R Square	0.92819467						
Adjusted R Square	0.82766722						
Standard Error	0.56208846						
Observations	13						
ANOVA							
	<i>df</i>	<i>SS</i>	<i>MS</i>	<i>F</i>	<i>Significance F</i>		
Regression	7	20.4202828	2.91718326	9.23324548	0.01316639		
Residual	5	1.57971716	0.31594343				
Total	12	22					
	<i>Coefficients</i>	<i>Standard Error</i>	<i>t Stat</i>	<i>P-value</i>	<i>Lower 95%</i>	<i>Upper 95%</i>	<i>Lower 95.0%</i> <i>Upper 95.0%</i>
Intercept	0.84647318	0.51523028	1.64290262	0.16132494	-0.4779684	2.17091479	-0.4779684 2.17091479
work with physical phenomena and complex data experience	1.77925043	0.61918307	2.87354502	0.0348499	0.18758968	3.37091119	0.18758968 3.37091119
volume rendering experience	-1.7397289	0.64504917	-2.6970485	0.04293525	-3.3978805	-0.0815772	-3.3978805 -0.0815772
multisensory interaction experience	-0.4899854	0.18203255	-2.6917463	0.04320832	-0.957915	-0.0220559	-0.957915 -0.0220559
Impression 1	-0.2323363	0.34562157	-0.6722275	0.53124586	-1.1207848	0.65611219	-1.1207848 0.65611219
Difficulty 1	0.18348242	0.43887842	0.41807118	0.69324338	-0.9446905	1.31165532	-0.9446905 1.31165532
Impression 2	0.77678858	0.32252849	2.40843402	0.06098191	-0.0522973	1.60587446	-0.0522973 1.60587446
Difficulty 2	-0.0449702	0.31793578	-0.1414444	0.89304113	-0.8622502	0.7723097	-0.8622502 0.7723097

(a)

SUMMARY OUTPUT							
Regression Statistics							
Multiple R	0.93635068						
R Square	0.87675259						
Adjusted R Square	0.81512889						
Standard Error	0.58217726						
Observations	13						
ANOVA							
	<i>df</i>	<i>SS</i>	<i>MS</i>	<i>F</i>	<i>Significance F</i>		
Regression	4	19.2885571	4.82213927	14.2275222	0.00103992		
Residual	8	2.71144291	0.33893036				
Total	12	22					
	<i>Coefficients</i>	<i>Standard Error</i>	<i>t Stat</i>	<i>P-value</i>	<i>Lower 95%</i>	<i>Upper 95%</i>	<i>Lower 95.0%</i> <i>Upper 95.0%</i>
Intercept	0.53525373	0.40808828	1.31161261	0.22603889	-0.4057995	1.47630699	-0.4057995 1.47630699
work with physical phenomena and complex data experience	1.20685129	0.39199977	3.0787041	0.01514664	0.3028982	2.11080437	0.3028982 2.11080437
volume rendering experience	-1.2370673	0.43538976	-2.8412871	0.02176882	-2.2410779	-0.2330567	-2.2410779 -0.2330567
multisensory interaction experience	-0.4887119	0.1338681	-3.6506975	0.00648782	-0.7974123	-0.1800115	-0.7974123 -0.1800115
Impression 2	0.69683483	0.13880115	5.02038208	0.00102639	0.37675879	1.01691087	0.37675879 1.01691087

(b)

Figure 7.7: Summary on preference to enhanced volume rendering technique . The screenshot of the linear regression results from the Analysis Toolpack(a) The regression with all independent variables (significant variables marked with yellow) (b) Regression for significant variables only

The estimated difficulty parameter of visual-auditory techniques does not significantly effect the user preference, as well as, impression produced by first technique. However, we assume that the second technique in this case produces a short term memory effect and thus is a significant variable, as well as, user experience in volume rendering and multi-sensory analysis variables (p-values of 0.06,0.03,0.042,0.043).

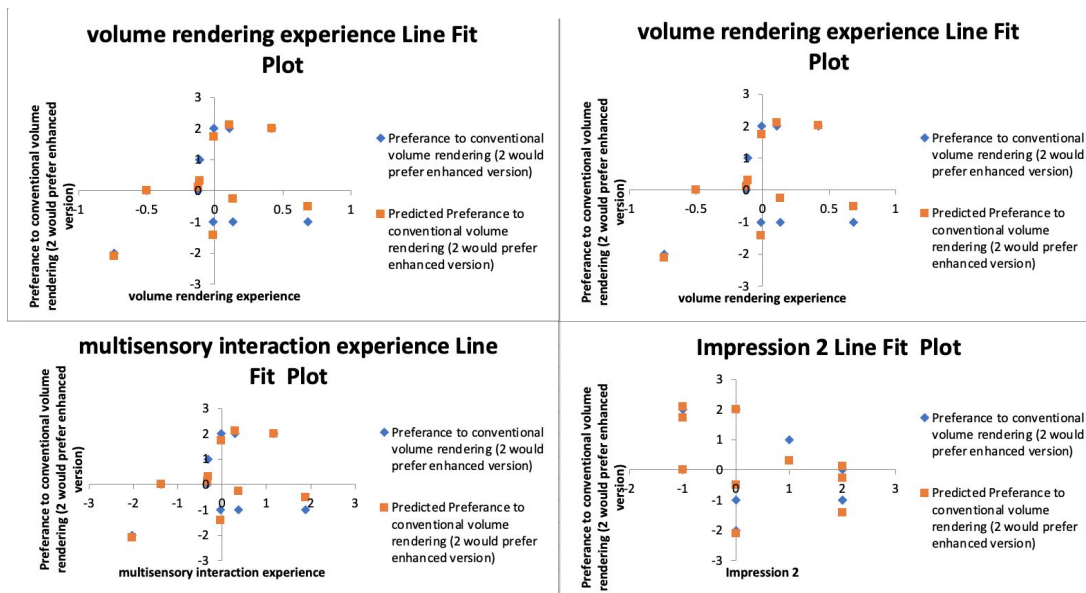


Figure 7.8: Approximated line plots for significant variables for enhanced volume rendering technique

t-Test: Two-Sample Assuming Unequal Variances		
	Variable 1	Variable 2
Mean	-0.5714286	0.6666667
Variance	0.95238095	2.2666667
Observations	7	6
Hypothesized Mean Difference	0	
df	8	
t Stat	-1.727203	
P(T<=t) one-tail	0.06120025	
t Critical one-tail	1.85954804	
P(T<=t) two-tail	0.1224005	
t Critical two-tail	2.30600414	

Figure 7.9: T-test results on population sample

With p-value higher than significance level 0.05, the difference between those means is statistically insignificant. The estimated with power analysis the effect size is 0.71 and the minimum sample size required for 20% type II error is 66 (see Fig. 7.10).

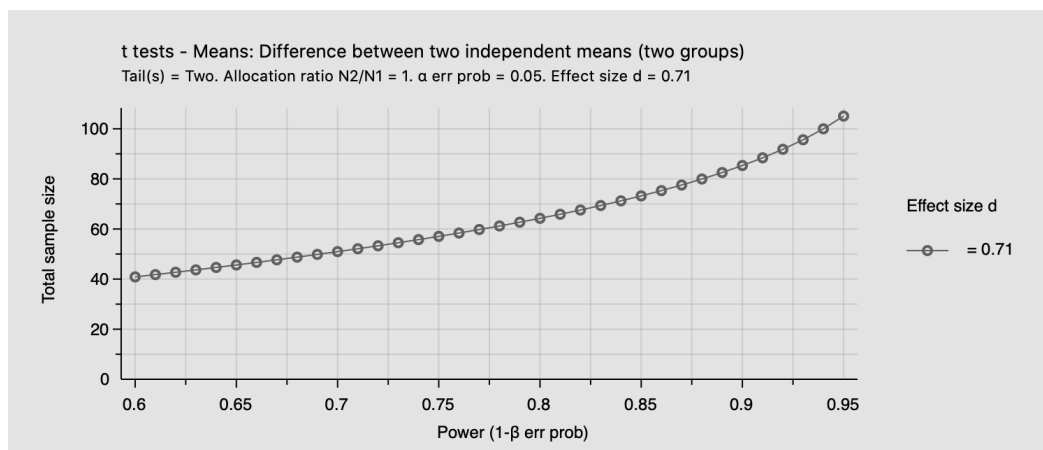


Figure 7.10: Power analysis. Estimation of sample size for defined II-type error with effects size of 0.71.

7.2.2 3D sound

7.2.2.1 Visual-auditory exploration of molecular structures

In previous evaluation case study 7.2.1 we have considered the principles of scanning 2D slices and simultaneous interpretation of colour and pitch to judge on properties of phenomena. We further explore the application of similar principles for heterogeneous objects, those are large scale molecular structures with distribution in space of internal volume properties. Similarly to visual volume ray-casting, we shoot the auditory rays from listener's position and use the human ability to locate the positions of objects producing sound.

In this part of the user study we consider the visual-auditory rendering of molecular structure. The activated part of the molecule is characterised by the specific produced as the result of auditory ray-casting 3D sound. As work in progress, we use the auditory transfer function to highlight with lower pitch the spatial distributions of atoms of selected type in big molecular structure. The activation atoms are visually highlighted when the initial impulse reaches them.

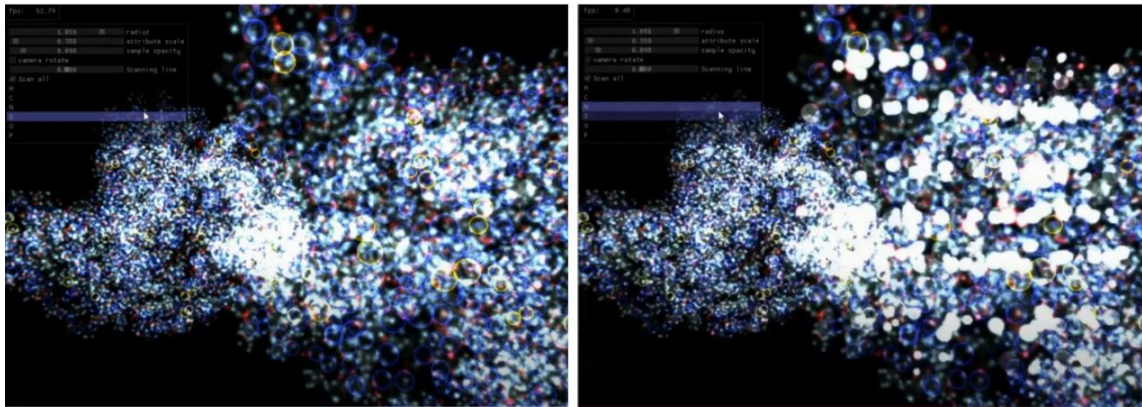


Figure 7.11: Visual-auditory volume ray-casting of the complex spatial object (molecule). Highlighting of "activated" with auditory impulse atoms

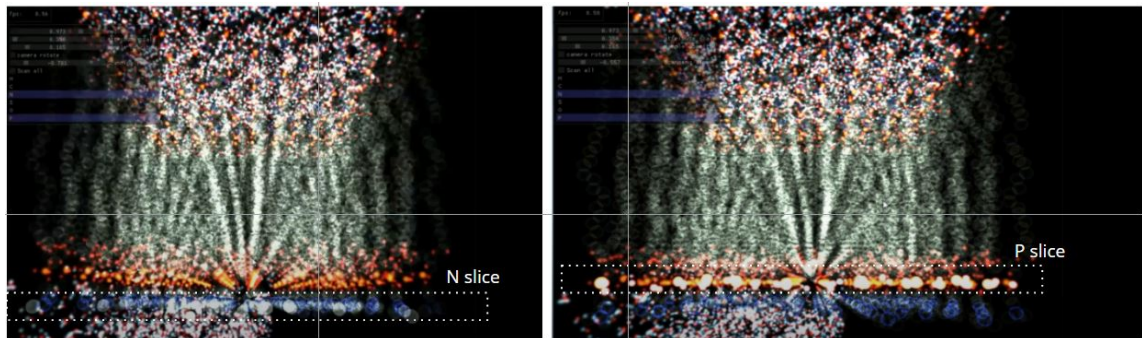


Figure 7.12: Auditory scanning of different layers of membrane molecular structure

As we have described the main technique principles in section 4.2.4, the auditory impulses propagate along with rays and activate objects that produce vibrations that are specified by object type. In this example, activating objects are atoms of a different type that compose a molecular structure (see figure below). Type of atom is interpreted visually as colour and auditory as pitch. To perform the task the users were asked to use the headphones to perceive the auditory spatial position of auditory rays propagation and spatial positions of activated atoms.

We have considered the two basic tasks:

1. Localisation of specified atoms in big volume molecular structure, those are P and N atoms. We have highlighted these atoms in structure with significantly lower pitch values to make them distinguishable and deployed spatial sound to highlight their spatial positions in volume molecular structure. We were interested if after visual-auditory visualisation the users would be able to approximately locate the highlighted

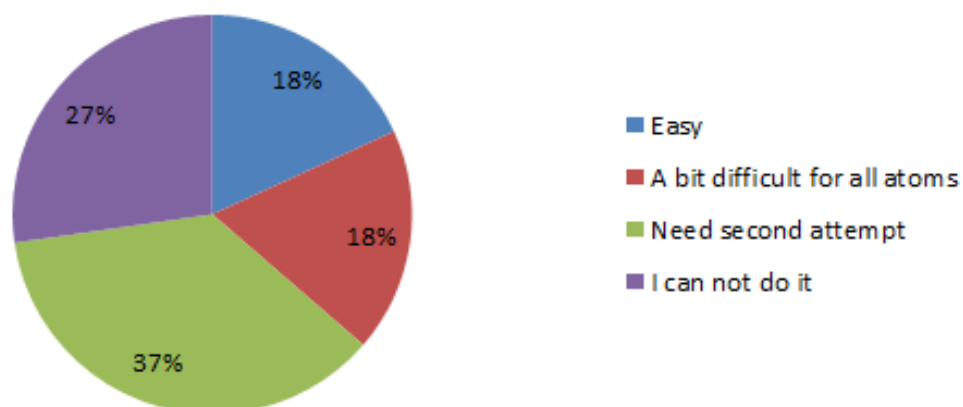
P and N atoms within volume molecular structure, in other words, zoom in to the approximate region of interest in the volume (see Fig. 7.11).

2. Auditory scanning of two different slices of molecular membrane structure. The slices are composed of P and N atoms accordingly that are highlighted with lower pitch values. Although they share some similar atoms, the P and N layers of the membrane will produce different auditory feedback. The technique assumes that the user will be able to memorise and compare auditory patterns each membrane layer is producing and further detect those layers even without visual information (see Fig. 7.12).

In both techniques we were interested in the applicability of spatial sound and sound patterns for the task of exploration and navigation within large scale molecular structures as the visual stimuli may be overload due to complex tasks execution and an additional source of information is needed. Most users were able to perform auditory localisation of specified atoms inside a big volume molecular structure. However, users had difficulties in case of dealing with large molecular structures with a lot of atoms of specified type for detection and localisation (see Fig. 7.13 (a)).

In the second technique, there are only two sound waves to compare and memorise. Most users were able to distinguish P and N layers only by sounds that they produce even after some time has passed since auditory scanning (see Fig. 7.13 (b)).

Auditory location of atoms in molecular structure



Auditory selection of membrane layer

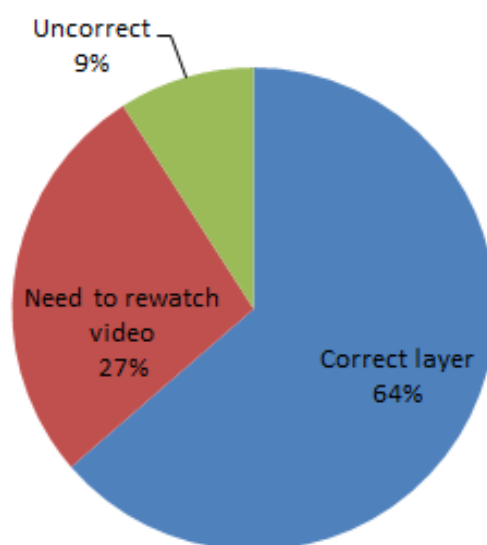


Figure 7.13: 3D sound for navigation and exploration. (a) Deployment of substructures localisation tasks in visual-auditory scene (atoms in molecular structure) (b) Deployment of solely auditory stimuli as source of additional information on substructure. The auditory feedback is based on 2 molecular membrane layers

7.2.2.2 Overall vision of extension of visual-auditory volume rendering

Despite that most of users of both groups admit efficiency and necessity of expansion of volume visualisation technique with auditory stimuli to enhance the analysis, at the same time most of the users consider auditory analysis as a complementary tool (average close to agree for first group and an average close to fully agree for second group see Fig. 7.15).

As it can be seen in Fig. 7.14, the following vision of the technique is defined by user estimated efficiency of different visual-auditory application cases (p-values 0.0671 and 0.0673), whether the users believe that there more cases are about to be considered (p-value 0.64) and how convenient was the sound analysis in total (p-value 0.054). Most of the users found the use of sound not disturbing, however have highlighted the necessity of additional application examples.

SUMMARY OUTPUT							
<i>Regression Statistics</i>							
Multiple R	0.88610799						
R Square	0.78518737						
Adjusted R Square	0.3555621						
Standard Error	0.95332191						
Observations	13						
<i>ANOVA</i>							
	<i>df</i>	<i>SS</i>	<i>MS</i>	<i>F</i>	<i>Significance F</i>		
Regression	8	13.2877862	1.66097328	1.82760986	0.29330645		
Residual	4	3.63529069	0.90882267				
Total	12	16.9230769					
	<i>Coefficients</i>	<i>Standard Error</i>	<i>t Stat</i>	<i>P-value</i>	<i>Lower 95%</i>	<i>Upper 95%</i>	<i>Lower 95.0%</i> <i>Upper 95.0%</i>
Intercept	2.18083679	0.74420098	2.93044065	0.042795	0.11460364	4.24706995	0.11460364 4.24706995
multisensory interaction experience	-1.9931547	0.73638691	-2.7066678	0.05372216	-4.0376926	0.05138308	-4.0376926 0.05138308
Impression 1	1.51953382	0.60911705	2.49464997	0.06714952	-0.1716462	3.21071385	-0.1716462 3.21071385
Difficulty 1	2.15814265	1.00922917	2.13840694	0.09926532	-0.6439267	4.96021204	-0.6439267 4.96021204
Impression 2	2.23230117	0.89588383	2.49173061	0.06735956	-0.2550711	4.71967346	-0.2550711 4.71967346
Difficulty 2	1.28528107	0.60435464	2.12670011	0.10058061	-0.3926764	2.96323855	-0.3926764 2.96323855
The use of sound was not disturbing	-1.4730154	0.54778769	-2.6890261	0.05471332	-2.9939178	0.04788705	-2.9939178 0.04788705
In current version the method is not difficult for application	0.75575532	0.4550356	1.66087078	0.17207597	-0.507626	2.01913668	-0.507626 2.01913668
No more examples are required	-1.9404324	0.76445587	-2.5383184	0.06409531	-4.0629022	0.18203735	-4.0629022 0.18203735

Figure 7.14: Screenshot of Analysis ToolPack linear regression results for the analysis of user vision of auditory analysis tools within volume rendering framework, in particular vision of using auditory analysis only as additional tool to visual analysis. The significant variables are marked with yellow.

t-Test: Two-Sample Assuming Unequal Variances		
	Variable 1	Variable 2
Mean	0.71428571	1.5
Variance	2.23809524	0.3
Observations	7	6
Hypothesized Mean Difference	0	
df	8	
t Stat	-1.2921816	
P(T<=t) one-tail	0.11618411	
t Critical one-tail	1.85954804	
P(T<=t) two-tail	0.23236822	
t Critical two-tail	2.30600414	

Figure 7.15: T-test results on population sample

With p-value more than significance level 0.05, the difference between those means is statistically insignificant. Also the estimated effect size is 0.49 and the minimum sample size required for 20% type II error is 130 (see Fig. 7.16).

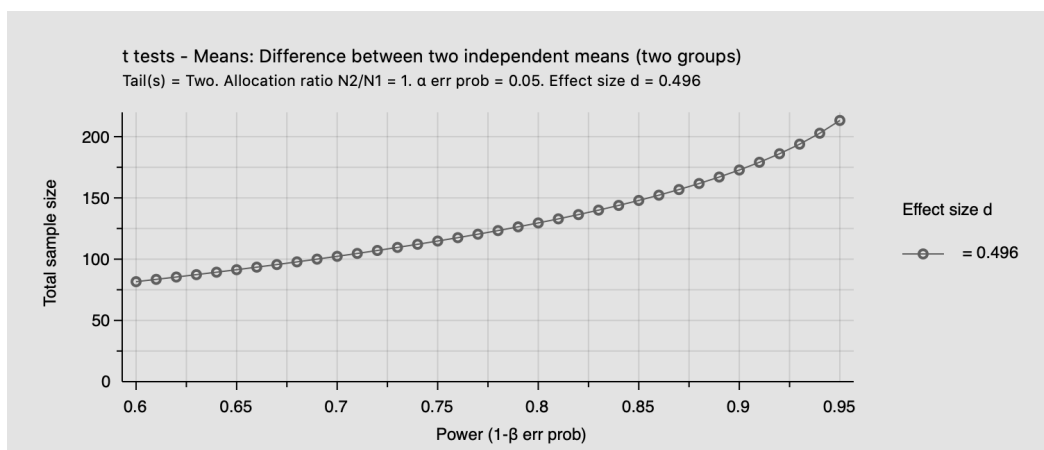


Figure 7.16: Power analysis. Estimation of sample size for defined II-type error with effects size of 0.49

7.2.3 Auditory perception based user interaction

In this part of the study, we were targeting the evaluation of the user interaction with volume data on the base of the obtained auditory image of the phenomena similarly to how in conventional volume rendering framework GUI is deployed to manipulate the optical TF (see section 3.5.4, 4.6.4). We are not aware of previous attempts to deploy such techniques. Thus, our primary goal was to collect reviews and opinion from users that have experience of interaction with volume and heterogeneous data.

Approximately half of the users were completely satisfied with conventional optical TF-based interaction techniques they were using for heterogeneous objects analysis, while others considered the possibility for further enhancement (see Fig. 7.17). The users have found the MIDI-based interaction technique interesting and having the potential to complement the existing techniques. However, there were concerns that complex cases of technique application may demand music/auditory training. Some users also found the technique needs further enhancement in terms of usability that similarly to optical TF can be achieved with combination with image processing techniques.

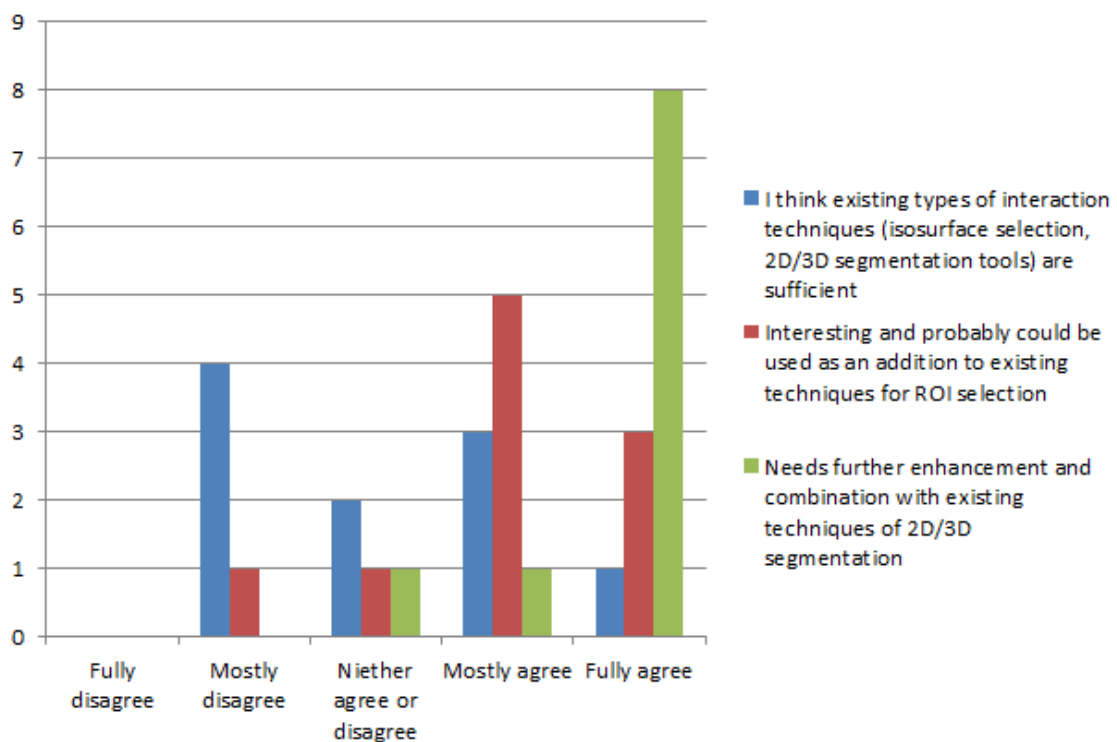


Figure 7.17: Interaction with volume data on base of obtained auditory image of the phenomena.

The results of the analysis of the user estimated vision of MIDI-interaction are presented in Fig. 7.18. The linear approximation is quite well and is well defined by users experience in multi-sensory analysis and work with physical data (p-values 0.056,0.034).

SUMMARY OUTPUT								
Regression Statistics								
Multiple R	0.93762561							
R Square	0.87914178							
Adjusted R Square	0.63742533							
Standard Error	0.57448753							
Observations	13							
ANOVA								
	<i>df</i>	<i>SS</i>	<i>MS</i>	<i>F</i>	<i>Significance F</i>			
Regression	8	9.60293325	1.20036666	3.63707886	0.11385748			
Residual	4	1.32014367	0.33003592					
Total	12	10.9230769						
	<i>Coefficients</i>	<i>Standard Error</i>	<i>t Stat</i>	<i>P-value</i>	<i>Lower 95%</i>	<i>Upper 95%</i>	<i>Lower 95.0%</i>	<i>Upper 95.0%</i>
Intercept	-0.0548649	0.45413493	-0.120812	0.90966548	-1.3157456	1.20601576	-1.3157456	1.20601576
work with physical phenomena and complex data volume rendering experience	1.22227337	0.45891491	2.66339868	0.05619096	-0.0518787	2.49642543	-0.0518787	2.49642543
multisensory interaction experience	-0.5887693	0.47273037	-1.2454653	0.28093482	-1.9012792	0.72374066	-1.9012792	0.72374066
In current version the method is not difficult for 3d meshes experience	0.50840964	0.16163193	3.14547768	0.03466447	0.05964745	0.95717183	0.05964745	0.95717183
The method logic is clear and will not be hard to Existing interaction VR method are good enough	0.03434867	0.22407038	0.15329413	0.8855888	-0.5877704	0.65646778	-0.5877704	0.65646778
Needs enhancement	-0.0169495	0.17022357	-0.0995719	0.9254749	-0.4895659	0.4556669	-0.4895659	0.4556669
	-0.1715459	0.2322684	-0.7385673	0.50115935	-0.8164263	0.47333461	-0.8164263	0.47333461
	-0.1870057	0.22116147	-0.845562	0.44541163	-0.8010484	0.42703695	-0.8010484	0.42703695

(a)

SUMMARY OUTPUT								
Regression Statistics								
Multiple R	0.89756844							
R Square	0.8056291							
Adjusted R Square	0.7408388							
Standard Error	0.48569861							
Observations	13							
ANOVA								
	<i>df</i>	<i>SS</i>	<i>MS</i>	<i>F</i>	<i>Significance F</i>			
Regression	3	8.79994865	2.93331622	12.4344093	0.00149261			
Residual	9	2.12312827	0.23590314					
Total	12	10.9230769						
	<i>Coefficients</i>	<i>Standard Error</i>	<i>t Stat</i>	<i>P-value</i>	<i>Lower 95%</i>	<i>Upper 95%</i>	<i>Lower 95.0%</i>	<i>Upper 95.0%</i>
Intercept	-0.227855	0.33398575	-0.6822296	0.51226802	-0.9833832	0.5276733	-0.9833832	0.5276733
work with physical phenomena and complex data experience	1.07144146	0.32132153	3.33448391	0.00873651	0.34456167	1.79832125	0.34456167	1.79832125
volume rendering experience	-0.5346383	0.35645356	-1.499882	0.16788067	-1.3409923	0.2717157	-1.3409923	0.2717157
multisensory interaction experience	0.43766913	0.11032589	3.96705735	0.00326916	0.18809463	0.68724363	0.18809463	0.68724363

(b)

Figure 7.18: Summary on preference to enhanced volume rendering technique . The screenshot of the linear regression results from the Analysis Toolpack(a) The regression with all independent variables (significant variables marked with yellow) (b) Regression for significant variables only

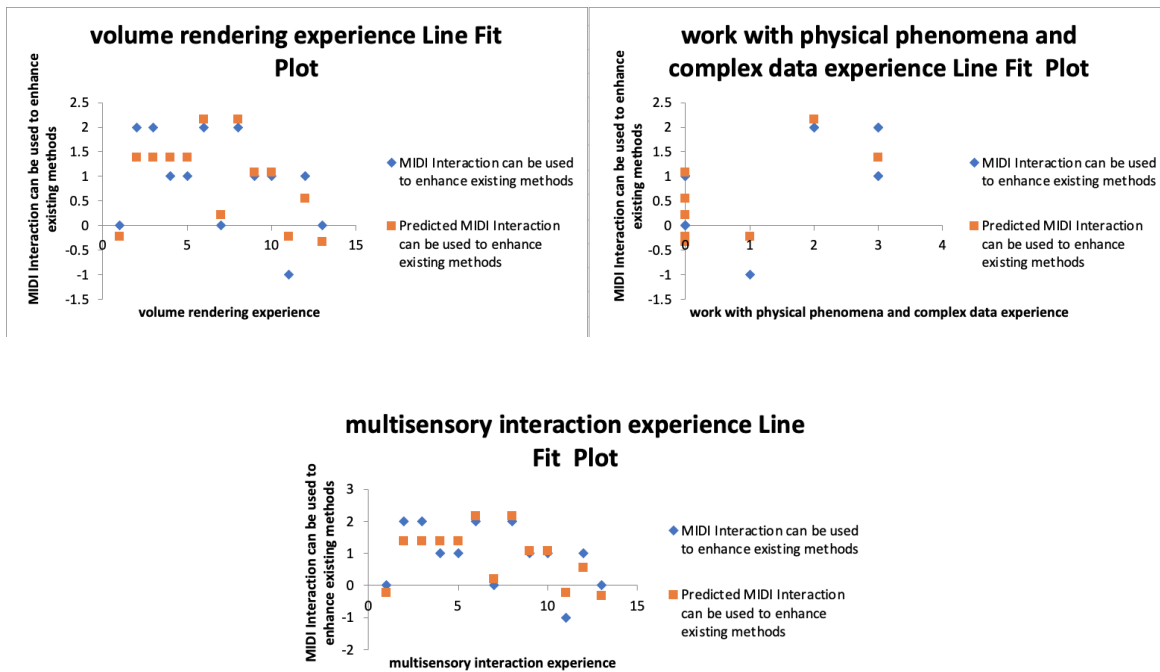


Figure 7.19: Approximated line plots for significant variables for vision of user interaction with visual-auditory image of the phenomena

t-Test: Two-Sample Assuming Unequal Variances		
	Variable 1	Variable 2
Mean	1.6666667	0.28571429
Variance	0.26666667	0.57142857
Observations	6	7
Hypothesized Mean Difference	0	
df	11	
t Stat	3.88920291	
P(T<=t) one-tail	0.00126152	
t Critical one-tail	1.79588482	
P(T<=t) two-tail	0.00252304	
t Critical two-tail	2.20098516	

Figure 7.20: T test results for user visual-auditory interaction vision within used population sample

The population analysis has demonstrated that with a p-value less than significance level 0.05, the difference between the means is statistically significant. Thus, we can reject the null hypothesis and say that estimated mean values are different, in other words, the users of the first group are between "agree" and "fully agree" on the importance of extension with more sophisticated tools for user interaction tools, while users of the second group are between "not sure" and "agree" with such necessity in average. The rate of occurrence of I-st Error

type (false positive) that leads to the fact there is no difference in means of our two groups (the null hypothesis was rejected incorrectly) is 0.05.

7.3 Summary

The goal of this preliminary evaluation was to understand the relevance of the entire direction of the research according to expectations of potential users and preliminary identify the main parameters for proposed techniques further enhancement and application for heterogeneous phenomena analysis. Based on the preliminary user study, we conclude that visual and auditory stimuli can complement each other in the analysis of both volume and spatial distribution properties of heterogeneous phenomena. Most of the users perceived the sound in our visual-auditory approach well. Applied for the tasks that are normally solved with volume rendering, the auditory stimuli can detect possible visual quality issues, the feature that is as preliminary evaluation shows is a significant factor for defining visual-auditory technique success. The results of regression analysis demonstrate that if the visual-auditory technique effectively addresses the visual perception limitations, its difficulty is not a primary factor that defines its preference by users.

Also, the reviews from specialists have highlighted that the proposed auditory techniques usability depends on the design of complex user interfaces. Although acknowledging the necessity of extension of volume rendering with auditory stimuli, the users consider the auditory analysis of heterogeneous phenomena as a complementary, on-demand tool. Thus we can conclude, that the main direction for extension of heterogeneous objects visual analysis with auditory stimuli has been identified correctly, although its application demands further enhancement in terms of usability and consideration of additional application cases. Also, in our preliminary study, we have expected a significant difference in the vision of volume rendering extension with auditory stimuli in the two groups of potential users. The first group are specialists with knowledge in volume rendering, physical phenomena analysis, aware of details of volume rendering technique. The specialists are interested in highlighting changes in complex data with specific characteristics of data, addressing perception issues. The second group is defined by mainly multi-sensory interaction experience. They usually pay a lot of attention to user interaction, enhancing and facilitating perception and see sonification as mainly a complementary tool in this area.

However, due to current limitations, we were able to obtain only a relatively small sample size for analysis and were unable to confirm that there is no significant difference in the vision of heterogeneous phenomena analysis extension with auditory stimuli for two groups of users. The results of power analysis demonstrate that for considered evaluation studies in sections

7.2.1.1,7.2.1.2,7.2.2.2 the sample sizes of at least 58,66 and 130 participants are required to make the judgements whether the usability estimation is different for representatives of the above two groups.

Chapter 8

Conclusions and discussion

In this research, we defined the framework for the simultaneous visual-auditory analysis of dynamic multi-scale heterogeneous objects. The GPU-accelerated volume rendering of such structures is an area of active research that significantly differs from conventional volume sampling of the 3D structured grid. The introduction of auditory sensory stimuli makes it even more challenging. The design of multisensory pipeline for heterogeneous phenomena analysis and further analysis with cross-stimuli interpretations deployment is not straightforward. The research in the area has to deal with a computationally expensive visual-auditory rendering of heterogeneous phenomena with dynamic and multi-scale features.

In this work, we have addressed the problem of visual-auditory analysis of heterogeneous objects from the more general, multi-modal point of view with introduction of the auditory material that is modelled and rendered similarly to optical one within a heterogeneous volume subdivision. We have discussed the aspects of low-level design, such as GPU accelerated ray-casting and application of computer graphics techniques for both visual and auditory analysis. We took advantage of the modern GPU hardware and have proposed a unified and flexible approach to visual-auditory pipeline design.

8.1 Overall conclusions

The main contributions that were stated in section 1.3 are outlined in this work as follows: In chapters 1,2 we have introduced the main challenges and did an overview of the subject area.

In chapter 3, we have investigated the works related to the multidisciplinary problem of visual-auditory analysis of heterogeneous objects and discussed the techniques needed for introduction of theoretical approach in chapter 4. We have presented the necessary background regarding modelling and GPU accelerated volume rendering of heterogeneous

structures. We have outlined the role of sound propagation in sound synthesis and auditory perception, the main features of the process that allow using the computer graphics techniques for auditory rendering. We have discussed the role of ray-casting and geometry modelling in interactive exploration with multimodal feedback.

Chapter 4 discusses the theoretical aspects of this work those are the first and second contribution of this research introduced in section 1.3. The chapter outlines a general approach for GPU accelerated volume visualisation of heterogeneous objects that compared to conventional volume visualisation frameworks considers the spatial distribution of dynamic and multi-scale properties of heterogeneous phenomena.

In that chapter we have proposed a framework for interactive visual-auditory visualisation that considers unified modelling of optical and auditory properties with ray-casting based rendering to a visual-auditory representation of heterogeneous phenomena. The main feature of the approach is a combination of GPU constructive hybrid modelling with volume ray-casting of visual and auditory properties.

We took advantage of the implicit complex (IC) representation to specify the rules of arbitrary multidimensional geometry modelling within an unstructured subdivision. We extended and deployed IC structures within interactive visual-auditory pipelines. We have considered the GPU implemented hybrid modelling that simultaneously operates several geometry representations (implicit functions, voxels, point-based data) as a core of heterogeneous objects visualisation. We have demonstrated that such a hybrid constructive structure is convenient for deployment in combination with volume ray-casting and allows designing complex visualisation techniques in a unified way.

Chapter 5 discusses the implementation aspects as a part of second contribution introduced in section 1.3. We have discussed the GPU implementation of the proposed framework and the benefits it provides for heterogeneous objects analysis. The GPU implemented IC allows addressing the challenges arising in the analysis of heterogeneous objects, such as simultaneous visual-auditory rendering and user interaction without restrictions on the type of geometry or design of complex interactive visualisation techniques for analysis of multi-scale dynamic features. We have used the structure of the constructive tree to control the efficiency of visualisation pipeline evaluation and the quality of volume rendering.

By using the modern ray-tracing graphic pipeline we have implemented the evaluation of visual-auditory pipeline for heterogeneous objects as a "black box". With this concept, we have designed an object-oriented API that facilitates the creation of visual-auditory pipelines for heterogeneous structures analysis and deploys GPU accelerated data-flow principles.

Chapter 6 discusses our third contribution that is the framework practical application for two problem areas those are molecular structures visualisation that deals with dynamic and

multi-scale phenomena and modelling and rendering of microstructures in digital fabrication. For these two considered problem areas, we have provided the practical details of framework deployment for designing interactive visualisation techniques and user interactive exploration and modelling with auditory feedback. We have discussed the design of the visual-auditory pipelines for analysis of these heterogeneous objects with the proposed API and how it allows addressing the interactive real-time visualisation challenges in considered problem areas in a unified way.

In chapter 7, we have assessed the applicability of the proposed method outside the scope of this research project by carrying out a preliminary evaluation and have identified the main aspects of the work future extension

We have assumed that the proposed unified approach to visual-auditory analysis is not only efficient but also facilitates the cross-interpretation of visual and auditory cues in the analysis of heterogeneous phenomena. We have evaluated to obtain the reviews from researchers that deal with problem area on various basic visual-auditory techniques that our approach allows introducing that target exploration of various features of heterogeneous phenomena and user interaction with optical and auditory properties. As a result of the evaluation, we may summarise that even applied straightforwardly in areas of conventional volume rendering, the auditory stimuli obtained with the proposed technique can assist in the enhancement of the quality of visual analysis of heterogeneous phenomena. The preliminary evaluation allows assuming that we have correctly identified the main direction for extension of the analysis of heterogeneous objects with auditory stimuli. However, its application demands further enhancement in terms of the design of more complex user interfaces and consideration of additional application cases that is out of the scope of this research. Due to current limitations, we were unable to confirm that there is no significant difference in the vision of heterogeneous phenomena analysis extension with auditory stimuli for two groups of potential users that specialise in the area of analysis of volume structures and deal with visual perception issues and users that deal with multi-sensory interaction for facilitation of the analysis of complex phenomena. Thus, we have provided the results of power analysis for the assumed sample size necessary for such analysis.

8.2 Future research

In this work, we have considered several aspects of heterogeneous objects analysis that are areas of further development and enhancement. We believe the most promising is the extension of this research in the following two directions:

8.2.1 HPC and complex GPU tasks within visualisation pipeline

In this work, we have addressed the problem of the growing complexity of geometric and material modelling within a visual pipeline. By using GPU-based hybrid constructive modelling we have demonstrated how the model allows addressing the efficiency and optimisation issues of the visual-auditory pipeline within a ray-tracing context.

Similarly to considered visual-auditory analysis area, other research areas take advantage of a combination of complex GPU tasks and ray-tracing in the context of scientific workflows or data analysis. The examples of such areas are processing of point clouds in computer vision or in-situ visualisation that combines real-time simulation and rendering. The research in the area uses GPU implementation and often benefits from conventional for ray-tracing acceleration structures and techniques. Complex tasks may deploy and operate simultaneously several types of GPU acceleration structures (BVH, KD-trees) to introduce more complex techniques, optimise GPU memory usage (SVO) or provide fast access part of data for in-situ visualisation. The flexibility the ray-tracing computer graphics pipeline makes it convenient for the integration of arbitrary geometry modelling procedures and GPU data manipulations (selection of subsets, evaluation of relationships). Our approach to heterogeneous objects analysis can be further deployed within a distributed scientific environment with a focus on a particular problem area and a combination of several GPU techniques.

Modern HPC research concentrates on issues of flexibility, memory sharing and data exchange in the context of multiple GPU implementation (Alex Ishii 2020, Li, Song, Chen, Li, Liu, Tallent & Barker 2020). The research deals with reducing the bandwidth of both CPU/GPU and GPU interconnect on both hardware and software levels. Exploring the above trends in the context of the design of more complex scientific interfaces that facilitate the analysis of scientific data can be an area challenging area of future research. Among most perspective areas we see the astrophysics research area that deals with particle-based simulation data (Gheller et al. 2016), (Vogelsberger et al. 2019) and datacubes data (Koribalski et al. 2018) of an extremely large scale.

8.2.2 User interaction with multisensory feedback

In this work, we have used similarities in light and sound propagation to propose a unified approach to the visual-auditory analysis of heterogeneous objects and implement it on the base of ray-tracing. However, not only the sound rendering but entire multisensory feedback generation and multimodal user interaction can benefit from GPU implementation and deploying ray-tracing techniques concepts.

In this work, we have explored possibilities of the GPU framework implementation to provide the real-time user interactive exploration procedures performed during data analysis. We stress that real-time interactive exploration of phenomena involves extensive multidimensional geometric modelling that can benefit from GPU acceleration and combination with ray-casting techniques. In this work, we have considered basic examples and principles that can be a basis for the design of various interactive exploration tasks in the analysis of heterogeneous objects. The evaluation has demonstrated that the usability of the techniques depends on the design of a user interface that deploys them.

In the same way as visual-auditory analysis design, the research in the area has demonstrated that modern GPU demonstrates the close relationships and combination of image processing, machine learning, computer vision tasks with ray-tracing (Jakob 2020),(Azinović et al. 2019), (Shankar & Michael 2020),(Alex Keller 2020). The techniques can allow enhancing the quality of analysis of the heterogeneous phenomena in many areas, for example by taking advantage of learning shape or internal features from additional data (Park et al. 2019). We consider the SDFs representation and combination with various ray-tracing structures (BVH, SVO, KD-trees, etc.) as the key to the integration of additional procedures and complex interactive techniques. Being a core of many image processing (DIOP et al. 2010),(Heimann & Meinzer 2009) and complex interaction tasks Xu & Barbic (2017), SDF is actively deployed as a part of ML and CV techniques (Slavcheva 2018),(Park et al. 2019), (Zeng et al. 2017), similarly to as ray-tracing structures (NVIDIA 2018),(Keller et al. 2018).

Also, ray-tracing and modern GPU techniques are actively applied for more complex and realistic visual-auditory rendering, not limited to volume rendering techniques. The related research in VR/AR area deals with realistic high-quality visual and auditory rendering (da Silva & Velho 2020). There are also quite specific application areas of auditory GPU accelerated rendering (Ulmstedt & Stålberg 2019), (Thoman et al. 2020). Overall, we see that our work can be used in wider range of disciplines and extended further for new possibilities in the area of scientific visualisation.

Appendix A

Additional materials

Because the presented in this work API for analysis of heterogeneous object was submitted for the High-Performance Graphics 2020 student competition (won), the source codes and examples, as well as general description are available from competition web page <https://www.highperformancegraphics.org/studcomp20/malikova/>

The following additional video materials related to this work and presented case studies are also available:

1. <https://www.youtube.com/watch?v=7QBGSXwgxO0> - HPG FastForward
2. <https://www.youtube.com/watch?v=k3wQ-ODzT8M> - Examples of GPU modelling and rendering of various heterogeneous objects
3. https://www.youtube.com/watch?v=9io0GBt_tJk - Leap Motion interaction example
4. <https://www.youtube.com/watch?v=k2SEhwZ-tZQ> - Visual-auditory localisation of atoms positions in molecular structure
5. <https://www.youtube.com/watch?v=Gv2RZ-1NVpI> - Visual-auditory analysis of different "slices" of membrane structure

Appendix B

List of Publications

- [1] Evgeniya Malikova, Valery Adzhiev, Oleg Fryazinov, Alexander Pasko, 2019. VISUAL-AUDITORY REPRESENTATION AND ANALYSIS OF MOLECULAR SCALAR FIELDS. Eurographics 2019 - Posters. DOI:10.2312/egp.20191051
- [2] Evgeniya Malikova, Valery Adzhiev, Oleg Fryazinov, Alexander Pasko, 2019. VISUAL-AUDITORY VOLUME RENDERING OF SCALAR FIELDS. 25th International Conference on Auditory Display (ICAD 2019), Northumbria University, Newcastle upon Tyne, UK. DOI:10.21785/icad2019.004
- [3] Evgeniya Malikova, Valery Adzhiev, Oleg Fryazinov, Alexander Pasko, 2020. VISUAL-AUDITORY VOLUME RENDERING OF DYNAMIC QUANTUM CHEMISTRY MOLECULAR FIELDS. VISIGRAPP (3: IVAPP), Pages: 193-200.
- [4] Evgeniya Malikova, 2020. RAY-CASTING INSPIRED VISUALISATION PIPELINE for MULTI-SCALE HETEROGENEOUS OBJECTS. High-Performance Graphics 2020, Poster. Online: <https://www.highperformancegraphics.org/studcomp20/malikova/>

Bibliography

Abadi, M., Agarwal, A., Barham, P., Brevdo, E., Chen, Z., Citro, C., Corrado, G. S., Davis, A., Dean, J., Devin, M., Ghemawat, S., Goodfellow, I., Harp, A., Irving, G., Isard, M., Jia, Y., Jozefowicz, R., Kaiser, L., Kudlur, M., Levenberg, J., Mané, D., Monga, R., Moore, S., Murray, D., Olah, C., Schuster, M., Shlens, J., Steiner, B., Sutskever, I., Talwar, K., Tucker, P., Vanhoucke, V., Vasudevan, V., Viégas, F., Vinyals, O., Warden, P., Wattenberg, M., Wicke, M., Yu, Y. & Zheng, X. (2015), ‘TensorFlow: Large-scale machine learning on heterogeneous systems’. Software available from tensorflow.org.

URL: <https://www.tensorflow.org/>

Abboud, S., Hanassy, S., Levy-Tzedek, S., Maidenbaum, S. & Amedi, A. (2014), ‘Eyemusic: Introducing a “visual” colorful experience for the blind using auditory sensory substitution’, *Restorative neurology and neuroscience* **32**(2), 247–257.

Adams, N. & Wakefield, G. (2005), ‘The binaural display of clouds of point sources’, *In IEEE Workshop on Application of Signal Proc. to Audio and Acoustics* .

Adamson, A. & Alexa, M. (2006), ‘Point-sampled cell complexes’, *ACM Trans. Graph.* **25**(3), 671–680.

URL: <https://doi.org/10.1145/1141911.1141940>

Adzhiev, V., Kartasheva, E., Kunii, T., Pasko, A. & Schmitt, B. (2002), ‘Hybrid cellular-functional modeling of heterogeneous objects’, *J. Comput. Inf. Sci. Eng.* **2**, 312–322.

Adzhiev, V., Ossipov, A. & Pasko, A. (1999), Multidimensional shape modeling in multimedia applications, *in* A. Karmouch, ed., ‘MultiMedia Modeling: Modeling Multimedia Information and Systems’, World Scientific, pp. 39–60.

Akenine-Moller, T., Haines, E. & Hoffman, N. (2008), *Real-Time Rendering*, 3rd edn, A. K. Peters, Ltd., USA.

Alex Ishii, N. W. (2020), ‘Under the hood of the new dgx a100 system architecture’, [://developer.nvidia.com/gtc/2020/video/s21884-vid](https://developer.nvidia.com/gtc/2020/video/s21884-vid).

- Alex Keller, N. B. (2020), 'Machine learning on the edge for 5g', [://developer.nvidia.com/gtc/2020/video/s21884-vid](https://developer.nvidia.com/gtc/2020/video/s21884-vid).
- Allusse, Y., Horain, P., Agarwal, A. & Saipriyadarshan, C. (2008), Gpucv: A gpu-accelerated framework for image processing and computer vision, Vol. 5359, pp. 430–439.
- Ament, M. (2014), 'Thesis: Computational visualization of scalar fields', https://www.researchgate.net/publication/272348816_Computational_Visualization_of_Scalar_Fields. Accessed on 2017-11-12.
- Angelidis, A. & Cani, M.-P. (2002), Adaptive implicit modeling using subdivision curves and surfaces as skeletons, in 'Proceedings of the Seventh ACM Symposium on Solid Modeling and Applications', SMA '02, Association for Computing Machinery, New York, NY, USA, p. 45–52.
URL: <https://doi.org/10.1145/566282.566292>
- An overview of auditory display to assist comprehension of molecular information* (2006), *Interacting with Computers* **18**(4), 853 – 868. Special Theme Papers from Special Editorial Board Members (contains Regular Papers).
- Anwar, S. & Sung, W. (2009), 'Digital signal processing filtering with gpu'.
- Appel, A. (1968), Some techniques for shading machine renderings of solids, in 'Proceedings of the April 30–May 2, 1968, Spring Joint Computer Conference', AFIPS '68 (Spring), Association for Computing Machinery, New York, NY, USA, p. 37–45.
URL: <https://doi.org/10.1145/1468075.1468082>
- Arbon, R., Jones, A., Bratholm, L., Mitchell, T. & Glowacki, D. (2018), 'Sonifying stochastic walks on biomolecular energy landscapes'.
- Argelaguet, F., Andujar, C. & Trueba, R. (2008), Overcoming eye-hand visibility mismatch in 3d pointing selection, in 'Proceedings of the 2008 ACM Symposium on Virtual Reality Software and Technology', VRST '08, Association for Computing Machinery, New York, NY, USA, p. 43–46.
URL: <https://doi.org/10.1145/1450579.1450588>
- A.S. Bregman (1990), *Auditory scene analysis: The perceptual organization of sound*, The MIT Press.
- Auvray, M., Hanneton, S. & O'Regan, J. K. (2007), 'Learning to perceive with a visuo—auditory substitution system: localisation and object recognition with 'the voice'', *Perception* **36**(3), 416–430.

- Ayachit, U. (2015), *The ParaView Guide: A Parallel Visualization Application*, Kitware, Inc., USA.
- Azinović, D., Li, T.-M., Kaplanyan, A. & Nießner, M. (2019), ‘Inverse path tracing for joint material and lighting estimation’.
- Backhaus, D., Engbert, R., Rothkegel, L. O. M. & Trukenbrod, H. A. (2019), ‘Task-dependence in scene perception: Head unrestrained viewing using mobile eye-tracking’.
- Bagaturyants, A., Vladimirova, K., Degtyarenko, N., Malikova, E., Minibaev, R., Pilyugin, V., Strikhanov, M. & Freidzon, A. (2010), ‘Visualization and design of nanostructures in multiscale approach: “nanomodeller” program’, *Scientific Visualization* (<http://sv-journal.org>) **2**(4), 40–60.
- Bálint, C. & Valasek, G. (2018), Accelerating sphere tracing, in ‘Proceedings of the 39th Annual European Association for Computer Graphics Conference: Short Papers’, EG, Eurographics Association, Goslar, DEU, p. 29–32.
- Ballweg, H., Bronowska, A. & Vickers, P. (2016), Interactive sonification for structural biology and structure-based drug design, pp. 41–47.
- Baloup, M., Pietrzak, T. & Casiez, G. (2019), Raycursor: A 3d pointing facilitation technique based on raycasting, in ‘Proceedings of the 2019 CHI Conference on Human Factors in Computing Systems’, CHI ’19, Association for Computing Machinery, New York, NY, USA, p. 1–12.
URL: <https://doi.org/10.1145/3290605.3300331>
- Balzano, G. & Clynes, M. (1982), ‘Music, mind, and brain’.
- Barrass, S. & Vickers, P. (2011), Sonification design and aesthetics, in T. Hermann, A. Hunt & J. G. Neuhoff, eds, ‘The Sonification Handbook’, Logos Publishing House, Berlin, Germany, chapter 7, pp. 145–171.
URL: <http://sonification.de/handbook/chapters/chapter7/>
- Basics of fMRI Analysis: Preprocessing, First Level Analysis, and Group Analysis* (2018), <https://ftp.nmr.mgh.harvard.edu/pub/docs/SavoyfMRI2014/fmri.april2011.pdf>. Accessed on 2018/12/7.
- Bastos, T. & Celes, W. (2008), Gpu-accelerated adaptively sampled distance fields, in ‘2008 IEEE International Conference on Shape Modeling and Applications’, pp. 171–178.

- Bathe, K.-J. & Zhang, L. (2017), 'The finite element method with overlapping elements a new paradigm for cad driven simulations', *Comput. Struct.* **182**(C), 526–539.
URL: <https://doi.org/10.1016/j.compstruc.2016.10.020>
- Becciani, U., Costa, A., Antonuccio-Delogu, V., Caniglia, G., Comparato, M., Gheller, C., Jin, Z., Krokos, M. & Massimino, P. (2010), 'Visivo-integrated tools and services for large-scale astrophysical visualization', *Publications of the Astronomical Society of the Pacific* **122**(887), 119–130.
- Beets, K. (2020), 'What is ray tracing and how is it enabling real-time 3d graphics?', *Embedded* .
URL: <https://www.embedded.com/what-is-ray-tracing-and-how-is-it-enabling-real-time-3d-graphics/>
- Begault, D. R. (1994), *3D Sound for Virtual Reality and Multimedia*, Academic Press Professional, Inc., San Diego, CA, USA.
- Ben-Av, M. B., Sagi, D. & Braun, J. (1992), 'Visual attention and perceptual grouping', *Perception & psychophysics* **52**(3), 277–294.
- Benbassat, A. (n.d.), 'Ear training – a direct and logical path', <https://www.miles.be/articles/ear-training-a-direct-and-logical-path/>. Accessed: 2017-10-24.
- Berg, J. M., Tymoczko, J. L. & Stryer, L. (2002), *Appendix: Depicting Molecular Structures*, New York: W. H. Freeman.
- Berger, C. C., Gonzalez-Franco, M., Tajadura-Jiménez, A., Florencio, D. & Zhang, Z. (2018), 'Generic hrtfs may be good enough in virtual reality. improving source localization through cross-modal plasticity', *Frontiers in Neuroscience* **12**, 21.
URL: <https://www.frontiersin.org/article/10.3389/fnins.2018.00021>
- Berger, M., Tagliasacchi, A., Seversky, L. M., Alliez, P., Guennebaud, G., Levine, J. A., Sharf, A. & Silva, C. T. (2017), 'A survey of surface reconstruction from point clouds', *Comput. Graph. Forum* **36**(1), 301–329.
URL: <https://doi.org/10.1111/cgf.12802>
- Beyer, J., Hadwiger, M. & Pfister, H. (2015), 'State-of-the-art in gpu-based large-scale volume visualization', *Comput. Graph. Forum* **34**(8), 13–37.
URL: <https://doi.org/10.1111/cgf.12605>

- Bianco, R., Harrison, P. M., Hu, M., Bolger, C., Picken, S., Pearce, M. T. & Chait, M. (2020), 'Long-term implicit memory for sequential auditory patterns in humans', *eLife* **9**, e56073.
- Blinn, J. F. (1982), 'A generalization of algebraic surface drawing', *ACM Trans. Graph.* **1**(3), 235–256.
URL: <https://doi.org/10.1145/357306.357310>
- Bly, S. (1982), Presenting information in sound, in 'Proceedings of the CHI '82 Conference on Human Factors in Computer Systems', ACM, pp. 371–375.
- Bonebright, T. L. & Flowers, J. H. (2011), Evaluation of auditory display, in T. Hermann, A. Hunt & J. G. Neuhoff, eds, 'The Sonification Handbook', Logos Publishing House, Berlin, Germany, chapter 6, pp. 111–144.
URL: <http://sonification.de/handbook/chapters/chapter6/>
- Bonneel, N., Drettakis, G., Tsingos, N., Viaud-Delmon, I. & James, D. (2008), 'Fast modal sounds with scalable frequency-domain synthesis', *ACM Trans. Graph.* **27**(3), 24:1–24:9.
URL: <http://doi.acm.org/10.1145/1360612.1360623>
- Boyce, W. P., Lindsay, T., Zgonnikov, A., Rano, I. & Wong-Lin, K. (2020), 'Optimality and limitations of audio-visual integration for cognitive systems'.
- Branets, L., Kubyak, V., Kartasheva, E., Shmyrov, V. & Kandybor, D. (2015), Capturing geologic complexity in a simulation grid, in 'SPE Reservoir Simulation Symposium (23-25 February, Houston, Texas, USA), SPE-173270-MS', Society of Petroleum Engineers.
- Brecheisen, R., Vilanova, A., Platel, B. & ter Haar Romeny, B. M. (2008), Flexible gpu-based multi-volume ray-casting, in 'VMV'.
- Brown, D. J., Simpson, A. J. R. & Proulx, M. J. (2015), 'Auditory scene analysis and sonified visual images. does consonance negatively impact on object formation when using complex sonified stimuli?', *Frontiers in Psychology* **6**, 1522.
URL: <https://www.frontiersin.org/article/10.3389/fpsyg.2015.01522>
- Brown, D., Macpherson, T. & Ward, J. (2011), 'Seeing with sound? exploring different characteristics of a visual-to-auditory sensory substitution device', *Perception* **40**(9), 1120–1135.
- Brown, G. & Cooke, M. (1994), 'Computational auditory scene analysis', *Computer Speech and Language* **8**, 297–336.

- Bryer, A. J., Hadden-Perilla, J. A., Stone, J. E. & Perilla, J. R. (2019), 'High-performance analysis of biomolecular containers to measure small-molecule transport, transbilayer lipid diffusion, and protein cavities', *Journal of Chemical Information and Modeling* **59**(10), 4328–4338. PMID: 31525965.
URL: <https://doi.org/10.1021/acs.jcim.9b00324>
- Cakmak, Y., Daniel, B., Hammer, N., Yilmaz, O., Irmak, C. & Khwaounjoo, P. (2020), 'The human muscular arm avatar as an interactive visualisation tool in learning anatomy: Medical students perspectives', *IEEE Transactions on Learning Technologies* **PP**, 1–1.
- Callahan, S. P., Bavoil, L., Pascucci, V. & Silva, C. T. (2006), Progressive volume rendering of unstructured grids on modern gpus, in 'ACM SIGGRAPH 2006 Sketches', SIGGRAPH '06, Association for Computing Machinery, New York, NY, USA, p. 78–es.
URL: <https://doi.org/10.1145/1179849.1179947>
- Cani, M.-P. & Hornus, S. (2001), 'Subdivision curve primitives: a new solution for interactive implicit modeling'.
URL: <http://maverick.inria.fr/Publications/2001/CH01>
- Carr, J. C., Beatson, R. K., Cherrie, J. B., Mitchell, T. J., Fright, W. R., McCallum, B. C. & Evans, T. R. (2001), Reconstruction and representation of 3d objects with radial basis functions, in 'Computer Graphics (SIGGRAPH '01 Conf. Proc.)', pages 67–76. ACM SIGGRAPH', Springer, pp. 67–76.
- Cassat, S., Serrano, M., Dubois, E. & Irani, P. (2018), A Novel Interaction Paradigm For Exploring Spatio-Temporal Data, in 'Workshop on Multimodal Interaction for Data Visualization, organized as part of the ACM AVI 2018 conference (MultimodalVis 2018)', Grosseto, Italy, p. 0.
URL: <https://hal.archives-ouvertes.fr/hal-02181910>
- Cebulla, J., Kim, E., Rhie, K., Zhang, J. & Pathak, A. P. (2014), 'Multiscale and multi-modality visualization of angiogenesis in a human breast cancer model', *Angiogenesis* **17**(3), 695–709.
URL: <https://doi.org/10.1007/s10456-014-9429-2>
- Chadzynski, T. (2018), 'Example of using gpu- and cpu-based solutions utilizing vulkan graphics and compute api'.
URL: <https://software.intel.com/content/www/us/en/develop/articles/parallel-techniques-in-modeling-particle-systems-using-vulkan-api.html>

- Chanda, P., Park, S. & Kang, T. (2006), A binaural synthesis with multiple sound sources based on spatial features of head-related transfer functions, pp. 1726 – 1730.
- Chatterjee, N., O'Connor, M., Lee, D., Johnson, D. R., Keckler, S. W., Rhu, M. & Dally, W. J. (2017), Architecting an energy-efficient dram system for gpus, *in* '2017 IEEE International Symposium on High Performance Computer Architecture (HPCA)', pp. 73–84.
- Chaudhary, A., Jhaveri, S. J., Sanchez, A., Avila, L. S., Martin, K. M., Vacanti, A., Hanwell, M. D. & Schroeder, W. (2019), 'Cross-platform ubiquitous volume rendering using programmable shaders in vtk for scientific and medical visualization', *IEEE Computer Graphics and Applications* **39**(1), 26–43.
- Chaudhary, A., Jhaveri, S., Sanchez, A., Avila, L., Martin, K., Lonie, D., Hanwell, M. & Schroeder, W. (2018), 'Cross-platform ubiquitous volume rendering using programmable shaders in vtk for scientific and medical visualization', *IEEE Computer Graphics and Applications* **39**.
- Chavent, M., Vanel, A., Tek, A., Levy, B., Robert, S., Raffin, B. & Baaden, M. (2011), 'Gpu-accelerated atom and dynamic bond visualization using hyperballs: A unified algorithm for balls, sticks, and hyperboloids', *Journal of Computational Chemistry* **32**(13), 2924–2935.
- Chen, M. & Tucker, J. V. (2000), 'Constructive volume geometry', *Computer Graphics Forum* **19**(4), 281–293.
URL: <https://onlinelibrary.wiley.com/doi/abs/10.1111/1467-8659.00464>
- Chen, Z., Zeng, W., Yang, Z., Yu, L., Fu, C. & Qu, H. (2020), 'Lassonet: Deep lasso-selection of 3d point clouds', *IEEE Transactions on Visualization and Computer Graphics* **26**(1), 195–204.
- Chen, Z. et al. (2007), An investigation of acoustic impulse response measurement and modeling for small rooms, PhD thesis, Montana State University-Bozeman, College of Engineering.
- Computing, S. & (SCI), I. I. (n.d.), 'Cibc:, 2015. imagevis3d: An interactive visualization software system for large-scale volume data'.
URL: <http://www.imagevis3d.org>
- Cook, P. R. (2002), *Real Sound Synthesis for Interactive Applications*, A. K. Peters, Ltd., Natick, MA, USA.

- Cook, P. R., ed. (1999), *Music, Cognition, and Computerized Sound: An Introduction to Psychoacoustics*, MIT Press, Cambridge, MA, USA.
- Corsini, M., Cignoni, P. & Scopigno, R. (2012), 'Efficient and flexible sampling with blue noise properties of triangular meshes', *IEEE transactions on visualization and computer graphics* **18**, 914–24.
- Cowan, N. (1984), 'On short and long auditory stores.', *Psychological bulletin* **96** **2**, 341–70.
- Crassin, C. (2011), GigaVoxels: A Voxel-Based Rendering Pipeline For Efficient Exploration Of Large And Detailed Scenes, PhD thesis, UNIVERSITE DE GRENOBLE. English and web-optimized version.
URL: <http://maverick.inria.fr/Publications/2011/Cra11>
- Crassin, C. & Green, S. (2012), Octree-based sparse voxelization using the gpu hardware rasterizer, in P. Cozzi & C. Riccio, eds, 'OpenGL Insights', CRC Press, pp. 303–319. <http://www.openglinsights.com/>.
URL: <https://www.seas.upenn.edu/~pcozzi/OpenGLInsights/OpenGLInsights-SparseVoxelization.pdf>
- Crassin, C., Neyret, F., Sainz, M., Green, S. & Eisemann, E. (2011), Interactive indirect illumination using voxel-based cone tracing: An insight, in 'ACM SIGGRAPH 2011 Talks', SIGGRAPH '11, ACM, New York, NY, USA, pp. 20:1–20:1.
URL: <http://doi.acm.org/10.1145/2037826.2037853>
- da Silva, V. & Velho, L. (2020), 'Ray-vr: Ray tracing virtual reality in falcor'.
- Dachuan, L., Li, J., Zhu, B.-Y., Wang, Q.-H., Wang, H.-B. & Wu, P.-H. (2017), 'Elliptical vortex and oblique vortex lattice in the fese superconductor based on the nematicity and mixed superconducting orders', *npj Quantum Materials* **3**.
- Dai, Y., Zheng, J., Yang, Y., Kuai, D. & Yang, X. (2013), 'Volume-rendering-based interactive 3d measurement for quantitative analysis of 3d medical images', *Computational and mathematical methods in medicine* **2013**, 804573.
- Deng, Y., Ni, Y., Li, Z., Mu, S. & Zhang, W. (2017), 'Toward real-time ray tracing: A survey on hardware acceleration and microarchitecture techniques', *ACM Comput. Surv.* **50**(4).
URL: <https://doi.org/10.1145/3104067>
- Deshpande, V., Ashby, M. & Fleck, N. (2001), 'Foam topology: bending versus stretching dominated architectures', *Acta Materialia* **49**(6), 1035 – 1040.
URL: <http://www.sciencedirect.com/science/article/pii/S1359645400003797>

- DIOP, E., Jerbi, T. & Burdin, V. (2010), 'Variational and shape prior-based level set model for image segmentation', *AIP Conference Proceedings* **1281**.
- Djurcilov, S., Kim, K., Lermusiaux, P. & Pang, A. (2001), Volume rendering data with uncertainty information, in D. S. Ebert, J. M. Favre & R. Peikert, eds, 'Data Visualization 2001', Springer Vienna, Vienna, pp. 243–252.
- Dobashi, Y., Yamamoto, T. & Nishita, T. (2003), 'Real-time rendering of aerodynamic sound using sound textures based on computational fluid dynamics', *ACM Trans. Graph.* **22**, 732–740.
URL: <http://doi.acm.org/10.1145/882262.882339>
- Donalek, C., Djorgovski, G., Davidoff, S., Cioc, A., Wang, A., Longo, G., Norris, J., Zhang, J., Lawler, E., Yeh, S., Mahabal, A., Graham, M. & Drake, A. (2014), Immersive and collaborative data visualization using virtual reality platforms.
- Duyne, S. A. V. & Smith, J. O. (1993), Physical modeling with the 2-d digital waveguide mesh, in 'ICMC'.
- Dyer, D. S. (1990), 'A dataflow toolkit for visualization', *IEEE Computer Graphics and Applications* **10**(4), 60–69.
- Dykes, T., Gheller, C., Rivi, M. & Krokos, M. (2016), 'Splotch: porting and optimizing for the xeon phi', *CoRR* **abs/1606.04427**.
URL: <http://arxiv.org/abs/1606.04427>
- Dykes, T., Hassan, A., Gheller, C., Croton, D. & Krokos, M. (2018), 'Interactive 3d visualization for theoretical virtual observatories', *Monthly Notices of the Royal Astronomical Society* **477**(2), 1495–1507.
URL: <http://dx.doi.org/10.1093/mnras/sty855>
- Eisenacher, C., Nichols, G., Selle, A. & Burley, B. (2013), Sorted deferred shading for production path tracing, in 'Proceedings of the Eurographics Symposium on Rendering', EGSR '13, Eurographics Association, Goslar, DEU, p. 125–132.
URL: <https://doi.org/10.1111/cgf.12158>
- El Saddik, A., Orozco, M., Eid, M. & Cha, J. (2011), *Haptics: General Principles*, 1st edn, Springer Publishing Company, Incorporated, pp. 1–20.
- Elorza, D. O. (2006), Room acoustics modeling using the ray-tracing method : implementation and evaluation.

- E.Malikova (2020), 'Visual-auditory api', <https://github.com/EvgMalikova/VAAPI>.
- Essl, G. (2002), 'Physical wave propagation modeling for real-time synthesis of natural sounds. ph.d. thesis'.
- Essl, G., Serafin, S., Cook, P. & Smith, J. (2004), 'Theory of banded waveguides', *Computer Music Journal* **28**(1), 37–50.
- Etiene, T., Kirby, R. & Silva, C. (2015), *An Introduction to Verification of Visualization Techniques*, Synthesis Lectures on Visual Computing: Computer Graphics, Animation, Computational Photography, and Imaging, Morgan & Claypool Publishers.
- Evans, K. K. & Treisman, A. (2010), 'Natural cross-modal mappings between visual and auditory features', *Journal of vision* **10**(1), 6–6.
- Falk, M., Hotz, I., Ljung, P., Treanor, D., Ynnerman, A. & Lundstrom, C. (2017), Transfer function design toolbox for full-color volume datasets, in '2017 IEEE Pacific Visualization Symposium (PacificVis)', pp. 171–179.
- Fang, S., Biddlecome, T. & Tuceryan, M. (1998), Image-based transfer function design for data exploration in volume visualization, in 'Proceedings Visualization '98 (Cat. No.98CB36276)', pp. 319–326.
- Feng, J., Jianzhong, F., Lin, Z., Shang, C. & Li, B. (2018), 'A review of the design methods of complex topology structures for 3d printing', *Visual Computing for Industry, Biomedicine, and Art* **1**.
- Fiebrink, R. & Cook, P. (2010), 'The wekinator: A system for real-time, interactive machine learning in music', *Proceedings of The Eleventh International Society for Music Information Retrieval Conference (ISMIR 2010)*.
- Fishman, E. K., Kuszyk, B. S., Heath, D. G., & Cabral, B. (1996), 'Surgical planning for liver resection', *Computer* **29**(1), 64–72.
- Florian Grond, M. & Dall'Antonia, F. (2008), SUMO. A SONIFICATION UTILITY FOR MOLECULES, in 'Proceedings of the 14th International Conference on Auditory Display, Paris, France, June 24-27'.
- Foley, J. & Ribarsky, B. (1994), *Next-generation data visualization tools*, Georgia Institute of Technology. Available online: <https://smartech.gatech.edu/handle/1853/3594?show=full>.

- Fong, J., Wrenninge, M., Kulla, C. & Habel, R. (2017), Production volume rendering: Siggraph 2017 course, in 'ACM SIGGRAPH 2017 Courses', SIGGRAPH '17, Association for Computing Machinery, New York, NY, USA.
URL: <https://doi.org/10.1145/3084873.3084907>
- Frank, T. (2007), Advanced visualization and modeling of tetrahedral meshes, in D. Wagner, ed., 'Ausgezeichnete Informatikdissertationen 2006', Gesellschaft für Informatik, Bonn, pp. 59–68.
- Franke, L. & Haehn, D. (2020), 'Modern scientific visualizations on the web', *Informatics* 7(4).
URL: <https://www.mdpi.com/2227-9709/7/4/37>
- Frauenberger, C. & Stockman, T. (2009), 'Auditory display design—an investigation of a design pattern approach', *International Journal of Human-Computer Studies* 67(11), 907–922.
- Freeman, E., Wilson, G., Vo, D.-B., Ng, A., Politis, I. & Brewster, S. (2017), The handbook of multimodal-multisensor interfaces, Association for Computing Machinery and Morgan & Claypool, New York, NY, USA, chapter Multimodal Feedback in HCI: Haptics, Non-speech Audio, and Their Applications, pp. 277–317.
URL: <https://doi.org/10.1145/3015783.3015792>
- Frisken, S. F., Perry, R. N., Rockwood, A. P. & Jones, T. R. (2000a), Adaptively sampled distance fields: A general representation of shape for computer graphics, in 'Proceedings of the 27th Annual Conference on Computer Graphics and Interactive Techniques', SIGGRAPH '00, ACM Press/Addison-Wesley Publishing Co., New York, NY, USA, pp. 249–254.
URL: <http://dx.doi.org/10.1145/344779.344899>
- Frisken, S., Perry, R., Rockwood, A. & Jones, T. (2000b), 'Adaptively sampled distance fields: A general representation of shape for computer graphics', *ACM SIGGRAPH* .
- Fryazinov, O., Vilbrandt, T. & Pasko, A. (2013), 'Multi-scale space-variant frep cellular structures', *Computer-Aided Design* 45, 26–34.
- Fuhrmann, A. & Sobottka, G. A. (2003), Distance fields for rapid collision detection in physically based modeling.

- Funkhouser, T., Carlbom, I., Elko, G., Pingali, G., Sondhi, M. & West, J. (1998), A beam tracing approach to acoustic modeling for interactive virtual environments, *in* 'Proceedings of the 25th Annual Conference on Computer Graphics and Interactive Techniques', SIGGRAPH '98, ACM, New York, NY, USA, pp. 21–32.
URL: <http://doi.acm.org/10.1145/280814.280818>
- Fyta, M. (2016), Multiscale, hybrid, and coarse-grained methods, *in* 'Computational Approaches in Physics', 2053-2571, Morgan Claypool Publishers, pp. 7–1 to 7–17.
URL: <http://dx.doi.org/10.1088/978-1-6817-4417-9ch7>
- Férey, N., Nelson, J., MARTIN, C., Picinali, L., Bouyer, G., Tek, A., Bourdot, P., Burkhardt, J.-M., Katz, B., Ammi, M., Etchebest, C. & Autin, L. (2009), 'Multisensory vr interaction for protein-docking in the corsaire project', *Vir. Real* **13**, 273–293.
- Gaither, K., Ebert, D., Geisler, B. & Laidlaw, D. (2004), Panel 2: In the eye of the beholder: The role of perception in scientific visualization, *in* 'IEEE Visualization 2004', pp. 567–568.
- Garanzha, K. (2008), Efficient clustered bvh update algorithm for highly-dynamic models, *in* '2008 IEEE Symposium on Interactive Ray Tracing', pp. 123–130.
- Gardner, B. (1994), Hrtf measurements of a kemar dummy-head microphone.
- Gardner, W., Vercoe, B. & Benton, S. (2000), 'The virtual acoustic room'.
- Gheller, C., Vazza, F., Brüggem, M., Alpaslan, M., Holwerda, B. W., Hopkins, A. M. & Liske, J. (2016), 'Evolution of cosmic filaments and of their galaxy population from mhd cosmological simulations', *Monthly Notices of the Royal Astronomical Society* **462**(1), 448–463.
URL: <http://dx.doi.org/10.1093/mnras/stw1595>
- Gionfrida, L. & Roginska, A. (2017), 'A novel sonification approach to support the diagnosis of alzheimer's dementia', *Frontiers in Neurology* **8**, 647.
URL: <https://www.frontiersin.org/article/10.3389/fneur.2017.00647>
- Gionfrida, L., Roginska, A., Keary, J., Mohanraj, H. & Friedman, K. P. (2016), The triple tone sonification method to enhance the diagnosis of alzheimer's dementia, *in* 'The 22nd International Conference on Auditory Display (ICAD)'.
- Giordano, M. (2016), 'Vibrotactile feedback and stimulation in music performance', http://digitool.library.mcgill.ca/webclient/StreamGate?folder_id=0&dvs=1523974484733~613. Accessed on 2017/12/7.

GLVis gallery (2018). Accessed on 01.01.2018.

URL: <http://glvis.org/gallery>

Goddard, T. D., Brilliant, A. A., Skillman, T. L., Vergenz, S., Tyrwhitt-Drake, J., Meng, E. C. & Ferrin, T. E. (2018), 'Molecular visualization on the holodeck', *Journal of Molecular Biology* **430**(21), 3982 – 3996.

URL: <http://www.sciencedirect.com/science/article/pii/S002228361830696X>

Gourmel, O., Pajot, A., Paulin, M., Barthe, L. & Poulin, P. (2010a), 'Fitted BVH for Fast Raytracing of Metaballs', *Computer Graphics Forum* **29**(2), 281–288.

Gourmel, O., Pajot, A., Paulin, M., Barthe, L. & Poulin, P. (2010b), 'Fitted BVH for Fast Raytracing of Metaballs', *Computer Graphics Forum* .

Grinstein, G. & Smith, S. (1990), Perceptualization of scientific data, in 'Proc. SPIE 1259, Extracting Meaning from Complex Data: Processing, Display, Interaction', pp. 190–199.

Grond, F., Janssen, S., Schirmer, S. & Hermann, T. (2010), 'Browsing rna structures by interactive sonification'.

Grottel, S., Krone, M., Muller, C., Reina, G. & Ertl, T. (2015), 'Megamol – a prototyping framework for particle-based visualization', *Visualization and Computer Graphics, IEEE Transactions on* **21**(2), 201–214.

Haber, R. & McNabb, D. (1990), 'Visualization idioms: a conceptual model for scientific visualization systems', *Visualization in scientific computing. Washington, DC: IEEE Computer Society* pp. 74—93.

Hacihabiboglu, H., Gunel, B. & Kondo, A. M. (2008), 'Time-domain simulation of directive sources in 3-d digital waveguide mesh-based acoustical models', *IEEE Transactions on Audio, Speech, and Language Processing* **16**(5), 934–946.

Hahn, J. K., Fouad, H., Gritz, L. & Lee, J. W. (1998), 'Integrating sounds and motions in virtual environments', *Presence* **7**(1), 67–77.

Haidacher, M., Bruckner, S., Kanitsar, A. & Gröller, M. E. (2008), Information-based transfer functions for multimodal visualization, in 'Proceedings of the First Eurographics Conference on Visual Computing for Biomedicine', EG VCBM'08, Eurographics Association, Aire-la-Ville, Switzerland, Switzerland, pp. 101–108.

- Han, M., Wald, I., Usher, W., Wu, Q., Wang, F., Pascucci, V., Hansen, C. & Johnson, C. (2019), 'Ray tracing generalized tube primitives: Method and applications', *Computer Graphics Forum* **38**.
- Hänel, C., Weyers, B., Hentschel, B. & Kuhlen, T. W. (2014), Interactive Volume Rendering for Immersive Virtual Environments, in 'IEEE VIS International Workshop on 3DVis: Does 3D really make sense for Data Visualization?'
- Hanwell, M., Martin, K., Chaudhary, A. & Avila, L. (2015), 'The visualization toolkit (vtk): Rewriting the rendering code for modern graphics cards', *SoftwareX* **1**.
- Hart, J. C. (1996), 'Sphere tracing: a geometric method for the antialiased ray tracing of implicit surfaces', *The Visual Computer* **12**(10), 527–545.
URL: <https://doi.org/10.1007/s003710050084>
- Hartling, P., Scott, B., Brown, J., Bierbaum, A. & Cruz-Neira, C. (2004), 'Avatar manipulation as a metaphor for virtual reality system simulator interaction'.
- Hatcher, A. (2000), *Algebraic topology*, Cambridge Univ. Press, Cambridge.
URL: <https://cds.cern.ch/record/478079>
- He, Y., Zheng, S., Zhu, F. & Huang, X. (2020), 'Real-time 3d reconstruction of thin surface based on laser line scanner', *Sensors* **20**(2).
URL: <https://www.mdpi.com/1424-8220/20/2/534>
- Heer, J. & Bostock, M. (2010), Crowdsourcing graphical perception: Using mechanical turk to assess visualization design, in 'Proceedings of the SIGCHI Conference on Human Factors in Computing Systems', CHI '10, Association for Computing Machinery, New York, NY, USA, p. 203–212.
URL: <https://doi.org/10.1145/1753326.1753357>
- Hege, H.-C., Hotz, I. & Munzner, T. (2009), 'Euro vis 2009-eurographics/ieee-vgtc symposium on visualization'.
- Hegemann, F., Manickam, P., Lehner, K., Koch, C. & König, M. (2013), 'A hybrid ground data model for interacting simulations in mechanized tunneling', *Journal of Computing in Civil Engineering* **27**.
- Heimann, T. & Meinzer, H.-P. (2009), 'Statistical shape models for 3d medical image segmentation: A review', *Medical image analysis* **13**, 543–63.

- Hendrich, J., Meister, D. & Bittner, J. (2017), 'Parallel bvh construction using progressive hierarchical refinement', *Computer Graphics Forum* **36**(2), 487–494.
URL: <https://onlinelibrary.wiley.com/doi/abs/10.1111/cgf.13143>
- Hermann, T. (2018), Wave space sonification, pp. 49–56.
- Hermann, T., Hunt, A. & Neuhoff, J. G., eds (2011), *The Sonification Handbook*, Logos Publishing House, Berlin, Germany.
URL: <http://sonification.de/handbook>
- Hidaka, S. & Ide, M. (2015), 'Sound can suppress visual perception', *Scientific Reports* **5**.
- Hines, A., Howington, S., White, B., Eslinger, O., Kees, C., Farthing, M., O'Bara, R., Blue, R., Yuan, Y., Bauer, A. & King, B. J. (2009), Computational model builder (cmb): A cross-platform suite of tools for model creation and setup, in '2009 DoD High Performance Computing Modernization Program Users Group Conference', pp. 370–373.
- Hoell, M., Oberweger, M., Arth, C. & Lepetit, V. (2018), Efficient physics-based implementation for realistic hand-object interaction in virtual reality.
- Hoetzlein, R. K. (2016), GVDB: Raytracing Sparse Voxel Database Structures on the GPU, in U. Assarsson & W. Hunt, eds, 'Eurographics/ ACM SIGGRAPH Symposium on High Performance Graphics', The Eurographics Association.
- Hormann, K. & Floater, M. (2006), 'Mean value coordinates for arbitrary planar polygons', *ACM Trans. Graph.* **25**, 1424–1441.
- Huang, W., Eades, P. & Hong, S.-H. (2009), 'Measuring effectiveness of graph visualizations: A cognitive load perspective', *Information Visualization* **8**(3), 139–152.
URL: <https://doi.org/10.1057/ivs.2009.10>
- Huang, Y. & Benesty, J. (2004), *Audio Signal Processing for Next-Generation Multimedia Communication Systems*, Kluwer Academic Publishers, USA.
- Hunt, A. & Hermann, T. (2011), Interactive sonification, in T. Hermann, A. Hunt & J. G. Neuhoff, eds, 'The Sonification Handbook', Logos Publishing House, Berlin, Germany, chapter 11, pp. 273–298.
URL: <http://sonification.de/handbook/chapters/chapter11/>
- Hurter, C., Riche, N. H., Drucker, S. M., Cordeil, M., Alligier, R. & Vuillemot, R. (2018), 'Fiberclay: Sculpting three dimensional trajectories to reveal structural insights', *IEEE transactions on visualization and computer graphics* **25**(1), 704–714.

Icosahedral water clusters (2018). Also we have used the open access data from this web resource.

URL: http://www.payonline.lsbu.ac.uk/water/icosahedral_water_clusters.html

Im, M.-Y., Fischer, P., Yamada, K., Sato, T., Kasai, S., Nakatani, Y. & Ono, T. (2012), ‘Symmetry breaking in the formation of magnetic vortex states in a permalloy nanodisk’, *Nature communications* **3**, 983.

Imagination announces PowerVR wizard GPU family: Rogue learns ray tracing (retrieved 2019).

URL: <https://www.anandtech.com/show/7870/imagination-announces-powervr-wizard-gpu-family-rogue-learns-ray-tracing>

Izadi, S., Kim, D., Hilliges, O., Molyneaux, D., Newcombe, R., Kohli, P., Shotton, J., Hodges, S., Freeman, D., Davison, A. & Fitzgibbon, A. (2011), Kinectfusion: Real-time 3d reconstruction and interaction using a moving depth camera, in ‘UIST ’11 Proceedings of the 24th annual ACM symposium on User interface software and technology’, ACM, pp. 559–568.

URL: <https://www.microsoft.com/en-us/research/publication/kinectfusion-real-time-3d-reconstruction-and-interaction-using-a-moving-depth-camera/>

J. Blauert (1999), *Spatial hearing – The psychophysics of human sound localization*, The MIT Press.

j. van Erp, B. & Self, B. (2008), ‘Tactile displays for orientation, navigation and communication in air, sea and land environments (les systemes d’affichage tactiles pour l’orientation, la navigation et la communication dans les environnements aerien, maritime et terrestre)’, p. 114.

Jackson, T., Jackson, T. R., Liu, H., Liu, H., Patrikalakis, N. M., Patrikalakis, N. M., Sachs, E. M., Sachs, E. M., Cima, M. J. & Cima, M. J. (1999), ‘Modeling and designing functionally graded material components for fabrication with local composition control’.

Jakob, W. (2020), ‘Differentiable simulation of light: Why it is important, and what makes it hard!’.

URL: <https://www.highperformancegraphics.org/2020/program/>

Jakob, W., Rhineland, J. & Moldovan, D. (2016), ‘pybind11 — seamless operability between c++11 and python’. <https://github.com/pybind/pybind11>.

- Jiang, Y., Ji, D., Han, Z. & Zwicker, M. (2019), 'Sdfdif: Differentiable rendering of signed distance fields for 3d shape optimization'.
- Johnson, C. (2004), 'Top scientific visualization research problems', *IEEE Comput. Graph. Appl.* **24**(4), 13–17.
URL: <http://dx.doi.org/10.1109/MCG.2004.20>
- Jones, M. W., Bærentzen, A. & Šrámek, M. (2006), '3d distance fields: A survey of techniques and applications', *IEEE Transactions on Visualization and Computer Graphics* **12**(4), 581–599.
- Jordan, D. & Shepard, R. (1987), 'Tonal schemas: evidence obtained by probing distorted musical scales', *Perception amp; psychophysics* **41**(6), 489—504.
URL: <https://doi.org/10.3758/bf03210484>
- Jung, Y., Kim, J., Kumar, A., Feng, D. & Fulham, M. (2018), 'Feature of interest-based direct volume rendering using contextual saliency-driven ray profile analysis', *Computer Graphics Forum* **37**(6), 5–19.
URL: <https://onlinelibrary.wiley.com/doi/abs/10.1111/cgf.13308>
- Juntu, J., Sijbers, J., Dyck, D. & Gielen, J. (2005), 'Bias field correction for mri images', *Computer Recognition Systems. Advances in Soft Computing* **30**, 543–551.
- Jönsson, D., Sundén, E., Ynnerman, A. & Ropinski, T. (n.d.), 'A survey of volumetric illumination techniques for interactive volume rendering', *Computer Graphics Forum* **33**(1), 27–51.
URL: <https://onlinelibrary.wiley.com/doi/abs/10.1111/cgf.12252>
- Kainz, B., Grabner, M., Bornik, A., Hauswiesner, S., Muehl, J. & Schmalstieg, D. (2009), 'Ray casting of multiple volumetric datasets with polyhedral boundaries on manycore gpus', *ACM Trans. Graph.* **28**(5), 1–9.
URL: <https://doi.org/10.1145/1618452.1618498>
- Kajiya, J. & von Herzen, B. (1984), 'Ray tracing volume densities', *ACM SIGGRAPH Computer Graphics* **18**, 165–174.
- Kalarat, K. & Koomhin, P. (2019), 'Real-time volume rendering interaction in virtual reality', *International Journal of Technology* **10**, 1307.
- Kalkofen, D., Sandor, C., White, S. & Schmalstieg, D. (2011), *Visualization Techniques for Augmented Reality*, pp. 65–98.

- Kam, H. R., Lee, S., Park, T. & Kim, C.-H. (2015), 'Rviz: a toolkit for real domain data visualization', *Telecommunication Systems* **60**, 337–345.
- Kaper, H., Wiebel, E. & Típei, S. (1999), Data sonification and sound visualization, in 'Computing in Science and Engineering', Vol. 1, pp. 48–58.
- Kapur, A., Cook, P. R., Salazar, S. & Wang, G. (2015), *Programming for Musicians and Digital Artists: Creating Music with ChucK*, 1st edn, Manning Publications Co., Greenwich, CT, USA.
- Kartasheva, E., Adzhiev, V., Comminos, P., Fryazinov, O. & Pasko, A. (2008), *An Implicit Complexes Framework for Heterogeneous Objects Modelling*, Springer Berlin Heidelberg, Berlin, Heidelberg, pp. 1–41.
URL: https://doi.org/10.1007/978-3-540-68443-5_1
- Kartasheva, E., Adzhiev, V., Comminos, P., Pasko, A. & Schmitt, B. (2005), 'Construction of implicit complexes: A case study'.
- Kaufman, A. & Mueller, K. (2005), *Overview of Volume Rendering*, Vol. 7, pp. 127–XI.
- Kauker, D., Falk, M., Reina, G., Ynnerman, A. & Ertl, T. (2016), 'Voxlink - combining sparse volumetric data and geometry for efficient rendering', *Comput. Vis. Media* **2**(1), 45–56.
URL: <https://doi.org/10.1007/s41095-016-0034-8>
- Kazhdan, M. & Hoppe, H. (2013), 'Screened poisson surface reconstruction', *ACM Trans. Graph.* **32**(3), 29:1–29:13.
URL: <http://doi.acm.org/10.1145/2487228.2487237>
- Keefe, D. F. & Isenberg, T. (2013), 'Reimagining the scientific visualization interaction paradigm', *Computer* **46**(5), 51–57.
- Keim, D. A., Mansmann, F., Schneidewind, J., Thomas, J. & Ziegler, H. (2008), Visual data mining, Springer-Verlag, Berlin, Heidelberg, chapter Visual Analytics: Scope and Challenges, pp. 76–90.
- Keinert, B., Schäfer, H., Korndörfer, J., Ganse, U. & Stamminger, M. (2014), Enhanced Sphere Tracing, in A. Giachetti, ed., 'Smart Tools and Apps for Graphics - Eurographics Italian Chapter Conference', The Eurographics Association.
- Keller, A., Křivánek, J., Novák, J., Kaplanyan, A. & Salvi, M. (2018), Machine learning and rendering, in 'ACM SIGGRAPH 2018 Courses', SIGGRAPH '18, Association for

- Computing Machinery, New York, NY, USA.
URL: <https://doi.org/10.1145/3214834.3214841>
- Kikinis, R., Pieper, S. D. & Vosburgh, K. G. (2014), *3D Slicer: A Platform for Subject-Specific Image Analysis, Visualization, and Clinical Support*, Springer New York, New York, NY, pp. 277–289.
- Kniss, J., Kindlmann, G. & Hansen, C. (2001), Interactive volume rendering using multi-dimensional transfer functions and direct manipulation widgets, in ‘Proceedings Visualization, 2001. VIS ’01.’, pp. 255–562.
- Kniss, J., Kindlmann, G. & Hansen, C. (2002), ‘Multidimensional transfer functions for interactive volume rendering’, *IEEE Transactions on Visualization and Computer Graphics* **8**(3), 270–285.
URL: <https://doi.org/10.1109/TVCG.2002.1021579>
- Kniss, J., Premoze, S., Hansen, C., Shirley, P. & McPherson, A. (2003), ‘A model for volume lighting and modeling’, *IEEE Transactions on Visualization and Computer Graphics* **9**(2), 150–162.
- Knoll, A. M. (2009), ‘Ray tracing implicit surfaces for interactive visualization. phd thesis’, <http://www.cs.utah.edu/~knolla/thesis.pdf>.
- Knoll, A. M., Wald, I. & Hansen, C. D. (2009), ‘Coherent multiresolution isosurface ray tracing’, *Vis. Comput.* **25**(3), 209–225.
URL: <http://dx.doi.org/10.1007/s00371-008-0215-2>
- Knoll, A., Morley, R. K., Wald, I., Leaf, N. & Messmer, P. (2019), *Efficient Particle Volume Splatting in a Ray Tracer*, Apress, Berkeley, CA, pp. 533–541.
URL: https://doi.org/10.1007/978-1-4842-4427-2_29
- Knoll, A., Wald, I., Navratil, P., Bowen, A., Reda, K., Papka, M. E. & Gaither, K. (2014), Rbf volume ray casting on multicore and manycore cpus, in ‘Proceedings of the 16th Eurographics Conference on Visualization’, EuroVis ’14, Eurographics Association, Aire-la-Ville, Switzerland, Switzerland, pp. 71–80.
- Kopta, D. (2016), Ray Tracing From a Data Movement Perspective, PhD thesis, The University of Utah.
- Kopta, D., Shkurko, K., Spjut, J., Brunvand, E. & Davis, A. (2015), ‘Memory considerations for low energy ray tracing’, *Computer Graphics Forum* **34**(1), 47–59.
URL: <https://onlinelibrary.wiley.com/doi/abs/10.1111/cgf.12458>

- Koribalski, B. S., Wang, J., Kamphuis, P., Westmeier, T., Staveley-Smith, L., Oh, S.-H., López-Sánchez, R., Wong, O. I., Ott, J., de Blok, W. J. G. & et al. (2018), 'The local volume hi survey (lvhis)', *Monthly Notices of the Royal Astronomical Society* **478**(2), 1611–1648.
URL: <http://dx.doi.org/10.1093/mnras/sty479>
- Koschier, D., Deul, C. & Bender, J. (2016), Hierarchical hp-adaptive signed distance fields, in 'Proceedings of the ACM SIGGRAPH/Eurographics Symposium on Computer Animation', SCA '16, Eurographics Association, Goslar, DEU, p. 189–198.
- Koungelis, D. K. & Augarde, C. E. (2008), 'Parameterised mesh generation for finite element analysis of tunnelling', *Computers and Geotechnics* pp. 1–41.
- Kouřil, D., Čmolík, L., Kozlíková, B., Wu, H., Johnson, G., Goodsell, D. S., Olson, A., Gröller, M. E. & Viola, I. (2019), 'Labels on levels: Labeling of multi-scale multi-instance and crowded 3d biological environments', *IEEE Transactions on Visualization and Computer Graphics* **25**(1), 977–986.
- Kozlikova, B., Schreck, T. & Wischgoll, T., eds (2017), *Molecular Visualization of Computational Biology Data: A Survey of Surveys*, EuroVis 2017 - Short Papers, The Eurographics Association, The Eurographics Association, Barcelona, Spain.
URL: <https://hal.archives-ouvertes.fr/hal-01644549>
- Kramer, G. (1994), *Auditory display: sonification, audification, and auditory interfaces*, Proceedings ; vol.18, Addison-Wesley, Reading, Mass Wokingham.
URL: <http://capitadiscovery.co.uk/bournemouth-ac/items/212475>
- Kulla, C. & Fajardo, M. (2012), 'Importance sampling techniques for path tracing in participating media', *Comput. Graph. Forum* **31**(4), 1519–1528.
URL: <https://doi.org/10.1111/j.1467-8659.2012.03148.x>
- Kurzeja, K. & Rossignac, J. (2019), 'Rangefinder: Accelerating ball-interference queries against steady lattices', *Computer-Aided Design* **112**, 14 – 22.
URL: <http://www.sciencedirect.com/science/article/pii/S0010448518303890>
- Laha, B. & Bowman, D. A. (2013), Interactive coarse segmentation and analysis of volume data with a suite of 3d interaction tools, in 'IEEE VR Workshop on Immersive Volume Interaction (WIVI)', Orlando, FL.

- Laha, B. & Bowman, D. A. (2014), Design of the bare-hand volume cracker for analysis of raw volumetric data, *in* 'IEEE VR Workshop on Immersive Volume Interaction (WIVI)', Minneapolis, MN.
- Lawonn, K., Smit, N., Bühler, K. & Preim, B. (2018), 'A survey on multimodal medical data visualization', *Computer Graphics Forum* **37**(1), 413–438.
URL: <https://onlinelibrary.wiley.com/doi/abs/10.1111/cgf.13306>
- Lee, B., Srinivasan, A., Stasko, J., Tory, M. & Setlur, V. (2018), Multimodal interaction for data visualization, *in* 'Proceedings of the 2018 International Conference on Advanced Visual Interfaces', AVI '18, Association for Computing Machinery, New York, NY, USA.
URL: <https://doi.org/10.1145/3206505.3206602>
- Lehericey, F., Gouranton, V. & Arnaldi, B. (2015), Gpu ray-traced collision detection for cloth simulation, *in* 'Proceedings of the 21st ACM Symposium on Virtual Reality Software and Technology', VRST '15, Association for Computing Machinery, New York, NY, USA, p. 47–50.
URL: <https://doi.org/10.1145/2821592.2821615>
- Leonard, J. & Villeneuve, J. (2019), mi-gen : An Efficient and Accessible Mass-Interaction Sound Synthesis Toolbox, *in* 'SMC 2019 - 16th Sound & Music Computing Conference', Malaga, Spain.
URL: <https://hal.archives-ouvertes.fr/hal-02270792>
- Lepage, G. P. (1980), 'VEGAS: AN ADAPTIVE MULTIDIMENSIONAL INTEGRATION PROGRAM'.
- Lepore, F., Green, A., Chapman, C. E. & Kalaska, J. F. (2011), *Enhancing Performance for Action and Perception: Multisensory integration, Neuroplasticity and Neuroprosthetics, Part II*, Elsevier.
- Lerdahl, F. (1988), 'Tonal pitch space', *Music perception* **5**(3), 315–349.
- Levoy, M. (1988), 'Display of surfaces from volume data', *IEEE Comput. Graph. Appl.* **8**(3), 29–37.
- Lewis, J. W., Beauchamp, M. S. & DeYoe, E. A. (2000), 'A Comparison of Visual and Auditory Motion Processing in Human Cerebral Cortex', *Cerebral Cortex* **10**(9), 873–888.
URL: <https://doi.org/10.1093/cercor/10.9.873>

- Leyrer, M., Linkenauger, S. A., Bühlhoff, H. H., Kloos, U. & Mohler, B. (2011), The influence of eye height and avatars on egocentric distance estimates in immersive virtual environments, *in* 'Proceedings of the ACM SIGGRAPH Symposium on Applied Perception in Graphics and Visualization', APGV '11, Association for Computing Machinery, New York, NY, USA, p. 67–74.
URL: <https://doi.org/10.1145/2077451.2077464>
- Li, A., Song, S. L., Chen, J., Li, J., Liu, X., Tallent, N. R. & Barker, K. J. (2020), 'Evaluating modern gpu interconnect: Pcie, nvlink, nv-sli, nvswitch and gpudirect', *IEEE Transactions on Parallel and Distributed Systems* **31**(1), 94–110.
URL: <http://dx.doi.org/10.1109/TPDS.2019.2928289>
- Li, B., Jianzhong, F., Feng, J., Shang, C. & Lin, Z. (2020), 'Review of heterogeneous material objects modeling in additive manufacturing', *Visual Computing for Industry, Biomedicine, and Art* **3**.
- Lin Lu, Andrei Sharf, H. Z. Y. W. Q. F. X. C. Y. S. C. T. D. C.-O. B. C. (2014), 'Build-to-last: Strength to weight 3d printed objects', *ACM Trans. Graph. (Proc. SIGGRAPH)* **33**(4), 97:1–97:10.
- Liu, D. & van der Heide, E. (2019), Interactive auditory navigation in molecular structures of amino acids: A case study using multiple concurrent sound sources representing nearby atoms, *in* '25th International Conference on Auditory Display (ICAD 2019) 23-27 June 2019, Northumbria University, Newcastle upon Tyne, UK.', Georgia Institute of Technology.
- Liu, L., Yu, X., Wan, W., Yu, H. & Liu, R. (2012), Rendering of large-scale 3d terrain point cloud based on out-of-core, *in* '2012 International Conference on Audio, Language and Image Processing', pp. 740–744.
- Liu, Q. & Sourin, A. (2006), 'Function-defined shape metamorphoses in visual cyberworlds', *The Visual Computer* **22**, 977–990.
- Liu, S. X. (2009), 'Symmetry and asymmetry analysis and its implications to computer-aided diagnosis: A review of the literature', *Journal of Biomedical Informatics* **42**(6), 1056 – 1064.
URL: <http://www.sciencedirect.com/science/article/pii/S1532046409000975>
- Liu, X. & Shapiro, V. (2018), 'Multiscale shape–material modeling by composition', *Computer-Aided Design* **102**, 194–203. Proceeding of SPM 2018 Symposium.
URL: <https://www.sciencedirect.com/science/article/pii/S0010448518302446>

- Liu, Y. (2013), Effects of mesh density on finite element analysis, Vol. 2.
- Ljung, P. (2006), Efficient Methods for Direct Volume Rendering of Large Data Sets, PhD thesis, Linköping University Linköping University, Visual Information Technology and Applications (VITA), The Institute of Technology.
- Ljung, P., Krüger, J., Groller, E., Hadwiger, M., Hansen, C. D. & Ynnerman, A. (2016), ‘State of the art in transfer functions for direct volume rendering’, *Computer Graphics Forum* **35**(3), 669–691.
URL: <https://onlinelibrary.wiley.com/doi/abs/10.1111/cgf.12934>
- Loboda, O., Goncharuk, V. & Dumanskii, A. (2009), ‘Theoretical study on icosahedral water clusters’, *Chemical Physics Letters - CHEM PHYS LETT* **484**.
- Lodha, S. K., Beahan, J., Heppe, T., Joseph, A. J. & Zane-Ulman, B. (1997), Muse : A musical data sonification toolkit.
- Long, B., Seah, S. A., Carter, T. & Subramanian, S. (2014), ‘Rendering volumetric haptic shapes in mid-air using ultrasound’, *ACM Trans. Graph.* **33**(6), 181:1–181:10.
URL: <http://doi.acm.org/10.1145/2661229.2661257>
- Luck, W. (1991), *Water — The Most Anomalous Liquid*, pp. 217–249.
- Lundström, C., Ljung, P. & Ynnerman, A. (2006), Multi-Dimensional Transfer Function Design Using Sorted Histograms, in R. Machiraju & T. Moeller, eds, ‘Volume Graphics’, The Eurographics Association.
- Luo, S. & Dingliana, J. (2017), Intuitive transfer function editing using relative visibility histograms, in ‘IEEE Visualization Posters’.
URL: <https://vimeo.com/230875337>
- Luongo, A., Falster, V., Doest, M., Ribo, M., Eiriksson, E., Pedersen, D. & Frisvad, J. (2020), ‘Microstructure control in 3d printing with digital light processing’, *Computer Graphics Forum (Online)* **39**(1), 347–359.
- MacDonald, D. & Stockman, T. (2014), ‘Towards a method, techniques and tools to support the development of auditory displays’, *HCI Engineering* p. 29.
- Maciejewski, R., Choi, S., Ebert, D. S. & Tan, H. Z. (2005), Multi-modal perceptualization of volumetric data and its application to molecular docking, in ‘First Joint Eurohaptics Conference and Symposium on Haptic Interfaces for Virtual Environment and Teleoperator Systems. World Haptics Conference’, pp. 511–514.

- Maidenbaum, S., Levy-Tzedek, S., Chebat, D.-R. & Amedi, A. (2013), 'Increasing accessibility to the blind of virtual environments, using a virtual mobility aid based on the "eyecane": Feasibility study', *PloS one* **8**(8), e72555.
- Maleike, D., Nolden, M., Meinzer, H. P. & Wolf, I. (2009), 'Interactive segmentation framework of the medical imaging interaction toolkit', *Comput. Methods Prog. Biomed.* **96**(1), 72–83.
URL: <http://dx.doi.org/10.1016/j.cmpb.2009.04.004>
- Malikova, E., Adzhiev, V., Fryazinov, O. & Pasko, A. (2019), Visual-auditory volume rendering of scalar fields, in '25th International Conference on Auditory Display (ICAD 2019)'.
URL: <https://smartech.gatech.edu/handle/1853/61517>
- Malikova, E., Adzhiev, V., Fryazinov, O. & Pasko, A. A. (2020), Visual-auditory volume rendering of dynamic quantum chemistry molecular fields, in A. Kerren, C. Hurter & J. Braz, eds, 'Proceedings of the 15th International Joint Conference on Computer Vision, Imaging and Computer Graphics Theory and Applications, VISIGRAPP 2020, Volume 3: IVAPP, Valletta, Malta, February 27-29, 2020', SCITEPRESS, pp. 193–200.
URL: <https://doi.org/10.5220/0008957001930200>
- Maloca, P., de Carvalho, J., Heeren, T., Hasler, P., Mushtaq, F., Mon-Williams, M., Scholl, H., Balaskas, K., Egan, C., Tufail, A., Witthauer, L. & Cattin, P. (2018), 'High-performance virtual reality volume rendering of original optical coherence tomography point-cloud data enhanced with real-time ray casting', *Translational Vision Science & Technology* **7**(4). Copyright 2018 The Authors. This work is licensed under a Creative Commons Attribution-NonCommercial-NoDerivatives 4.0 International License. A copy of the licence can be found at: <https://creativecommons.org/licenses/by-nc-nd/4.0/>.
URL: <http://eprints.whiterose.ac.uk/133207/>
- Malpica, S., Gutiérrez, D. & Masia, B. (2020), 'Auditory stimuli degrade visual performance in virtual reality', *Scientific Reports* **10**, 12363.
- Manssour, I., Furuie, S., Nedel, L. & Freitas, C. (2001), A framework to visualize and interact with multimodal medical images, in K. Mueller & A. E. Kaufman, eds, 'Volume Graphics 2001', Springer Vienna, Vienna, pp. 385–398.
- Martí-Bonmati, L., Sopena, R., Bartumeus, P. & Sopena, P. (2010), 'Multimodality imaging techniques', *Contrast Media & Molecular Imaging* **5**(4), 180–189.
URL: <https://onlinelibrary.wiley.com/doi/abs/10.1002/cmimi.393>

- Max, N. & Chen, M. (2010), Local and global illumination in the volume rendering integral, in 'Scientific Visualization: Advanced Concepts', pp. 259–274.
- Max, N., Hanrahan, P. & Crawfis, R. (1990), 'Area and volume coherence for efficient visualization of 3d scalar functions', *SIGGRAPH Comput. Graph.* **24**(5), 27–33.
URL: <https://doi.org/10.1145/99308.99315>
- May, K. R., Sobel, B., Wilson, J. & Walker, B. N. (2019), Auditory displays to facilitate object targeting in 3d space, in '25th International Conference on Auditory Display (ICAD 2019) 23-27 June 2019, Northumbria University, Newcastle upon Tyne, UK.', Georgia Institute of Technology.
- McArthur, A., Sandler, M. & Stewart, R. (2017), Distance in audio for vr: Constraints and opportunities, in 'Proceedings of the 12th International Audio Mostly Conference on Augmented and Participatory Sound and Music Experiences', AM '17, ACM, New York, NY, USA, pp. 28:1–28:7.
- McCormick, B. H. (1988), 'Visualization in scientific computing', *SIGBIO Newsl.* **10**(1), 15–21.
URL: <http://doi.acm.org/10.1145/43965.43966>
- McGookin, D. K. & Brewster, S. A. (2004), 'Understanding concurrent earcons: Applying auditory scene analysis principles to concurrent earcon recognition', *ACM Trans. Appl. Percept.* **1**(2), 130–155.
URL: <https://doi.org/10.1145/1024083.1024087>
- McNeely, W. A., Puterbaugh, K. D. & Troy, J. J. (1999), Six degree-of-freedom haptic rendering using voxel sampling, in 'Proceedings of the 26th Annual Conference on Computer Graphics and Interactive Techniques', SIGGRAPH '99, ACM Press/Addison-Wesley Publishing Co., New York, NY, USA, pp. 401–408.
URL: <http://dx.doi.org/10.1145/311535.311600>
- Meibner, M., Pfister, H., Westermann, R. & Wittenbrink, C. (2000), 'Volume visualization and volume rendering techniques'.
- Meredith, J. S., Ahern, S., Pugmire, D. & Sisneros, R. (2012), EAVL: The Extreme-scale Analysis and Visualization Library, in H. Childs, T. Kuhlen & F. Marton, eds, 'Eurographics Symposium on Parallel Graphics and Visualization', The Eurographics Association.

- Merimaa, J. (2006), 'Analysis, synthesis, and perception of spatial sound – binaural localization modeling and multichannel loudspeaker reproduction. phd thesis'.
URL: <http://lib.tkk.fi/Diss/2006/isbn9512282917/isbn9512282917.pdf>
- Miao, H., Klein, T., Kouřil, D., Mindek, P., Schatz, K., Gröller, M. E., Kozlíková, B., Isenberg, T. & Viola, I. (2019), 'Multiscale Molecular Visualization', *Journal of Molecular Biology* **431**(6), 1049–1070.
URL: <https://hal.inria.fr/hal-01873724>
- Miao, H., Klein, T., Kouřil, D., Mindek, P., Schatz, K., Gröller, M. E., Kozlíková, B., Isenberg, T. & Viola, I. (2019), 'Multiscale molecular visualization', *Journal of Molecular Biology* **431**(6), 1049 – 1070.
- Microsoft (2020), 'Analysis toolpack'.
URL: <https://support.microsoft.com/en-us/office/load-the-analysis-toolpak-in-excel-6a63e598-cd6d-42e3-9317-6b40ba1a66b4>
- Minghim, R. & Forrest, A. R. (1995), An illustrated analysis of sonification for scientific visualisation, in 'Proceedings Visualization '95', pp. 110–117.
- MITK Release notes 2016* (2016).
URL: http://mitk.org/wiki/MITK_ReleaseNotes2016.11
- Mohan, J., Krishnaveni, V. & Guo, Y. (2014), 'A survey on the magnetic resonance image denoising methods', *Biomedical Signal Processing and Control* **9**, 56 – 69.
URL: <http://www.sciencedirect.com/science/article/pii/S1746809413001407>
- Moloney, J., Spehar, B., Globa, A. & Wang, R. (2018), 'The affordance of virtual reality to enable the sensory representation of multi-dimensional data for immersive analytics: from experience to insight', *Journal of Big Data* **5**.
- Moon, B., Byun, Y., Kim, T.-J., Claudio, P., Kim, H.-S., Ban, Y.-J., Nam, S. W. & Yoon, S.-E. (2010), 'Cache-oblivious ray reordering', *ACM Trans. Graph.* **29**(3), 1–10.
- Moore, B. (2012), *An Introduction to the Psychology of Hearing*, Emerald.
URL: <https://books.google.co.uk/books?id=LM9U8e28pLMC>
- Moreau, P. & Clarberg, P. (2019), *Importance Sampling of Many Lights on the GPU*, Apress, Berkeley, CA, pp. 255–283.
URL: https://doi.org/10.1007/978-1-4842-4427-2_18

- Moreland, K. (2013), 'A survey of visualization pipelines', *IEEE Transactions on Visualization and Computer Graphics* **19**(3), 367–378.
URL: <https://doi.org/10.1109/TVCG.2012.133>
- Moreland, K., Ayachit, U., Geveci, B. & Ma, K.-L. (2011), 'Dax toolkit: A proposed framework for data analysis and visualization at extreme scale', *1st IEEE Symposium on Large-Scale Data Analysis and Visualization 2011, LDAV 2011 - Proceedings* .
- Moreland, K., Sewell, C., Usher, W., Lo, L.-t., Meredith, J., Pugmire, D., Kress, J., Schroots, H., Ma, K. L., Childs, H., Larsen, M., Chen, C. M., Maynard, R. & Geveci, B. (2016), 'Vtk-m: Accelerating the visualization toolkit for massively threaded architectures', *IEEE Computer Graphics and Applications* **36**(3).
- Morriscal, N., Usher, W., Wald, I. & Pascucci, V. (2019), Efficient space skipping and adaptive sampling of unstructured volumes using hardware accelerated ray tracing, *in* '30th IEEE Visualization Conference, IEEE VIS 2019 - Short Papers, Vancouver, BC, Canada, October 20-25, 2019', IEEE, pp. 256–260.
URL: <https://doi.org/10.1109/VISUAL.2019.8933539>
- M.S.Gordon & M.W.Schmidt (2005), *Advances in electronic structure theory: GAMESS a decade later*, Elsevier.
- Müller, K., Techmann, T. & Fellner, W.-D. (2003), 'Adaptive ray tracing of subdivision surfaces.', *Computer Graphics Forum* **22**(3), 553–562.
- Murphy, D., Kelloniemi, A., Mullen, J. & Shelley, S. (2007), 'Acoustic modeling using the digital waveguide mesh', *IEEE Signal Processing Magazine* **24**, 55–66.
- Museth, K. (2013), 'Vdb: High-resolution sparse volumes with dynamic topology', *ACM Trans. Graph.* **32**(3), 27:1–27:22.
URL: <http://doi.acm.org/10.1145/2487228.2487235>
- Muzic, M. L., Autin, L., Parulek, J. & Viola, I. (2015), cellVIEW: a Tool for Illustrative and Multi-Scale Rendering of Large Biomolecular Datasets, *in* K. Bühler, L. Linsen & N. W. John, eds, 'Eurographics Workshop on Visual Computing for Biology and Medicine', The Eurographics Association.
- Neuhoff, J. G. (2011), Perception, cognition and action in auditory display, *in* T. Hermann, A. Hunt & J. G. Neuhoff, eds, 'The Sonification Handbook', Logos Publishing House, Berlin, Germany, chapter 4, pp. 63–85.
URL: <http://sonification.de/handbook/chapters/chapter4/>

- Neuhoff, J., Kramer, G. & Wayand, J. (2002), 'Pitch and loudness interact in auditory displays: Can the data get lost in the map?', *Journal of experimental psychology. Applied* **8**, 17–25.
- Nguyen, A. (2006), *Implicit Bounding Volumes and Bounding Volume Hierarchies*, PhD thesis, Stanford, CA, USA. AAI3235306.
- Nie, B., Chen, G., Luo, X. & Liu, B. (2019), 'Error mechanism and self-calibration of single-axis rotational inertial navigation system', *Mathematical Problems in Engineering* **2019**, 1–11.
- Norman, M. R. (2016), 'Materials design for new superconductors', *Reports on Progress in Physics* **79**(7), 074502.
URL: <https://doi.org/10.1088/0034-4885/79/7/074502>
- North, C. (2006), 'Toward measuring visualization insight', *IEEE Computer Graphics and Applications* **26**(3), 6–9.
- Nukarinen, T., Kangas, J., Rantala, J., Koskinen, O. & Raisamo, R. (2018), Evaluating ray casting and two gaze-based pointing techniques for object selection in virtual reality, pp. 1–2.
- NVIDIA (2018), 'Nvidia gvdb voxels 1.1. programming guide', https://github.com/NVIDIA/gvdb-voxels/blob/master/GVDB_Programming_Guide_1.1.pdf.
- O., C. (n.d.), 'Dear imgui'.
URL: <https://github.com/ocornut/imgui>
- O'Brien, J. F., Cook, P. R. & Essl, G. (2001), Synthesizing sounds from physically based motion, in 'Proceedings of ACM SIGGRAPH 2001', pp. 529–536.
- O'Brien, J. F., Shen, C. & Gatchalian, C. M. (2002), Synthesizing sounds from rigid-body simulations, in 'Proceedings of the 2002 ACM SIGGRAPH/Eurographics Symposium on Computer Animation', SCA '02, ACM, New York, NY, USA, pp. 175–181.
URL: <http://doi.acm.org/10.1145/545261.545290>
- of York, U. (n.d.), 'Dynamic 3d digital waveguide mesh voice synthesis', <https://www.york.ac.uk/electronic-engineering/research/communication-technologies/projects/3d-mesh-voice/>.

- Ogi, T. & Hirose, M. (1996), Multisensory data sensualization based on human perception, in 'VRAIS '96 Proceedings of the 1996 Virtual Reality Annual International Symposium', pp. 66–71.
- Ojha, D., Karhan, K. & Kühne, T. (2018), 'On the hydrogen bond strength and vibrational spectroscopy of liquid water', *Scientific reports* **8**.
- Ostromoukhov, V., Donohue, C. & Jodoin, P.-M. (2004), 'Fast hierarchical importance sampling with blue noise properties', **23**(3).
URL: <https://doi.org/10.1145/1015706.1015750>
- Otaduy, M. A. & Lin, M. C. (2005), Introduction to haptic rendering, in 'ACM SIGGRAPH 2005 Courses', SIGGRAPH '05, ACM, New York, NY, USA.
URL: <http://doi.acm.org/10.1145/1198555.1198603>
- Pantaleoni, J. & Luebke, D. (2010), Hlbvh: Hierarchical lbvh construction for real-time ray tracing of dynamic geometry, in 'Proceedings of the Conference on High Performance Graphics', HPG '10, Eurographics Association, Goslar, DEU, p. 87–95.
- Park, J. J., Florence, P., Straub, J., Newcombe, R. & Lovegrove, S. (2019), DeepSDF: Learning continuous signed distance functions for shape representation, in 'The IEEE Conference on Computer Vision and Pattern Recognition (CVPR)'
- Park, S. & Bajaj, C. L. (2004), Multi-dimensional transfer function design for scientific visualization, in 'ICVGIP'.
- Parker, S. G., Bigler, J., Dietrich, A., Friedrich, H., Hoberock, J., Luebke, D., McAllister, D., McGuire, M., Morley, K., Robison, A. & Stich, M. (2010), Optix: A general purpose ray tracing engine, in 'ACM SIGGRAPH 2010 Papers', SIGGRAPH '10, Association for Computing Machinery, New York, NY, USA.
URL: <https://doi.org/10.1145/1833349.1778803>
- Parulek, J. & Viola, I. (2012), Implicit representation of molecular surfaces, in '2012 IEEE Pacific Visualization Symposium', pp. 217–224.
- Pasko, A. A., Fryazinov, O., Vilbrandt, T., Fayolle, P.-A. & Adzhiev, V. (2011a), 'Procedural function-based modelling of volumetric microstructures', *Graphical Models* **73**, 165–181.
- Pasko, A. A., Fryazinov, O., Vilbrandt, T., Fayolle, P.-A. & Adzhiev, V. (2011b), 'Procedural function-based modelling of volumetric microstructures', *Graphical Models* **73**, 165–181.

- Pasko, A., Adzhiev, V., Schmitt, B. & Schlick, C. (2001), 'Constructive hypervolume modeling', *Graph. Models* **63**(6), 413–442.
URL: <http://dx.doi.org/10.1006/gmod.2001.0560>
- Pasko, A., Adzhiev, V., Sourin, A. & Savchenko, V. (1995), 'Function representation in geometric modeling: concepts, implementation and applications', *The Visual Computer* **11**(8), 429–446.
URL: <https://doi.org/10.1007/BF02464333>
- Pasko, A., Okunev, O. & Savchenko, V. (2003), 'Minkowski sums of point sets defined by inequalities', *Computers Mathematics with Applications* **45**, 1479–1487.
- Pasko, A., Savchenko, A. & Savchenko, V. (1999), 'Implicit curved polygons', *Technical Report 96-1-004*.
- Pasko, A. & Savchenko, V. (1997), 'Projection operation for multidimensional geometric modeling with real functions'.
- Pasko, G., Pasko, A. & Kunii, T. (2004a), 'Space–time blending', *Computer Animation and Virtual Worlds* **15**(2), 109–121.
URL: <https://onlinelibrary.wiley.com/doi/abs/10.1002/cav.12>
- Pasko, G., Pasko, A. & Kunii, T. (2004b), 'Space–time blending', *Computer Animation and Virtual Worlds* **15**(2), 109–121.
URL: <https://onlinelibrary.wiley.com/doi/abs/10.1002/cav.12>
- Patric, L., Jens, K., Eduard, G., Markus, H., D., H. C. & Anders, Y. (2016), 'State of the art in transfer functions for direct volume rendering', *Computer Graphics Forum* **35**(3), 669–691.
- Payandeh, S. & Azouz, N. (2001), Finite elements, mass-spring-damper systems and haptic rendering, in 'Proceedings 2001 IEEE International Symposium on Computational Intelligence in Robotics and Automation (Cat. No.01EX515)', pp. 224–229.
- Peck, E. M., Yuksel, B. F., Harrison, L., Ottley, A. & Chang, R. (2012), Towards a 3-dimensional model of individual cognitive differences: Position paper, in 'Proceedings of the 2012 BELIV Workshop: Beyond Time and Errors - Novel Evaluation Methods for Visualization', BELIV '12, Association for Computing Machinery, New York, NY, USA.
URL: <https://doi.org/10.1145/2442576.2442582>

- Pérez-Bellido, A., Ernst, M., Soto-Faraco, S. & López-Moliner, J. (2015), ‘Visual limitations shape audio-visual integration.’, *Journal of vision* **15** **14**, 5.
- Pham, M.-S., Liu, C., Todd, I. & Lertthanasarn, J. (2019), ‘Publisher correction: Damage-tolerant architected materials inspired by crystal microstructure.’, *Nature* **567**.
URL: <http://dx.doi.org/10.1038/s41586-019-0968-y>
- Pharr, M. & Humphreys, G. (2004), *Physically Based Rendering: From Theory to Implementation*, Morgan Kaufmann Publishers Inc., San Francisco, CA, USA.
- Pharr, M., Jakob, W. & Humphreys, G. (2016), *Physically Based Rendering: From Theory to Implementation*, 3rd edn, Morgan Kaufmann Publishers Inc., San Francisco, CA, USA.
- Phillips, M., Georgiev, I., Hildebrandt, A., Nickels, S., Marsalek, L., Lenhof, H.-P., Hildebrandt, A. & Slusallek, P. (2010), Measuring properties of molecular surfaces using ray casting, pp. 1–7.
- Pike, C. (2019), Evaluating the perceived quality of binaural technology.
- Plaisant, C. (2004), The challenge of information visualization evaluation, in ‘Proceedings of the Working Conference on Advanced Visual Interfaces’, AVI ’04, Association for Computing Machinery, New York, NY, USA, p. 109–116.
URL: <https://doi.org/10.1145/989863.989880>
- Pressnitzer, D. & Gnansia, D. (2005), ‘Real-time auditory models’, *International Computer Music Conference, ICMC 2005* .
- Projection operation for multidimensional geometric modeling with real functions* (1996), in W. S. (Ed.), ed., ‘Theory and Practice of Geometric Modeling, Blaubeuren II conference’.
- Purcell, T. J., Buck, I., Mark, W. R. & Hanrahan, P. (2002), ‘Ray tracing on programmable graphics hardware’, *ACM Transactions on Graphics* **21**(3), 703–712. ISSN 0730-0301 (Proceedings of ACM SIGGRAPH 2002).
- Putanowicz, R. (2015), ‘Implementation of pore microstructure model generator and pore space analysis tools’, *Procedia Engineering* **108**, 355–362.
- Raab, M., Seibert, D. & Keller, A. (2008), Unbiased global illumination with participating media, in A. Keller, S. Heinrich & H. Niederreiter, eds, ‘Monte Carlo and Quasi-Monte Carlo Methods 2006’, Springer Berlin Heidelberg, Berlin, Heidelberg, pp. 591–605.

- Rathke, B., Wald, I., Chiu, K. & Brownlee, C. (2015), SIMD Parallel Ray Tracing of Homogeneous Polyhedral Grids, in C. Dachsbacher & P. Navrátil, eds, 'Eurographics Symposium on Parallel Graphics and Visualization', The Eurographics Association.
- Ray Tracing In Vulkan* (2018), <https://www.khronos.org/blog/ray-tracing-in-vulkan>. Accessed: 2019-10-23.
- Reiner, T., Muckl, G. & Dachsbacher, C. (2011), 'Interactive modeling of implicit surfaces using a direct visualization approach with signed distance functions', *Computers Graphics* **35**(3).
- Ren, Z., Yeh, H. & Lin, M. C. (2013), 'Example-guided physically based modal sound synthesis', *ACM Trans. Graph.* **32**(1).
URL: <https://doi.org/10.1145/2421636.2421637>
- Ribeiro, F., Florêncio, D., Chou, P. A. & Zhang, Z. (2012), Auditory augmented reality: Object sonification for the visually impaired, in '2012 IEEE 14th International Workshop on Multimedia Signal Processing (MMSP)', pp. 319–324.
- Rincon-Nigro, M., Navkar, N., Tsekos, N. & Deng, Z. (2014), 'Gpu-accelerated interactive visualization and planning of neurosurgical interventions', *Computer Graphics and Applications, IEEE* **34**, 22–31.
- Röber, N., Kaminski, U. & Masuch, M. (2007), Ray acoustics using computer graphics technology.
- Roberts, J. C., Ritsos, P. D., Badam, S. K., Brodbeck, D., Kennedy, J. & Elmqvist, N. (2014), 'Visualization beyond the desktop—the next big thing', *IEEE Computer Graphics and Applications* **34**(6), 26–34.
- Roodaki, H., Navab, N., Eslami, A., Stapleton, C. & Navab, N. (2017), 'Sonifeye: Sonification of visual information using physical modeling sound synthesis', *IEEE Transactions on Visualization and Computer Graphics* **23**(11), 2366–2371.
URL: doi.ieeecomputersociety.org/10.1109/TVCG.2017.2734327
- Ropinski, T., Praßni, J., Steinicke, F. & Hinrichs, K. (2008), Stroke-Based Transfer Function Design, in H.-C. Hege, D. Laidlaw, R. Pajarola & O. Staadt, eds, 'IEEE/ EG Symposium on Volume and Point-Based Graphics', The Eurographics Association.
- Rubin, J. (2016), 'What is haptics? part 2: Vibrotactile (vibration) feedback'.
URL: <https://haptx.com/what-is-haptics-really-part-2/>

- Ruijters, D. & Vilanova, A. (2006), Optimizing gpu volume rendering, in ‘WSCG - Winter School of Computer Graphics’, Vol. 14, pp. 9–16.
URL: <http://graphics.tudelft.nl/Publications-new/2006/RV06>
- Ruspini, D. C., Kolarov, K. & Khatib, O. (1997), The haptic display of complex graphical environments, in ‘Proceedings of the 24th Annual Conference on Computer Graphics and Interactive Techniques’, SIGGRAPH ’97, ACM Press/Addison-Wesley Publishing Co., New York, NY, USA, pp. 345–352.
URL: <https://doi.org/10.1145/258734.258878>
- Röber, N., Andres, S. & Masuch, M. (2006), ‘Hrtf simulations through acoustic raytracing’.
- Sachin, N. & Khairnar, V. (2014), ‘Brain tumor detection based on symmetry information’, *CoRR* **abs/1401.6127**.
URL: <http://arxiv.org/abs/1401.6127>
- Saket, B. & Endert, A. (2018), ‘Evaluation of visualization by demonstration and manual view specification’, *ArXiv* **abs/1805.02711**.
- Salisbury, K., Conti, F. & Barbagli, F. (2004), ‘Haptic rendering: introductory concepts’, *IEEE Computer Graphics and Applications* **24**(2), 24–32.
- Samanta, K. & Koc, B. (2008), *Feature-Based Material Blending for Heterogeneous Object Modeling*, Springer Berlin Heidelberg, Berlin, Heidelberg, pp. 142–166.
URL: https://doi.org/10.1007/978-3-540-68443-5_6
- Sanchez, M., Fryazinov, O. & Pasko, A. (2012), Efficient evaluation of continuous signed distance to a polygonal mesh, in ‘Proceedings of the 28th Spring Conference on Computer Graphics’, SCCG ’12, ACM, New York, NY, USA, pp. 101–108.
URL: <http://doi.acm.org/10.1145/2448531.2448544>
- Santosh, K. C. & Antani, S. (2017), ‘Automated chest x-ray screening: Can lung region symmetry help detect pulmonary abnormalities?’, *IEEE Transactions on Medical Imaging* **PP**(99), 1–1.
- Sarkka, O., Nieminen, T., Suuriniemi, S. & Kettunen, L. (2017), ‘A multi-position calibration method for consumer-grade accelerometers, gyroscopes, and magnetometers to field conditions’, *IEEE Sensors Journal* **PP**, 1–1.
- Savioja, L. & Svensson, U. P. (2015), ‘Overview of geometrical room acoustic modeling techniques’, *The Journal of the Acoustical Society of America* **138**(2), 708–730.
URL: <https://doi.org/10.1121/1.4926438>

- Savioja, L. & Välimäki, V. (2002), Interpolated 3-d digital waveguide mesh for room acoustic simulations, in 'Conference: Forum Acusticum'.
- Schaedler, T. A. & Carter, W. B. (2016), 'Architected cellular materials', *Annual Review of Materials Research* **46**(1), 187–210.
- Schissler, C. & Manocha, D. (2011), 'Gsound: Interactive sound propagation for games', *Proceedings of the AES International Conference* .
- Schlegel, P., Makhinya, M. & Pajarola, R. (2011), 'Extinction-based shading and illumination in gpu volume ray-casting', *IEEE Transactions on Visualization and Computer Graphics* **17**(12), 1795–1802.
- Schmidt, C. & Budge, B. (2002), 'Simple nested dielectrics in ray traced images', *Journal of Graphics Tools* **7**.
- Schmidt, N. (2020), A cad interface for drawing with signed distance functions, in 'ACM SIGGRAPH 2020 Posters', SIGGRAPH '20, Association for Computing Machinery, New York, NY, USA.
URL: <https://doi.org/10.1145/3388770.3407435>
- Schmitt, B., Pasko, A., Adzhiev, V., Pasko, G. & Schlick, C. (2008), *Modelling Function-Based Mixed-Dimensional Objects with Attributes*, Vol. 4889, pp. 90–117.
- Scholl, I., Suder, S. & Schiffer, S. (2018), *Direct Volume Rendering in Virtual Reality*, pp. 297–302.
- Schroeder, W., Martin, K. & Lorensen, B. (2006), *The Visualization Toolkit—An Object-Oriented Approach To 3D Graphics*, fourth edn, Kitware, Inc.
- Schroeder, W., Martin, K. M. & Lorensen, W. E. (1998), *The Visualization Toolkit (2Nd Ed.): An Object-oriented Approach to 3D Graphics*, Prentice-Hall, Inc., Upper Saddle River, NJ, USA.
- Schürer, R. (2004), Adaptive quasi-monte carlo integration based on miser and vegas, in H. Niederreiter, ed., 'Monte Carlo and Quasi-Monte Carlo Methods 2002', Springer Berlin Heidelberg, Berlin, Heidelberg, pp. 393–406.
- Schwind, V., Mayer, S., Comeau-Vermeersch, A., Schweigert, R. & Henze, N. (2018), Up to the finger tip: The effect of avatars on mid-air pointing accuracy in virtual reality, in 'Proceedings of the 2018 Annual Symposium on Computer-Human Interaction in Play',

- CHI PLAY '18, Association for Computing Machinery, New York, NY, USA, p. 477–488.
URL: <https://doi.org/10.1145/3242671.3242675>
- Seyb, D., Jacobson, A., Nowrouzezahrai, D. & Jarosz, W. (2019a), 'Non-linear sphere tracing for rendering deformed signed distance fields', *ACM Transactions on Graphics (Proceedings of SIGGRAPH Asia)* **38**(6).
- Seyb, D., Jacobson, A., Nowrouzezahrai, D. & Jarosz, W. (2019b), 'Non-linear sphere tracing for rendering deformed signed distance fields', *ACM Trans. Graph.* **38**(6).
URL: <https://doi.org/10.1145/3355089.3356502>
- Shankar, K. & Michael, N. (2020), Mrfmap: Online probabilistic 3d mapping using forward ray sensor models.
- Sherstyuk, A. (1999), 'Kernel functions in convolution surfaces: A comparative analysis', *The Visual Computer* **15**.
- Shi, J., Zhang, A., Encarnação, J. & Göbel, M. (1993), 'A modified radiosity algorithm for integrated visual and auditory rendering', *Computers Graphics* **17**(6), 633–642.
URL: <https://www.sciencedirect.com/science/article/pii/009784939390112M>
- Shusterman, A. & Strauss, L. (2001), 'Teaching chemistry with electron density models. 2. can atomic charges adequately explain electrostatic potential maps?', *The Chemical Educator* **6**, 36–40.
- Shusterman, G. P. & Shusterman, A. J. (1997), Teaching chemistry with electron density models.
- Signal Processing Essentials* (2005), John Wiley Sons, Ltd, chapter 2, pp. 13–49.
URL: <https://onlinelibrary.wiley.com/doi/abs/10.1002/9780470041970.ch2>
- Sik, M. & Krivanek, J. (2013), Fast Random Sampling of Triangular Meshes, in B. Levy, X. Tong & K. Yin, eds, 'Pacific Graphics Short Papers', The Eurographics Association.
- Siltanen, S., Lokki, T., Kiminki, S. & Savioja, L. (2007), 'The room acoustic rendering equation', **122**, 1624.
- Silva, C., Comba, J., Callahan, S. & Bernardon, F. (2005), 'A survey of gpu-based volume rendering of unstructured grids.', *RITA* **12**, 9–30.

Silva, N., Blascheck, T., Jianu, R., Rodrigues, N., Weiskopf, D., Raubal, M. & Schreck, T. (2019), Eye tracking support for visual analytics systems: Foundations, current applications, and research challenges, in 'Proceedings of the 11th ACM Symposium on Eye Tracking Research Applications', ETRA '19, Association for Computing Machinery, New York, NY, USA.

URL: <https://doi.org/10.1145/3314111.3319919>

Silva, R., Rodrigues, P., Oliveira, J. & Giraldo, G. (2004), Augmented reality for scientific visualization: Bringing datasets inside the real world.

Slavcheva, M. (2018), Signed distance fields for rigid and deformable 3d reconstruction.

Smith, J. O. (1992), 'Physical modeling using digital waveguides', *Computer Music Journal* **16**.

Smith, S. W. (1997), *The Scientist and Engineer's Guide to Digital Signal Processing*, California Technical Publishing, San Diego, CA, USA.

URL: <https://users.dimi.uniud.it/antonio.dangelo/MMS/materials/Guide₁oDigitalSignalProcess.pdf>

Sommefeldt, R. (2020), 'Coherency gathering in ray tracing: the benefits of hardware ray tracking'.

URL: <https://www.imaginationtech.com/blog/coherency-gathering-in-ray-tracing-the-benefits-of-hardware-ray-tracking/>

Song, X., Cheng, M., Wang, B., Huang, S. & Huang, X. (2011), 'Computer-aided preoperative planning for liver surgery based on ct images', *Procedia Engineering* **24**, 133 – 137. International Conference on Advances in Engineering 2011.

URL: <http://www.sciencedirect.com/science/article/pii/S1877705811054671>

Sonification Report: Status of the Field and Research Agenda (2010), <https://digitalcommons.unl.edu/cgi/viewcontent.cgi?article=1443&context=psychfacpub>.

Soundararajan, K. P. & Schultz, T. (2015), 'Learning probabilistic transfer functions: A comparative study of classifiers', *Computer Graphics Forum* **34**(3), 111–120.

URL: <https://onlinelibrary.wiley.com/doi/abs/10.1111/cgf.12623>

Sourin, A. & Pasko, A. (1995), Function representation for sweeping by a moving solid.

Spence, C. (2011), 'Crossmodal correspondences: A tutorial review', *Attention, Perception, & Psychophysics* **73**(4), 971–995.

- Strohmeier, P. & Hornbæk, K. (2017), Generating haptic textures with a vibrotactile actuator, in 'Proceedings of the 2017 CHI Conference on Human Factors in Computing Systems', CHI '17, ACM, New York, NY, USA, pp. 4994–5005.
URL: <http://doi.acm.org/10.1145/3025453.3025812>
- Sua, S., Chaudhary, A., O'Leary, P., Geveci, B., Sherman, W., Nieto, H. & Francisco-Revilla, L. (2015), Virtual reality enabled scientific visualization workflow, pp. 29–32.
- Subtil, N. (2018), 'Vintroduction to real-time ray tracing with vulkan', <https://developer.nvidia.com/blog/vulkan-raytracing/>. Accessed: 2019-10-23.
- Suderow, H., Guillamon, I., Rodrigo, J. G. & Vieira, S. (2014), 'Imaging superconducting vortex cores and lattices with a scanning tunneling microscope', *Superconductor Science and Technology* **27**(6), 063001.
- Sussman, E. (2005), 'Integration and segregation in auditory scene analysis', *The Journal of the Acoustical Society of America* **117**, 1285–98.
- Sussman, E. (2017), 'Auditory scene analysis: An attention perspective', *Journal of Speech Language and Hearing Research* **60**, 2989.
- Syam, W. P., Jianwei, W., Zhao, B., Maskery, I., Elmadih, W. & Leach, R. (2018), 'Design and analysis of strut-based lattice structures for vibration isolation', *Precision Engineering* **52**, 494 – 506.
URL: <http://www.sciencedirect.com/science/article/pii/S0141635917302726>
- Tak, S. & Toet, A. (2013), Towards interactive multisensory data representations.
- Takala, T. & Hahn, J. (1992), Sound rendering, in 'Proceedings of the 19th Annual Conference on Computer Graphics and Interactive Techniques', SIGGRAPH '92, ACM, New York, NY, USA, pp. 211–220.
URL: <http://doi.acm.org/10.1145/133994.134063>
- Tang, J., Han, X., Tan, M., Tong, X. & Jia, K. (2020), 'Skeletonnet: A topology-preserving solution for learning mesh reconstruction of object surfaces from rgb images.', *arXiv: Computer Vision and Pattern Recognition* .
- Tappenbeck, A., Preim, B. & Dicken, V. (2006), Distance-based transfer function design: Specification methods and applications, in 'SimVis2006', pp. 259–274.
- Team, R. D. (2018a), *RAPIDS: Collection of Libraries for End to End GPU Data Science*.
URL: <https://rapids.ai>

- Team, R. D. (2018b), *RAPIDS: Collection of Libraries for End to End GPU Data Science*.
URL: <https://rapids.ai>
- Tejima, T., Fujita, M. & Matsuoka, T. (2015), ‘Direct ray tracing of full-featured subdivision surfaces with bezier clipping’, *Journal of Computer Graphics Techniques (JCGT)* **4**(1), 69–83.
URL: <http://jcgt.org/published/0004/01/04/>
- Thoman, P., Wippler, M., Hranitzky, R. & Fahringer, T. (2020), Rtx-rsim: Accelerated vulkan room response simulation for time-of-flight imaging, in ‘Proceedings of the International Workshop on OpenCL’, IWOCL ’20, Association for Computing Machinery, New York, NY, USA.
URL: <https://doi.org/10.1145/3388333.3388662>
- Tory, M. & Moller, T. (2005), ‘Evaluating visualizations: do expert reviews work?’, *IEEE Computer Graphics and Applications* **25**(5), 8–11.
- Trainor, L. (2015a), ‘The origins of music in auditory scene analysis and the roles of evolution and culture in musical creation’, *Philosophical transactions of the Royal Society of London. Series B, Biological sciences* **370**.
- Trainor, L. (2015b), ‘The origins of music in auditory scene analysis and the roles of evolution and culture in musical creation’, *Philosophical transactions of the Royal Society of London. Series B, Biological sciences* **370**.
- Tsai, T.-C. (2017), *Position Based Dynamics*, Springer International Publishing, Cham, pp. 1–5.
URL: https://doi.org/10.1007/978-3-319-08234-9_2 – 1
- Turk, M. (2014), ‘Multimodal interaction: A review’, *Pattern Recognition Letters* **36**, 189 – 195.
URL: <http://www.sciencedirect.com/science/article/pii/S0167865513002584>
- UCLA (2020), ‘G*power’.
URL: <https://stats.idre.ucla.edu/other/gpower/>
- Ulmstedt, M. & Stålberg, J. (2019), Gpu accelerated ray-tracing for simulating sound propagation in water, Master’s thesis, Linköping University, Computer Engineering.
- Urbanietz, C., Enzner, G., Orth, A., Kwiatkowski, P. & Pohl, N. (2019), A radar-based navigation assistance device with binaural sound interface for vision-impaired people, pp. 236–243.

- Usher, W. (2020), 'The rtx shader binding table three ways', <https://www.willusher.io/graphics/2019/11/20/the-sbt-three-ways>.
- Usher, W., Amstutz, J., Brownlee, C., Knoll, A. & Wald, I. (2017), Progressive cpu volume rendering with sample accumulation, in 'Proceedings of the 17th Eurographics Symposium on Parallel Graphics and Visualization', PGV '17, Eurographics Association, Goslar, DEU, p. 21–30.
URL: <https://doi.org/10.2312/pgv.20171090>
- Usher, W. & Pascucci, V. (2020), Interactive visualization of terascale data in the browser: Fact or fiction?, in '2020 IEEE 10th Symposium on Large Data Analysis and Visualization (LDAV)', pp. 27–36.
- van den Doel, K. & K. Pai, D. (2003), 'Modal synthesis for vibrating objects', *Audio Anecdotes* pp. 1–8.
- Van, G. & Bergen, D. (2004), Ray casting against general convex objects with application to continuous collision detection.
- Van Uitert, R. & Bitter, I. (2007), 'Subvoxel precise skeletons of volumetric data based on fast marching methods', *Medical Physics* **34**(2), 627–638.
URL: <https://aapm.onlinelibrary.wiley.com/doi/abs/10.1118/1.2409238>
- Vasiou, E., Shkurko, K., Mallett, I., Brunvand, E. & Yuksel, C. (2018), 'A detailed study of ray tracing performance: render time and energy cost', *The Visual Computer* **34**.
- Vasuki, P., Kanimozhi, J. & Devi, M. B. (2017), A survey on image preprocessing techniques for diverse fields of medical imagery, in '2017 IEEE International Conference on Electrical, Instrumentation and Communication Engineering (ICEICE)', pp. 1–6.
- Vickers, P. & Alty, J. (2002), 'Musical program auralisation: A structured approach to motif design', *Interacting with Computers* **14**, 457–485.
- Vilbrandt, T., Pasko, A. & Vilbrandt, C. (2009), 'Fabricating nature', *Technoetic Arts, Intellect* **7**, 165–174.
- Villanueva, A. J., Marton, F. & Gobetti, E. (2017), 'Symmetry-aware sparse voxel DAGs (SSVDAGs) for compression-domain tracing of high-resolution geometric scenes', *Journal of Computer Graphics Techniques (JCGT)* **6**(2), 1–30.
URL: <http://jcgt.org/published/0006/02/01/>

- Vitello, F., Sciacca, E., Becciani, U., Costa, A., Bandieramonte, M., Benedettini, M., Brescia, M., Butora, R., Cavuoti, S., Giorgio, A. M. D., Elia, D., Liu, S. J., Molinari, S., Molinaro, M., Riccio, G., Schisano, E. & Smareglia, R. (2018), ‘Vialactea visual analytics tool for star formation studies of the galactic plane’, *Publications of the Astronomical Society of the Pacific* **130**(990), 084503.
URL: <https://doi.org/10.1088/1538-3873/aac5d2>
- Vogelsberger, M., Marinacci, F., Torrey, P. & Puchwein, E. (2019), ‘Cosmological simulations of galaxy formation’.
- Volume Rendering with Python and VTK* (n.d.), <https://pyscience.wordpress.com/2014/11/16/volume-rendering-with-python-and-vtk/>. Accessed: 2018-10-23.
- VRWorks - Audio* (2018), <https://developer.nvidia.com/vrworks/vrworks-audio>. Accessed on 2018/12/7.
- Vulkan compute pipelines* (n.d.).
URL: <https://www.khronos.org/registry/vulkan/specs/1.1-extensions/html/chap10.html#pipelines-compute>
- Wächter, C. & Raab, M. (2019), *Automatic Handling of Materials in Nested Volumes*, Apress, Berkeley, CA, pp. 139–147.
URL: https://doi.org/10.1007/978-1-4842-4427-2_11
- Wahle, M. & Wriggers, W. (2015), Multi-scale visualization of molecular architecture using real-time ambient occlusion in sculptor, *in* ‘PLoS Computational Biology’.
- Wald, I. (2007), On fast construction of sah-based bounding volume hierarchies, *in* ‘Proceedings of the 2007 IEEE Symposium on Interactive Ray Tracing’, RT ’07, IEEE Computer Society, USA, p. 33–40.
URL: <https://doi.org/10.1109/RT.2007.4342588>
- Wald, I., Dietrich, A., Benthin, C., Efremov, A., Dahmen, T., Gunther, J., Havran, V., Seidel, H. & Slusallek, P. (2006), Applying ray tracing for virtual reality and industrial design, *in* ‘2006 IEEE Symposium on Interactive Ray Tracing’, pp. 177–185.
- Wald, I., Johnson, G., Amstutz, J., Brownlee, C., Knoll, A., Jeffers, J., Gunther, J. & Navratil, P. (2017), ‘Ospray - a cpu ray tracing framework for scientific visualization’, *IEEE Transactions on Visualization and Computer Graphics* **23**(1), 931–940.
URL: <https://doi.org/10.1109/TVCG.2016.2599041>

- Wald, I. & Parker, S. G. (2019), Rtx accelerated ray tracing with optix, in 'ACM SIGGRAPH 2019 Courses', SIGGRAPH '19, Association for Computing Machinery, New York, NY, USA.
URL: <https://doi.org/10.1145/3305366.3340297>
- Wang, B., Jiang, W., Dai, X., Gao, Y., Wang, Z. & Zhang, R. Q. (2016), 'Molecular orbital analysis of the hydrogen bonded water dimer', *Scientific reports* **6**.
- Wang, L., Yu, Y., Zhou, K. & Guo, B. (2011), 'Multiscale vector volumes', *ACM Trans. Graph.* **30**(6), 167:1–167:8.
- Wang, W., Wang, T. Y., Yang, Z., Liu, L., Tong, X., Tong, W., Deng, J., Chen, F. & Liu, X. (2013), 'Cost-effective printing of 3d objects with skin-frame structures', *ACM Trans. Graph.* **32**(6).
URL: <https://doi.org/10.1145/2508363.2508382>
- Wang, X., Tang, M., Manocha, D. & Tong, R. (2018), 'Efficient BVH-based Collision Detection Scheme with Ordering and Restructuring', *Computer Graphics Forum* .
- Ward, J. & Meijer, P. (2010), 'Visual experiences in the blind induced by an auditory sensory substitution device', *Consciousness and cognition* **19**(1), 492–500.
- Ward, M. & Yang, J. (2004), Interaction spaces in data and information visualization., pp. 137–145.
- Watson, C. S., Wroton, H. W., Kelly, W. J. & Benbassat, C. A. (1975), 'Factors in the discrimination of tonal patterns. i. component frequency, temporal position, and silent intervals', *The Journal of the Acoustical Society of America* **57**(5), 1175–1185.
- Weiler, M., Kraus, M., Merz, M. & Ertl, T. (2003), Hardware-based ray casting for tetrahedral meshes, in 'Proceedings of the 14th IEEE Visualization 2003 (VIS'03)', VIS '03, IEEE Computer Society, USA, p. 44.
URL: <https://doi.org/10.1109/VISUAL.2003.1250390>
- Wenzel, E. M., Arruda, M., Kistler, D. J. & Wightman, F. L. (1993), 'Localization using nonindividualized head-related transfer functions', *The Journal of the Acoustical Society of America* **94**(1), 111–123.
URL: <https://doi.org/10.1121/1.407089>
- Whitted, T. (1980), 'An improved illumination model for shaded display', *Commun. ACM* **23**(6), 343–349.
URL: <https://doi.org/10.1145/358876.358882>

- Winkler, I., Denham, S. L. & Nelken, I. (2009), 'Modeling the auditory scene: predictive regularity representations and perceptual objects', *Trends in Cognitive Sciences* **13**(12), 532–540.
URL: <http://www.sciencedirect.com/science/article/pii/S1364661309002095>
- wu, K., Truong, N., Yuksel, C. & Hoetzlein, R. (2018), 'Fast fluid simulations with sparse volumes on the gpu', *Computer Graphics Forum* **37**, 157–167.
- Wu, R. & Yu, G. (2016), Improvements in hrtf dataset of 3d game audio application, in '2016 International Conference on Audio, Language and Image Processing (ICALIP)', pp. 185–190.
- Wyman, C. (2020), 'Lighting scenes with millions of lights using rtx direct illumination', <https://developer.nvidia.com/blog/lighting-scenes-with-millions-of-lights-using-rtx-direct-illumination/>.
- Xu, H. & Barbič, J. (2017), '6-dof haptic rendering using continuous collision detection between points and signed distance fields', *IEEE Transactions on Haptics* **10**(2), 151–161.
URL: doi.ieeecomputersociety.org/10.1109/TOH.2016.2613872
- Xu, H. & Barbič, J. (2014), 'Continuous collision detection between points and signed distance fields', *Workshop on Virtual Reality Interaction and Physical Simulation VRIPHYS 2014*.
- Yagel, R. & Shi, Z. (1993), Accelerating volume animation by space-leaping, in 'Proceedings Visualization '93', pp. 62–69.
- Yan, Obias & ÖLLERER (2004), Touching the visualized invisible: Wearable ar with a multimodal interface.
- Yang, J., Hermann, T. & Bresin, R. (2019), 'Introduction to the special issue on interactive sonification', *Journal on Multimodal User Interfaces* **13**.
- Yeung, E. (1980), 'Pattern recognition by audio representation of multivariate analytical data', *Analytical Chemistry* **52**(7), 1120–1123.
- Zahorik, P., Brungart, D. & Bronkhorst, A. (2005), 'Auditory distance perception in humans: A summary of past and present research', *Acta Acustica united with Acustica* **91**, 409–420.
- Zatorre, R. J. (1988), 'Pitch perception of complex tones and human temporal-lobe function', *The Journal of the Acoustical Society of America* **84**(2), 566–572.

- Zeng, A., Song, S., Nießner, M., Fisher, M., Xiao, J. & Funkhouser, T. (2017), 3dmatch: Learning local geometric descriptors from rgb-d reconstructions, *in* 'CVPR'.
- Zhao, L., Ma, K. & Yang, Z. (2015), 'Changes of water hydrogen bond network with different externalities', *International journal of molecular sciences* **16**(4), 8454–8489.
- Zhao, X. & Kaufman, A. (2010), Multi-dimensional Reduction and Transfer Function Design using Parallel Coordinates, *in* R. Westermann & G. Kindlmann, eds, 'IEEE/ EG Symposium on Volume Graphics', The Eurographics Association.
- Zhao, Y., Ji, Z., Jiaoying, S. & Zhigeng, P. (2001), A fast algorithm for large scale terrain walkthrough.
- Zhou, H.-X. (2014), 'Theoretical frameworks for multiscale modeling and simulation', *Current opinion in structural biology* **25C**, 67–76.
- Zhou, K., Gong, M., Huang, X. & Guo, B. (2008), 'Highly parallel surface reconstruction'.
- Zhou, K., Hou, Q., Wang, R. & Guo, B. (2008), Real-time kd-tree construction on graphics hardware, *in* 'ACM SIGGRAPH Asia 2008 Papers', SIGGRAPH Asia '08, Association for Computing Machinery, New York, NY, USA.
URL: <https://doi.org/10.1145/1457515.1409079>
- Zhou, L. & Hansen, C. (2013), Transfer function design based on user selected samples for intuitive multivariate volume exploration, *in* '2013 IEEE Pacific Visualization Symposium (PacificVis)', pp. 73–80.
- Zhou, L., Schott, M. & Hansen, C. (2012), 'Transfer function combinations'.
URL: <http://hdl.handle.net/10754/600057>
- Ziemer, T. & Schultheis, H. (2019), 'Psychoacoustic auditory display for navigation: an auditory assistance system for spatial orientation tasks', *Journal on Multimodal User Interfaces* **13**(3), 205–218.
- Ziemkiewicz, C., Ottley, A., Crouser, R., Chauncey, K., Su, S. & Chang, R. (2012), 'Understanding visualization by understanding individual users', *Computer Graphics and Applications, IEEE* **32**.
- Zilles, C. B. & Salisbury, J. K. (1995), A constraint-based god-object method for haptic display, *in* 'Proceedings of the International Conference on Intelligent Robots and Systems- Volume 3 - Volume 3', IROS '95, IEEE Computer Society, Washington, DC, USA,

pp. 3146–.

URL: <http://dl.acm.org/citation.cfm?id=846238.849727>

Ó Maidín, D. & Fernström, M. (0001), ‘The best of two worlds: Retrieving and browsing’.